Wearable Systems For Health Monitoring Towards Active Aging

Wearable Systems For Health Monitoring

Towards Active Aging

BY

SUMIT MAJUMDER

B. Sc. BANGLADESH UNIVERSOTY OF ENGINEERING AND TECHNOLOGY, 2007

M. A, Sc. MCMASTER UNIVERSITY, 2011

A THESIS

SUBMITTED TO THE DEPARTMENT OF ELECTRICAL & COMPUTER

ENGINEERING

AND THE SCHOOL OF GRADUATE STUDIES

OF MCMASTER UNIVERSITY

IN PARTIAL FULFILMENT OF THE REQUIREMENTS

FOR THE DEGREE OF PHILOSOPHY

McMaster University
Hamilton, Canada

Doctor of Philosophy (2020)
Electrical and Computer Engineering

TITLE: Wearable Systems For Health Monitoring Towards Active Aging

AUTHOR: Sumit Majumder
B. Sc., Bangladesh University of Engineering and Technology, Dhaka, Bangladesh
M. A. Sc., McMaster University, Hamilton, Canada

SUPERVISOR: Dr. M. Jamal Deen

NUMBER OF PAGES: xix, 174

Lay Abstract

Wearable health monitoring systems can be a viable solution to meet the increased demand for affordable healthcare and monitoring services. However, such systems need to be energy–efficient, accurate and ergonomic to enable long–term monitoring of health reliably while preserving user comfort.

In this thesis, we develop efficient algorithms to obtain real–time estimates of on–body sensors' orientation, gait parameters such as stride length, and gait velocity and lower–limb joint angles. Furthermore, we develop a simple, low–cost and computationally efficient gait–analyzer using miniature and low–power inertial motion units to track the health of human gait in a continuous fashion.

In addition, we design flexible, dry capacitive electrodes and use them to develop a portable single–lead electrocardiogram (ECG) device. The flexible design ensures better conformity of the electrode to the skin, resulting in better signal quality. The capacitive nature allows for obtaining ECG signals over insulating materials such as cloth, thereby potentially enabling a comfortable means of long–term cardiac health monitoring at home. Besides, we implement an automatic anomaly detection algorithm that detects Atrial Fibrillation with good accuracy from short single–lead ECGs.

Finally, we investigate the association between gait and cardiac activities. We observe that some important cardiac signs, such as heart rate and heart rate variability and physical parameters, such as age and BMI show good association with gait asymmetry and gait variation.

Abstract

Global rise in life expectancy has resulted in an increased demand for affordable healthcare and monitoring services. The advent of miniature and low–power sensor technologies coupled with the emergence of the Internet–of–Things has paved the way towards affordable health monitoring tools in wearable platforms. However, ensuring power–efficient operation, data accuracy and user comfort are critical for such wearable systems. This thesis focuses on the development of accurate and computationally efficient algorithms and low–cost, unobtrusive devices with potential predictive capability for monitoring mobility and cardiac health in a wearable platform.

A three–stage complementary filter–based approach is developed to realize a computationally efficient method to estimate sensor orientation in real–time. A gradient descent–based approach is used to estimate the gyroscope integration drift, which is subsequently subtracted from the integrated gyroscope data to get the sensor orientation. This predominantly gyroscope–based orientation estimation approach is least affected by external acceleration and magnetic disturbances.

A two–stage complementary filter–based efficient sensor fusion algorithm is developed for real–time monitoring of lower–limb joints that estimates the IMU inclinations in the first stage and uses a gradient descent–based approach in the second stage to estimate the joint angles. The proposed method estimates joint angles primarily from the gyroscope measurements without incorporating the magnetic field measurement, rendering the estimated angles least affected by any external acceleration and insensitive to magnetic disturbances.

An IMU–based simple, low–cost and computationally efficient gait–analyzer is developed to track the course of an individual's gait health in a continuous fashion. Continuous monitoring of gait patterns can potentially enable detecting musculoskeletal or neurodegenerative diseases at the early onset. The proposed gait analyzer identifies an anomalous gait with moderate to high accuracy by evaluating the gait features with respect to the baseline clusters corresponding to an individual's healthy peer group. The adoption of a computationally efficient signal analysis technique renders the analyzer suitable for systems with limited processing capabilities.

A flexible dry capacitive electrode and a wireless ECG monitoring system with automatic anomaly detection capability are developed. The flexible capacitive electrode reduces motion artifacts and enables sensing bio–potential over a dielectric material such as cotton cloth. The virtual ground of the electrode allows for obtaining single–lead ECG using two electrodes only. ECG measurements obtained over different types of textile materials and in presence of body movements show comparable performance to other reported ECG monitoring systems. An algorithm is developed separately as a potential extension of the software to realize automatic identification of Atrial Fibrillation from short single–lead ECGs.

The association between human gait and cardiac activities is studied. The gait is measured using wearable IMUs and the cardiac activity is measured with a single–lead handheld ECG monitor. Some key cardiac parameters, such as heart rate and heart rate variability and physical parameters, such as age and BMI show good association with gait asymmetry and gait variation. These associations between gait and heart can be useful in realizing low–cost in–home personal monitoring tool for early detecting CVD–related changes in gait features before the CVD symptoms are manifested.

Acknowledgements

It is my immense pleasure to thank those people who, by their assistance, support and valuable advice helped me to prepare and complete this dissertation.

First and foremost, I would like to express my utmost gratitude to my supervisor Dr. M. Jamal Deen for his consistent support, invaluable guidance and countless technical advice during the entire course of my graduate studies and research work. It has been a great honor and privilege to be a student of such an accomplished researcher and academician. The training that I received from Dr. Deen on different aspects of research such as critical thinking, problem–solving, experiment planning, data analysis, technical writing, and presentation to people with different education levels and backgrounds is truly invaluable.

I would like to sincerely thank my committee member, Dr. Tapas Mondal, and Dr. Chih–Hung Chen, for the helpful discussions and for their continuous support during my research. I would also like to thank them for taking the time to review my thesis. I also would like to sincerely thank Dr. David Cowan for his time and effort in recruiting volunteers for experiments and for his valuable insights in designing the experiments.

I am also privileged to have some top–notch researchers as my lab–mates in Dr. Deen's team. I would like to thank Dr. Yiheng Qin, Dr. Arif U. Alam, Dr. Si Pan, Dr. Mrwan Alayed, Dr. Mahdi Naghshvarianjahromi, Dr. Ahmed Elsharabasy, Yamn Chalich, Ryan Scott, Hytham Afifi, Wei Jiang, and Abu Ilius Faisal for their valuable suggestions and feedback on my research.

I also sincerely thank my parents and sister for their unconditional love, support and encouragement over all these years. I cannot thank enough to my dear wife, Mouri Biswas, for her endless love, sacrifice and support, and my little bundle of joy, Pratyush. Last but not least, I would like to express my heartfelt gratitude to my uncle Rupan Kanti Das and my late grandfather Nirmal Bihari Das, who along with my mother, Minakshi Majumder, had great influence in laying the foundation of my long pursuit of academic endeavors. I dedicate this thesis to them.

Table of Contents

Lay Abstract iii

Abstract iv

Acknowledgements vi

List of Figures xi

List of Tables xiv

List of Abbreviations xv

Chapter 1 Introduction 1

1.1 Research motivation 2

1.2 Smart health–monitoring framework 5

1.2.1 Sensors and actuators 7

1.2.2 Communication network 7

1.2.3 Computing and decision making platform 9

1.2.4 Services 9

1.3 Interoperability and standardization 10

1.4 Sensors and devices 13

1.4.1 Smartphone–based systems 15

1.4.2 Wearable devices 24

1.4.3 Textile–based sensors 26

1.5 Regulatory concerns 34

1.6 Research contributions and thesis organization 40

Chapter 2 A robust orientation filter 45

2.1 Related works 46

2.2 Proposed orientation filter 49

2.2.1 Stage one: Estimation of Roll and Pitch 49

2.2.2 Stage two: Coarse estimation of yaw 51

2.2.3 Stage three: Fine estimation of yaw 53

2.3 Performance evaluation 53

2.3.1 Orientation estimation 53

2.3.2 Filter robustness 55
2.3.3 Gait parameter estimation 59
2.4 Conclusions 63
Chapter 3 Real–time monitoring of lower–limb joints 65
3.1 Background 66
3.2 Proposed method 69
3.2.1 Stage one: estimation of inclination 70
3.2.2 Second stage: estimation of joint angle 72
3.3 Performance evaluation 75
3.3.1 Joint angle estimation 75
3.3.2 Filter robustness 78
3.4 Conclusions 81
Chapter 4 A gait analyzer for healthcare applications 83
4.1 Background 84
4.2 Data acquisition system and protocols 87
4.2.1 Participants and protocols 87
4.2.2 Data acquisition system 87
4.2.3 Data acquisition Protocol 88
4.3 Signal analysis and assessment 88
4.3.1 Preprocessing 89
4.3.2 Signal decomposition 89
4.3.3 Feature extraction 90
4.3.4 Dimensional reduction 92
4.3.5 Classification of the baseline gait data 92
4.3.6 Cross validation 93
4.4 Results and discussion 93
4.4.1 Stride characteristics 93
4.4.2 Gender–specific clustering of gait behavior 97
4.4.3 Age–specific clustering of gait behavior 99

4.5 Conclusions 101
Chapter 5 Wearable ECG system with automatic anomaly detection 103
5.1 Related works on ambulatory ECG systems 105
5.1.1 ECG systems in the literature 106
5.1.2 Commercial portable ECG systems 112
5.2 Proposed ECG system 113
5.2.1 Overview 113
5.2.2 Capacitive electrodes 114
5.2.3 Portable ECG device 116
5.2.4 Computer monitoring system 117
5.3 Performance evaluation 117
5.3.1 Experimental results 117
5.3.2 Comparison with existing results 121
5.4 Automatic anomaly detection 123
5.4.1 Data collection protocols 124
5.4.2 Signal processing 125
5.4.3 Feature extraction 125
5.4.4 Predictive model 126
5.4.5 Model performance 127
5.5 Conclusions 128
Chapter 6 Association between gait and heart 130
6.1 Background 131
6.2 Data acquisition and protocols 134
6.2.1 Participants and protocols 134
6.2.2 Data acquisition systems 135
6.2.3 Data acquisition protocol 135
6.3 Results and discussion 136
6.3.1 Association between Resting HR and Gait 136
6.3.2 Association between HRV and Gait 139

6.4 Conclusions 143
Chapter 7 Conclusions, perspectives and future work 145
7.1 Conclusions 145
7.2 General perspectives 148
7.3 Future work 150
References 153
Appendix Copyright permissions 172

List of Figures

Figure 1.1 IoT–enabled Smart Homes, integrated with automated with automated healthcare systems. 2

Figure 1.2 General framework of smart health–monitoring system showing the network among different stakeholders. 5

Figure 1.3 A four–layer architecture of the smart health–monitoring system [1.22]. 6

Figure 1.4 Fragmentation of wireless communication platforms. 11

Figure 1.5 Cardiovascular monitoring: (a) a typical lead I ECG signal (not scaled); (b) Electrode placement in a standard 12–lead ECG system; 13

Figure 1.6 Photoplethysmograph (PPG) signal from the pulsatile flow of blood volume is used to measure HR and HRV using smartphone 15

Figure 1.7 General architecture of a smartphone–based activity monitoring system. 18

Figure 2.1 Proposed three–stage orientation filter. 49

Figure 2.2 Aligning sensor frame to the earth frame. 52

Figure 2.3 Estimated integration drift in the roll and pitch angles. 54

Figure 2.4 Estimated roll and pitch at first stage with respect to the ground truth. 54

Figure 2.5 Estimated yaw with respect to the ground truth. 55

Figure 2.6 Accelerometer data contaminated at different noise levels. 56

Figure 2.7 Error in the estimated roll and pitch at different noise levels. 57

Figure 2.8 Magnetic field data contaminated with simulated low–frequency disturbances. 58

Figure 2.9 Error in the estimated orientation in the presence of magnetic disturbance. 58

Figure 2.10 Magnetic field disturbance in presence of a magnet. 59

Figure 2.11 Estimated yaw using the proposed filter. 59

Figure 2.12 Inertial measurement unit (a) commercial sensor (Mbientlab MetaMotionR) (b) mounting of the sensor. 60

Figure 2.13 Gait parameter estimation– a) measured acceleration b) orientation corrected linear acceleration along three dimensions, c) drift–corrected instantaneous velocity and d) estimation of stride length. 61

Figure 2.14 Photograph of the staircase and estimated trajectory of staircase climbing using the proposed orientation filter. 63
Figure 3.1 Proposed two–stage filter for joint angle estimation. 70
Figure 3.2 Aligning sensor frame to the earth frame assuming no rotation around the vertical *z*–axis..... 73
Figure 3.3 Rotation of the joint in the reference frame. 74
Figure 3.4 Estimated integration drift in the roll and pitch angles. 76
Figure 3.5 Estimated roll and pitch at the end of first stage. 76
Figure 3.6 Estimated angles with respect to the ground truth for– a) thigh joint b) knee joint, and c) ankle joint. 77
Figure 3.7 Accelerometer data contaminated at different noise levels. Data along the y–axis data is presented only. 79
Figure 3.8 Error in the estimated angles at 0.5 ms^{-1} speed from a) hip joint, b) knee joint and c) ankle joint. 80
Figure 4.1 Inertial measurement unit (a) commercial sensor (Invensense MPU–9150) (b) position of the sensor. 88
Figure 4.2 Wavelet packet decomposition tree up to 2nd level. 90
Figure 4.3 Four components of the medio–lateral signal decomposed at 2nd level with wavelet packet decomposition using sym4 as the mother wavelet. 90
Figure 4.4 Block diagram of the gait analyzer. 93
Figure 4.5 Comparison between male and female gait (a) cadence (b) GA (c) CV. 94
Figure 4.6 Comparison between male and female gait energies (a) acceleration energy (b) rotational energy. 95
Figure 4.7 Comparison between two age groups (a) cadence (b) GA (c) CV. 96
Figure 4.8 Comparison between two age groups (a) acceleration energy (b) rotational energy. 97
Figure 4.9 Classification results showing two distinct groups (excluding outliers). 98
Figure 4.10 One instance of cross–validation showing one subject is falsely classified. ... 98

Figure 4.11 Classification results showing two distinct age groups (excluding outliers).. 100
Figure 4.12 One instance of cross–validation showing one subject falls in a different age group than his/her actual age. 101
Figure 5.1 Basic features in the waveform of an ECG signal. 104
Figure 5.2 General architecture of the ambulatory ECG monitoring system. 105
Figure 5.3 Block diagram of the proposed ECG sensing system. 114
Figure 5.4 Electrode–body interface with capacitive coupling of ECG bio–potential..... 114
Figure 5.5 Schematic diagram of the capacitive electrode. 115
Figure 5.6 Photograph of the ECG measurement set–up. 116
Figure 5.7 ECG acquisitions in the time domain without body movement, with electrodes on (a) bare dry skin and (b) cotton fabric covered dry skin. 118
Figure 5.8 ECG measured from the bare dry skin with body movements: (a) slow abduction–adduction of both hands, (b) fast abduction–adduction of both hands, (c) body rotation, and (d) normal walking. 119
Figure 5.9 ECG measured from the textile covered dry skin with body movements: (a) slow abduction–adduction of both hands, (b) fast abduction–adduction of both hands, (c) body rotation, and (d) normal walking. 120
Figure 5.10 Single–lead ECG signal (a) normal rhythm and (b) atrial fibrilation [5.86]... 124
Figure 6.1 The brain has three main parts: the cerebrum, cerebellum and brain stem..... 131
Figure 6.2 Change in HR due to submaximal workloads..... 134
Figure 6.3 Experimental setup a) IMU attachment in the shank b) 20 m walking loop. ... 136
Figure 6.4 Biplot of the first three principal component coefficients. 138
Figure 6.5 Association of key gait features with resting HR. 139
Figure 6.6 Heart rate variability evolves from the interaction between the sympathetic and parasympathetic parts of ANS. 140
Figure 6.7 Relations between age and resting–HRV of healthy participants determined by a) pNN20 and b) pNN50. 141
Figure 7.1 (a) Pulse transit time (PTT) (b) Four sensor health monitoring system. 151

List of Tables

Table 1.1 Communication technologies for Smart health–monitoring systems. 8

Table 1.2 Smartphone–sensors for cardiovascular health monitoring. 16

Table 1.3. Typical features extracted from motion signals [1.20]. 18

Table 1.4. Smartphone–sensor based activity monitoring systems. 19

Table 1.5. Comparison among cardiovascular monitoring systems. 25

Table 1.6. Activity monitoring systems. 27

Table 1.7. Summary of textile electrodes. 30

Table 1.8. Summary of textile–based strain sensors. 33

Table 2.1 Comparison of root Mean Square error in estimated orientation (radians) 55

Table 2.2. RMSE (radians) in estimated orientation in presence of external acceleration. . 57

Table 2.3 Experimental validation of stride length calculation. 62

Table 3.1 Performance of the proposed filter with respect to the ground truth. 78

Table 3.2 RMS error of estimated joint angles in presence of external acceleration. 80

Table 4.1 Participants' characteristics 87

Table 4.2 Extracted features. 92

Table 4.3 Confusion matrix for gender–specific gait classifier. 99

Table 4.4 Confusion matrix for age–specific gait classifier. 100

Table 5.1 Effects of interface materials and moisture on the ECG signal quality. 121

Table 5.2 Comparison between the proposed methods and recent alternatives for ECG sensing systems. 122

Table 5.3 Performance of the anomalous ECG detector. 128

Table 6.1 Performance of the models after 5–fold cross validation. 137

Table 6.2 Description of the five key gait features. 138

Table 6.3 HRV indices in time domain. 140

Table 6.4 HRV indices with age both at rest and after walk. 141

Table 6.5 Association of resting–HRVs with gait speed and stride length. 142

List of Abbreviations

IoT	Internet–of–Things
WHO	World Health Organization
GDP	Gross Domestic Product
OECD	Organization for Economic Co–Operation and Development
MEMS	Microelectromechanical Systems
SHS	Smart Health–Monitoring System
NIC	National Intelligence Council
BLE	Bluetooth Low Energy
FPGA	Field Programmable Gate Array
HR	Heart Rate
HRV	Heart Rate Variability
SpO_2	Arterial Oxygen Saturation
BP	Blood Pressure
GSR	Galvanic Skin Response
RR	Respiratory Rate
T	Body Temperature
RFID	Radio–Frequency Identification
PIR	Passive Infrared
BSN	Body Sensor Network
LAN	Local Area Network
PAN	Personal Area Networks
WSN	Wireless Sensor Network
AES	Advanced Encryption Standard
WEP	Wired Equivalent Privacy
WPA	Wi–Fi Protected Access
RF	Radio–Frequency
NFC	Near–Field Communication
P2P	Peer–to–Peer
HART	Highway Addressable Remote Transducer Protocol
HomePlug GP	Homeplug Green PHY
AI	Artificial Intelligence
ANN	Artificial Neural Network
SVM	Support Vector Machine
KNN	K–Nearest Neighbors
EMS	Emergency Medical Service
GSM	Global System for Mobile Communications
EDGE	Enhanced Data Rates for GSM Evolution
3G	Third Generation Wireless Mobile Telecommunications Technology
HSPA	High Speed Packet Access
LTE	Long–term Evolution
IEEE	Institute of Electrical and Electronics Engineers
ISO	International Organization for Standardization
IEC	International Electrotechnical Commission
ITU	International Telegraph Union
ITU–T	ITU–Telecommunication Standardization Sector
IETF	Internet Engineering Task Force
ETSI	European Telecommunications Standards Institute
SDO	Standard Development Organization

IoTSP	Internet Of Things, Services and People
IP	Internet Protocol
IPv4	Internet Protocol Version 4
IPv6	Internet Protocol Version 6
BACnet	Building Automation and Control Networks
TCP	Transmission Control Protocol
6LoWPAN	Ipv6 Over Low–Power Wireless Personal Area Networks
DECT	Digital European Cordless Telecommunications
DECT ULE	DECT Ultra Low Energy
IPSO	Internet Protocol for Smart Objects
CoAP	Constrained Application Protocol
LR–WPANs	Low–Rate Wireless Personal Area Networks
PHY/MAC	Physical / Media Access Control
RFC	Request for Comments
REST	Representational State Transfer
HTTP	Hypertext Transfer Protocol
API	Application Programming Interface
OPC UA	Open Platform Communications Unified Architecture
oBIX	Open Building Information Xchange
ADL	Activities of Daily Living
ECG	Electrocardiogram
MI	Myocardial Infarction
PPG	Photoplethysmograph
NIR	Near–Infrared
PC	Pearson Correlation Coefficient
ICA	Independent Component Analysis
ROI	Region of Interest
GPS	Global Positioning System
RMS	Root Mean Square
HAR	Human Activity Recognition
WISDM	Wireless Sensor Data Mining
HMM	Hidden Markov Model
NN	Neural Network
FMM	Fuzzy Min–Max
CART	Classification and Regression Tree
MLP	Multilayer Perceptron
DTW	Dynamic Time Warping
DNN	Deep Neural Network
CRF	Conditional Random Field
PCA	Principal Component Analysis
HIER	Hierarchical Agglomerative Clustering
DBSCAN	Density–Based Spatial Clustering of Applications With Noise
GMM	Gaussian Markov Model
LDA	Linear Discriminant Analysis
DBN	Deep Belief Network
IndRNN	Independently Recurrent Neural Network
ICC	Intra–Class Correlation Coefficients
KPCA	Kernel Principal Component Analysis
SMA	Signal Magnitude Area
SMV	Signal Magnitude Vector

MMS	Multimedia Messaging Service
ABF	Audio Bio–Feedback
HLFPN	High–Level Fuzzy Petri Net
ROM	Range of Motion
NB	Naive Bayes
MA	Motion Artifacts
Ni	Nickel
Cu	Copper
FCCL	Flexible Copper Clad Laminates
PPV	Positive Predictive Value
NPV	Negative Predictive Value
TPR	True Positive Rate
FPR	False Positive Rate
CVD	Chemical Vapor Deposition
DOF	Degree of Freedom
IMU	Inertial Measurement Unit
CRF	Conditional Random Field
USB	Universal Serial Bus
STD	Standard Deviation
EMG	Electromyography
PU	Polyurethane
PEDOT:PSS	Poly(3,4–Ethylenedioxythiophene) Polystyrene Sulfonate
PVDF	Polyvinylidene Difluoride
FFT	Fast Fourier Transform
TENS	Transcutaneous Electrical Nerve Stimulation
PCB	Printed Circuit Board
PDMS	Polydimethylsiloxane
FBG	Fiber Bragg Grating
FDA	Food and Drug Administration, USA
MHRA	Medicines and Healthcare Products Regulatory Agency, UK
EU	European Union
MDD	Medical Device Directive
CE	Conformité Européenne
EEA	European Economic Area
BSA	Body Surface Area
MDR	Medical Device Regulation
AIMD	Active Implantable Medical Devices
UDI	Unique Device Identification
BMI	Body Mass Index
NB	Notified Body
MDL	Medical Device License for Canada
MDEL	Medical Device Establishment License for Canada
TGA	Therapeutic Goods Administration, Australia
PMDA	Pharmaceutical and Medical Devices Agency, Japan
IMDRF	International Medical Device Regulators Forum
MDSAP	Medical Device Single Audit Program
ANVISA	Agência Nacional De Vigilância Sanitária, Brazil
MHLW	Ministry of Health and Labor and Welfare, Japan
CMDCAS	Canadian Medical Device Conformity Assessment System
AFib	Atrial Fibrillation

CVD	Cardiovascular Disease
MIMU	Magnetic and Inertial Measurement Units
MFC	Minimum Foot Clearance
EKF	Extended Kalman Filter
QUEST	Quaternion Estimator
CF	Complementary Filter
RMSE	Root Mean Square Error
SNR	Signal–to–Noise Ratio
ZUPT	Zero Velocity Update
BPF	Band–Pass Filter
HPF	High–Pass Filter
LPF	Low–Pass Filter
UKF	Unscented Kalman Filter
SPINE	Signal Processing In Node Environment
CNS	Central Nervous System
DWPA	Discrete Wavelet Packet Analysis
EMD	Empirical Mode Decomposition
CEEMD	Complete Ensemble EMD
IMF	Intrinsic Mode Functions
DWT	Discrete Wavelet Transform
WPD	Wavelet Packet Decomposition
GA	Gait Asymmetry
CV	Coefficient of Variation
REB	Research Ethics Board
AFE	Analog Front End
ETI	Electrode–Tissue Impedance
EPDM	Ethylene Propylene Diene Monomer
CNT	Carbon Nanotube
MNA	Microneedles Array
CDA	Conductive Dry Adhesives
CMRR	Common Mode Rejection Ratio
DDA	Differential Difference Amplifier
RSSI	Relative Received Signal Strength
HBC	Human Body Communication
BER	Bit Error Rate
CMOS	Complementary Metal–Oxide–Semiconductor
IIR	Infinite Impulse Response
CSV	Comma Separated Value
LA	Left Arm
RA	Right Arm
pNN10	% of consecutive NN intervals that differ by more than 10 ms
pNN20	% of consecutive NN intervals that differ by more than 20 ms
pNN50	% of consecutive NN intervals that differ by more than 50 ms
SDNN	Standard Deviation of NN Intervals
SDSD	Standard Deviation of Successive Differences
RMSSD	Root Mean Square of Successive Differences between NN intervals
SVD	Singular Value Decomposition
Bagged tree	Bootstrap Aggregated Tree
MTC	Minimum Toe Clearance
CHF	Chronic Heart Failure

PCI	Physiological Cost Index
ANOVA	Analysis of Variance
WAT	White Adipose Tissue
LG	Logistic Regression
PC1	First Principal Component
PC2	Second Principal Component
PC3	Third Principal Component
ANS	Autonomic Nervous System
COVID	Coronavirus Disease
PTT	Pulse Transit Time
BGL	Blood Glucose Level

Chapter 1
Introduction

In recent years, the Internet–of–Things (IoT) has attracted much attention from researchers, entrepreneurs, and tech giants [1.1]–[1.3] around the globe. IoT is an emerging technology that connects to the internet, collects and shares data from a variety of devices and systems such as sensors, actuators, appliances, computers, and cellular phones, thus leading towards a highly distributed intelligent system capable of communicating with other devices and human beings [1.1]–[1.3]. The dramatic advancements in computing and communication technologies coupled with modern low–power, low–cost sensors, actuators and electronic components have unlocked the door of ample opportunities for the IoT applications. Remote health monitoring in a Smart home platform through wearable systems is such an example of IoT application that can potentially play a pivotal role in revolutionizing the healthcare system, particularly for the elderly, facilitating active aging at home. As the world is rapidly moving towards the new era of the IoT, a fully functional smart home with heath monitoring capability is closer to reality than ever before (See Figure 1.1).

In this chapter, we describe the motivation of this research that is followed by a discussion on the IoT–based health monitoring framework. We briefly present the current state–of–the–

---

* Adapted from -

S. Majumder, T. Mondal, and M. J. Deen, "Wearable sensors for remote health monitoring," *Sensors*, vol. 17, no. 1, 45 pages, 2017.

S. Majumder *et al.*, "Smart homes for elderly healthcare—Recent advances and research challenges," *Sensors*, vol. 17, no. 11, 32 pages, 2017.

S. Majumder and M. J. Deen, "Smartphone sensors for health monitoring and diagnosis," *Sensors*, vol. 19, no. 9, 45 pages, 2019.

art of wearable systems, following a discussion on device interoperability and standardization. Next, a short discussion on the regulatory concerns associated with the smartphone applications for health monitoring is presented. Then, the research contributions are given. Finally, the organization of this thesis is presented.

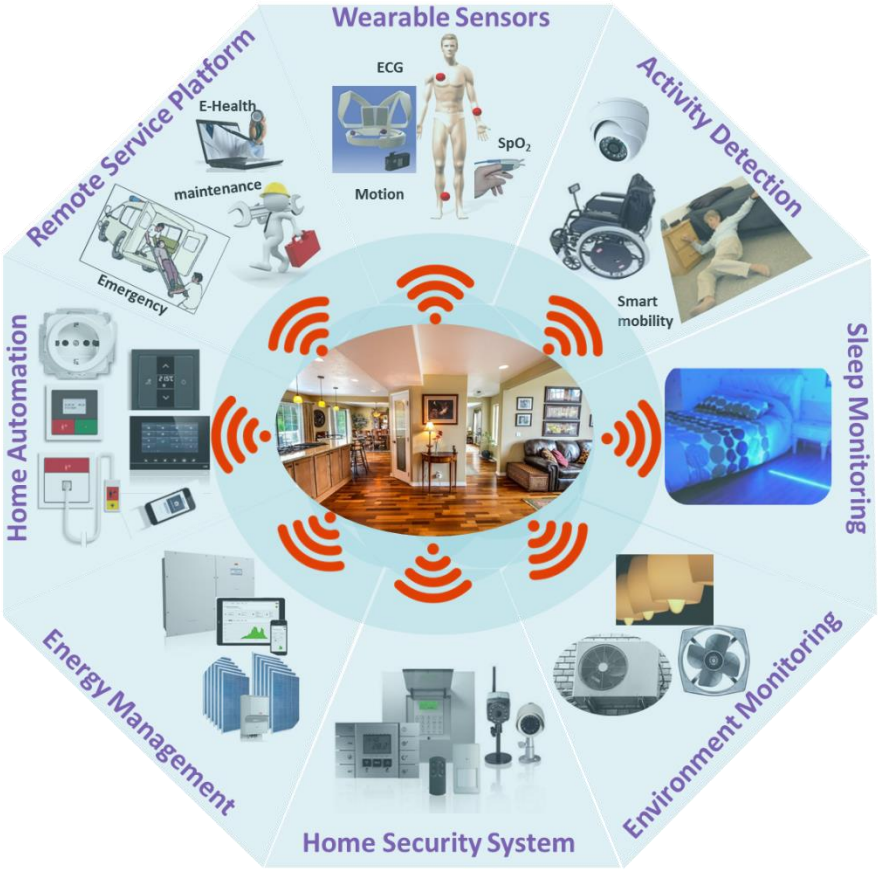

Figure 1.1 IoT–enabled Smart Homes, integrated with automated with automated healthcare systems.

1.1 Research motivation

In the last few decades, the life expectancy in most countries has increased dramatically. This improvement is achieved primarily due to significant advancements in medical science and diagnostic technology, as well as the rising awareness about personal and environmental hygiene, health, nutrition, and education [1.4]–[1.7]. However, increased life expectancy coupled with falling birthrates is expected to result in a large aging population in the near future. In fact, according to the World Health Organization (WHO), the elderly population over 65 years of age would outnumber the children under the age of 14 by 2050 [1.6]. In

addition, about 15% of the world's population suffers from various disabilities, with 110–190 million adults having significant functional difficulties [1.8]. People with disabilities are often deprived of their regular healthcare needs due to their limited mobility and independence. Furthermore, chronic diseases and conditions such as heart disease, stroke, cancer and diabetes, are among the most common health problems in adults. Half of all American adults aged 18 years or older are reported to have at least one chronic condition, and one in three adults suffering from multiple chronic conditions. Out of the ten leading causes of death, chronic diseases account for ~65–70% of total mortality [1.9]. In particular, heart disease and cancer together are the leading causes of death, accounting for 48% of all deaths [1.10].

Therefore, it is no wonder that the demand for healthcare services increases with the rise of average life expectancy. An important issue related to providing adequate healthcare services is the continuously increasing cost of pharmaceuticals, modern medical diagnostic procedures and in–facility care services, which together renders the existing healthcare services unaffordable for many. To give one example, in the 2017 budget of the Province of Ontario in Canada, an additional $11.5 billion was allocated for the next three years in healthcare sectors [1.11]. Further, the total health spending per Canadian was expected to be $6839 in 2018, representing more than 11% of Canada's GDP and these numbers are similar to most other OECD (Organization for Economic Co–operation and Development) countries [1.12]. Therefore, present–day healthcare services are likely to cause a substantial socio–economic burden on many nations, particularly the developing and least developed countries [1.13]–[1.17]. Furthermore, a large fraction of the elderly relies on other persons such as family members, friends and volunteers, or expensive formal care services such as caregivers and elderly care centers for their daily living and healthcare needs [1.18]–[1.20]. Therefore, enabling superior healthcare and monitoring services at an affordable price is urgently needed, particularly for persons having limited access to healthcare facilities or to those living under constrained or fixed budget conditions. However, through long–term monitoring of key physiological parameters and activities of the elderly in a continuous fashion, many of

the medical complications can be avoided or managed properly [1.20]–[1.23]. Long–term monitoring of health enables early diagnoses of developing diseases. However, current practice requires frequent visits to or long–term stays at expensive healthcare facilities. In addition, a shortage of skilled healthcare personnel and limited financial capability, coupled with increasing healthcare costs [1.24] contribute to the bottleneck in realizing long–term health monitoring. On the other hand, wearable healthcare systems can potentially enable a cost–effective alternative for long–term health monitoring and may allow the healthcare personnel to monitor and assess their patients remotely without interfering with their daily activities [1.20],[1.25].

In order to be compatible for long–term monitoring purposes, wearable health monitoring systems need to satisfy certain medical and ergonomic requirements. For example, the system needs to be comfortable; the components should be flexible, small in dimensions and must be chemically inert, nontoxic, and hypo–allergenic to the human body. In addition, limitation of hardware resources is a major concern for a multi–sensor system where the central on–body processing node needs to handle a large amount of data from different sensor nodes. It also impacts the system power requirements significantly that needs to be minimized in order to extend the battery life for long–term use. Finally, the system needs to be inexpensive and user–friendly in order to ensure its widespread acceptance among the people for ubiquitous health monitoring. Therefore, the critical design challenge for wearable health monitoring system is to integrate several electronic and sensing components while ensuring data accuracy, efficient processing for real–time monitoring, and low–power consumption as well as user's wearing comfort.

To obtain the abovementioned goals, this research focuses on the development of highly accurate yet computationally efficient algorithms and low–cost, unobtrusive devices with potential predictive capability to realize reliable health monitoring in the wearable platform. This research particularly focuses on developing monitoring solutions for cardiovascular health and mobility *i.e.* health of the lower–limb — two key factors that are strongly associated with the human aging process.

1.2 Smart health–monitoring framework

The advancement of miniaturized and inexpensive sensors, embedded computing devices, and wireless networking technologies as well as growing penetration of internet, tablets and smartphones, have paved the way for realizing in–home health monitoring systems. People can stay in their familiar home environment and enjoy their normal lives with friends and family while their health is being monitored, analyzed and assessed from a remote facility based–on the physiological data collected by different on–body sensors. The system can perform long–term health trend analysis, detect anomalies, and generate alert signals in the case of an emergency (See Figure 1.2).

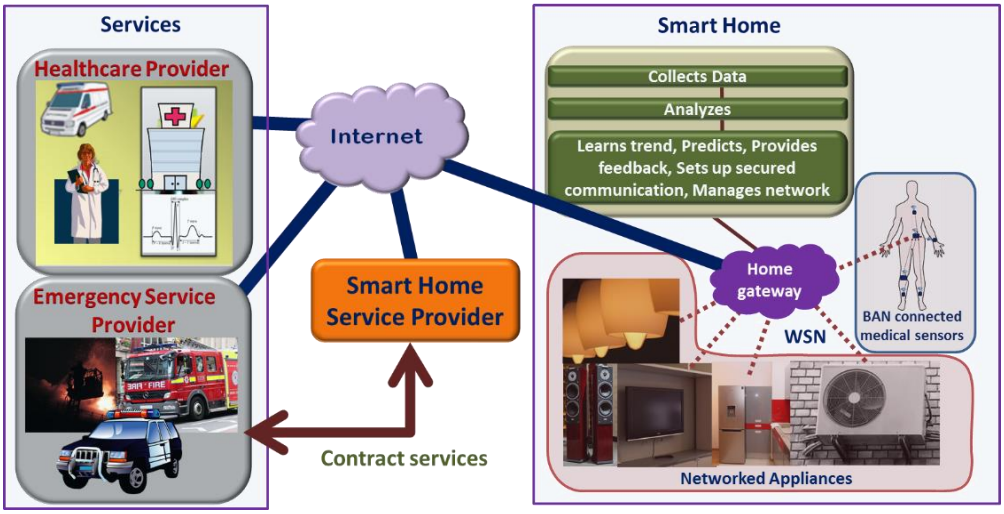

Figure 1.2 General framework of smart health–monitoring system showing the network among different stakeholders.

Such a smart health–monitoring system (SHS) can be realized by exploiting the IoT framework and incorporating sensors, actuators, and smart devices in a 'Smart Home' to potentially facilitate monitoring of the occupants' health, safety, wellbeing, comfort and security remotely, over the internet from anywhere. The IoT can be defined as a network of intelligent objects that is capable of organizing and sharing information, data and resources, decision making, and responding to feedback [1.26]. It allows human–to–human, human–to–things and things–to–things interaction by providing a unique identity to each and every object [1.27]. The US National Intelligence Council (NIC) considered the IoT technology as one of the six disruptive civil technologies that can potentially impact US national power

[1.28]. Some researchers envisioned the IoT as an emerging field that can enable new ways of living by bridging the physical world with the digital computing platform by means of smart sensing and actuating devices, and appropriate communication technologies such as Bluetooth Low Energy (BLE), ZigBee, and ANT [1.29]–[1.32]. Therefore, the concept of IoT can be exploited in a wide range of applications such as E–health, assisted living, enhanced learning, intelligent transportation, environmental protection, government work, public security, smart homes, intelligent fire control, industrial monitoring and automation [1.33].

The SHS may include a set of environmental, activity and physiological sensors and actuators, connected through a wireless communication medium. The advancement in low–power, smaller dimension sensing, actuating and transceiver systems coupled with modern communication technologies and inexpensive computing platforms such as field programmable gate array (FPGA), microcontrollers, microprocessors paved the way for low–cost smart health–monitoring systems. A four–layer architecture of SHS [1.22] is presented in Figure 1.3.

Figure 1.3 A four–layer architecture of the smart health–monitoring system [1.22].

1.2.1 Sensors and actuators

Sensors and actuators are critical in monitoring systems described in Section 1.2 that bridges the gap between the physical world and the digital domain. This in–home health monitoring system may make use of wearable sensors to monitor physiological parameters such as heart rate (HR), heart rate variability (HRV), arterial oxygen saturation (SpO_2), blood pressure (BP), galvanic skin response (GSR), respiratory rate (RR) and body temperature (T). This system may also incorporate fixed–position sensors to collect data about the home environment such as light illumination level, temperature, pressure, gas leakage and oxygen level, and about the activity or location of the occupants by using inertial measurement units, RFID tags or passive infrared (PIR) sensors to ensure the occupants' safety and comfort.
Actuators, on the other hand, can respond to the feedback from the occupants or from the central decision making platform by performing small scale maneuvers to control the environment or to deliver drugs such as insulin to the occupant's body. These sensors and actuators can communicate with the central computing and decision making platform over the wireless communication medium. The sensors, particularly the on–body sensors, need to be energy efficient and unobtrusive in order to facilitate long–term monitoring. Also, adoption of energy harvesting technologies can effectively increase the run–time of the ambulatory devices.

1.2.2 Communication network

All sensors and actuators in the SHS are connected with the central communication and decision–making platform though a communication network, which forms the second layer of the health monitoring framework. Signals measured by the sensors are transmitted to a central computing node over a wireless and/or wired communication medium. Although wired connection is a feasible solution for fixed–position based environmental sensors, it is not suitable for wearable and long–term monitoring systems. Wired connections for the wearable BSN may cause inconvenience to the user and restrict their mobility. It may also cause occasional connection failure among the on–body sensors. Textile based conductive medium such as conductive fabrics can be used to communicate with the on–body sensors as an alternative to the wired connection. However, conductive textiles suffer from low durability and limited washability, thus resulting in poor or failed connectivity after prolonged use [1.34]. Therefore, modern low–power wireless communication technologies appear to be the most viable and reliable medium for short–range communication. Table 2

presents the key features of some commonly used wireless technologies for short range communication.

The wearable sensors can be connected in a Body Sensor Network (BSN), where the central BSN node is connected with all fixed–position sensors and actuators through the Wireless Sensor Network (WSN). All the sensors and actuators in the Smart Home are connected, thus forming a Local Area Network (LAN) or Personal Area Networks (PAN) to enable data communication inside the home [1.35]. The central decision making platform can communicate with any sensors and actuators in the network through the WSN to collect data or send feedback to perform necessary actions, if required.

Table 1.1 Communication technologies for Smart health–monitoring systems.

Wireless tech.	Frequency	Range	Data rate	Power (mW)	Max # nodes	Network topologies	Security
RFID	13.56 MHz 860–960 MHz	0–3 m	640 kbps	200	1 at a time	peer–to–peer (P2P) passive	—
Bluetooth	2.4–2.5 GHz	1 – 100 m	1–3 Mbps	2.5–100	1 M[1], 7 S[2]	P2P, star	56–128 bit key
BLE	2.4–2.5 GHz	1 – 100 m	1 Mbps	10	1 M, 7 S	P2P, star	128–bit AES[3]
HomePlug GP	1.8–30 MHz	~100 m	4–10 Mbps	500	–	P2P, star, tree and mesh	128–bit AES
EnOcean	902, 928, 868 MHz	30 – 300 m	125 kbps	~0.05 with energy harvesting	–	P2P, star, tree and mesh	128–bit AES
ZigBee	2.4–2.5 GHz	10 – 100 m	250 kbps	50	65,533	P2P, star, tree and mesh	128–bit AES
WiFi	2.4–2.5 GHz	150 – 200 m	54 Mbps	1000	255	P2P, star	WEP,WPA, WPA2
DASH7	315–915 MHz	200 m –2 km	167 kbps	<1	–	P2P, star, tree and mesh	128–bit AES
Insteon	RF:869.85, 915, 921 MHz powerline: 131.65kHz	40 – 50 m	38 kbps (RF) 2–13 kbps (powerline)	–	64,000 nodes per network	P2P, star, tree and mesh	256–bit AES
Sigfox	868/902 MHz	10 – 50 km	10–1000 bps	0.01–100	–	P2P, star	No default encryption
NFC	13.56 MHz	5 cm	424 kbps	15	1 at a time	P2P	AES
Wireless HART™	2.4 GHz	50 – 100 m		10	–	P2P, star, tree and mesh	128–bit AES
6LoWPAN	2.4 GHz	25 – 50 m	250 kbps	2.23	–	P2P, star, tree and mesh	128–bit AES
ANT	2.4–2.5 GHz	30 m	20–60 kbps	0.01–1	65,533 in one channel	P2P, star, tree and mesh	64–bit key
Z–Wave	860–960 MHz	100 m	9.6–100 kbps	100	232	mesh	128–bit AES

[1]M: Master, [2]S: Slave, [3]AES: Advanced Encryption Standard

1.2.3 Computing and decision making platform

The third layer of smart health–monitoring architecture is responsible for computing and decision making, thus functioning as the brain of the system. This layer is equipped with computing systems such as smartphones, computers or custom–built processing nodes based on Field Programmable Gate Arrays (FPGAs) or microprocessors. It gathers data from the sensors and actuators over the WSN, processes, stores, and analyzes the measured data.

It may also perform trend analysis, run prediction algorithms and send feedback to the user or to the actuators. The prediction algorithms can exploit the features of artificial intelligence (AI) and make use of deep learning and machine learning techniques such as artificial neural network (ANN), support vector machine (SVM), and K–Nearest Neighbors (KNN) to model the behavioral and physiological patterns of the occupants, and potentially predict and/or identify anomalies at their onset. Such models are used by the computing platform to make predictive decisions about the occupant's health status or home environment based on the information received from several sensors. The adoption of AI will also allow this platform to exploit robotics [1.36],[1.37] to control the system's peripherals and to provide services to the occupants in an automatic fashion with continuous improvements in accuracy and precision over time. One such platform, Lab–of–Things (LoT), developed by Microsoft Research, used an operating system named HomeOS to monitor, manage, and control interconnected devices in homes, and to analyze data received from the sensors [1.38]. This layer is also responsible for ensuring a secured, long–range communication channel to the remote service provider. It can transmit the measured data, key physiological or environmental parameters over the internet or cellular network, thus functioning as the home gateway to the remote facility. This platform monitors and assesses the measured physiological or environmental data continuously. If any abnormality in the home environment or in the vital signs of the user's health is detected, it can raise an alarm or send alert messages to the service providers in the form of a voice call, a text message or an e–mail.

1.2.4 Services

The top layer of the smart health–monitoring architecture consists of the services delivered to the user by the service providers. These services may be associated with the health of the occupants, environment, safety, or security of the home and the residents. Services provided to the Smart health–monitoring system can be tailored according to the

requirements of the occupants based on the level of medical attention or safety and security required. In such systems, the gateway platform functions as the primary service provider, for example, by activating necessary actuators to control the home environment, door locks or dosage of medical drugs, in the case of automated drug delivery. The gateway system may adopt AI technologies to assess the safety, security and environment of the homes and control the smart devices to provide the occupants with better services [1.36],[1.37]. The gateway can learn and keep continuous track of the occupants' physiological conditions with the help of the BSN–connected wearable health sensors. The AI technologies implemented in the gateway will allow the smart devices in the SHS to be controlled to adjust the home environment according to the occupants' requirement. It can also monitor the home environment and can detect any hazardous situation such as the presence of smoke or gas leakage using the environmental sensors installed at different places in the home. In case of any anomalous physiological or environmental conditions, the gateway raises alarms and sends electronic notifications such as emails, text messages, and phone calls to the secondary service provider.

The secondary service provider is the central hub for all the subscriber and responsible for management, maintenance, connectivity, and information security of the SHS network and systems. It continuously monitors for alarms or emergencies and immediately notifies other third party services such as emergency medical service (EMS), caregivers, police station and fire station, if necessary.

1.3 Interoperability and standardization

One of the key concerns in adopting the IoT technologies for SHS and Smart Homes evolves from the fragmentation of the technologies [1.39]–[1.41]. The fragmentation of the IoT technologies, which is not only driven by technology constraints but marketing and business policies also [1.39],[1.42] causes lack of interoperability among the devices, platforms and systems. These issues need to be addressed for ubiquitous adoption of the IoT in such smart monitoring systems. Smart health–monitoring systems, as the term implies, are envisioned to be fully automated, energy efficient, and sustainable as well as capable of monitoring, and assessing the health, safety and wellbeing of the users. It also requires a robust communication platform and may also assist the users to monitor the ADLs. Therefore, the SHS, and thereby the Smart Homes are expected to be equipped with a wide variety of

devices, systems and platforms from different suppliers in order to provide the users with a wide range of services. However, the communication technologies used in those devices and systems may vary from supplier to supplier, thus leaving a fragmented IoT market and thereby posing a great challenge for the service providers in bringing together different technologies in a cost–effective and energy–efficient manner. For example, there exists long–range cellular communication technologies such as GSM, EDGE, 3G, HSPA, and LTE along with several non–cellular short or medium range wireless connectivity solutions presented in Figure 1.4, while new technologies such as ABB–free@home® [1.43] and Thread Protocol [1.44] are emerging. Each of these non–cellular technologies offer its own advantages and also has its limitations. However, a key concern is that they are often not compatible with each other.

Figure 1.4 Fragmentation of wireless communication platforms.

A common, extensible and standardized platform is thus required to ease the integration of different technologies, systems and services from different manufacturers. The internet of things, services and people (IoTSP) is such a platform that is particularly designed for building automation [1.39],[1.45]. In fact, there exists a number of standards for the IoT developed by major standard development organizations (SDOs) such as Institute of Electrical and Electronics Engineers (IEEE), International Organization for Standardization/International Electrotechnical Commission (ISO/IEC), International Telegraph Union–Telecommunication Standardization Sector (ITU–T), Internet Engineering Task Force (IETF), and European Telecommunications Standards Institute (ETSI)

[1.40],[1.41]. Each SDO has their own point–of–view towards the IoT; however they are putting their efforts to bridge the gap among the standards. The interoperability issue is currently being addressed by adopting the internet protocol (IP) as the common platform, which, by assigning local IP addresses to the devices and systems, allows for realizing a cost–effective solution for device level connectivity and system integration [1.39],[1.41]. BACnet/IP, KNXnet/IP, HomePlug, and Modbus TCP/IP (transmission control protocol /internet protocol) are some examples of IP–based wired communication technologies. There also exist some IP–based versions of wireless communication technologies such as IPv6 over Low–Power Wireless Personal Area Networks (6LoWPAN) over Bluetooth, ZigBee IP, 6LoWPAN over DECT ULE, and Thread. In fact, ETSI and the IPSO Alliance organized their fourth Constrained Application Protocol (CoAP) Plugtests™ event in London, UK in March 2014 [1.46]. They also organized the first 6LoWPAN Interop event in Berlin, Germany in July 2013 [1.47]. These events allowed the vendors to assess the level of interoperability of their systems and verified whether the IETF base specifications were interpreted correctly. The tests were performed using the 2006 release of the 2.4 GHz low–rate wireless personal area networks (LR–WPANs) PHY/MAC standards. Although all implementations were observed to send and interpret data correctly, they exhibited poor compliance with IETF RFC 6775, which describes optimization of neighbor discovery and addressing mechanisms for 6LoWPANs [1.48].

In addition, there is a growing consensus among the engineering and scientific community of using Representational State Transfer or RESTful web services to develop the application programming interfaces (APIs) for the IoT applications [1.39],[1.40]. RESTful web services are light weight and highly flexible, which uses Hypertext Transfer Protocol (HTTP) for data communication. It allows the system to communicate with different devices in the network running on different communication platforms. It thus allows for building a bridging platform for all the sensors, actuators and systems used in the Smart Homes, irrespective of the manufacturer and can successfully fulfill the integration requirements, which are critical for seamless operation of these smart systems [1.49],[1.50]. The adoption of RESTful web

services in the IoT may also enable adopting other semantic technologies such as OPC UA (Open Platform Communications Unified Architecture) and oBIX (Open Building Information Xchange) from the internet industry in future.

1.4 Sensors and devices

A Smart health–monitoring system may comprise several on–body sensors connected in a BSN and/or several stand–alone devices and systems connected in a LAN or PAN to facilitate monitoring of different physiological signs such as HR, HRV, SpO_2, GSR, BP, body temperature, RR, and BP as well as ADL, gait quality, joint–health and mobility. In order to enable unobtrusive long–term monitoring of the aforementioned health parameters it is critical that the sensors and devices be at least portable, and preferably wearable. In this section, a brief review on such devices and sensors proposed in the literature for cardiovascular health and activity monitoring is presented.

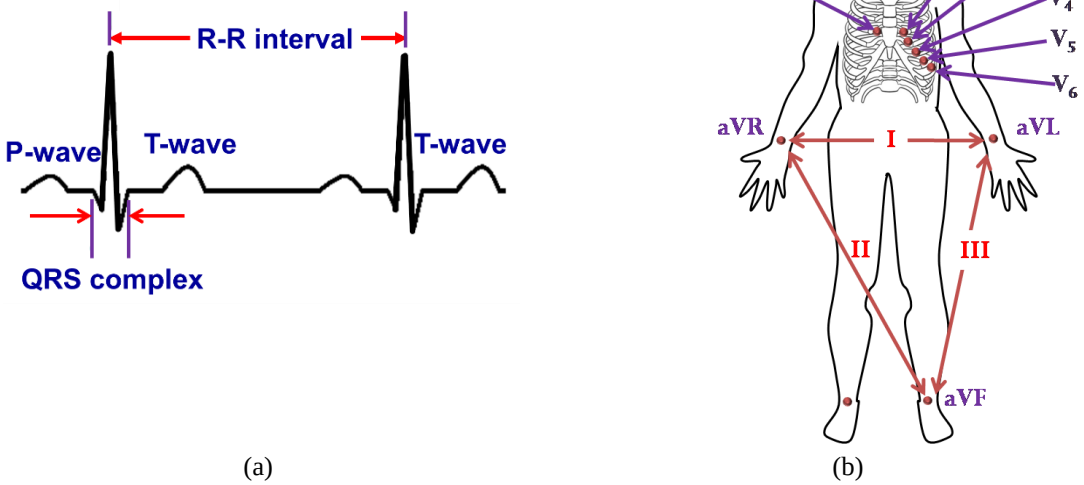

(a) (b)

Figure 1.5 Cardiovascular monitoring: (a) a typical lead I ECG signal (not scaled); (b) Electrode placement in a standard 12–lead ECG system;

Heart rate (HR) or pulse rate is one of the four 'vital signs' that is routinely monitored by physicians to diagnose heart–related diseases such as different types of arrhythmias [1.20],[1.34]. HR and HR variability (HRV) are typically extracted from the Electrocardiogram (ECG) (Figure 1.5(a)). Electrocardiograms (ECGs) represent a non–

invasive approach for measuring and recording fluctuations of the cardiac potential. A standard 12–lead ECG (Figure 1.5(b)) is the most widely used and effective diagnostic tool that physicians have used for decades to identify heart–related problems such as different forms of arrhythmias. Although many arrhythmias are not life–threatening, some results from weak or damaged heart such as myocardial infarction (MI) that may lead to cardiac arrest, if not managed immediately. After a heart attack, patients are required to receive immediate medical attention, which otherwise may turn fatal. These complications can be avoided if any inconsistency in cardiac activity is detected and treated in an early stage that calls for outpatient ambulatory monitoring of ECG. Some rare, but serious arrhythmias such as, Brugada syndrome, arrhythmogenic right ventricular cardiomyopathy, long QT syndrome, and hypertrophic cardiomyopathy are infrequent and can only be detected in prolonged monitoring.

Daily physical activities such as walking, running and climbing stairs involve several joints and muscles of the body and require proper coordination between the nervous system and the musculoskeletal system. This activities involve several joints including the spine, hip, knee, ankle, tarsal and metatarsal joints. They also involve several muscles, for example, muscles of the back, around hip joints, thighs, calf muscles and several small muscles in the feet. Therefore, any abnormalities in the functioning of these biological systems may potentially affect the natural patterns of these activities. For example, persons at the early onset of Parkinson's disease tend to exhibit small and shuffled steps, and occasionally experience difficulties to start, stop and take turns while walking [1.20],[1.51]. Additionally, due to gradual deterioration of motor control with age, older adults are at high risk of fall and mobility disability. In fact, an estimated 10% (2.7 million) of Canadians, aged 15 years and over, suffered from mobility–related disabilities in 2017 [1.52]. Furthermore, falls in the older adults may cause hip and bone fractures, joint injuries, and traumatic brain injury, which not only require longer recovery time, but also restrict physical movement, thereby affecting an individual's daily activities. In addition, fall–related fractures reportedly have a strong correlation with mortality [1.53]. Therefore, quantitative assessment of gait, knee

joints and daily activities are critical in early diagnosing of musculoskeletal or cognitive diseases, fall and balance assessment, as well as in the post–injury rehabilitation period.

1.4.1 Smartphone–based systems

A. Cardiovascular health monitoring

HR and HRV can be measured using portable and hand–held single–lead ECG devices [1.20],[1.34]. Furthermore, with the advancement of wearable sensor technologies, HR and HRV can now be obtained using commercial fitness trackers such as Fitbit® (San Francisco, CA, USA), Jawbone® (San Francisco, CA, USA), Striiv® (Redwood City, CA, USA), and Garmin®, (Olathe, KS, USA) [1.20].

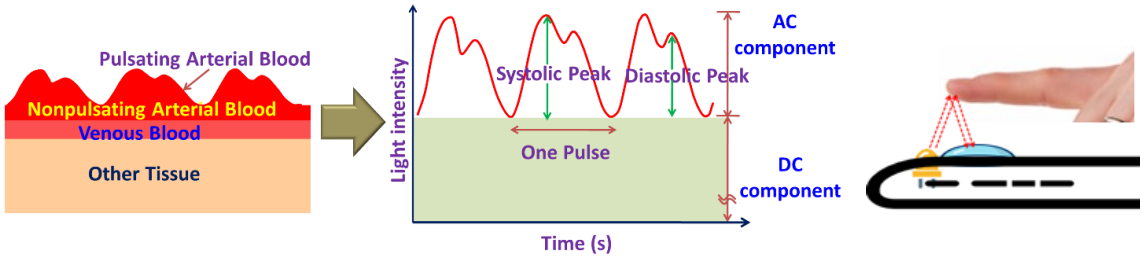

Figure 1.6 Photoplethysmograph (PPG) signal from the pulsatile flow of blood volume is used to measure HR and HRV using smartphone

However, these portable and wearable systems require additional accessories, which can be avoided by exploiting the embedded sensors such as a camera and microphone in a smartphone for monitoring HR and HRV. Using smartphone camera sensors, it is possible to estimate HR and HRV from the photoplethysmogram (PPG) signal derived from a video of the bare skin such as of the fingertip or the face. The light absorption characteristics of hemoglobin in blood differ from the surrounding body tissues such as flesh and bone. PPG estimates the volumetric changes in blood by detecting the fluctuation of transmissivity and/or reflectivity of light with arterial pulsation through the tissue (Figure 1.6) [1.20],[1.54]. Although near–infrared (NIR), red light sources are used in most commercial systems [1.20],[1.54], some researchers [1.55]–[1.59]exploited the smartphone embedded white flashlight to illuminate the tissue to measure the PPG.

Table 1.2 Smartphone–sensors for cardiovascular health monitoring.

Ref.	Year	Measured signs	Type	Smartphone model	Sensor used	Video Resolution	Frame rate (fps)	Video length	Method	Performance wrt standard monitors	# of subjects
[1.56]	2018	HR, HRV	Contact–based (index finger)	iPhone 6, Apple Inc., Cupertino CA	Front camera	1280 × 720	240	5 min	•Reflection of light from the finger is measured.	Pearson Correlation coefficient (PC) for most parameters between PPG and ECG: >0.99	50 (11 F, 39 M)
[1.58]	2016	HR, HRV	Contact–based (index finger)	iPhone 4S, Apple Inc., Cupertino CA	Rear camera		30	5 min	•Combination of the steepest slope detection of pulse wave derived from the green channel of the reflected light and its correlation to an optimized pulse wave pattern.	PC: >0.99 (HR), ≥0.90 (HRV)	68 (28 F, 40 M)
[1.57]	2016	HR, RR	Contact–based (HR) and contactless (RR)	HTC One M8, HTC Corporation, New Taipei City, Taiwan	Front (for RR) and rear (for HR) camera	RR: 320 × 240 (ROI: 49 × 90 abdomen) HR: 176 × 144 (ROI:176 × 72)	30 (down–sampled to 20 (RR), 25 (HR))	—	•Frequency domain analysis of the noncontact video recordings of chest and abdominal motion.	Average of median errors for RR: 1.43%–1.62% between 6 and 60 breaths per minute	11 (2 F, 9 M)
[1.64]	2012	HR	Contactless (face)	iPhone 4, Apple Inc., Cupertino CA	Front camera	640 × 480	30	20 s	•Analysis of the raw video signal (green channel) and ICA–decomposed signals of the face in the frequency domain.	Error rate: 1.1% (raw signal), 1.5% (ICA–decomposed signals)	10 (2 F, 8 M)
[1.68]	2018	HR, RR	Contactless (face)	LG G2, LG Electronics Inc., Korea	Rear camera	—	30 (down–sampled to 10)	20 s	•Frequency domain analysis of the color variations in the reflected light (hue) from the face.	PC: 0.9201 (HR) and 0.6575 (RR)	25 (10 F, 15 M)
[1.55]	2016	HR	Contact–based (index finger)	—	Rear camera	1920 × 1080	—	—	•Frame–difference based motion detection for improving data quality. •Uses all 3 channels (R, G, B) for PPG extraction. •Blood volume flow was observed clearly in the Red channel.	Average accuracy: 98%	20
[1.69]	2015	Pulse, HR, HRV	Contact–based (index finger)	Motorola Moto X, Motorola, Libertyville, IL and Samsung S 5	Rear camera	640 × 480	30	100 s	•Extracts PPG by averaging the Green channel data of the video. •HR is calculated by detecting the consecutive PPG peaks.	PC of pulse and R–R interval from two phone models > 0.95	11

Table 1.2 Smartphone sensors for cardiovascular monitoring (contd.).

Ref.	Year	Measured signs	Type	Smartphone model	Sensor used	Video Resolution	Frame rate (fps)	Video length	Method	Performance wrt standard monitors	# of subjects
[1.59]	2014	HR, NPV	Contact–based (index finger)	iPhone 4S, Apple Inc., Cupertino CA	Rear camera	ROI: 192 × 144	30	20 s	•HR and NPV were measured in the presence of a controlled motion (6 Hz) of the left hand. •Evaluated the effect of motion artifact (MA) on the PPG in all three color (R, G, B) channels.	Higher SNR for B and G channel PPG in presence of 6Hz MA. PC: HR>0.996 (R, B, G), NPV = 0.79 (G)	12 (M)
[1.70]	2014	HR, HRV	Contact–based (index finger)	Sony Xperia S, Sony Corporation, Tokyo, Japan.	Rear camera	—	—	60 s	•HR was estimated by detecting the consecutive PPG peaks and also the dominant frequency. •Combines several parameters (HR, HRV, Shannon entropy) to detect Atrial fibrillation (AFib).	HR error rate: 4.8% AFib detection: 97% specificity, 75% sensitivity	
[1.71]	2012	HR, HRV	Contact–based (index finger)	iPhone 4s and Motorola Droid, Motorola, Libertyville, IL	Rear camera	ROI: 50 × 50	30 (iPhone), 20 (Droid)	2, 5 min (iPhone, Droid)	•Several ECG parameters were extracted with two different models of smartphone both in supine and tilt position and performed comparative analysis with the data obtained from a standard five lead ECG.	PC: ~ 1.0 (HR), PC for Other ECG parameters: 0.72–1 (Droid), 0.8–1 (iPhone)	9 (iPhone) 13 (Droid)
[1.63]	2012	HR	Contact–based (index finger)	HTC HD2 and Samsung Galaxy S	Rear camera	ROI: 288 × 352 (HTC) 480 × 720 (Samsung)	25 (HTC) 30 (Samsung)	6 s	•HR is calculated by detecting the consecutive PPG peaks.	Error: ± 2 bpm	10
[1.72]	2012	HR	Contact–based (index finger)	Motorola Droid, Motorola, Libertyville, IL	Rear camera	ROI: 176 × 144	20	5 min	•HR from the PPG signals was obtained at sitting, reading and video gaming by using an Android–based software.	PC: ≥ .99 Error: ± 2.1 bpm	14 (11 F, 3 M)

Most published smartphone–based HR and HRV monitoring applications [1.55]–[1.59] follow a similar approach where these parameters are extracted from the PPG signal either by measuring pulse–to–pulse time difference in time–domain [1.58] or by finding the dominant frequency in the frequency domain [1.55],[1.57]. Table 1.2 presents some smartphone–sensor based cardiovascular health monitoring systems presented in the literature.

B. Activity monitoring

Most existing activity monitoring systems rely on a network of cameras fixed at key locations in a home [1.20],[1.73]. Although such systems can provide comprehensive information about complex gait activities, they are expensive and generally have a limited field–of–view. In recent years, there has been a growing interest in using smartphone embedded motion sensors such as accelerometers, gyroscopes, and magnetometers as well as location sensors such as the GPS sensor for real–time monitoring of human gait and activities of daily living (ADL) [1.74]–[1.101].

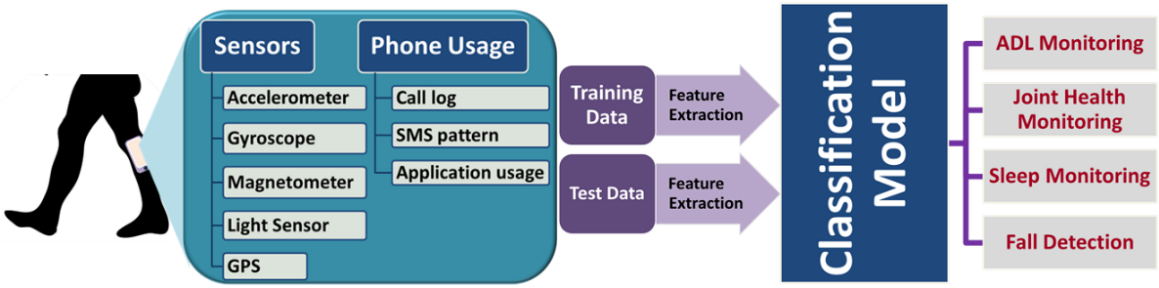

Figure 1.7 General architecture of a smartphone–based activity monitoring system.

These sensors measure the linear and angular movement of the body, and the location of the user, which can be used to quantify and classify human gait events and activities in real time. A general architecture of smartphone–based activity monitoring is presented in Figure 1.7.

Table 1.3. Typical features extracted from motion signals [1.20].

Spatial Domain	Temporal Domain	Frequency Domain	Statistical Domain
Step length	Double support time	Spectral power	Correlation
Stride length	Stance time	Peak frequency	Mean
Step width	Swing time	Maximum spectral amplitude	standard deviation
RMS acceleration	Step time		Covariance
Walking speed	Stride time		energy
Signal vector magnitude	Cadence (steps/min)		Kurtosis

Table 1.4. Smartphone–sensor based activity monitoring systems.

Ref.	Proposition	Phone(Sensors)	Experiment Protocol	n	Method	Performance/ Comment
[1.74]	Human activity and gait recognition	Samsung Nexus S (a, ω)	• Subjects walked ~30 m for each of three different walking speeds • Smartphone in the trouser pocket • Sampling rate: 150 sample/s	25	• Each gait cycle was detected and normalized in length. • Several distance metrics between the test and template cycle were calculated as features. • Statistical analysis and machine learning used for recognition.	• Gait recognition accuracy 89.3% with dynamic time warping (DTW) distance metric. • Activity recognition accuracy >99%.
[1.75]	Human activity recognition	Samsung Galaxy S II (a, ω)	• University of California Irvine (UCI) Human activity recognition (HAR) dataset • Subjects performed an activity twice, with the phone 1) mounted on the belt at the left side 2) placed according to the user's preference.	30	• Feature selection using random forests variable importance measures. • Two–stage continuous HMM for activity recognition. • First and 2nd level for coarse classification and fine classification, respectively.	• Activity (walking, ascending and descending stairs, sitting, standing, and laying) recognition accuracy 91.76%.
[1.76]	Human activity recognition	Samsung Galaxy S II (a, ω)	• UCI HAR dataset • Activities are: walking, ascending and descending stairs, sitting, standing, and laying	30	• A hybrid model based on the fuzzy min–max (FMM) neural network and the classification and regression tree (CART).	• Activity (walking, ascending and descending stairs, sitting, standing, and laying) recognition accuracy 96.52%.
[1.77]	Evaluation of hyperbox (HB) NN for classifying activities	Samsung Galaxy S II (a, ω)	• UCI HAR dataset • Five subsets of varying sizes (5%, 10%, 20%, 50% and 100% of the dataset) were created for training purpose	30	• One HB is assigned for all attributes of a class and has one or more associated neurons for class distribution. • Points falling into 1) only one HB are immediately classified 2) overlapping regions of HBs use the neural outputs for prediction.	• Performance was comparable to SVM, decision tree, KNN and MLP classifier. •Activity (walking, ascending and descending stairs, sitting, standing, and laying) recognition accuracy 75%–87.4%
[1.78]	Human activity recognition	Nexus One, HTC Hero, Motorola Backflip (a)	• Wireless sensor data mining (WISDM) dataset from http://www.cis.fordham.edu/wisdm/dataset.php • Sampling rate: 20 samples/s	36	• Extracted 43 features from the mean and standard deviation of acceleration, mean absolute difference, mean resultant acceleration, time between peaks and binned distribution. • A Voting scheme to combine the results from the J48 decision tree, logistic regression and MLP.	• Accuracy > ~97% (walking, jogging, sitting and standing), ~86% (ascending stairs), and ~73% (descending stairs)
[1.100]	Human activity recognition	iPod Touch (a, ω)	• Measured activities: sitting, walking, jogging, and ascending and descending stairs at different paces	16	• Evaluated different classification models (decision tree, multilayer perception, Naive Bayes, logistic regression, KNN and meta–algorithms such as boosting and bagging) in terms of recognition accuracy.	• Accuracy for sitting, walking, and jogging at different paces: 90.1%–94.1% • Accuracy for ascending and descending stairs: 52.3%–79.4%

Table 1.4: *Cont.*

Ref.	Proposition	Phone (Sensors)	Experiment Protocol	n	Method	Performance/ Comment
[1.79]	Complex activity recognition system	Samsung Galaxy S IV (a, ω, P, T, H (and Gimbal beacons))	• Four smartphones worn on the waist lower back, thigh, and wrist. • Participants performed 19 activities in 45 minutes according to their own order of choice and repetition.		• Conditional random field based classification was performed on each device separately. • Final recognition was based on the result from the most relevant device to that particular activity. • 19 activities are: walk and run indoors, clean utensil, cook, sit and eat, use – bathroom sink and refrigerator, move from/to indoor to/from outdoor, ascending and descending stairs, stand, lie on the – bed, floor, and, sofa, sit on the bed, floor, sofa, and, toilet.	• Activity recognition accuracy > 80%
[1.80]	A feature selection approach for faster recognition	Samsung Galaxy S II (a, ω)	• UCI HAR dataset • Activities are: walking, ascending and descending stairs, sitting, standing, and laying.	30	• Data segmentation by sliding window and extraction of time and frequency domain features • A hybrid of the filter and the wrapper (FW) methods for feature selection • Performance verified by naïve Bayes and KNN.	• Activity recognition Accuracy, precision and F1–score to 87.8%, 88.0% and 87.7% (with a, ω data) • Significant reduction in recognition time.
[1.81]	Algorithm for Human activity recognition	Google NEXUS 4 (a, ω)	• Subjects performed each activity twice for 30 s each, keeping the device at five different orientations.	5	• Employed coordinate transformation and principal component analysis (CT–PCA) on the data to eliminate the effect of orientation variation. • Used several classification models for evaluation.	•Activity (static, walking, running, going upstairs, and going downstairs) recognition accuracy 88.74% with online–independent SVM (OISVM)
[1.82]	A hardware friendly SVM for HAR	Samsung Galaxy S II (a, ω)	• UCI HAR dataset • Activities are: walking, ascending and descending stairs, sitting, standing, and laying.	30	• Standard support vector machine (SVM) with fixed–point arithmetic for computational cost reduction.	Activity recognition accuracy ~89% (similar to standard SVM)
[1.83]	Unsupervised learning for activity recognition	Samsung Galaxy Nexus (a, ω)	• Smartphone was kept in a pants pocket for measurements • n = 5 activities: walking, running, sitting, standing, and lying down • Each activity was performed for 10 min.	—	• Experiment 1: known n. k–means, Gaussian mixer model, and average–linkage hierarchical agglomerative clustering (HIER) were used for recognition. • Experiment 2: unknown n. Density–based spatial clustering of applications with noise (DBSCAN) along with three other models used for classification. • DBSCAN requires setting two parameters (*eps* and *minPts*) and for other models, n was chosen based on local maxima of the Calin´ ski–Harabasz index (CH).	• GMM achieved 100% recognition accuracy when n is known • HIER and DBSCAN achieved over 90% recognition accuracy when n is unknown.
[1.84], [1.85]	DNN for Human activity recognition	Samsung Galaxy S II (a, ω)	• UCI HAR dataset • Activities are: walking, ascending and descending stairs, sitting, standing, and laying.	30	• DNN was formed by stacking several convolutional and pooling layers to extract discriminative features. • Number of layers, number of feature maps, pooling and convolutional filter size were adjusted to maximize test–accuracy by 'softmax' classifier. • Multilayer perceptron for final recognition.	• Accuracy: 94.79%–95.75%

Table 1.4: *Cont.*

Ref.	Proposition	Phone(Sensors)	Experiment Protocol	n	Method	Performance/ Comment
[1.92]	Human activity recognition	Samsung Galaxy and Huawei P20 Pro S II (a, ω)	• Smartphone was attached to the waist. • Sampling frequency = 50 Hz • 10,299 samples with Samsung Galaxy SII and 4752 samples with Huawei P20	30	• An Ensemble Extreme learning machine with Gaussian random projection (GRP). • GRP was used for the initialization of input weights of base ELMs.	Activity (sitting, standing, laying, walking, walking upstairs and downstairs) recognition accuracies: 97.35% (Samsung), 98.88% (Huawei)
[1.98]	Human activity recognition	Samsung Galaxy Note I, Motorola Droid, Nokia N900 (GPS)	• Collected 2 weeks of GPS data continuously • Subjects prepared a journal of real–time information about their everyday activities.	3	• A fuzzy logic –based approach for classification. • Location uncertainty improved by calculating the probabilities of different activities at a single location. • Recognized activities by a segment aggregation method while adjusting for location uncertainties.	Classification accuracy: ~96%
[1.93]	Human activity recognition	Samsung Galaxy S 4 (a, ω)	• Free walk at a natural pace and run in a straight path, maintain a standing position and minimize additional bodily movement (25 s each).	1	• Feature set consisted of linear acceleration, normal acceleration and angular velocity. • Naive Bayes and k–means clustering for classification	Classification accuracy: 85%
[1.94]	Human activity recognition	(a, ω)	• A database of 12 activities (standing, sitting, lying down, walking, ascending and descending stairs, stand–to/from–sit, sit–to/from–lie, stand–to/from–lie, and lie–to/from–stand).	—	• Extracted features were processed by a kernel principal component analysis (KPCA) and linear discriminant analysis (LDA). • Deep belief network (DBN) for classification.	Mean recognition rate: 89.61% and overall accuracy: 95.85%
[1.95]	Human activity recognition	Huawei Mate 9 (a, ω)	• Activities were logged approximately 5–8 hours a day for 4 months	1	• A six–layer independently recurrent neural network (IndRNN) processed data of different lengths and captured the temporal patterns at different time intervals.	Classification accuracy: ~96%
[1.96]	Human activity recognition	Samsung Galaxy S II (a, ω, ϕ, and P)	• UCI HAR dataset • Activities are: walking, ascending and descending stairs, sitting, standing, and laying	30	• DNN–based subassembly divides sensor data into various motion states. The transformation subassembly derives the intrinsic correlation between the sensor data and personal health.	• Accuracy :95.9% with unsupervised feature extraction • 96.5% with manual feature extraction
[1.97]	Walk@Work (W@W)–App for HAR	(a, ω)	•1 h laboratory protocol and two continuous hours of occupational free–living activities	17 (10F 7 M)	• Calculated agreement, intra–class correlation coefficients (ICC) and mean differences of sitting time against the inclinometer ActivPAL3TM, and step counts against the SW200 Yamax Digi–Walker pedometer for performance comparison.	• ICC: 0.85 for self–paced walking, 0.80 for active working tasks. • ICC (free–living): 0.99, 0.92 with a difference of 0.5 min and 18 steps for sitting time and stepping, respectively.

Table 1.4: *Cont.*

Ref.	Proposition	Phone(Sensors)	Experiment Protocol	n	Method	Performance/ Comment
[1.99]	Human activity recognition	Samsung Galaxy S II (a, ω, ϕ)	• Four smartphones attached to four body position: right pocket, belt, right arm, and right wrist • Measured activities: walking, running, sitting, standing, walking upstairs and downstairs	4	• Data from three types of sensors were evaluated in terms of recognition accuracy using seven classifiers (naïve Bayes, SVM, neural networks, logistic regression, KNN, rule–based classifiers and decision trees).	• Best performance was achieved using both gyroscope and accelerometer data together. • Magnetometer data played little role.
[1.91]	Balance analysis and Audio Bio–Feedback (ABF) system	iPhone 4 (a, ω, ϕ, mic)	• Smartphone was mounted on a belt. • Subjects wore the belt on the posterior low back at the level of the L5 vertebra and a pair of earphones, and placed arms close to the trunk, stood barefoot, with their eyes closed.	20 (11F 9 M)	• Tilt angles and heading were calculated from accelerometer and gyroscope, respectively as well as from the magnetometer. • Kalman filter was used to correctly estimate the rotation angles from the difference between the two previous estimates. • Audio feedback sent through the mic when trunk orientation is above a threshold.	—
			• Subjects kept sway minimum in parallel feet (10 cm apart), tandem stance–positions, and 2 experimental conditions with and without ABF. • Each experimental condition was performed in random order six times, each for 30 s.			
[1.88]	Fall detection and notification system	Lenovo Le–phone (a)	• Smartphone mounted on the waist	—	• Extracted signal magnitude area (SMA), signal magnitude vector (SMV) and tilt angle from the median filtered accelerometer data. • Fall detection with a decision tree–based algorithm. • In case of a fall, a multimedia messaging service (MMS) was sent with time and location info.	• Performance comparison not reported.
[1.89]	Fall detection	Samsung Galaxy S III (a)	• Collected acceleration data		• Detected a fall if the acceleration along a direction changed at a faster rate than that in normal daily activities.	• Performance comparison not reported.
[1.101]	Fall detection, tracking and notification system	(a)	• Evaluated the tracking error range at two outdoors and one indoor fall location. • Tests conducted near a school and a subway station at three periods of the day: 7:00–12:00, 12:00–18:00, and 18:00–24:00 to evaluate the accuracy of tracking with mobile obstacles.	10	• Calculated accelerometer SMV. • Rapid change in the SMV to a large value indicated a fall. • In case of a fall detected, the GPS location of the smartphone is communicated. • The real–time location tracking system used Google's 3D mapping services.	• Overall accuracy of the location tracking system: < 9 m. • Larger error range observed between 12:00 and 18:00. • High density of Wi–Fi installations improves location accuracy.
[1.102]	Fall detection and daily activity recognition	Sony C6002 Xperia Z, Apple iPhone 4s (a, ω, ϕ)	• Subjects kept phones in the right, left and front–pockets and fall onto a 15 cm thick cushion. • Activities: four types of fall (forward, backward, toward the left and right) and ADL.	8	• Activities were classified using supervised machine learning (SVM, Decision tree, KNN and discriminant analysis) algorithms. • A fall is detected when SMV goes above a threshold value (24.2 ms^{-2}).	• ADL (sitting, standing, walking, laying, walking upstairs and walking downstairs) recognition accuracy 99% with the SVM.

Table 1.4: *Cont.*

Ref.	Proposition	Phone(Sensors)	Experiment Protocol	n	Method	Performance/ Comment
[1.103]	Fall detection algorithm	Sony Z3 (a)	• Smartphone was placed in the front pocket • Subjects performed six activities of daily living and six fall activities	10 (7 M and 3 F	• Six features (SMV, sum vector excluding gravity magnitude, max and min value of acceleration in gravity vector direction, mean of the absolute derivation of acceleration in gravity vector direction, and gravity vector changing angle) were derived from the accelerometer data. • SVM was used to classify fall and non–fall events.	• 96.67% sensitivity, 95% specificity
[1.104]	Fall detection based on high–level fuzzy petri net (HLFPN)	HTC Desire S (a)	• Smartphone was placed in the thigh pocket • Activities: Falls (forward, backward, vertical, and sideways) and ADLs (walking, jogging, jumping, sitting, and squatting).	12 (7 F and 5 M)	• Calculated accelerometer SMV and frequency of occurrences from the accelerometer data. • Fuzzy degree was generated by substituting the calculated values into the membership function formulated by the experiment. • Final classification with HLFPN.	• Fall detection accuracy 90% with HLFPN
[1.107]	Knee Joint ROM	iPhone 6 (a)	• Dynamic knee extension ROM was measured three times with an interval of 5 min. • Phone was attached to the tibia • An isokinetic dynamometer used to generate and measure the knee motion for validation.	21 (M)	• A MATLAB program automatically detected the min/max values of knee extension angles from the accelerometer data. • The difference between the min and max values was calculated as the dynamic knee extension ROM.	• Highly correlated (r_s = 0.899) and low error (~0.62°) *wrt* the commercial system (Biodex System 4 Pro) • Limits of agreement: −9.1to 8.8 deg. • ICCE between two methods >0.862
[1.108]	Assessment of smartphone apps for measuring knee range of motion	Camera, inclinometer (a, ω, ϕ)	• Five measurements of knee range of motion from each subject by a commercial system, two apps – Goniometer Pro and Dr. Goniometer • Goniometer Pro (by 5fuf5) and Dr. Goniometer (by CDM S.R.L.) were based on smartphone inclinometer and camera, respectively.	10 (5 F and 5 M)	• Goniometer Pro: attached to the anterior of the thigh proximal to the skin incision, and on the anterior of the distal tibia distal to the skin incision and knee flexion angle (θ_{Fx}) was derived by adding the two measured angles. • Dr. Goniometer: calculated θ_{Fx} by taking pictures from the lateral side of the operated knee with markers virtually placed at the level of the greater trochanter, the knee joint and the ankle joint.	• θ_{Fx} by Dr. Goniometer was clinically identical to θ_{Fx} from the commercial system, with a mean difference of <1° and 1/50 difference >3°

a: accelerometer, ω: gyroscope, P: pressure sensor, T: temperature sensor, H: humidity sensor, ϕ: magnetometer, n: number of subjects

At the heart of an activity monitoring and recognition system is the classification or recognition algorithm. However, signal processing techniques and extraction of appropriate features also play critical roles in realizing a computationally efficient and reliable system. Signal processing techniques may include filtering, data normalization and/or data windowing or segmentation. Subsequently, a number of key features from the statistical, temporal, spatial and frequency domains are extracted to feed into the classification model. Table 1.3 presents a list of typical features that are extracted from the motion signals. Finally, an appropriate classification model such as support vector machine (SVM) [1.81],[1.82],[1.99],[1.102],[1.103], naive Bayes (NB) [1.80],[1.93],[1.99],[1.100], k–means clustering [1.82],[1.93], logistic regression [1.78],[1.99],[1.100], k–nearest neighbor (KNN) [1.77],[1.80],[1.99],[1.100],[1.102], neural network (NN) [1.84],[1.85],[1.87],[1.95],[1.96] or a combination of models [1.78],[1.84],[1.85],[1.92],[1.94] are employed for activity recognition. Table 1.4 summarizes several recent smartphone–sensor based activity and sleep monitoring systems.

1.4.2 Wearable devices

A. Cardiovascular health monitoring

In a conventional 12–lead ECG system, electrical activities of the heart along 12 particular spatial orientations are measured using ten Ag–AgCl electrodes (hydrogel method/wet ECG), which are affixed to some specific parts of the body. The electrodes contain conducting gel in the middle of the pad that functions as a conduction medium between the skin and the electrode. This conducting gel has potential toxic and irritant effects on the skin and is thus not best suitable to use for long–term ambulatory monitoring system though currently, it is the only system available [1.109]–[1.111]. However, only a few numbers of electrodes are used in ambulatory ECG monitoring system at the cost of limited information. A continuous ambulatory monitoring device requires a wearable and portable system that could be used comfortably without affecting an individual's daily activities. Table 1.5 presents a comparison among the cardiovascular monitoring systems published in the literature.

Table 1.5. Comparison among cardiovascular monitoring systems.

Ref.	Proposition	Signs	Electrode type	Active material	Electrode size	Attac–hment method	Comm.	Accuracy	Signal acquisition module			
									Size	Fs	A/D	Bat. life, Power
[1.112]	Sensorized T–shirt and textile belt	ECG, HR	Dry textile electrodes	Silver based conductive yarns		Snap buttons	BLE		—	512 Hz	24 bit	—
[1.113]	Wearable mobile electrocardiogram monitoring system	ECG, HR, loca–tion	Dry foam electrode	Ni/Cu coated compressed urethane polymer foam	14 mm × 8 mm × 8 mm		Bluetooth v2.0, and GSM	99.51% correlation with prerecorded ECG data, QRS detection accuracy ~98.14%	4 cm × 2.5 cm × 0.6 cm	512 Hz	12 bit	33 hours, 1100 mAh Li–ion battery
[1.109]	Wireless, portable capacitive ECG sensor	ECG, HR	Capacitive electrode with cotton insulator		33 mm × 33 mm × 2 mm	Woven under a stretcha ble belt	ANT		45 mm × 60 mm × 9 mm	500 Hz	10 bit	15 hours with 256 mAh 3 V Li battery
[1.114]	Use of flexible capacitive electrodes for reducing MA	ECG, HR	Flexible capacitive electrodes	Ni/Cu coated foam (polyolefin covered by polyurethane)	300 mm × 20 mm × (1.1 ± 0.2 mm)	Integrat ed into a chest belt	Bluetooth	Up to 91.32% QRS detection at 7 km/h walking speed	—	256 Hz	—	—
[1.115]	Common Electrode–Free ECG monitoring System	ECG, HR	Active capacitive electrodes	Copper layer	5 cm × 3 cm	Adhesiv e tape	—		—	2 kHz	24 bit	—
[1.116]	HR monitoring from pressure variance in ear canal	HR	Piezoelectric film sensor		3.5 mm × 3.5 mm	Earpiec e like device	2.4 GHz RF	Sensitivity 97.25%, PPV 97.18%.	15 mm × 17 mm	100 Hz	12 bit	Coin–cell battery
[1.117]	Heart Rate Monitoring with pressure sensor	HR	Piezoresist–ive pressure sensing	C black/silicone rubber nanocomposite encapsulated in conductive FCCL films	15 mm × 30 mm	Embedd ed in elastic belt	—	Accuracy > 97%	—	—	—	—

B. Activity monitoring

Monitoring an individual's physical activities and locomotion can be useful in rehabilitation, sports, early detection of musculoskeletal or cognitive diseases, and fall and balance assessment. As mentioned earlier, fixed position monitoring systems such as camera–based systems are useful tool for activity monitoring. Although these systems are capable of recognizing complex gait activities, they, however, restrict the user within a limited range and are complex and expensive. Thus, they are not feasible for long–term continuous monitoring. In recent years, the use of wearable motion sensors such as accelerometers, gyroscopes, and magnetometers are gaining in popularity for measuring human gait activities [1.20],[1.21]in real time. The sensors measure linear and angular motion of the body from which a number of key features are extracted as presented in Table 1. 3 earlier. Table 1.6 presents a comparison of the key features and performance characteristics among the activity monitoring systems published in the literature.

1.4.3 Textile–based sensors

Smart textiles associated with healthcare include sensors, actuators, communication, computing, and electronic systems that are made of textile or are suitable for embedding into textiles, thus enabling unobtrusive and comfortable means of monitoring physiological signals of the individuals. It makes use of conventional fabric manufacturing techniques such as weaving, knitting, embroidery, and stitching to realize or integrate sensing materials in clothes. Advanced fabrication methods, for example, inkjet–printing, coating, lithography, chemical vapor deposition (CVD) are also used in order to achieve high performance in terms of noise and sensitivity. The active or sensing material is usually built on a substrate and can either be in direct contact with the body surface or remain encapsulated in a fabric–based layer.

Table 1.6. Activity monitoring systems.

Ref.	Proposition	Feature extraction	Classification method	Sensors and sensor placement	Detected activities and performance
[1.118]	Activity and gait recognition system on a smartphone	Fixed set of features	SVM, Bayes network, and Random Tree	Accelerometer is embedded in smartphone	• Different walking speed • Accuracy> 99%.
[1.119]	In–home, fine–grained activity recognition multimodal wearable sensors	Fixed feature set	Conditional random field (CRF)	Smartphone's onboard sensors (accelerometer, gyroscope, barometer, temperature and, humidity sensor), along with Gimbal Bluetooth beacons Waist, lower back, thigh and wrist	• Walk and run indoors, use refrigerator, clean utensil, cook, sit and eat, use bathroom sink, move from indoor to outdoor, move from outdoor to indoor, walk upstairs, and walk downstairs, stand, lie on the bed, sit on the bed, lie on the floor, sit on the floor, lie on the sofa, sit on the sofa, and sit on the toilet • Accuracy > 80%
[1.120]	Wearable device based on a 9–DOF IMU	Fixed set of features		• Accelerometer, gyroscope, and magnetometer • Limb or trunk • Bluetooth	• Balance hazards, balance monitoring for fall prediction • High correlation • Streaming ~6 hours, Logging > 16 hours
[1.121]	Algorithm development	Time–Frequency analysis	Hidden Markov Model	• 3–axis accelerometer, 3–axis gyroscope • Chest • USB	• Walking, running, ascending upstairs, descending downstairs and standing • Accuracy ~95%
[1.122]	A real–time, adaptive algorithm for gait–event detection			• Two inertial and magnetic sensors (1 IMU = 1 accelerometer, 1 gyroscope) • External part of both shanks	• Gait events: Initial Contact (IC), End Contact (EC) and Mid–Swing for both legs while walking at three different speed • F1–scores 1(IC, EC), 0.998 (IC) and 0.944 (EC) for stroke subjects
[1.123]	Recognition method for similar gait action	Inter–class relation Ship	Support vector machine, K–nearest neighbor	• 3 IMUs (each IMU: 1 tri–axial accelerometer,1 tri–axial gyro) • Fixed at the back, left, and right waist	• Walking on flat ground, up/down stairs, and up/down slope • Accuracy ~93% average
[1.124]	Stochastic approximation framework	Fixed set of features	K –means and Gaussian Mixture Models	• Accelerometer • Belt–like strap around the waist	• 3 intensity level of walking: 93.8%; • 3 intensity level of running 95.6%
[1.125]	Power–aware feature selection for minimum processing energy	Minimum cost feature selection by using a redundancy graph	KNN	• 6 IMUs (each IMU has one 3–axis accelerometer and a 2–axis gyroscope) • Waist, right wrist, left wrist, right arm, left thigh, right ankle BSN	• Switching between stand and sit, sit and lie, bend to grasp , rising from bending, kneeling right, rising from kneeling, look back and return, turn clockwise, step forward and backward, jumping • 30% energy savings with 96.7% accuracy

Table 1.6. Activity monitoring systems.(*Cont*.)

Ref.	Proposition	Feature extraction	Classification method	Sensors, Sensor placement	Detected activities and performance
[1.126]	Optimization for phase–dependent locomotion mode recognition	Fixed set of features		• 2 IMUs, 2 pressure insoles (each having 4 pressure sensors) • IMUs on the shank and the shoe, pressure sensors insole	• Walking, up/down stairs, and up/down slope, passive mode • Accuracy: 88%–98%
[1.127]	Electronic insole for motor activities and shoe comfort monitoring	Fixed set of features		• Humidity and temperature sensors, accelerometer and 4 pressure sensors • Insole • ZigBee	• Foot accelerations, orientation in space, temperature and moisture data • 10 hours of data logging
[1.128]	Shoe–based activity monitoring system (smartshoe)	Fixed set of features	SVM, MLP	• 5 pressure sensors (PS) and one 3–D accelerometer • PS on insole and accelerometer on heel of shoe	• Sit, stand, walk, ascend stairs, descend stairs and cycling • Accuracy: 99.8% ± 0.1% with MLP
[1.129]	A wearable device for monitoring daily use of the wrist and fingers	Fixed set of features	K–means	• Two 3–D magnetometers • Watch–like enclosure worn on the wrist and a small neodymium ring worn on the index finger	• Finger and wrist movement • Accuracy: 92%–98% with a 19%–28% STD • Power requirement: 20.5 mA at 3.3 V
[1.130]	Combined kinematic models to estimate human joint angles	Unscented Kalman filter		• 3 IMUs • Upper arm, forearm, and wrist	• Shoulder internal/external rotation; flexion/extension of shoulder, elbow, and wrist, supination/pronation of forearm, wrist twist • Average RMS angle error ~3°
[1.131]	Wearable device with automatic gait and balance analyzer for Alzheimer patients	Fixed set of features		• 3 IMUs (each IMU has a 3–d accelerometer, a uni–axial gyroscope, and a biaxial gyroscope • On feet for gait analysis on waist for balance analysis	• Gait parameters and balance • Power requirement: 30 mA at 3.7 V
[1.132]	IMU based fall Detection system	Madgwick orientation filter		Accelerometer, gyroscope, and magnetometer Waist Bluetooth	• Backward fall, forward fall, lateral left fall, lateral right fall, syncope • Accuracy: 90.37%–100% • Sensitivity: 80.74%–100% • Power requirement: 15 mA–34 mA using 3.7 V

A. Bio–potential sensor

Smart textiles can be used to develop wearable on–body electrodes in order to measure electro–physiological signals such as ECG, electroencephalography (EEG), GSR, and electromyography (EMG). Textile based electrodes were reported to be as reliable as the traditional wet gel Ag–AgCl electrodes [1.133],[1.134]. Textile electrodes can be classified into two basic categories: active and passive. Passive textile electrodes sense electrical properties from the skin surface. It can be used to monitor cardiac or muscle activities by sensing potential fluctuations caused by the heart or muscle. They also have applications in GSR measurement where the change in the skin conductivity due to sweating is detected by attaching electrodes on the body surface. Traditional electrodes use adhesive and conductive gel to affix them to the skin. It requires skin preparation such as shaving and cleaning the attachment site. In addition, the conductive gel may cause irritation, allergic reactions, or inflammation [1.109],[1.110]. Furthermore, the gel dries out with time causing degraded signal quality. Although wet electrodes provide superior signal quality, they are not suitable for wearable and long–term monitoring system [1.109],[1.110].

On the other hand, dry electrodes do not use adhesive or conductive gel and are usually biocompatible. Owing to their ‘dry’ nature, they are more suitable for long–term monitoring and are being used extensively in textile–based health monitoring systems [1.135]–[1.139]. However, dry electrodes suffer from very high electrode–skin impedance and thus are more vulnerable to noise and motion artifacts compared to the wet electrodes. Active electrodes often incorporate a high input impedance preamplifier that reduces the impact of noise and motion artifacts by reducing the electrode–skin impedance [1.135],[1.140]. This also helps to reduce the impedance mismatch between the electrodes resulting in lower differential common mode voltage, which may otherwise cause signal saturation.

.

Table 1.7. Summary of textile electrodes.

Ref	Proposition	Electrode type	Size	Base material	Conductive material	Technology	Performance
[1.135]	Direct attach and Interposer electrode	Active electrode	20 × 13 mm^2 (direct–attach) 11.6 × 11.6 mm^2 (Interposer)	Nonwoven Evolon fabrics	Conductive ink (CMI 112–15)	Screen printing, stenciling, curing, and encapsulation	*PSDs for sitting and jogging are close to Ag/AgCl electrodes *Durable up to 5 washing cycles
[1.140]	Active electrodes on woven textiles	Active electrode	28 mm × 23 mm (skin contact area)	Woven textile of cotton, polyester and Lycra fibers	Silver polymer paste (Fabinks TC–C–4001)	Screen and stencil printing	Printed active and Ag/AgCl electrodes had very similar rms levels after filtering
[1.142]	2 textile nanofiber web electrodes	Dry electrode	9 mm diameter	PVDF Nanofiber Web	PEDOT	Electrospinning–vapor phase polymerization	ECG is 95% similar to Ag/AgCl electrodes Contact resistance: ~1000 Ω
				PVDF Nano fiber Web	Silver	Silver mirror reaction	ECG is ~92% similar to Ag/AgCl electrodes Contact resistance: ~100 Ω
[1.143]	Textile electrode	Dry electrode	4 cm × 6 cm	Polypropylene nonwoven fabric	Copper nanoparticles on fabric	Multiple dip chemical processes	Max conductivity: 142.8 kΩm
[1.147]	8 types of electro–thread	Dry fabric electrode	2 × 2 cm^2, 2 × 5 cm^2	Polyester 75 denier	Silver thread	Inclusion of one strand or two strands of 50 μm silver thread	32 kΩ at 120 Hz (for 2 Ag strand based 1300TM polyester fabric)
[1.145]	Several textile–based electrodes	Dry fabric electrode	1.5 cm × 3 cm	PU laminated or dry–coated nylon	Copper coating	Sputtering	5.7 Ω (PU laminated nylon), 10.26 Ω(PU dry–coated nylon).
				Ripstop, Mesh fabric	Cu/Ni coating	Electroless Plating	0.23 Ω/sq (Ripstop), 0.29 Ω/sq (Mesh)
			5 cm × 5 cm	Cotton, Steel/cotton	Stainless Steel Filament Yarn	Embroidering or Knitting	R peak detection accuracy: 58.8% and 64.2% 32.55 Ω/m (linear resistance)
[1.146]	Knitted fabric electrodes	Dry electrodes	20 mm × 20 mm	Wool and polyester	Ag coated nylon, stainless steel yarn , and Ag coated Cu	Knitting	FFT response of the multifilament electrodes retains ECG spectral components
[1.148]	Embroidered textile electrode	Wet, water vapor with polyester pad.	2 cm × 7 cm	Polyethylene terephthalate yarn of 50 μm diameter	Silver and ultra–thin titanium	Coating by plasma sputtering	Similar signal quality and signal strength after 1 h as after 72 hours of use

Some active textile electrodes can stimulate muscle or nerve cells by applying an electrical current to the underlying tissues. This technique of muscle and nerve activation, commonly referred to transcutaneous electrical nerve stimulation (TENS) is widely applied in rehabilitation and therapeutic applications [1.137]–[1.139]such as chronic and postoperative pain management.

Textile electrodes can be realized by integrating prefabricated electrodes into finished garments by simply stitching them at suitable locations on clothes. They can also be developed by directly depositing conductive layers on the fabric. The conductive layers can be formed on the surface of the fabric by depositing nano–fibers [1.141]–[1.143] using electrodeposition method or by applying a conductive layer with the help of screen–printing [1.144], sputtering, carbonizing and evaporation [1.145].

Although conductive coating on the surface of the fabric results in superior conductivity, the performance may deteriorate with time, especially after a number of wash cycles. Another attractive technique of textile electrode fabrication is weaving or knitting garment fabrics using conductive yarn [1.140],[1.144],[1.145]. The conductive yarn can be made of metal filaments [1.145]–[1.147], conductive nano–filaments [1.148] or produced by applying a metal coating on fibers such as cotton [1.140],[1.141],[1.144], nylon [1.145], Kevlar or polyester [1.140],[1.146]–[1.149]. Nano–fibers can be grown by the electrospinning method [1.142] whereas metal coating on the fiber is formed by employing chemical deposition process such as polymerization [1.150], electroless plating [1.145],[1.149], electroplating [1.151] and sputtering [1.145],[1.148]. Table 1.7 presents the summary of several textile electrodes reported in the literature.

B. Activity sensor

Most researchers have used MEMS–based inertial sensors to measure the signal corresponding to human locomotion. They are mounted on small PCB boards, which are then embedded in belts, elastic bands or Velcro straps. MEMS–based motion sensors are cheap and small in size. Having good sensitivity, accuracy, and low power features, they are suitable

for long–term and real–time activity monitoring systems. However, the rigid PCB boards can be uncomfortable to some users. A MEMS accelerometer was fabricated in [1.152]on cotton cloth for measuring pelvic tilt angle. The accelerometer exploited the piezoresistive effect of the conductive Ag nanoparticles that was patterned on the textile by stamping and ironing.

Flexible and stretchable strain sensors were also used by many researchers in textile–based activity monitoring systems. Strain sensors measure the physical deformation by changing its electrical characteristics such as resistance and capacitance in response to mechanical stress. The strain sensors for textile applications need to be highly flexible, stretchable, and durable. In addition, high sensitivity, and fast response/recovery time are critical for real–time activity detection. Such sensors can be fabricated by embedding metal nanowire [1.153] and nanoparticles [1.154]in or between PDMS layers, using elastic and conductive webbing [1.155], embedding conductive fibers in textiles [1.156], [1.157], using flexible polymer fiber such as PU/PEDOT:PSS [1.158].

A few researchers also investigated textile–based optical sensors for activity monitoring. In [1.159], a single optical Fiber Bragg Grating (FBGs) sensor encapsulated with a polymer foil was integrated into an elastic knee band. The flexion–extension movement of the knee causes strain variations resulting deflection in the resonance wavelength of the FBG. Instead of optical power, the FBG sensor performed measurement based on the wavelength thus was less sensitive to external noise and fluctuations in the optical source. Krehel et al. [1.160] designed an optical fiber based flexible force sensor that could be potentially be integrated into textiles. In the presence of an external force, the optical fiber experiences an elliptical deformation along the plane of its cross section. This deformation causes increased deflection of light within the fiber resulting reduced light intensity at the output, from which the force can be estimated. The sensor is flexible and can be integrated into textile for detecting moderate to strong forces corresponding to, for example, limb motion, and respiratory rate. However, the sensor is sensitive to temperature, causing inaccuracies in the measured data. Table 1.8 presents the summary of textile–based strain sensors.

Table 1.8. Summary of textile–based strain sensors.

Ref.	Proposition	Sensing mechanism	Structure /Base	Sensing material	Gauge factor	Stable strain range	Applications
[1.156]	Textile–structured flexible strain sensor	Contact resistance of fiber/ yarn/fabric	Single warp fabric	Carbon fiber	10–200 depending on fiber length	Max 200%	Wearable strain sensor
[1.157]	Textile–based strain sensor	Contact resistance of conductive fiber loops	Fabric with elastomeric yarns	Silver coated polymeric yarn made loops	0.75	40%	Wearable strain sensor
[1.153]	Stretchable and Sensitive Strain Sensor	Piezoresistive	PDMS	Ag nano–walls thin film	2 to 14	70%	Finger movements
[1.155]	Textile–based strain sensor for monitoring the elbow and knee movements	Piezoresistive	Elastic yarns made from Lycra fiber wrapped with two polyester yarns.	Carbon particles coated polyamide fiber twisted with polyester yarn	~0.3	30%	Flexion angle of elbow and knee movements
[1.154]	Stretchable strain sensor based on a metal nanoparticle thin film for human motion detection	Piezoresistive	PDMS	Silver nanoparticle	2.5	20%	Finger movements
[1.159]	Knee's kinematic monitoring using single optical FBG sensor	Fiber Bragg grating	Optical Fiber	Polymer encapsulated FBG sensor	~0.8	0.04%	Knee, finger movements, HR, RR
[1.160]	Force sensors based on light pipes in the form of multimode optical fibers made of copolymers.	Loss of light due to deflection of the fiber with force	Multimodal optical fiber	Copolymers containing silicon and polyurethane			Force sensing
[1.152]	Textile–based MEMS accelerometer	Piezoresistive	Cotton fiber	Silver nanoparticles	7.796 ± 2.835		Motion sensing
[1.158]	All–polymeric knitted textile strain sensor	Piezoresistive	Commercial Spandex yarn	PU/PEDOT:PSS fibers	0.2 to 1	160%	Knee bending movements

1.5 Regulatory concerns

As portable health monitoring devices including smartphone–based systems and applications are increasing rapidly and becoming more pervasive in society, there is a growing concern about the safety issues and associated potential dangers [1.161],[1.162]. Concerns also remain among many researchers about whether and/or how a regulatory policy would be adopted and enforced by the government bodies such as the US Food and Drug Administration (FDA), or the Medicines and Healthcare Products Regulatory Agency (MHRA) in the United Kingdom (UK) [1.163],[1.164].

Many experts[1.165]–[1.173]have raised questions about the accuracy and reliability of smartphone–based health monitoring applications/systems, the vast majority of which reportedly lacked enough involvement of medical professionals during the design and evaluation phases. For example, in [1.167], the authors studied and tested a dermatology app called 'Skin Scan', which was found to recognize only 10.8% images correctly as high–risk melanomas against 93 clinical images from the National Cancer Institute and Fitzpatrick's Dermatology in General Medicine. Furthermore, in January 2017, a team of researchers [1.174] conducted a search for suitable apps in the iTunes App Store and Google Play that can assist people to deal with anxiety disorders and selected 52 apps for study. They found that 63.5% (33 out of 52) of the apps were reported as having no information about the intervention approach. In addition, no information related to the manufacturers' professional credentials were available for more than two–thirds (35 out of 52) of the applications. Only two out of the 52 anxiety apps were found to be thoroughly tested by the psychiatrists [1.174]. Therefore, cautious use of many of these applications was advised in [1.168],[1.170] due to their diagnostic inaccuracies and unreliability. Some of them are reported to be unsafe to use [1.166],[1.171],[1.172] and may even cause life–threatening consequences [1.173]. Hence, adoption and enforcement of some regulatory policies were recommended by the experts [1.165],[1.169] to ensure accountability, data–privacy, information security and patient welfare in terms of safety and diagnostic effectiveness.

Following the FDA's release of a draft guideline for regulating mobile medical apps in 2011, key experts in this industry expressed their expectations regarding the policies for medical apps [1.175]. These experts urged the FDA to draw a clear demarcation line between the medical apps and the fitness or wellness app, as well as between diagnosing apps and monitoring apps. They recommended for defining the risk–level threshold of regulatory significance for medical apps. They also suggested defining the boundaries of FDA regulations for apps serving as device accessories and making a guideline to deal with the modular applications. In February 2015, the FDA released the latest version of the guidelines defining the categories of smartphone–based healthcare applications that must require regulatory oversight [1.176]. According to the guideline, FDA will regulate only those medical applications that can turn a smartphone into a medical device such as ophthalmoscopes and dermatoscopes using external and/or internal sensors and devices. Regulatory oversight will also be applied to those applications that can be used as an accessory to the FDA–approved medical devices such as a smartphone–based ECG monitor. In short, regulatory oversight from the FDA is required if any application that can possibly affect the 'performance or functionality' of the FDA–regulated medical devices, and thus may pose a risk to patient safety. However, some mobile applications, although being a medical device by the definition, enjoy "enforcement discretion" as they pose a low risk to patients [1.176]. Regardless, all high–risk class III devices and about 75% of medium–risk Class II devices require clinical trials and/or other evidence to demonstrate their safety and compliance with the intended operation [1.162].

However, if a device demonstrates substantially similar performance to an already approved and legally marketed device (predicate device), it may enjoy an exemption from new clinical trials upon proper evidence that shows the device has same intended use and technological characteristics as the predicate device [1.177]. In the case when the new device has different technological characteristics in terms of device safety and effectiveness—first, it must not raise any new concerns, and second, it must meet the minimum standards of the predicate device [1.177]. Nevertheless, there remain serious concerns about safety assurances in the process of device approval based on predicate

devices. Therefore, both the Institute of Medicine [1.178] and the U.S. Congress [1.179] understandably urged to curtail this approach of device approval. So far, the FDA has approved several healthcare applications developed for the mobile platform [1.180]. The diagnostic radiology app 'Mobile MIM' is the first such application ever available in iTunes stores [1.181]. This app allows a healthcare professional to view, assess and securely share images with patients, peers or partner institutions, thus reducing diagnosis and treatment delay. KardiaMobile (AliveCor, Inc.) is another FDA approved device that comes with an application, which can turn a smartphone into a portable single–lead electrocardiogram (ECG) machine [1.182]. Other FDA approved healthcare apps for smartphones include the iExaminer™ (Welch Allyn, Inc.) adapter for PanOptic™ Ophthalmoscope [1.183], BlueStar® (WellDoc, Inc.) for type 2 diabetes management [1.184], and ResolutionMD® (PureWeb Inc., Calgary, Canada) for viewing and assessing diagnostic images [1.185].

In Europe, according to the EU Medical Device Directive MDD 93/42/EEC [1.186], published on 14 June 1993 and amended in the Directive 2007/47/EC [1.187], any stand–alone or combination of 'instrument, apparatus, appliance, software, material or other article' intended for healthcare purposes including diagnosis, monitoring, prevention and treatment will be considered be as 'medical device'. Therefore, most smartphone–based healthcare applications including those that monitor and assess cardiovascular health, eye and skin health through imaging, and lung health, will fall under the umbrella of 'medical device' and thus require Conformité Européenne (CE) certification for marketing the product within the European Economic Area (EEA). The CE certification or 'CE marking' ensures the product's conformity with the health, safety, and environmental protection standards set by the EU's harmonization legislation [1.188]. For example, an Irish app ONCOassist™ [1.189] was designed as a decision support tool for professional oncologists at the point–of–care and incorporated prognostic tools, drug interaction checker, survival rate predictors for diseases such as breast cancer, colon cancer and lung cancer. In addition, this app also incorporated some algorithms to determine, for example, liver cirrhosis severity, level of consciousness, the prognostic score for patients with advanced Hodgkin lymphoma and appropriate dosage of chemotherapy agents based on patient's body surface

area (BSA) and thereby, was considered as a medical device. ONCOassist™ received the CE certification in 2013 and displays the CE mark on its welcome screen.

A new medical device regulation (MDR) [1.190] (EU) 2017/745 was published in the Official Journal of the European Union repealing the MDD 93/42/EEC on 5 May 2017. The new MDR brings previously unregulated non–medical and cosmetic devices under the umbrella of 'medical device', with many of them being reclassified as medium to high risk (such as class IIa, IIb and III) devices. The other key changes in the MDR over the MDD includes inclusion of medical purpose devices and active implantable medical devices (AIMD), requirements for the manufacturers to update clinical data, technical documentation, and labeling; and generate and provide detailed clinical data to validate safety and performance claims and enforce unique device identification (UDI) for tracking. A wider range of smartphone–based commercial healthcare apps will now be defined as the 'medical devices' according to the MDR that require the manufacturers, and app development companies to revisit their safety and quality control processes to ensure compliance with the new MDR, that was scheduled to be enforced on May 26, 2020. Although these changes are meant to ensure a much safer, transparent and sustainable regulatory framework for the consumer, changeover on such a scale in a limited timeframe is a mammoth task for manufacturers and regulatory bodies to achieve. Furthermore, the parting of the United Kingdom (UK) from the EU—popularly termed as 'Brexit'—is causing more confusion for the manufactures in this already highly challenging task. It was unclear whether the UK would comply with EU regulations [1.191]. However, the UK Government, on 4 July 2017, vowed to work closely with the EU in terms of medicines regulation to ensure public health and safety even after leaving the EU [1.192]. In a recent statement, the UK's Department of Health and Social Care declared that it will comply with the key elements of the MDR and recognize all medical devices approved for the EU market and CE–marked after leaving the EU, in the case a no Brexit deal is reached [1.193].

Currently, the Medicines and Healthcare Products Regulatory Agency (MHRA) of the UK complies with the existing Medical Device Directive (MDD) and defines any healthcare app or software as a 'medical device' based on the functionality or service it provides to

the users and the associated risks in terms of patient's safety [1.194]. According to the MHRA, an app/software is most likely to be considered as a 'medical device' if it is designed to perform some calculations or run some algorithms on the raw data to detect, diagnose and prevent disease, or to monitor the course of a disease or injury. Apps that are intended for archiving records without modification, providing existing information, and making general recommendations for an expert's advice, can safely be excluded from 'medical devices' category. However, if the decision–support apps perform some calculations or interpret or interpolate the data and do not allow the clinicians to review the raw data, then such apps/software are highly likely to fall into the 'medical device' category. Apps that perform simple and straightforward calculations to track physical fitness such as heart rate, step–count or BMI (body mass index) are not considered as 'medical devices'. However, apps/software that perform complex calculations, for example, to determine medicine doses can potentially fall into the high–risk class III 'medical device' category [1.195]–[1.197]. The MHRA recommends the users to use a CE marked medical purpose app to ensure user safety.

In order to receive a 'CE mark' for the medical purpose apps—a 'medical device' by the MDD 93/42/EEC—the manufacturers need to identify the class of the device based on the perceived risk associated with it and select the corresponding conformity assessment procedure. The conformity assessment procedure ensures tighter control to be applied to the device in the case of higher perceived risks associated with it. Next, the manufacturer prepares a document that generally includes the technical details about the design and manufacturing process of the device as well as the intended operation of the product to demonstrate the product's compliance with the MDD 93/42/EEC. For a low–risk i.e., class I device, the manufacturer can self–declare the device's compliance with the Directive. For class IIa devices, manufacturers must also declare the device's compliance with the corresponding regulatory requirements of the Directive. Additionally, class IIa devices as well as class IIb and class III devices must require a notified body (NB) to carry out a detailed conformity assessment and receive a 'Declaration of Conformity' certificate from

the NB to submit as an evidence of the app/software's being compliant with the MDD 93/42/EEC [1.186].

However, It was argued in a report to the U.S. Congress of the Global Legal Research Center that the 'CE mark' on a medical device does not necessarily ensure the quality of the device in terms of its performance and clinical effectiveness, rather it merely shows its compliance with the EU legislation [1.198]. Medical devices in the EU are approved based on the safety and performance standards, and demonstration of the devices' clinical efficacy is not required by the MDD [1.162]. However, the new MDR, which is scheduled to be in force in 2020 has put more emphasis on clinical trials and evidence [1.190]. On the other hand, the US Food and Drug Administration (FDA) requires the devices to ensure not only the safety and performance, but also their clinical efficacy [1.199]. Furthermore, only one organization, the FDA, governs the entire process of device approval in the US. While this ensures better surveillance on the regulatory processes, however, often it turns out to be an expensive, rigid and lengthy process for manufacturers [1.200]. In contrast, in the EU, the manufacturers can flexibly appoint one of the many EU approved private, for–profit 'notified bodies' to assess and approve the devices in terms of regulatory standards, thus expediting the process for obtaining a 'CE' mark, but this may be, at a potential risk of compromised safety [1.201],[1.202]. In addition, some 'high–risk' medical devices developed, for instance, by an academic institution, can likely be distributed through/among the associated entities for non–commercial use without a CE mark, whereas in the US, prior FDA–approval is necessary before distribution [1.203]. However, the approval process of medical devices based on the predicate device and without rigorous new clinical evidence can deter the manufacturers to carry out expensive and time–consuming clinical trials, which not only raise concerns in terms of device safety and efficacy but also may lessen the scope of device improvement and innovation [1.203].

While the US and the EU represent 40% of the global markets for medical devices [1.204], other markets such as Canada, Australia, and Japan have their own regulatory bodies to enforce regulatory policies for medical devices. Health Canada, for example, categorizes the medical devices into four classes from, Class I to Class IV, based on the risks associated

with the devices [1.205]. Prior to marketing a medical device in Canada, the manufactures or the distributors must apply for and receive the Canadian Medical Device License (MDL) for class II, III, and IV devices and the Medical Device Establishment License (MDEL) for class I devices [1.205]. However, the information required to file an application for Health Canada approval is approximately the same as that required in the US and EU [1.206]. On the other hand, Australia's Therapeutic Goods Administration (TGA) relies mostly on the EU regulations and CE mark certification from the European NBs before granting approval to market medical devices there [1.207]. Recently, Australia's TGA decided to begin recognizing registrations and certifications from additional foreign medical device regulators including US FDA, Health Canada, the Japanese Pharmaceutical and Medical Devices Agency (PMDA) [1.208].

In 2014, the International Medical Device Regulators Forum (IMDRF) launched the Medical Device Single Audit Program (MDSAP) pilot to develop an efficient and standardized global directive to auditing and monitoring medical devices [1.209]. The regulatory bodies participating in this program include TGA of Australia, Agência Nacional de Vigilância Sanitária (ANVISA) of Brazil, Health Canada, the U.S. FDA, and the Ministry of Health and Labor and Welfare (MHLW) of Japan, while the EU participated as an observer [1.209]. TGA has recently decided to recognize registrations and certifications from MDSAP auditing organizations [1.208]. Starting in January 2019, Health Canada also planned to discard the Canadian Medical Device Conformity Assessment System (CMDCAS) and replace it with the MDSAP certification. In fact, Health Canada urged the MDL holders to submit evidence for MDSAP transition from CMDCAS and/or MDSAP certificates by the 31st December 2018 [1.210].

1.6 Research contributions and thesis organization

The research work conducted in this thesis aims at developing highly accurate yet computationally efficient algorithms and low–cost, unobtrusive devices with potential predictive capability to realize reliable health monitoring in the wearable platform. This research particularly focuses on developing monitoring solutions for cardiovascular health

and mobility i.e. health of the lower–limb — two key factors that are strongly associated with the human aging process. The major contributions of this work are summarized as follows:

Design, implementation, and validation of a three–stage sensor fusion algorithm. A gradient descent approach was used to estimate the gyroscope integration drift, which was subtracted from the cumulatively integrated gyroscope data to obtain the orientation of the IMU in real time. The roll and pitch angles were obtained from the first stage, whereas the second and third stages outputs a coarse and fine estimate of yaw angle, respectively. Since the estimation was obtained primarily from the gyroscope data, the estimated orientation was least affected by the external acceleration and magnetic disturbances. This complementary filter–based orientation estimation method is presented in Chapter 2.

Design, implementation, and validation of a two–stage sensor fusion algorithm for real–time estimation of lower–limb joint angles. The drift in the cumulatively integrated gyroscope data was estimated in real–time using a gradient descent approach that was subsequently used to correct the inclination of the IMU sensors. The roll and pitch angles thus obtained for each sensor mounted above and below the joint were then fused in the second stage to obtain a real–time estimate of joint angle by exploiting a gradient descent method. Since the joint angles were estimated primarily from the gyroscope data and without incorporating any magnetic field measurement, the joint angles thus obtained were least affected by the external acceleration and insensitive to magnetic disturbances. This two–stage sensor fusion algorithm for real–time monitoring of lower–limb joints is presented in Chapter 3.

Development of a simple, low–cost and non–invasive gait analyzer. The analyzer uses low–cost, wireless and miniature micro–electromechanical sensor based IMUs to obtain acceleration and angular velocity of walking from both legs. The information thus obtained are used to quantitatively identify the healthy gait corresponding to gender and age, and can thereby evaluate an individual's gait with respect to the baseline characteristics of his/her peer group. The gait features obtained from the apparently healthy subjects were

further analyzed, forming two distinct clusters in the baseline gait characteristics corresponding to gender and age. This simple and inexpensive gait analyzer can potentially be transformed into a portable and continual remote monitoring tool to evaluate and early diagnose the decline of the musculoskeletal or cognitive health of the user, thus facilitating healthy aging at home. This simple, low–cost and computationally efficient gait–analyzer is presented in Chapter 4.

Development of flexible and dry capacitive electrodes, a two–electrode wireless ECG monitoring system and an automatic detection method of anomalous ECGs. The capacitive–coupled dry electrodes can measure ECG signals over a textile–based interface material between the skin and electrodes. The flexible nature of the sensing part reduces motion artifacts and makes it suitable for long–term monitoring of cardiovascular health. Furthermore, the use of virtual ground in designing the electrodes enables realizing a two–electrode ECG system instead of conventional three–electrode systems used in the portable ECG devices. The raw ECG signals obtained from the electrodes are transmitted to a computer by a data acquisition system over Bluetooth medium. A software application was developed to process, store and display the ECG signal in real time. An algorithm was developed separately as a potential extension of the software to realize automatic identification of Atrial Fibrillation (AFib) from short single–lead traces. Design of this flexible and dry capacitive electrode and a wireless ECG monitoring system with automatic anomaly detection capability is presented in Chapter 5.

A study on the association between human gait and cardiac activities. The gait characteristics and the cardiac activity are measured using wearable IMUs and a single–lead handheld ECG monitor. The gait asymmetry between two legs and variation in the gait show good association with some key cardiac parameters and physical parameters. These Quantitative association between gait and heart can potentially lead towards realizing a low–cost in–home personal monitoring tool for early detection of signs associated with CVD–related changes in gait features before the actual CVD symptoms are manifested. We investigate the association between human gait and cardiac activities in Chapter 6.

In addition, an introduction to smart health–monitoring system as a potential application of the IoT is presented in Chapter 1. Then, the motivation of developing computationally efficient algorithms and low–cost, unobtrusive devices is presented. The framework of a complete smart health–monitoring system is presented. The concerns regarding the interoperability of devices and the recent efforts on developing standardized platform are discussed. A comparative discussion on the recent research activities in portable and wearable sensors and devices for cardiovascular health and activity monitoring is presented that is followed by a brief discussion on the regulatory concerns associated with the portable and smartphone–based health monitoring systems. Finally, a summary of the main contributions of this research and the structure of this thesis are given. In Chapter 7, this thesis is concluded with a summary of the research and several recommendations for future research possibilities in the field of smart wearable health–monitoring systems.

Publications:

- S. Majumder and M. J. Deen, "Wearable IMU–based System for Real–time Monitoring of Lower–limb Joints," *IEEE Sens. J.*, pp. 1–1, 2020.
- S. Majumder and M. J. Deen, "A Robust Orientation Filter for Wearable Sensing Applications," *IEEE Sens. J.*, vol. 20, no. 23, pp. 14228-14236, 1 Dec.1, 2020.
- A. I. Faisal, S. Majumder, R. Scott, T. Mondal, D. Cowan, and M. J. Deen, "A Simple, Low-cost Multi-sensor-based Smart Wearable Knee Monitoring System," *IEEE Sens. J.*, pp. 1–1, 2020.
- S. Majumder and M. J. Deen, "Smartphone sensors for health monitoring and diagnosis," *Sensors*, vol. 19, no. 9. 2019.
- S. Majumder, T. Mondal, and M. J. Deen, "A Simple, Low–Cost and Efficient Gait Analyzer for Wearable Healthcare Applications," *IEEE Sens. J.*, vol. 19, no. 6, pp. 2320–2329, 2019.
- **Feature paper:** A. I. Faisal, S. Majumder, T. Mondal, D. Cowan, S. Naseh, and M. J. Deen, "Monitoring methods of human body joints: State–of–the–art and research challenges," *Sensors*, vol. 19, no. 11, p. 2629, 2019.

- S. Majumder, L. Chen, O. Marinov, C. H. Chen, T. Mondal, and M. J. Deen, "Noncontact Wearable Wireless ECG Systems for Long–Term Monitoring," *IEEE Rev. Biomed. Eng.*, vol. 11, pp. 306–321, 2018.
- S. Majumder *et al.*, "Smart homes for elderly healthcare—Recent advances and research challenges," *Sensors*, vol. 17, no. 11, pp. 2496–2527, 2017.
- **Feature paper:** S. Majumder, T. Mondal, and M. J. Deen, "Wearable sensors for remote health monitoring," *Sensors*, vol. 17, 45 pages, no. 1, p. 130, 2017.
- W. Jiang, S. Majumder*, S. Kumar, S. Subramaniam, X. Li, R. Khedri, T. Mondal, M. Abolghasemian, I. Satia, and M. J. Deen, "A Wearable Tele-Health System towards Monitoring COVID-19 and Chronic Diseases," *IEEE Rev. Biomed. Eng.*, 2020. (*Submitted*)
- X. Li, C. Shen, L. Wang, S. Majumder, D. Zhang; M. J. Deen et al., "Pulmonary fibrosis and its related factors in discharged patients with new coronavirus pneumonia: A cohort study of 90–150 days follow–up after onset," *Respir. Res.*, 2020. (*Submitted*)
- **Invited paper:** A. U. Alam, S. Majumder, C.–H. Chen, O. Marinov, and M. J. Deen, "Low Frequency Noise in Electrochemical Sensors for Water Quality Monitoring," in *25th International Conference on Noise and Fluctuations (ICNF 2019)*, 2019.

*co-first author

Accolade:

- **3rd place winner:** S. Majumder, "Walking speaks!," *ECE Three Minute Thesis (3MT) competition, McMaster University*, 2019.

Chapter 2

A robust orientation filter

Rapid advances in the micro–electromechanical systems (MEMS) technology have enabled us to realize low power, low cost and highly sensitive miniature sensors and actuators. MEMS–based magnetic field measurement devices (magnetometers) and inertial measurement devices such as accelerometers and gyroscopes have become an integral part of many consumer applications such as smartphones, automobiles, flying drones and fitness trackers [2.1]–[2.3]. In fact, the global market penetration of smartphones is increasing rapidly and is expected to exceed 3.8 billion by 2021 [2.4]. In addition, Magnetic and Inertial Measurement Units (MIMU) are expected to be an integral part of smart devices and systems in the upcoming era of Smart Home technologies, Internet–of–Things (IoT), and Internet–of–Everything (IoE) [2.5],[2.6]. Therefore, the integrated MIMU, when coupled with present–day energy efficient and high–speed computing and communication technologies, can enable continuous and in–home monitoring and assessment of activity, mobility, fitness and overall health of people without interrupting their daily living [2.1],[2.7],[2.8]. Furthermore, these miniature and low–power MIMUs, if integrated with smart textiles may potentially pave the way for unobtrusive remote monitoring of elderly health, allowing the healthcare personnel to monitor, assess and keep record of the overall health condition of individuals in terms of their fitness, activity, mobility and rehabilitation from distant facilities [2.1],[2.7],[2.8].

---

* Adapted from S. Majumder and M. J. Deen, "A Robust Orientation Filter for Wearable Sensing Applications," in *IEEE Sensors Journal*, doi: 10.1109/JSEN.2020.3009388. (Appendix A)

A MIMU–based gait analyzer can be one such tool to measure and analyze human gait characteristics, which is reported to have a strong association with health condition [2.1],[2.6]. For example, among middle–aged adults, slow walkers are found to be more vulnerable to die from heart failure than the brisk walkers of the same age group [2.8]. In addition, gait parameters such minimum foot clearance (MFC), step length, and step time as well as the variability in these parameters can provide useful predictive information about an individual's health [2.10],[2.11]. However, the orientation of the on–body MIMUs for gait analysis are arbitrary. Therefore, estimation and correction of the sensor's orientation is critical for accurate assessment of the gait parameters.

The orientation of the sensor can be represented by the Euler angles or Quaternions. The roll (Φ) and pitch (θ) orientations of the sensor can ideally be obtained from a tri–axial accelerometer from its orientation with respect to the direction of the gravity, whereas a tri–axial magnetometer can be used to obtain the yaw (ψ) of the MIMU by measuring the geomagnetic field. Furthermore, all three orientations can ideally be obtained by integrating the angular velocity around the three axes measured by a tri–axial gyroscope.

However, the accelerometer and magnetometer measurements are highly susceptible to noise due to external vibrations and magnetic disturbances, respectively. In particular, the magnetic field generated by ambient ferromagnetic materials can dominate the relatively weak geomagnetic field and thus can introduce large errors in the estimated orientation. In addition, estimation of orientation solely from the gyroscope is not reliable due to the drift introduced during integration. Nevertheless, measurement acquired by all three sensors can be exploited to obtain a more accurate estimation of orientation.

2.1 Related works

In a typical orientation filter, measurements acquired by the accelerometers, gyroscopes and magnetometers are combined to obtain an estimate of the device orientation. However, an efficient sensor fusion algorithm in terms of ease of implementation and computational complexity is critical for real time systems. Many researchers used Kalman filter–based approaches for orientation estimation [2.12]–[2.16]. For example, an Extended Kalman Filter (EKF) was used in [2.12] to estimate the attitude of a body–worn MIMU. There, they

determined the global frame from the accelerometer and magnetometer measurements and exploited the Gauss–Newton techniques to bring the arbitrary attitude (roll and pitch) measured by the gyroscopes closer to global frame by minimizing the error in the quaternion. However, the measurement equations obtained in [2.12] were complicated, non–linear and computationally intensive, thus making the approach unfeasible for real time applications. These issues were addressed in [2.13], where the authors computed the quaternion from the accelerometer and magnetometer data using a previously reported quaternion estimator (QUEST) [2.17]. The computed quaternion along with the gyroscope measurements were afterwards fed to the input of the Kalman filter. Although the QUEST algorithm introduced some complexities to the approach, the overall computational cost reduced due to the linear nature of the measurement equations. However, linearization can make the system sensitive to initial conditions and may cause issues with convergence and stability, particularly at a low sampling rate [2.18]. In addition, none of the above approaches compensate for external acceleration and magnetic disturbances.

In [2.14], an adaptive approach for orientation estimation was proposed that used a quaternion–based indirect Kalman filter to estimate the external acceleration, which was then compensated by increasing the measurement noise covariance. However, the authors did not compensate for the magnetic disturbances and did not report the accuracy of the estimated attitude and heading. In [2.15] and [2.16], the researchers performed observability analysis to identify large disturbances in measured acceleration and magnetic field. The information thus obtained were incorporated in an EKF–based approach to improve the accuracy of the estimated orientation. In fact, Kalman filter based approaches are considered as a superior tool for sensor fusion, motion prediction and filtering in terms of speed and accuracy [2.19]. However, the Kalman filter based approaches require experimentally determining its parameters such as the covariance matrices of process noise and measurement noise. In addition, its inherent computational complexity that arises from the inversion of large matrices can significantly reduce the battery life of the portable and wearable systems [2.20],[2.21].

Complementary Filter (CF)–based estimation approaches, on the other hand, are computationally efficient and require only a few tuning parameters. It estimates the orientation by combining information from at least two separate sources,

1) accelerometer and magnetometer data, that are contaminated with noise and disturbances but free from drift problems, and

2) gyroscope data, which are least affected by the high frequency noise, however, suffers from low–frequency drift [2.20],[2.22].

Such a CF–based approach was proposed in [2.22], where the reference gravity and magnetic field information in the global reference were projected on the sensor frame and subtracted from the actual measurements to calculate the error. This error information was used to correct the gyroscope data and obtain an estimate of the quaternion. A somewhat similar approach was used in [2.23], where the estimation was made by minimizing the calculated error using a gradient descent algorithm. However, neither of the above approach addressed the disturbances present in the measured acceleration and magnetic field.

A quaternion–based adaptive orientation filter was proposed in [2.24], which used an algebraic approach to minimize the effect of magnetic disturbances in the attitude estimation. The impact of external acceleration on the estimation of heading was minimized by adopting an adaptive gain control approach. However, the authors tested their orientation filter in the presence of a short burst of external acceleration that lasted for only four seconds. In [2.25], an external acceleration detector was designed to identify the dynamic condition of the body. In the case when an external acceleration due to the movement of the body was detected, the gain of the filter was adjusted accordingly to compensate for the external acceleration. A CF–based approach for external acceleration compensation was proposed in [2.26], where they estimated and compensated the external acceleration separately, outside of the attitude estimator. The filter's performance was validated with a rotating turntable. However, the performance of the filter in complex dynamic situations was not tested. In a two–step complementary filter implemented in [2.27], the authors exploited a state–machine based approach to mitigate the effect of external acceleration and magnetic disturbance. The performance of the system was

validated in different dynamic conditions including daily–living environments and magnetically distorted conditions.

2.2 Proposed orientation filter

In this work, we propose a three–stage complementary filter that estimates the orientation of the MIMU by estimating and compensating for the integration drift from the gyroscope measurements, making the estimation least affected by the external acceleration and magnetic disturbances. In the first stage, the drift in the roll and pitch are estimated from the accelerometer and gyroscope data, which are subtracted from the roll and pitch obtained by integrating the gyroscope measurements along the *x*– and *y*–axes, respectively. A crude estimation of the yaw was made in the second stage by fusing the magnetometer measurements and the information obtained from the first stage. Finally, a similar approach to the first stage was used to combine the output of the second stage and the gyroscope data (z–axis) to improve the estimation accuracy of the yaw. The block diagram of the proposed orientation filter is shown in Figure 2.1.

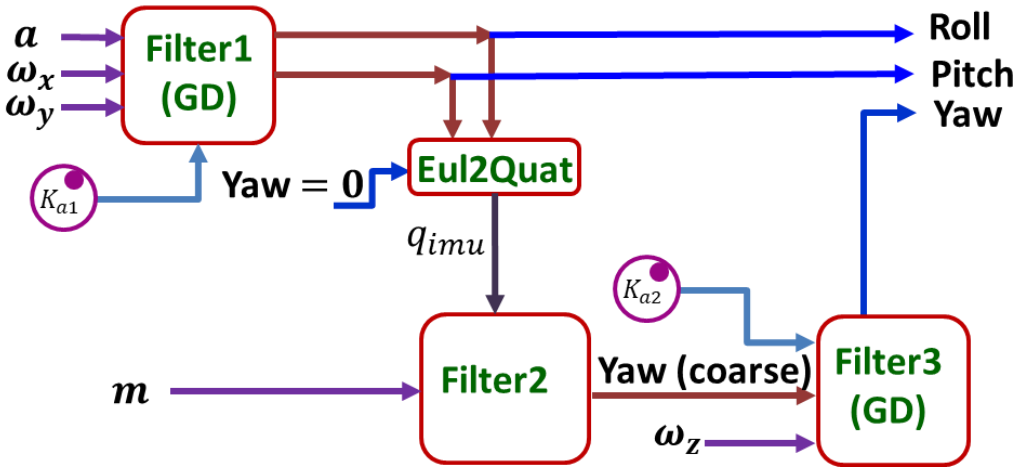

Figure 2.1 Proposed three–stage orientation filter.

2.2.1 Stage one: Estimation of Roll and Pitch

The angular velocity ω_m of the device about the x, y and z axes are measured with a tri–axial gyroscope, and it is expressed as,

$$\omega_m = [\omega_{mx} \quad \omega_{my} \quad \omega_{mz}]. \tag{2.1}$$

The orientation of the sensor φ_m can be obtained by integrating ω_m over time, i.e.

$$\varphi_m = [\Phi_m \quad \theta_m \quad \psi_m] = \int_{t_i}^{t_f} \omega_m dt = \sum_{i=1}^{t_f - t_i / T} T\omega_{m,i} \ , \tag{2.2}$$

where, Φ_m, θ_m and ψ_m represent the roll, pitch, and yaw of the device, respectively, and T is the sampling interval of the gyroscope. However, the gyroscope measurement drifts over time, which along with the measurement noise accumulate during integration. This causes the calculated orientation to drift over time. Therefore, at any given time, φ_m can be expressed as,

$$\varphi_m = \varphi_{tr} + \varphi_{dr}, \tag{2.3}$$

where, φ_{tr} is the true orientation and φ_{dr} denotes the amount of drift in the measured orientation from the gyroscope. Eq. 2.3 can be rearranged as,

$$\varphi_{dr} = \varphi_m - \varphi_{tr}. \tag{2.4}$$

Eq. 2.4 allows for formulating an optimization problem, where φ_{dr} may be obtained as the solution to the Eq. 2.5,

$$\min_{\varphi_{dr} \in \Re} f(\varphi_{dr}, \varphi_m, \varphi_{tr}), \tag{2.5}$$

where, the optimization problem is defined as Eq. 2.6.

$$f(\varphi_{dr}, \varphi_m, \varphi_{tr}) = \varphi_{dr} - (\varphi_m - \varphi_{tr}). \tag{2.6}$$

The drift, φ_{dr} can be estimated iteratively by using the gradient descent algorithm with an initial orientation, $\varphi_{dr,0}$ and a step–size β, as presented in Eq. 2.7.

$$\varphi_{dr,k+1} = \varphi_{dr,k} - \beta \frac{\nabla f(\varphi_{dr}, \varphi_m, \varphi_{tr})}{\|\nabla f(\varphi_{dr}, \varphi_m, \varphi_{tr})\|} \ . \qquad k = 1,2,3 \ldots \tag{2.7}$$

Here, ∇f denotes the gradient of the solution surface and is given by,

$$\nabla f(\varphi_{dr}, \varphi_m, \varphi_{tr}) = J^T(\varphi_{dr}) f(\varphi_{dr}, \varphi_m, \varphi_{tr}), \tag{2.8}$$

where, J is the Jacobian of the objective function $f(\varphi_{dr}, \varphi_m, \varphi_{tr})$.

The drift, φ_{dr} evolving from the integration of the gyroscope measurements is independent of the true orientation φ_{tr}. Ideally, φ_{tr} can be obtained from the accelerometer; however, is contaminated with external noise and disturbances. Therefore, the Jacobian J can be presented as,

$$J^T(\varphi_{dr}) = 1 - \frac{\partial \varphi_m}{\partial \varphi_{dr}}.$$

(2.9)

Assuming that the sensor undergoes a small incremental change in the orientation at every sample, the Eq. 2.9 can be approximated as,

$$J^T(\varphi_{dr}) \approx 1 \tag{2.10}$$

Consequently, Eq. 2.8 can be simplified as,

$$\nabla f(\varphi_{dr}, \varphi_m, \varphi_{tr}) \approx f(\varphi_{dr}, \varphi_m, \varphi_{tr}). \tag{2.11}$$

Therefore, Eq. 2.7 can be rearranged as

$$\varphi_{dr,k+1} \approx \varphi_{dr,k} - \beta \left(\varphi_{dr,k} - \left(\varphi_{m,k} - \varphi_{tr,k}\right)\right), k = 1,2,3 \ldots \tag{2.12}$$

where,

$$\varphi_{m,i} = \sum_{i=1}^{k} T\omega_{m,i}, \tag{2.13}$$

and

$$\begin{aligned} \Phi_{tr,k} &= \arctan\left(\frac{a_{y,k}}{a_{z,k}}\right), && \text{roll} \\ \theta_{tr,k} &= -\arctan\left(\frac{a_{x,k}}{\sqrt{a_{y,k}^2 + a_{z,k}^2}}\right). && \text{pitch} \end{aligned} \tag{2.14}$$

Here, $a_{x,k}$, $a_{y,k}$ and $a_{z,k}$ are the k–th measurements from the accelerometer along the x, y and z axes, respectively. Then, the drift–free estimate of the roll and pitch angle $\breve{\varphi}_{tr,k+1}$can be obtained by,

$$\breve{\varphi}_{tr,k+1} \approx \varphi_{m,k+1} - \varphi_{dr,k+1}. \tag{2.15}$$

2.2.2 Stage two: Coarse estimation of yaw

The drift–corrected roll ($\breve{\Phi}_{tr}$) and pitch ($\breve{\theta}_{tr}$) information obtained in the first stage are used to calculate a quaternion, q_{imu}, while assuming a zero rotation around the z–axis (Yaw), i.e.

$$q_{imu} = f(\breve{\varphi}_{tr}), \tag{2.16}$$

where, $\breve{\varphi}_{tr} = [\breve{\Phi}_{tr} \quad \breve{\theta}_{tr} \quad 0]$. A rotation by an amount of q_{imu} brings the sensor frame (F_S) on the $x-y$ plane of the earth frame (F_E), aligning the unit's z–axis to the z–axis of the

earth frame. However, the orientation of the x– and y– axes of the sensor with respect to that of the earth's frame (α_N) remains unknown (Figure 2.2).

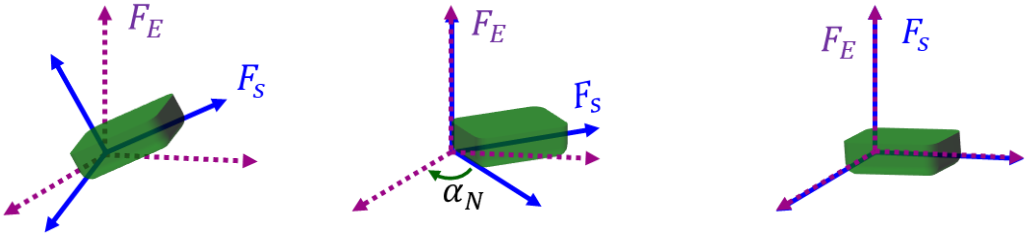

(a) (b) (c)

Figure 2.2 Aligning sensor frame to the earth frame.

Let the measured magnetic field in the sensor frame be $\boldsymbol{m} = [m_x \quad m_y \quad m_z]$, then the magnetic field in the earth frame $\boldsymbol{b} = [b_x \quad b_y \quad b_z]$, can be obtained by,

$$[0 \quad b_x \quad b_y \quad b_z] = q_{imu} \otimes [0 \quad m_x \quad m_y \quad m_z] \otimes q_{imu}^{*}. \tag{2.17}$$

Now, α_N can be obtained by rotating the resultant of the magnetic field vector on the $x-y$ plane of the earth frame, b_{xy} towards the reference north, $\boldsymbol{E}_N = [1 \quad 0 \quad 0]$, where

$$\boldsymbol{b_{xy}} = [b_x \quad b_y \quad 0]. \tag{2.18}$$

Rotation of an object by an angle α_N around a vector, $\hat{\boldsymbol{u}}_N$ can be described by a quaternion q_{mag},

$$q_{mag} = \left[\cos\frac{\alpha_N}{2}, \quad \hat{\boldsymbol{u}}_N \sin\frac{\alpha_N}{2}\right]. \tag{2.19}$$

where, $\hat{\boldsymbol{u}}_N$ can be obtained from the vector cross product of $\boldsymbol{b_{xy}}$ and $\boldsymbol{E}_N$, i.e.

$$\hat{\boldsymbol{u}}_N = \frac{\boldsymbol{b_{xy}} \times \boldsymbol{E}_N}{\|\boldsymbol{b_{xy}} \times \boldsymbol{E_N}\|}, \tag{2.20}$$

and the angle α_N between $\boldsymbol{b_{xy}}$ and $\boldsymbol{E}_N$ can be obtained from the vector dot product of $\boldsymbol{b_{xy}}$ and $\boldsymbol{E}_N$, i.e.

$$\alpha_N = \cos^{-1}\left(\frac{\boldsymbol{b_{xy}} \bullet \boldsymbol{E}_N}{\|\boldsymbol{b_{xy}}\|\|\boldsymbol{E_N}\|}\right) = \arctan\left(\frac{|b_y|}{b_x}\right). \tag{2.21}$$

The orientation of the sensor q can then be obtained by,

$$q = q_{mag} \otimes q_{imu} = [q_0 \quad q_1 \quad q_2 \quad q_3]. \tag{2.22}$$

Finally, a coarse estimate of the yaw angle ψ_c can be obtained from the quaternion q according to Eq. 2.23,

$$\psi_{c,k} = \arctan\big(2\big(q_{0,k}q_{3,k} + q_{1,k}q_{2,k}\big), 1 - 2(q_{2,k}^2 + q_{3,k}^2)\big) \tag{2.23}$$

2.2.3 Stage three: Fine estimation of yaw

A similar approach to stage one is used in stage three to combine the information from the gyroscope with the output from the stage two to further improve the accuracy of the estimated yaw. The drifted yaw angle $\psi_{m,k}$ can be obtained from the gyroscope by Eq. 2.13, which along with the estimated yaw from the second stage, i.e. $\psi_{c,k} = \psi_{tr,k}$ were used in Eq. 2.12 to estimate the amount of drift in the yaw $\psi_{dr,k+1} = \varphi_{dr,k+1}$. Then, the drift–free estimate of the yaw angle $\breve{\psi}_{tr,k+1}$ can be obtained by,

$$\breve{\psi}_{tr,k+1} \approx \psi_{m,k+1} - \psi_{dr,k+1}. \tag{2.24}$$

2.3 Performance evaluation

The performance of the proposed orientation filter was evaluated under different conditions and compared with other approaches described in the literature. In this section, we present the performance of our proposed filter in terms of estimation accuracy, robustness against noise and disturbances, and its application in gait monitoring.

2.3.1 Orientation estimation

In order to evaluate the estimation accuracy of the proposed filter, we tested the designed filter on a publicly available benchmark dataset [2.28]. The dataset was collected by a set of sensors mounted on an AscTec "Pelican" quadrotor. The sensors include a forward–looking camera, a downward–looking camera, and an inertial measurement unit, which measured the quadrotor's acceleration, angular velocity and magnetic field along three axes. The sensor–mounted quadrotor was flown in one, two and three loops in an indoor space (10m ×10m ×10m) equipped with eight Vicon cameras mounted on the four sides of the ceiling walls. The Vicon system allowed for obtaining the ground truth orientation of the quadrotor.

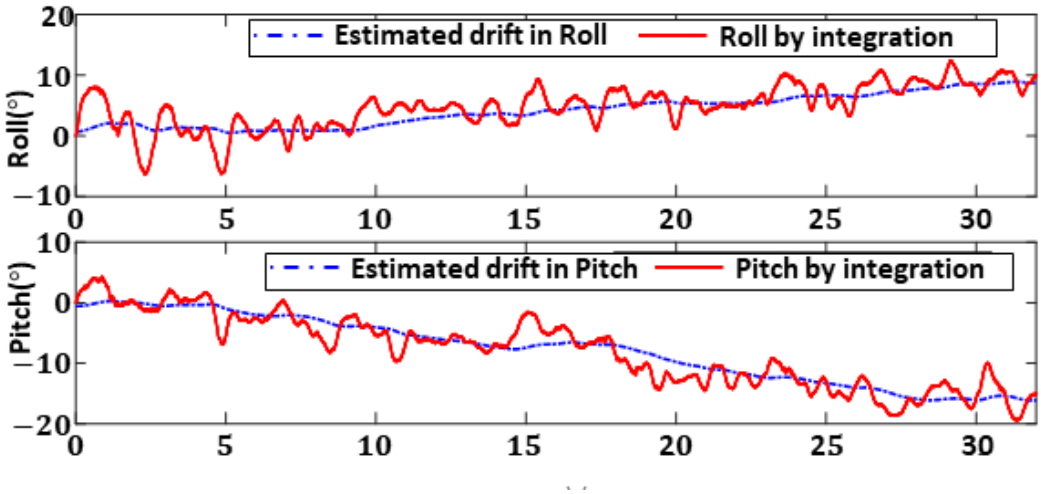

Figure 2.3 Estimated integration drift in the roll and pitch angles.

Figure 2.3 presents the drift estimated from the accelerometer data and the angular velocity measurements for the first set of data ('1LoopDown'). The drift thus estimated is subtracted from the roll and pitch angles obtained by integrating the angular velocity around the x– and y– axes. This results into a drift free estimate of roll and pitch at the end of stage 1. Figure 2.4 presents the estimated roll and pitch at the end of stage 1 for the first set of data in comparison to the ground truth.

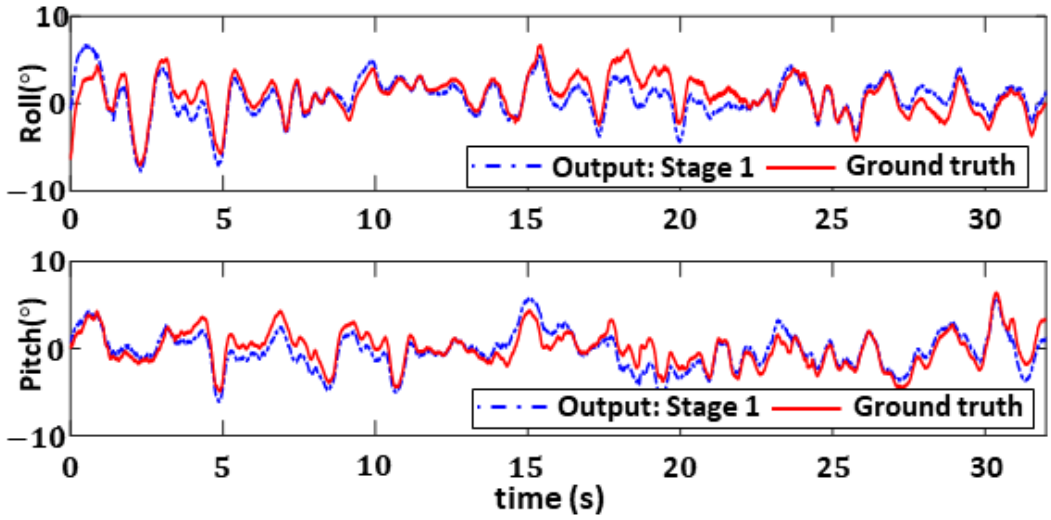

Figure 2.4 Estimated roll and pitch at first stage with respect to the ground truth.

A coarse estimate of the yaw angle was obtained at the end of stage 2. The accuracy of this coarse estimate was further improved by fusing the z–axis information of the gyroscope in

stage 3. Figure 2.5 shows the comparison of estimated yaw at the end stage 2 and stage 3 in reference to the ground truth.

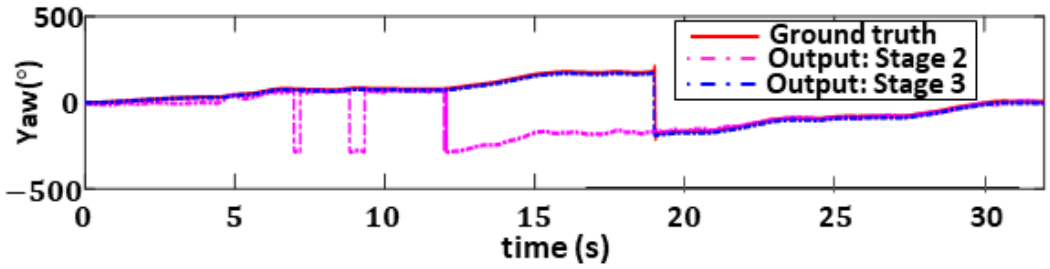

Figure 2.5 Estimated yaw with respect to the ground truth.

Similarly, the proposed orientation filter was used to estimate the roll, pitch and yaw from the two other experiments. The Root Mean Square Error (RMSE) of the estimated roll, pitch and yaw were computed for all three experiments and compared with respect to the published results (Table 2.1) [2.29]. It can be seen that the proposed orientation filter gives the best estimation accuracy for most cases.

Table 2.1 Comparison of root Mean Square error in estimated orientation (radians)

	1loopDown			2loopsDown			3loopsDown		
	RMSE			RMSE			RMSE		
	Roll	**Pitch**	**Yaw**	**Roll**	**Pitch**	**Yaw**	**Roll**	**Pitch**	**Yaw**
Our Work	0.0250	0.0208	0.1282	0.0245	0.0316	0.1199	0.0246	0.0336	0.1755
[2.29]	0.0233	0.0209	0.1429	0.0292	0.0223	0.1309	0.0277	0.0202	0.2890
On-board	0.0464	0.0369	0.3388	0.0338	0.0313	0.3182	0.0315	0.0329	0.3255
EKF	0.0287	0.0284	0.1888	0.0314	0.0384	0.3345	0.0331	0.0392	0.3545
Madgwick	0.0370	0.0336	0.2543	0.0470	0.0369	0.9229	0.0405	0.0360	1.3327

2.3.2 Filter robustness

In the proposed filter, the orientation was calculated by estimating and correcting for the drift from the integrated gyroscope data. Since the gyroscope measurement is less likely to be affected by high–frequency noise, it is expected that the estimated orientation would be least affect by any external acceleration and magnetic disturbance. In this section, we analyze the robustness of the proposed filter in presence of external acceleration and magnetic disturbance.

A. External acceleration

In order to verify the filter's performance in the presence of external noise, we generated zero–mean white Gaussian noise and added it to the measured acceleration of the benchmark dataset. This allows for simulating contamination of the dynamic accelerometer data at different signal–to–noise ratio (SNR) levels for different durations. Figure 2.6 shows the accelerometer data along the x–axis contaminated at three different SNR levels, where the acceleration fluctuated from ± 0.05g to ± 1g.

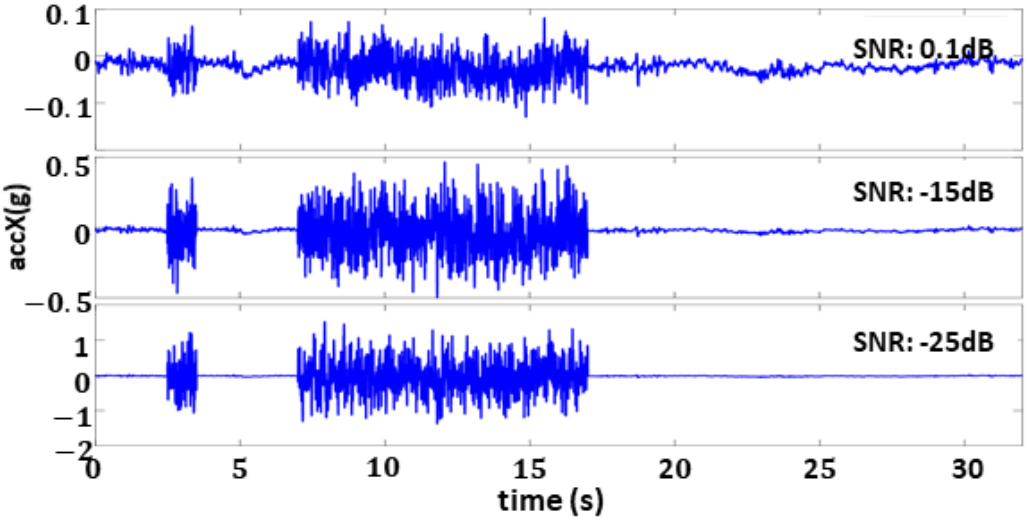

Figure 2.6 Accelerometer data contaminated at different noise levels.

The error in the estimated roll and pitch with respect to the ground truth is shown in Figure 2.7. It can be seen that the error increases somewhat when the contamination in the accelerometer data is high thus having a poor SNR. Nevertheless, the errors quickly converge to the same level as the external acceleration disappears. However, the RMSE for both the roll and pitch angles during the duration of the external acceleration change a little in comparison to the error presented in Table 2.1 for the actual accelerometer measurement. The RMS error of estimation in presence of external acceleration is presented in Table 2.2. It can be noted that, the presence of external acceleration does not affect the estimated yaw and thereby the error in the estimated yaw remains unchanged. This is due to the fact that the yaw estimation stage is fully decoupled from the first stage and does not rely on the

accelerometer measurement directly. It rather uses the estimated roll and pitch angles from the first stage and combines this information with the measured magnetic field and gyroscope measurement around the *z*–axis to obtain a fine estimate of yaw.

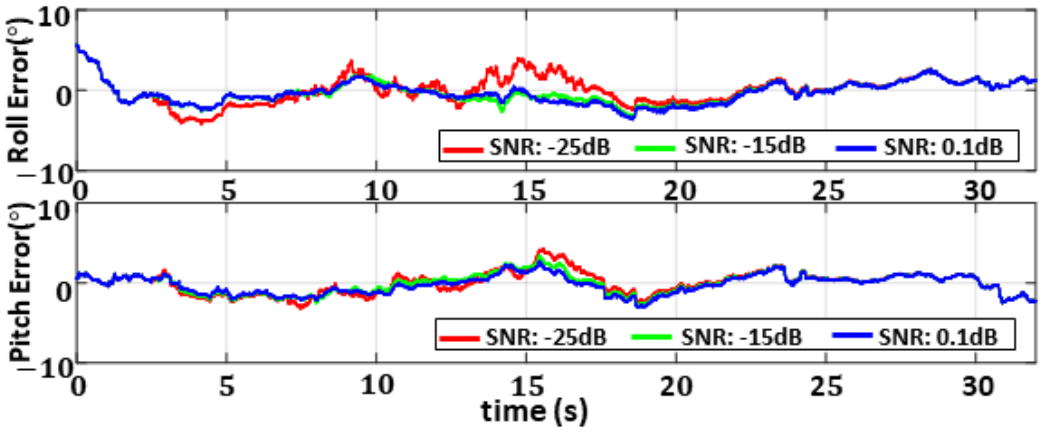

Figure 2.7 Error in the estimated roll and pitch at different noise levels.

Table 2.2. RMSE (radians) in estimated orientation in presence of external acceleration.

Noise duration	Orientation	SNR		
		0.1dB	**-15dB**	**-25dB**
1s	**Roll**	0.0192	0.0219	0.0103
	Pitch	0.0082	0.0108	0.0170
	Yaw	0.0345	0.0345	0.0345
10s	**Roll**	0.0122	0.0152	0.0335
	Pitch	0.0180	0.0237	0.0281
	Yaw	0.1154	0.1154	0.1154

B. Magnetic disturbance

In order to verify the filter's performance in presence of magnetic disturbance, we generated low–frequency Gaussian noise and added it to the measured magnetic field along the all three axes of the benchmark dataset. This allows for simulating contamination of magnetic field data in dynamic condition for different durations. Figure 2.8 shows the magnetic field data contaminated with simulated low–frequency disturbances and Figure 2.9 presents the error in the estimated orientation with respect to the ground truth.

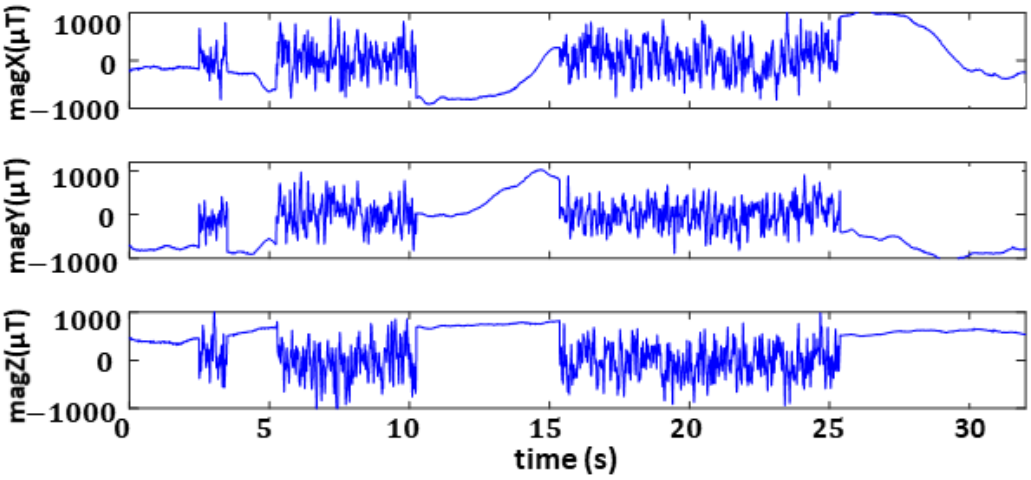

Figure 2.8 Magnetic field data contaminated with simulated low–frequency disturbances.

It can be seen that the estimated orientation angles and the error using the ground truth field and the externally disturbed magnetic field follow each other very closely, inferring a little effect of the external magnetic disturbance on the estimated yaw (See Figure 2.9).

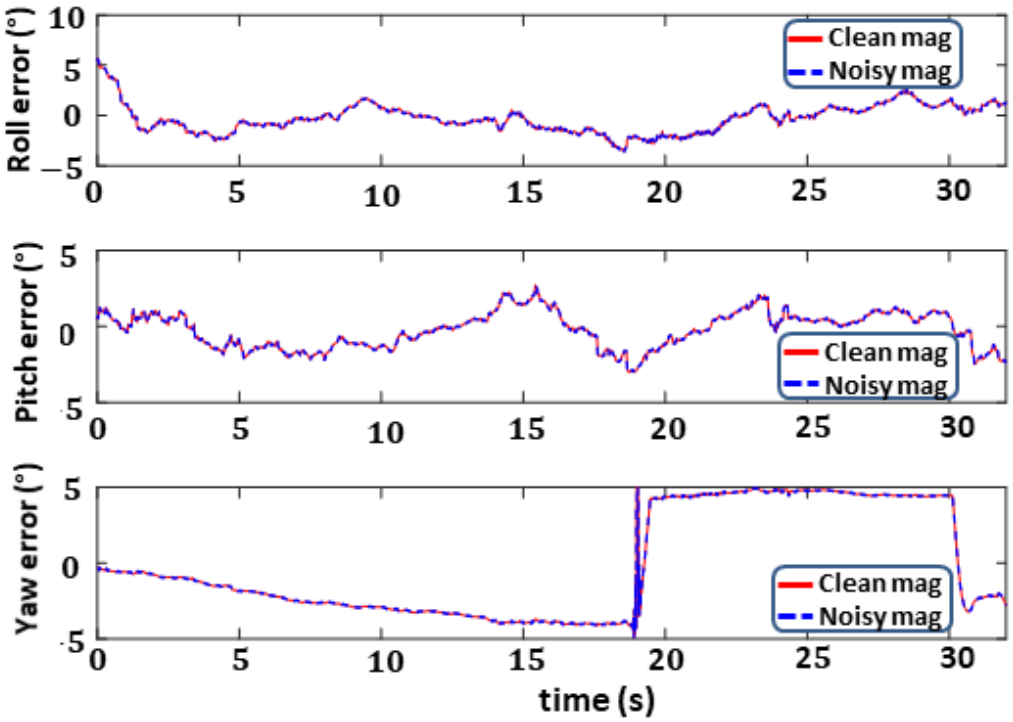

Figure 2.9 Error in the estimated orientation in the presence of magnetic disturbance.

This is due to the fact that, the orientation is obtained by estimating and subtracting the drift from the gyroscope measurement, which are not affected by any external acceleration or magnetic disturbances.

In addition to the simulation, we also performed an experiment where a MIMU was mounted on a wooden wheel and placed a magnet near the wheel. As we rotated the wheel the ambient magnetic field measured by the magnetometer was disturbed when the MIMU came closer to magnet (Figure 2.10). The MIMU was positioned in such a way that it rotated around its *z*–axis.

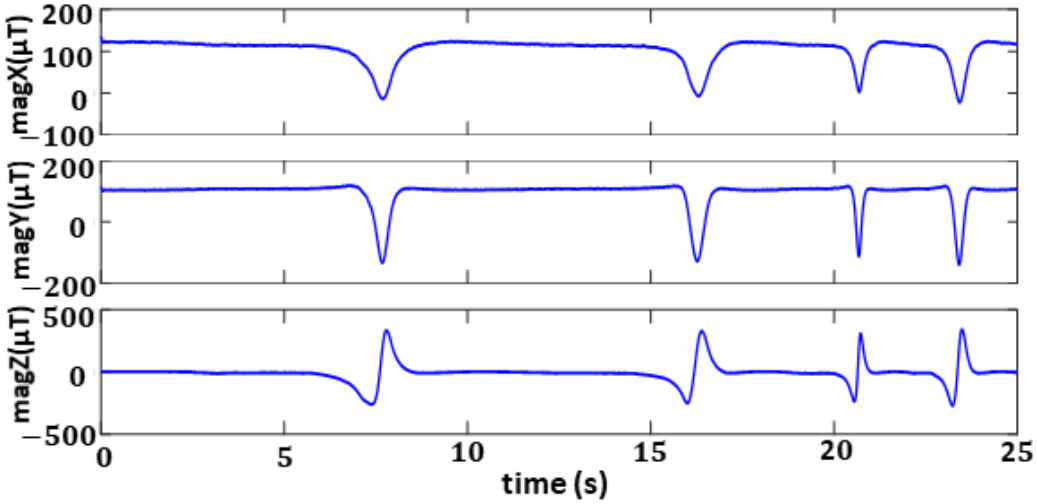

Figure 2.10 Magnetic field disturbance in presence of a magnet.

The Euler angles were estimated using the proposed filter. It can be seen from Figure 2.11 that the estimated yaw was little affected by the presence of external magnetic field and achieved a complete 360° rotation on every occasion.

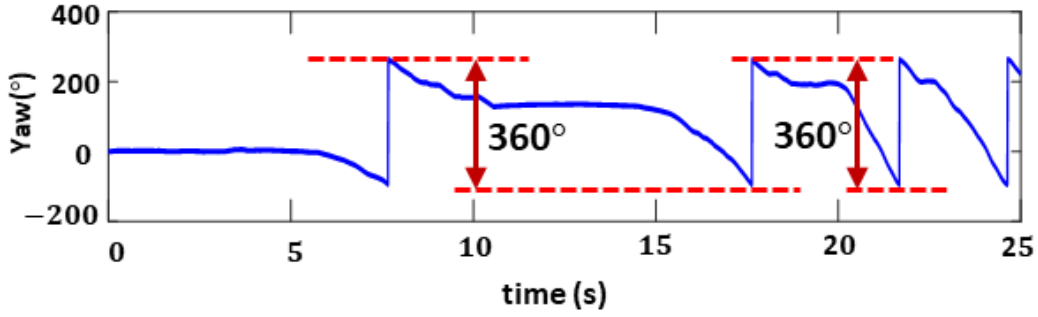

Figure 2.11 Estimated yaw using the proposed filter.

2.3.3 Gait parameter estimation

As discussed earlier, gait is strongly associated with our health condition. For example, people at the early onset of Parkinson's tend to walk with short and shuffled steps

[2.6],[2.30]. In addition, gait speed was reported to be strongly associated with cardiovascular disease related mortality [2.31]. Furthermore, older adults with high variability in the minimum foot clearance (MFC) are vulnerable to falling [2.32]. MIMUs, however, pave the way for simple, low–power, and unobtrusive solutions for in–home gait monitoring and assessment. In the final set of experiments, the proposed orientation filter is used to estimate some key gait parameters such as gait speed, and step length.

We mounted a MIMU from Mbientlab Inc (MetaMotionR) on an elastic band and attached the device on the top of a shoe (See Figure 2.12). The MIMU houses a set of sensors including a tri–axial accelerometer, a tri–axial gyroscope and a tri–axial magnetometer and can communicate with a Smartphone over the Bluetooth Low Energy Smart platform.

(a) (b)

Figure 2.12 Inertial measurement unit (a) commercial sensor (Mbientlab MetaMotionR) (b) mounting of the sensor.

A. Walk on plain surface

We recruited two participants to walk on a well illuminated and obstacle free 10–meter–long path at their preferred pace. The walking was video–recorded in an attempt to track the stride length for validation purposes. In order to minimize any possible bias, we repeated the experiment four times for each participant at different times of the day.

The orientation information obtained from the proposed filter was used to correct the acceleration measured in the sensor frame by using,

$$\boldsymbol{a} = \mathbf{R}(\varphi)\boldsymbol{a}' \tag{2.25}$$

where, $\boldsymbol{a}' = [a'_x \quad a'_y \quad a'_z]$, is the measured acceleration, $\boldsymbol{a} = [a_x \quad a_y \quad a_z]$, is the orientation corrected acceleration in the earth's frame, and $\mathbf{R}$ is the 3×3 rotation matrix,

which is a function of the estimated orientation φ. Therefore, an accurate estimation of orientation will result in an accurate rotation matrix.

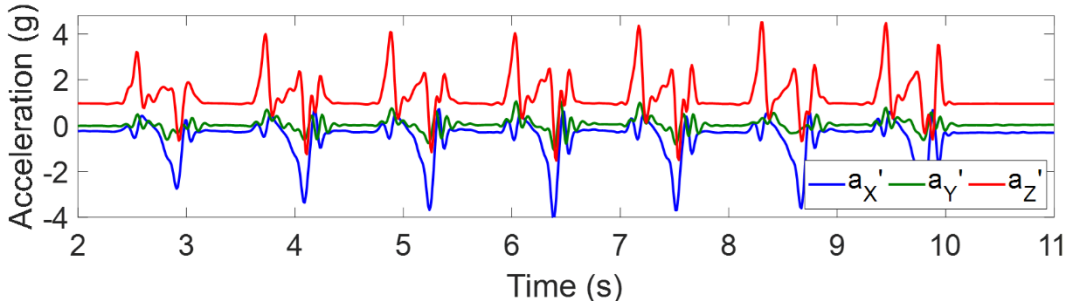

(a)

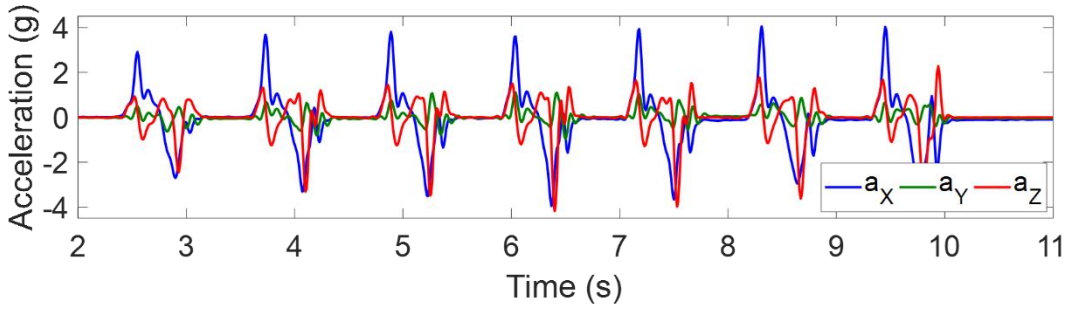

(b)

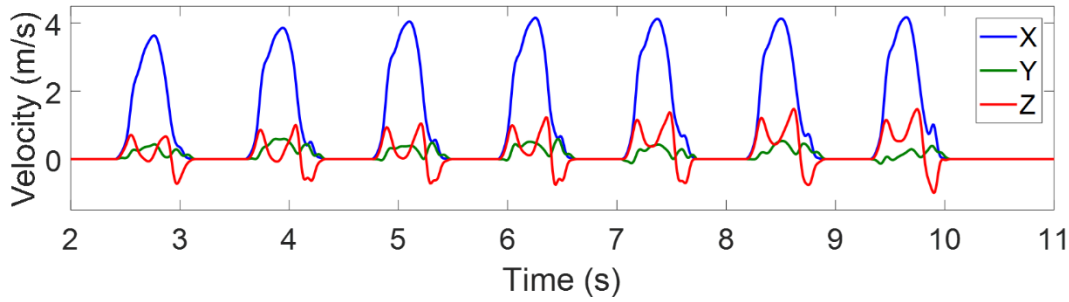

(c)

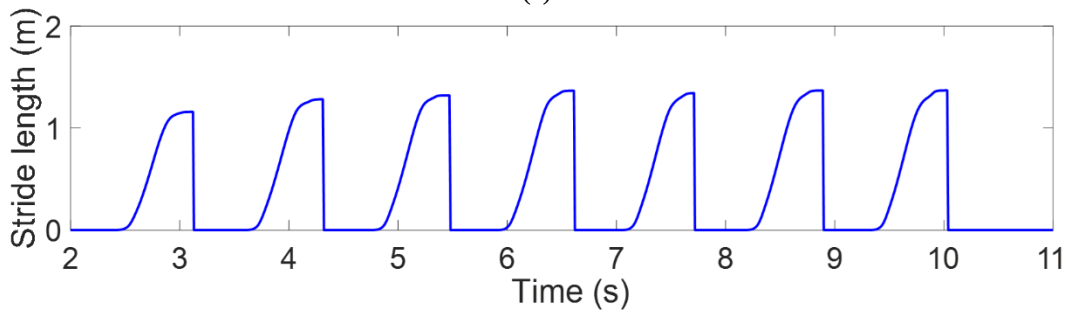

(d)

Figure 2.13 Gait parameter estimation– a) measured acceleration b) orientation corrected linear acceleration along three dimensions, c) drift–corrected instantaneous velocity and d) estimation of stride length.

This will eventually lead to an accurate estimation of linear acceleration, velocity and distance.is a function of the estimated orientation φ. Therefore, an accurate estimation of orientation will result in an accurate rotation matrix, which will eventually lead to an accurate estimation of linear acceleration, velocity and distance. The acceleration due to gravity, g, was subtracted from the corrected acceleration in the earth frame to obtain the linear acceleration. We employed a simple zero velocity update (ZUPT) approach while integrating the linear acceleration to obtain a drift–free estimate of velocity. The velocity thus obtained was then integrated to obtain the stride length. Figure 2.13 shows an example of measured acceleration, corrected acceleration, instantaneous gait speed, and forward displacement of the foot during walking. The results from all eight sets of experiments are presented in Table 2.3. The root mean square error (RMSE) of the calculated stride length is 1.64 cm. It can be seen that the average stride length remains consistent for each participant throughout the experiments.

Table 2.3 Experimental validation of stride length calculation.

Subject	**Experiment**	**Average Stride Length (cm)**		
		True	**Calculated**	**RMSE**
1	1	158	157	1.64
	2	152	151	
	3	158	157	
	4	157	156	
2	1	126	123	
	2	121	120	
	3	126	123	
	4	121	120	

B. Staircase climbing

In another experiment, we asked a participant to climb a staircase with the MIMU sensor mounted on the top of the shoe as shown in Figure 2.12. The measured acceleration, angular velocity and magnetic field data were fed into the proposed orientation filter to obtain the three–dimensional trajectory of the staircase climbing. The measured magnetic field and acceleration during the staircase climbing were found to be contaminated with external disturbances at every step, with the acceleration reaching to as high as 8g. Figure 2.14

presents the photograph of the staircase and the estimated trajectory of the staircase climbing obtained from the proposed orientation filter. Each step of the staircase was 17 cm high and 26 cm wide. We employed the simple ZUPT approach to calculate the height and length of each step of the staircase. The mean height and width of each step was 16.8 cm and 26.1 cm, respectively with an RMSE of 8.7% and 8.5%, respectively. However, the accuracy of estimated dimensions can be further improved by using high–accuracy position estimation approaches such as adaptive threshold–based ZUPT [2.33] or a Kalman filter–based approach [2.34].

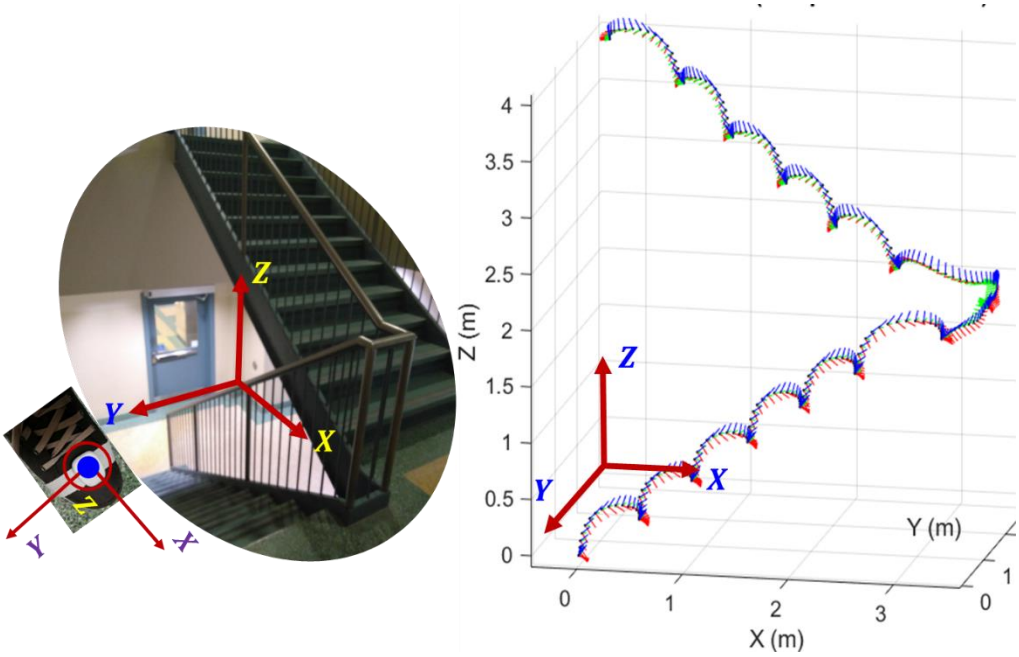

Figure 2.14 Photograph of the staircase and estimated trajectory of staircase climbing using the proposed orientation filter.

2.4 Conclusions

Inertial motion and magnetic field sensors have become an integral part of modern–day smart gadgets. They can potentially be important components in the forthcoming era of smart home technologies, Internet–of–Things (IoT), and Internet–of–Everything (IoE). These miniature, low–power sensors, coupled with high–speed computing and communication technologies may enable in–home monitoring and assessment of people's gait pattern, mobility, fitness and overall health in a continuous fashion without interrupting

their daily living. However, the orientation of the on–body sensors can be arbitrary, and if it is not corrected, may result in inaccuracies in the estimation and assessment of gait parameters. In this work, we have designed, implemented and validated a three–stage sensor fusion algorithm that outputs sensor orientation in Euler angles. We estimated the drift in the integrated gyroscope data using a gradient descent approach and subtracted it from the integrated gyroscope data to obtain the orientation in real time. The inclusion of the third stage of yaw estimation increased the estimation accuracy. As the estimation was made primarily based–on the gyroscope data, the estimated orientation was observed to be least affected by external acceleration and magnetic disturbances. Due to the adoption of a complementary filter–based approach, the proposed algorithm is inherently computationally efficient and well suited for real–time applications. However, in order to demonstrate a fair comparison with other filters, the proposed algorithm was validated using a publicly available dataset, and it showed better results for most parameters. The robustness of the algorithm was further tested in the presence of simulated external acceleration and magnetic disturbances. Finally, the proposed filter was used to derive some key gait parameters, such as stride length, gait asymmetry, gait speed, minimum foot clearance and gait variation, from gait measurements, which show high conformity to the ground–truth values.

Chapter 3
Real–time monitoring of lower–limb joints

An IMU–based system for monitoring the lower–limb joint health can be a cost–effective solution to measure and analyze human mobility that is known to have a strong association with one's muscle strength, fitness and overall health [3.1]–[3.10]. For example, the range of motion (ROM) of the lower–limb joints (hip, knee and ankle) decreases significantly with the progression of age as a result of age–related deterioration of the musculoskeletal system [3.9], [3.11]. In addition, ROM of lower–limb joints can provide useful predictive information about the early onset of the knee and hip osteoarthritis, which are reportedly associated with an increased risk of death from cardiovascular disease (CVD) [3.9],[3.12]. Therefore, regular monitoring of lower–limb joints is critical to assess the health of the joint, gait and activity performance, rehabilitation following an injury, and the onset of osteoarthritis. At present, clinicians primarily use video imaging–based tracking systems for the assessment of lower–limb joints and gait [3.6],[3.9]. Although these systems can provide accurate and comprehensive information, they, however, require skilled manpower, specialized infrastructure with several mounted cameras, high computational resources for image processing and analysis, and large memory size for storage. Therefore, imaging–based systems are not particularly suitable for continuous and in–home monitoring of lower–limb joints. Many researchers also proposed alternative measures for monitoring knee joints using optical fiber sensors [3.13], [3.14], textile–based strain sensors

[3.15], and flexible conductive wire [3.16]. The performance of these optical and flexible sensors, however, deteriorates over time due to mechanical wear and tear. In addition, these solutions are obtrusive and thus are not suitable for long–term applications.

There is a growing interest among researchers in using miniature and low–power IMUs to realize unobtrusive, accurate and sensitive joint monitoring systems [3.6], [3.17], [3.18]. Multiple IMUs can be embedded in a wearable platform and connected wirelessly through a Body Sensor Network (BSN) to enable real–time monitoring of lower–limb joint movement [3.1], [3.6], [3.8]. In this chapter, we present a two–stage complementary filter–based approach to estimate the lower–limb joint angles from IMU data in real–time.

3.1 Background

In a typical IMU–based joint monitoring system, measurements acquired by the accelerometer, gyroscope and magnetometer of each IMU attached above and below the joint are combined to obtain an estimate of the joint angle. It is critical to develop an efficient sensor fusion algorithm for joint angle estimation in terms of ease of its implementation and computational complexity for real–time applications.

Ideally, the absolute angles of the neighbouring limb–segments of a joint can be obtained by simply integrating the gyroscope data. However, the problem of estimating absolute angles by integrating gyroscope data arises from the presence of integration drift in the calculated angle resulting from the accumulation of noise over time. Therefore, some researchers attempted using only accelerometers for obtaining joint angles. For example, the authors in [3.19] estimated the knee joint angle by using four accelerometers where two accelerometers were attached to each limb segments above and below the joint. The difference of signals from two accelerometers attached to a segment was passed through a band–pass filter (BPF) to obtain the absolute angle of the segment. The absolute angles obtained from the two segments were subtracted to obtain the joint angle. However, the joint angle thus obtained still had a drift problem that was minimized by a second–order low–pass Butterworth filter. The drift was further improved by incorporating a high–pass filter (HPF) in conjunction with the low–pass filter (LPF). However, the proposed approach

suffers from poor estimation accuracy, particularly at lower gait speeds. In addition, the use of a number of filters may introduce significant delay in the system output. Furthermore, using four accelerometers to estimate the angle of one joint is not a feasible solution for wearable systems in terms of ease–of–use, comfort and power requirements. Another key problem of accelerometer–based joint monitoring systems is that accelerometers are sensitive to high–frequency noise and vibrations associated with gait events and muscle movements. In an attempt to avoid dependence on noisy accelerometer data, the authors in [3.20] developed a gyroscope–based algorithm to estimate joint angles. There, they identified the knee angle minima at every gait cycle, and then integrated the gyroscope data until the next knee angle minima to obtain a drift–free estimate of the joint angle. This model requires accurate detection of the knee angle minima at every stride that may limit the application of the algorithm, making it inappropriate for users who cannot extend their knee completely. However, this algorithm, as mentioned by the authors, can be useful for users who exhibit decreased swing flexion during gait.

As discussed earlier, measurements by the accelerometer can be contaminated with external noise and disturbances but are free from drift problems [3.21], [3.22]. In contrast, gyroscope measurements are inherently robust against external high–frequency noise; however, may suffer from low–frequency drift. To deal with integration drift of the accelerometers and the low–frequency drift of the gyroscopes while estimating joint angles, researchers mostly exploited Kalman filter–based approaches. For example, an unscented Kalman Filter (UKF) was used in [3.23] to estimate joint angles using body–worn IMUs. There, they exploited the kinematic models developed for control of robotic arms and expressed the model in state–space form, which was later used in the UKF to track the joint angle. The algorithm can potentially be used with any combination of sensors and can handle sensor malfunction or missing information. However, the authors verified the performance of the algorithm with synthetic data only. Moreover, the equations for the process model and the observation model were complicated and non–linear, thus making the approach computationally intensive for real time applications.

Kalman filter was used in [3.24] to estimate the roll and pitch of each IMU attached above

and below the joint. Then they took advantage of biomechanical constraints based on joint anatomy to estimate the knee joint angle. Although the authors reported achieving good accuracy with respect to the measurement from a standard camera–based system for knee joint estimation, the non–linear nature of Gauss–Markov process, which was used to model accelerations, angular velocity and gyro biases, can potentially make this method computationally intensive for real–time applications. A quaternion–based extended Kalman filter (EKF), derived from a first–order linear model of the human musculoskeletal system, was implemented for joint ROM tracking in [3.25]. The model expressed the motion dynamics of the human musculoskeletal system while assuming the limb segments as rigid bodies of three degrees of freedom (DOF) that move independently of each other. Unlike in [3.23] and [3.24], the linear nature of the measurement equations of the Kalman filter proposed in [3.25] can significantly reduce the overall computational cost, thus making the algorithm potentially suitable for real–time systems. However, linearization of the model may lead to a system that is sensitive to initial conditions and vulnerable in terms of convergence and stability, especially at lower sampling rates [3.22], [3.26].

Nevertheless, in applications such as motion tracking, signal filtering and sensor fusion, Kalman filter based methods generally offer superior performance in terms of accuracy and speed [3.21], [3.27]. However, one major concern for such Kalman filter–based approaches is their requirement of covariance matrices of process noise and measurement noise that need to be determined experimentally. Furthermore, Kalman filter requires inversion of large matrices that increases the computational complexity of the algorithm, and thereby can potentially adversely affect the computing time and the battery life of portable and wearable systems [3.22],[3.28].

Complementary Filter (CF)–based techniques have the advantage of being computationally efficient because they exploit information from at least two separate sources to obtain a final estimate [3.22]. CF–based joint angle estimation techniques combines information from the gyroscope, accelerometer, and/or magnetometer to estimate the joint angle and thus overcome the limitations of each source. Such CF–based approaches were proposed in [3.29], [3.30], where the accelerometer and gyroscope data were fused to determine the

knee and joint angles. Similar to [3.24] they made use of biomechanical constraints based on the joint anatomy to simplify the formulation of the problem and assumed the dynamical acceleration is negligible with respect to the acceleration due to gravity. Although the acceleration due to gravity dominates the dynamic acceleration signals in most practical situations, this assumption is not valid at low frequencies.

The authors in [3.31] addressed this problem and proposed a complementary filter–based method that exploited a previously published [3.32] acceleration propagation–based method for the low frequency regime and gyroscope data for high frequency estimation. In order to avoid dealing with a large estimation error due to magnetic disturbances from ambient ferromagnetic materials in the indoor measurements, most researchers understandably preferred to not use the magnetometer data when developing joint monitoring algorithms. However, the accelerometer data can get also contaminated by external acceleration associated with gait anomalies, prosthetic lower–limbs, scar and adipose tissue, particularly during the stance phase of the gait [3.20]. The presence of high external acceleration can lead to inaccuracies in the estimated joint angles. However, none of the above approaches compensate for external acceleration or assess its impact on the accuracy of the estimated joint angles.

3.2 Proposed method

In this work, we propose a two–stage complementary filter that can estimate the joint angles of the lower limb using the accelerometer and gyroscope data from two MIMUs attached above and below the joint. The accelerometer data is exploited in the first stage based–on an approach proposed in [3.22] to estimate and compensate for the integration drift in the roll and pitch of the IMUs obtained thorough integration of the gyroscope measurements around the *x*– and *y*– axes, respectively. This approach allows for obtaining roll and pitch information of the IMUs from the gyroscope measurements, which are inherently robust against high–frequency noise and vibrations, thus making the estimation least affected by the external acceleration. In the second stage, the joint angle is estimated by fusing the

inclination (roll and pitch) information of both the MIMUs obtained in the first stage. The block diagram of the proposed orientation filter is shown in Figure 3.1.

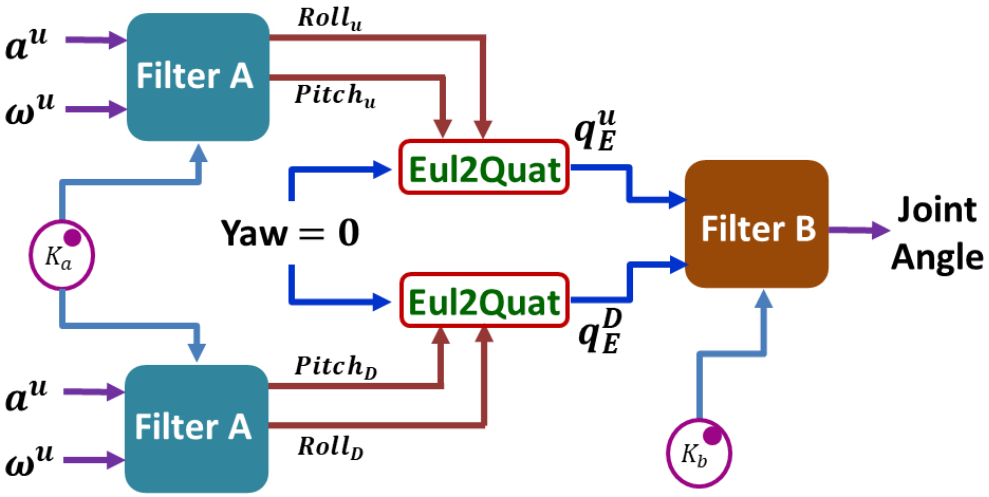

Figure 3.1 Proposed two–stage filter for joint angle estimation.

3.2.1 Stage one: estimation of inclination

Since the orientation of each IMU attached to the limb segments above and below the joint is arbitrary, it is first necessary to correct the sensor orientation. In the first stage, Filter–A estimates and corrects the orientation of the IMUs to align them with the earth's reference frame.

The angular velocity of the IMU above the joint (ω_m^u) about the x, y and z axes are measured with a tri–axial gyroscope that can be expressed as,

$$\omega_m^u = [\omega_{mx}^u \quad \omega_{my}^u \quad \omega_{mz}^u]. \tag{3.1}$$

The three–dimensional orientation of this sensor φ_m^u can be obtained by integrating ω_m^u over time, i.e.

$$\varphi_m^u = [\Phi_m^u \quad \theta_m^u \quad \psi_m^u] = \int_{t_i}^{t_f} \omega_m^u dt = \sum_{k=1}^{{t_f - t_i}/{T}} T\omega_{m,k}^u \ , \tag{3.2}$$

where, Φ_m^u, θ_m^u and ψ_m^u represent the roll, pitch and yaw of the IMU above the joint, respectively, and T is the sampling interval of the gyroscope.

However, the measured angular velocity drifts over time, which is in addition to the measurement noise accumulates during the integration of the gyroscope data. This causes

the calculated orientation to drift over time. Therefore, at any given time, φ_m^u can be expressed as,

$$\varphi_m^u = \varphi_{tr}^u + \varphi_{dr}^u, \tag{3.3}$$

where, φ_{tr}^u represents the true orientation and φ_{dr}^u is the amount of integration drift in the orientation obtained from the gyroscope.

Eq. 3.3 can be rearranged as,

$$\varphi_{dr}^u = \varphi_m^u - \varphi_{tr}^u. \tag{3.4}$$

An optimization problem can be formulated from Eq. 3.4, where φ_{dr}^u may be estimated from the solution to the Eq. 3.5,

$$\min_{\varphi_{dr}^u \in \Re} f(\varphi_{dr}^u, \varphi_m^u, \varphi_{tr}^u), \tag{3.5}$$

where, Eq. 3.6 defines the optimization problem.

$$f(\varphi_{dr}^u, \varphi_m^u, \varphi_{tr}^u) = \varphi_{dr}^u - (\varphi_m^u - \varphi_{tr}^u). \tag{3.6}$$

By exploiting the gradient descent algorithm with an initial orientation $\varphi_{dr,0}^u$, and a step–size K_a, the drift φ_{dr}^u can be estimated iteratively as presented in Eq. 3.7.

$$\varphi_{dr,i+1}^u = \varphi_{dr,i}^u - K_a \frac{\nabla f(\varphi_{dr}^u, \varphi_m^u, \varphi_{tr}^u)}{\left\| \nabla f(\varphi_{dr}^u, \varphi_m^u, \varphi_{tr}^u) \right\|} \quad . \qquad i = 1,2,3 \ldots \tag{3.7}$$

Here, ∇f represents the gradient of the solution surface and is given by,

$$\nabla f(\varphi_{dr}^u, \varphi_m^u, \varphi_{tr}^u) = J_f^T(\varphi_{dr}^u) f(\varphi_{dr}^u, \varphi_m^u, \varphi_{tr}^u), \tag{3.8}$$

where, J_f represents the Jacobian of the objective function $f(\varphi_{dr}^u, \varphi_m^u, \varphi_{tr}^u)$.

The drift, φ_{dr}^u, which evolves from the accumulation of noise during the integration of the gyroscope measurements is independent of the true orientation φ_{tr}^u. In the ideal case, φ_{tr}^u can be obtained from the accelerometer. However, in practical and dynamic applications, accelerometer measurements are contaminated with external noise and disturbances. Therefore, the Jacobian J_f of the objective function can be presented using Eq. 3.6 as,

$$J_f^T(\varphi_{dr}^u) = 1 - \frac{\partial \varphi_m^u}{\partial \varphi_{dr}^u}. \tag{3.9}$$

Assuming that the sensor undergoes a small incremental change in the orientation at every sample, then Eq. 3.9 can be approximated as,

$$J_f^T(\varphi_{dr}^u) \approx 1. \tag{3.10}$$

Consequently, Eq. 3.8 can be simplified as,

$$\nabla f(\varphi_{dr}^u, \varphi_m^u, \varphi_{tr}^u) \approx f(\varphi_{dr}^u, \varphi_m^u, \varphi_{tr}^u). \tag{3.11}$$

Therefore, Eq. 3.7 can be rearranged as

$$\varphi_{dr,i+1}^u \approx \varphi_{dr,i}^u - K_a\left(\varphi_{dr,i}^u - \left(\varphi_{m,i}^u - \varphi_{tr,i}^u\right)\right), \quad i = 1,2,3 \ldots \tag{3.12}$$

where,

$$\varphi_{m,i}^u = \sum_{k=1}^{i} T\omega_{m,k}^u, \tag{3.13}$$

and

$$\begin{aligned} \Phi_{tr,i}^u &= \arctan\left(\frac{a_{y,i}}{a_{z,i}}\right), && \text{roll} \\ \theta_{tr,i}^u &= -\arctan\left(\frac{a_{x,i}}{\sqrt{a_{y,i}^2 + a_{z,i}^2}}\right). && \text{pitch} \end{aligned} \tag{3.14}$$

Here, $a_{x,i}$, $a_{y,i}$ and $a_{z,i}$ are the i–th measurements from the accelerometer along the x, y and z axes, respectively.

Then, the drift–free estimate of the roll and pitch angle $\breve{\varphi}_{tr,i+1}^u$ of the IMU above the joint can be obtained from

$$\breve{\varphi}_{tr,i+1}^u \approx \varphi_{m,i+1}^u - \varphi_{dr,i+1}^u. \tag{3.15}$$

A drift–free estimate of the roll and pitch angle $\breve{\varphi}_{tr,i+1}^D$ of the IMU below the joint can also be obtained similarly and is given as

$$\breve{\varphi}_{\mathrm{tr},i+1}^D \approx \varphi_{\mathrm{m},i+1}^D - \varphi_{dr,i+1}^D. \tag{3.16}$$

3.2.2 Second stage: estimation of joint angle

For the healthy population, it is sufficient to assume that the flexion–extension of the lower limb joints such as hip, knee and ankle occurs only around the transverse axis of the body (y–axis) [3.19]. Therefore, any movement of the IMUs around the vertical z–axis (Yaw) can be reasonably neglected.

(a) (b)

Figure 3.2 Aligning sensor frame to the earth frame assuming no rotation around the vertical *z*–axis.

The drift–corrected roll ($\breve{\Phi}_{tr}^{u}$) and pitch ($\breve{\theta}_{tr}^{u}$) information obtained in the first stage for the upper IMU are used to calculate a quaternion, q_E^u while assuming a zero rotation around the *z*–axis (Yaw), i.e.

$$q_E^u = f(\breve{\varphi}_{tr}^{u}) \,, \tag{3.17}$$

where, $\breve{\varphi}_{tr}^{u} = [\breve{\Phi}_{tr}^{u} \quad \breve{\theta}_{tr}^{u} \quad 0]$ and $q_E^u = [q_0^u \quad q_1^u \quad q_2^u \quad q_3^u]$. Assuming the device does not experience any rotation around the *z*–axis, a rotation by an amount of q_E^u aligns the upper IMU frame F_U, to the earth frame F_E, (see Figure 3.2).

Similarly, the drift–corrected roll ($\breve{\Phi}_{tr}^{D}$) and pitch ($\breve{\theta}_{tr}^{D}$) information of the IMU below the joint obtained in the first stage are used to calculate a quaternion q_E^D, while assuming a zero rotation around the *z*–axis (Yaw), i.e.

$$q_E^D = f(\breve{\varphi}_{tr}^{D}) \,, \tag{3.18}$$

where, $\breve{\varphi}_{tr}^{D} = [\breve{\Phi}_{tr}^{D} \quad \breve{\theta}_{tr}^{D} \quad 0]$ and $q_E^D = [q_0^D \quad q_1^D \quad q_2^D \quad q_3^D]$.

The upper IMU frame, q_E^u rotates by q_u^D to align with the lower IMU frame q_E^D (See Figure 3.3), i.e.

$$q_E^D = q_E^u \otimes q_u^D, \tag{3.19}$$

where, $q_u^D = [q_{u0}^D \quad q_{u1}^D \quad q_{u2}^D \quad q_{u3}^D]$.

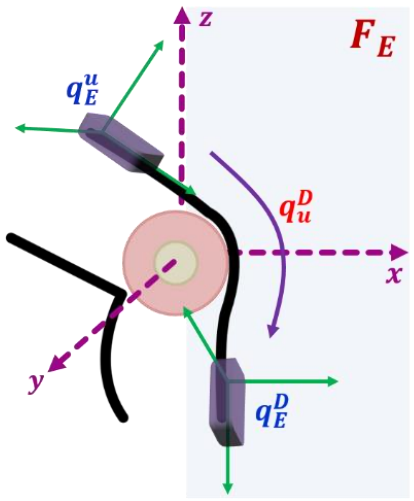

Figure 3.3 Rotation of the joint in the reference frame.

Eq. 3.18 allows for formulating an optimization problem, where q_u^D may be obtained as the solution to the Eq. 3.20,

$$\min_{q_u^D \in \Re} G(q_u^D, q_E^D, q_E^u), \tag{3.20}$$

where, the optimization problem is defined as Eq. 3.21.

$$G(q_u^D, q_E^D, q_E^u) = q_E^D - (q_E^u \otimes q_u^D). \tag{3.21}$$

The quaternion corresponding to the joint angle q_u^D, can be estimated iteratively by using the gradient descent algorithm with an initial orientation, $q_{u,0}^D$ and a step–size K_b, as presented in Eq. 3.22.

$$q_{u,i+1}^D = q_{u,i}^D - K_b \frac{\nabla G(q_u^D, q_E^D, q_E^u)}{\|\nabla G(q_u^D, q_E^D, q_E^u)\|} \quad . \qquad i = 1,2,3 \ldots \tag{3.22}$$

Here, ∇G denotes the gradient of the solution surface and is given by,

$$\nabla G(q_u^D, q_E^D, q_E^u) = J_G^T(q_u^D) G(q_u^D, q_E^D, q_E^u), \tag{3.23}$$

where, J_G is the Jacobian of the objective function $G(q_u^D, q_E^D, q_E^u)$.

Considering the flexion–extension (α) of the lower–limb joints (i.e. hip, knee and ankle) occur only around the y–axis of the earth frame, the quaternion q_u^D can be simplified as,

$$q_u^D = [q_{u0}^D \quad 0 \quad q_{u2}^D \quad 0], \tag{3.24}$$

where

$$\alpha = 2\arctan\left(\frac{q_{u2}^D}{q_{u0}^D}\right). \tag{3.25}$$

Then, Eq. 3.21 can be reorganized as,

$$G = \begin{bmatrix} q_0^D - q_0^u q_{u0}^D + q_2^u q_{u2}^D \\ q_1^D - q_1^u q_{u0}^D + q_3^u q_{u2}^D \\ q_2^D - q_2^u q_{u0}^D - q_0^u q_{u2}^D \\ q_3^D - q_1^u q_{u2}^D - q_3^u q_{u0}^D \end{bmatrix}, \tag{3.26}$$

and the Jacobian J_G of the of the objective function $G(q_u^D, q_E^D, q_E^u)$ becomes

$$J_G(q_u^D) = \begin{bmatrix} -q_0^u & 0 & q_2^u & 0 \\ -q_1^u & 0 & q_3^u & 0 \\ -q_2^u & 0 & -q_0^u & 0 \\ -q_3^u & 0 & -q_1^u & 0 \end{bmatrix}. \tag{3.27}$$

Eq. 3.21, Eq. 3.25, and Eq. 3.26 are then combined to obtain a real–time estimate of the quaternion, $q_{u,i+1}^D$ corresponding to the joint angle. The joint angle can then be obtained by rearranging Eq. 3.25 as

$$\alpha_{i+1} = 2 \arctan\left(\frac{q_{u2,i+1}^D}{q_{u0,i+1}^D}\right). \tag{3.28}$$

Finally, α_{i+1} is passed through a second–order Butterworth low–pass filter (cut–off frequency 10 Hz) to remove the high–frequency components from the estimated angle.

3.3 Performance evaluation

The performance of the proposed joint monitoring algorithm was evaluated at three different walking speeds and compared with the ground truth measurements obtained using a camera–based standard system. In this section, we present the performance of our proposed filter in terms of estimation accuracy and robustness against external acceleration.

3.3.1 Joint angle estimation

In order to evaluate the performance of the proposed algorithm, we tested the designed filter on a publicly available benchmark dataset [3.33], [3.34]. Four IMU sensors were attached on the trunk, thigh, shank and foot of each participant, who walked on the treadmill at four different speeds of $0.5\, ms^{-1}, 1.0\, ms^{-1}$, $1.5\, ms^{-1}$ and their own comfort. The participants wore a marker set of Strathclyde functional cluster model [3.34], [3.35] to enable video tracking of their gait phases. A twelve camera Vicon motion capture system

obtained the ground truth measurements of the lower–limb joints synchronously with the IMU data at a rate of 100 samples per second.

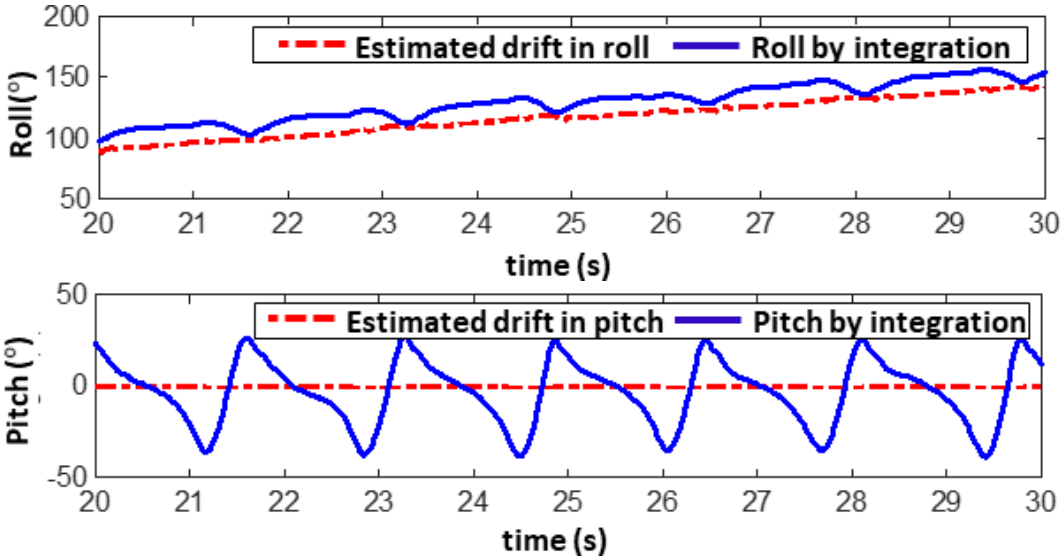

Figure 3.4 Estimated integration drift in the roll and pitch angles.

An instance of the integrated gyroscope data and the real–time estimate by Filter–A of the integration drift from the accelerometer data is presented in Figure 3.4. The integration drift thus obtained is subsequently subtracted from the roll and pitch angles obtained by integrating the gyroscope measurements around the x– and y– axes, respectively.

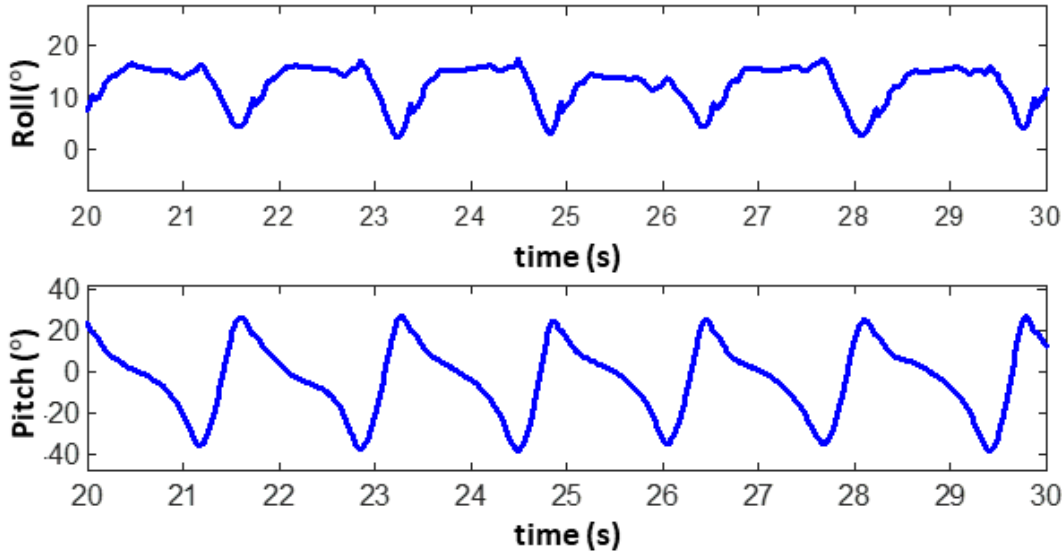

Figure 3.5 Estimated roll and pitch at the end of first stage.

Filter–A thus outputs a drift free real–time estimate of roll and pitch of the IMU. An example of the estimated roll and pitch of the IMU at the output of Filter–A is presented in

Figure 3.5. The estimated roll and pitch of both IMUs above and below the joint are fused in Filter–B, which then outputs the trajectory of the flexion–extension angle of the joint in real–time. An example of the estimated angles from each of the hip, knee and ankle joints at 0.5 ms^{-1} walking speed on a treadmill with respect to the ground–truth measurements obtained from the Vicon motion capture system is shown in Figure 3.6. The proposed joint monitoring method was tested using the IMU data obtained from three subjects, who walked on a treadmill at four different speeds of 0.5 ms^{-1}, 1.0 ms^{-1}, 1.5 ms^{-1} and their own comfort.

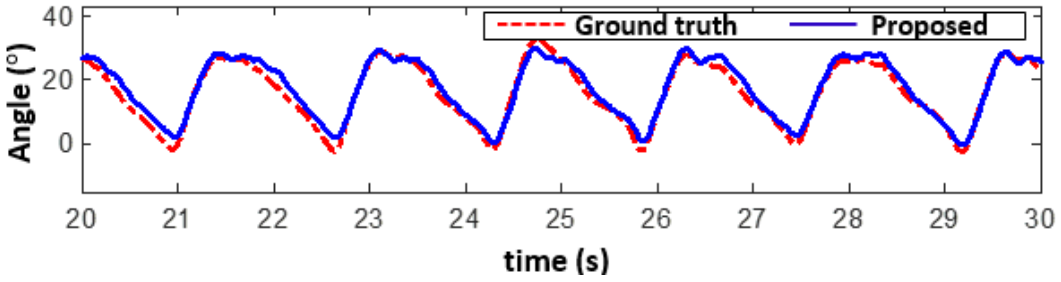

(a)

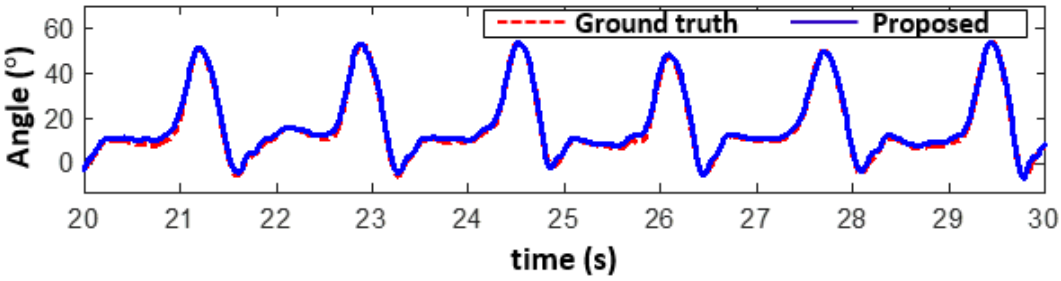

(b)

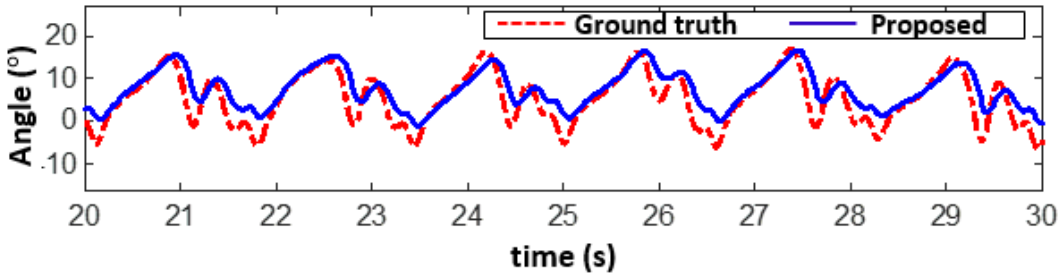

(c)

Figure 3.6 Estimated angles with respect to the ground truth for– a) thigh joint b) knee joint, and c) ankle joint.

The performance of the proposed filter was evaluated with respect to the camera–based system in terms of Root Mean Square Error ($RMSE$) and Pearson correlation coefficient (r) that are presented in Table 3.1.

Table 3.1 Performance of the proposed filter with respect to the ground truth.

Speed	0.5 ms^{-1}		1.0 ms^{-1}		1.5 ms^{-1}		Average	
	RMSE	*r*	RMSE	*r*	RMSE	*r*	RMSE	*r*
Thigh	1.91 °	0.978	2.61 °	0.981	3.02 °	0.983		
Knee	1.73 °	0.996	1.94 °	0.997	2.07 °	0.997	**2.50** °	**0.951**
Ankle	3.15 °	0.832	2.69 °	0.894	3.17 °	0.897		

It can be seen that the proposed method yields a highly accurate estimate of the lower–limb joint angles, showing a good agreement to the ground–truth with a mean r and mean $RMSE$ of 0.951 and 2.50°. In particular, the estimated knee and thigh joint angles shows excellent agreement with the ground–truth with a mean r of 0.997 and 0.982, respectively, thus making the proposed algorithm a suitable candidate for realizing a wearable in–home monitoring system of lower–limb joints. In addition, the average r for all joints at different speeds were found consistent. However, the average $RMSE$ for all joints were observed to increase slightly ($\sim$0.4°) with a 0.5 ms^{-1} increase of the walking speed. Nevertheless, the $RMSE$ in all cases remain within the mean error limit of 5°, which is accepted by the American Medical Association as reliable measurements for clinical evaluation of movement impairments [3.36].

3.3.2 Filter robustness

In the proposed knee joint monitoring method, the joint angle was calculated in the second stage using the roll and pitch of the IMUs obtained from the first stage. Since the proposed method does not use any magnetometer data for angle estimation, this approach is inherently insensitive to magnetic disturbances in the ambient magnetic field generated by ferromagnetic materials. In addition, the roll and pitch of the IMUs were obtained by estimating and adjusting for the drift in the integrated gyroscope data. Since the gyroscope measurements are inherently robust against high–frequency noise and vibration, the estimated orientation obtained at the output of the first stage, and thereby the joint angle estimated in the second stage is expected to be least affected by any external acceleration.

In this section, the robustness of the proposed method in the presence of an external acceleration is validated experimentally.

In order to verify the performance of the proposed method in the presence of an external acceleration, the simulated zero–mean white Gaussian noise was generated and added to the measured acceleration of both the IMUs in the benchmark dataset. This allows for simulating the dynamic accelerometer data contaminated at different signal–to–noise ratio (SNR) levels for different durations. Figure 3.7 shows the accelerometer data of both IMUs above and below the joint contaminated at two different SNR levels, where the acceleration fluctuated within a range of $\pm$2g.

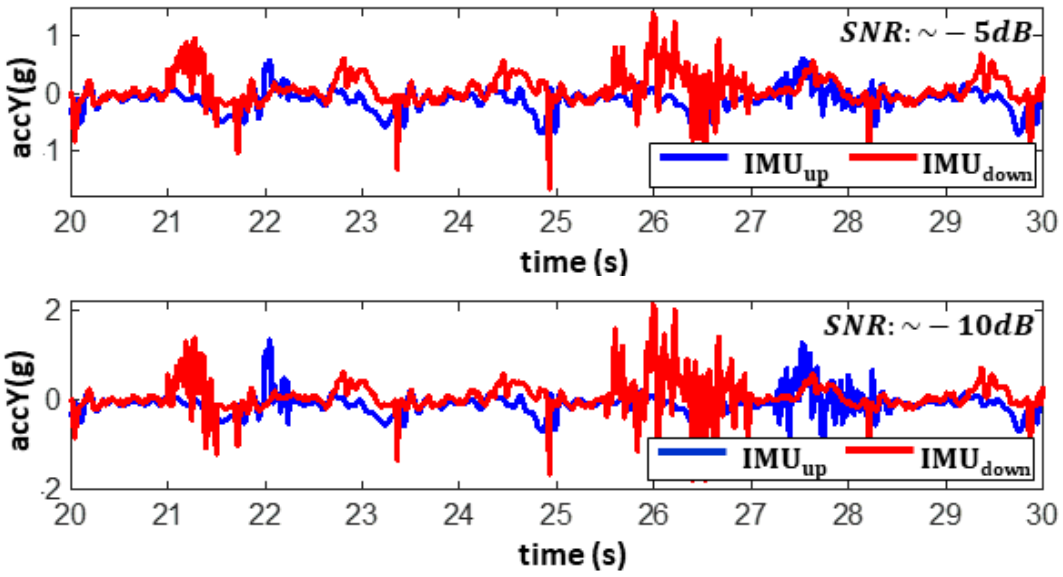

Figure 3.7 Accelerometer data contaminated at different noise levels. Data along the y–axis data is presented only.

The error in the estimated joint angles with respect to the ground truth at a walking speed of 0.5 ms^{-1} is shown in Figure 3.8. It can be seen that the error in the estimated joint angles changes slightly at a moderate level of SNR (~ –5dB) with respect to the error obtained using the actual accelerometer measurements. On the other hand, the error increase to some extent when the contamination is higher, but it quickly converges to the level of error from the actual accelerometer measurement as the external acceleration disappears. Therefore, the RMSE and the Pearson correlation coefficient (r) of the estimated angles for all three

joints change slightly during the duration of the external acceleration with respect to the error presented in Table 3.1 with the actual accelerometer measurements.

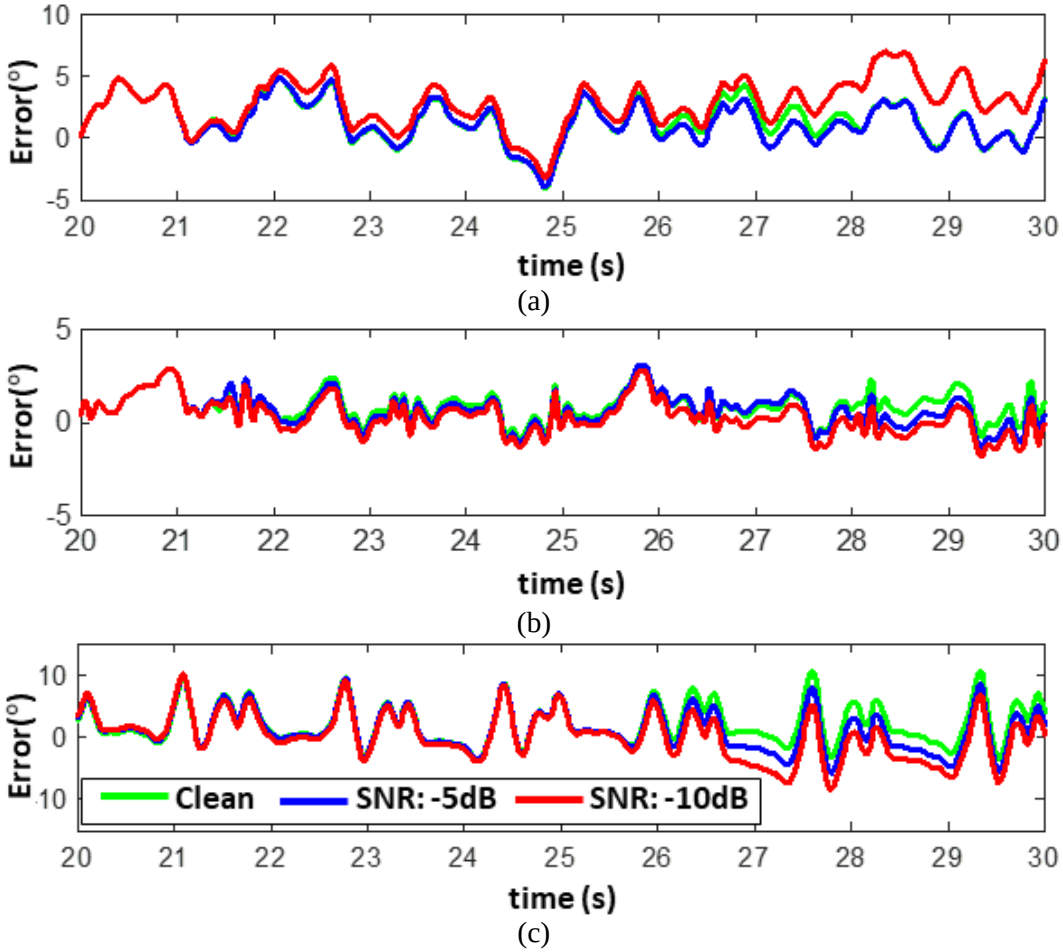

Figure 3.8 Error in the estimated angles at 0.5 ms^{-1} speed from a) hip joint, b) knee joint and c) ankle joint.

The RMS error of estimated joint angles in presence of external acceleration at all four different speeds are presented in Table 3.2.

Table 3.2 RMS error of estimated joint angles in presence of external acceleration.

	Thigh						Knee						Ankle					
Speed	**0.5 ms^{-1}**		**1.0 ms^{-1}**		**1.5 ms^{-1}**		**0.5 ms^{-1}**		**1.0 ms^{-1}**		**1.5 ms^{-1}**		**0.5 ms^{-1}**		**1.0 ms^{-1}**		**1.5 ms^{-1}**	
SNR	**RMSE**	***r***	**RMSE**	***r***	**RMSE**	***r***	**RMSE**	***r***	**RMSE**	***r***	**RMSE**	***r***	**RMSE**	***r***	**RMSE**	***r***	**RMSE**	***r***
Clean	1.91°	0.978	2.61°	0.981	3.02°	0.983	1.73°	0.996	1.94°	0.997	2.07°	0.997	3.15°	0.832	2.69°	0.894	3.17°	0.897
-5 dB	2.10°	0.973	2.67°	0.980	3.21°	0.981	1.71°	0.995	2.03°	0.997	2.14°	0.996	3.15°	0.829	3.53°	0.826	3.61°	0.853
-10 dB	2.15°	0.972	2.91°	0.975	3.05°	0.981	1.77°	0.996	2.22°	0.996	2.34°	0.995	3.33°	0.810	3.76°	0.808	4.04°	0.823
Mean			**2.63°**	**0.978**					**1.99°**	**0.996**					**3.38°**	**0.841**		

It can be seen from Figure 3.8 and Table 3.2 that the proposed algorithm can withstand a moderate level of variation ($\pm$1g) in the external acceleration while estimating the joint angles for thigh and ankle. It is particularly robust against external acceleration as high as $\pm$2g for knee joint angle estimation. Also, the *RMSE* in all cases reside within the clinically acceptable mean error limit of 5°.

3.4 Conclusions

Inertial motion sensors play an integral role in present–day smart gadgets such as smartphones, tablets and fitness trackers. They can potentially be the part of new technologies such as smart homes, Internet–of–Things (IoT), and Internet–of–Everything (IoE). These small, low–power and potentially wearable sensors, coupled with advanced and power–efficient high–speed computing and communication technologies can be used in home–based monitoring and to asses people's activity, mobility, gait pattern, fitness and overall health in a continuous fashion without interrupting their day–to–day living. The lower limb joints play critical role in locomotion and they deteriorate gradually with age, thereby affecting people's mobility. Therefore, it is important to keep track of the health of the lower limb joints. One important metric of assessing joint health is its range of motion.

In this work, we have designed, implemented and validated a two–stage sensor fusion algorithm that outputs joint angle in real–time. In the first stage, the drift in the integrated gyroscope data of each IMU was estimated using a gradient descent approach and later subtracted from the integrated gyroscope data to obtain the inclination of the IMU in real time. In the second stage, the inclination information of both IMUs were fused using a gradient descent approach to obtain a real–time estimate of the joint angle. Since the joint angle was estimated primarily based–on the gyroscope measurements and without incorporating the magnetic field measurement, the estimated orientation and joint angles were observed to be least affected by any external acceleration and insensitive to magnetic disturbances. In addition, the complementary nature of the proposed method made it computationally efficient and well suited for real–time systems, thus enabling a potential wearable tele–rehabilitation solution for objective measurement of lower–limb joint angles

in home or community settings. The proposed algorithm was validated against a standard video–based system using a publicly available dataset and showed superior performance at different gait speeds than that required for clinical acceptance. The robustness of the algorithm was also tested against different levels and duration of simulated external accelerations.

Chapter 4

A gait analyzer for healthcare applications

Continuous increase in life expectancy will translate into a large aging population in the near future. However, in spite of the present healthcare system being highly advanced, especially in the developed world, or first–world countries, it is not yet cost–effective due to high costs associated with prescription drugs, diagnostic tools and in–hospital care [4.1],[4.2]. Therefore, predictive diagnostic and monitoring systems, which are simple, non–invasive, and low–cost yet reliable and precise, are of utmost necessity in order to provide affordable healthcare services to the elderly while ensuring their comfort and independence. The recent advances in wireless communications, information and computing technologies, as well as miniaturized sensors and actuators have paved the way for smart and cost–effective solutions for healthcare [4.3]–[4.6]. One such system, an inertial sensor based walking pattern analyzer, can potentially offer a simple and low–cost solution to monitoring the overall status of the health of the elderly.

Walking and gait are the process of balance and locomotion that require proper coordination between the nervous and the musculoskeletal systems. Also, proper

---

* Adapted from S. Majumder, T. Mondal and M. J. Deen, "A Simple, Low-Cost and Efficient Gait Analyzer for Wearable Healthcare Applications," in *IEEE Sensors Journal*, vol. 19, no. 6, pp. 2320-2329, 15 March, 2019, doi: 10.1109/JSEN.2018.2885207. (Appendix A)

functioning of the respiratory and cardio–vascular organs as well as the nervous and musculoskeletal systems is critical for maintaining a normal and healthy gait [4.1]. Therefore, human gait is strongly associated with health condition [4.1],[4.3],[4.7], and any deviation in the walking pattern from its baseline characteristics can be indicative of a potential disease or malfunctioning of the musculoskeletal and/or nervous systems. Walking and gait patterns are distinctive in nature and vary with physical traits such as gender, age, height and weight owing to the inherent differences or gradual changes in musculoskeletal structure [4.1],[4.7],[4.8]. For example, females tend to have larger hip swing compared to males, whereas males exhibit larger shoulder swing [4.9]. On the other hand, elderly people tend to walk differently than the younger ones owing to the gradual decline in the motor control and muscle strength [4.10]. Therefore, a tool for the quantitative assessment of gait is needed to detect the early onset of any anomaly in the gait pattern and to monitor the rehabilitation of gait following an injury or illness such as to the knee or stroke.

One such tool can be based on micro–electro–mechanical systems (MEMS). The integrated Inertial Measurement Units (IMUs), coupled with the wireless connectivity and superior processing capability of the smart devices, can be used for real–time gait monitoring and performing quantitative assessment of gait without interrupting the daily activities of individuals. In this chapter, we investigate the gait characteristics quantitatively using inertial sensors and propose an inertial sensor–based low–cost and computationally efficient gait analyzer for healthcare applications. We used an efficient signal analysis and features extraction technique, thus reducing the computational complexities for a continual gait monitoring system. In this way, our gait analyzer is suitable for real–time systems using limited processing resources such as microcontrollers or FPGAs (field programmable gate arrays).

4.1 Background

At present, clinicians mainly use pressure sensors [4.14],[4.15] or video imaging–based systems [4.13],[4.16],[4.17] for gait analysis and assessment. Pressure sensors are either

arranged in an array configuration and embedded in the floor [4.14], or integrated in the shoe to measure foot plantar pressure characteristics while walking [4.14],[4.15]. However, pressure sensors, being linearly dependent on external pressure, are unable to provide useable information about gait during the swing phase. On the other hand, video–based imaging systems can provide comprehensive information about the mechanical parameters such as gait speed, acceleration and tilting of the legs. However, video systems require specialized and expensive infrastructure with multiple mounted cameras and high computational resources with large memory sizes. An attractive alternative of the pressure sensor and video imaging based gait analysis systems can be the inexpensive, small–in–size and low–power IMU–based systems for gait monitoring. These systems can be of immense benefit for continual assessment of human gait as one health metric.

Researchers have been using IMUs for activity monitoring [4.1],[4.3],[4.4],[4.18], and motion tracking [4.19],[4.20]. IMUs can be embedded in a wearable platform [4.1],[4.3],[4.4] and connected through a Body Sensor Network (BSN) [4.21] to facilitate activity and gait monitoring. However, computational resources [4.21]–[4.23] and energy requirements [4.1],[4.24],[4.25] are some bottlenecks in such systems [4.1],[4.22] which were addressed in [4.21]–[4.25]. For example, the authors in [4.21] reported an efficient, modular and open–source software framework named Signal Processing In Node Environment (SPINE), which was used to implement a Hidden Markov Model (HMM)–based classifier to classify four gait events.

Apart from activity monitoring and motion tracking, there has been a growing interest in exploiting IMU–based gait analytics for health assessment and diseases prediction. Walking or gait requires proper coordination between the musculoskeletal system and the central nervous system (CNS). Therefore, any abnormalities in walking patterns are strongly associated with and thereby indicative of some health conditions [4.26]. For example, individuals with neurodegenerative disorders such as Alzheimer's or Parkinson's tend to exhibit short and shuffling steps [4.27]. Some IMU–based gait analysis tools in the literature focus on distinguishing the pathological gaits from the healthy ones [4.28],[4.29]. The gait pattern and features such as heel–strike and toe–off events, variability and

asymmetry, or stride length and speed in gait characteristics are found to change distinctively [4.30],[4.31] from its normal characteristics following a disease like Parkinson's, Alzheimer's and stroke. However, the changes in gait characteristics develop gradually and can potentially be detected with the IMUs through continual monitoring, thus facilitating early diagnosis and intervention of health problems.

In this chapter, we propose a simple, efficient and low–cost IMU–based gait analyzer that can provide regular quantitative assessment of human walking patterns by comparing the gait of an individual with respect to the baseline gait parameters of his/her peer group. The gait characteristics of an individual with healthy musculoskeletal and nervous system are expected to be contained within the cluster corresponding to his/her gender and age. However, an anomalous gait pattern in an individual may fall outside the respective baseline clusters, which can be symptomatic of potential health issues [4.1],[4.6],[4.7]. We employed the DWPA (discrete wavelet packet analysis) to analyze the IMU signals corresponding to human walking and extract energy, and statistical and temporal features. DWPA can localize the signal components in both frequency and time domain, thus overcoming the limitation of Fourier Transform [4.32],[4.33], which provides frequency localization only. It also removes the limitations of computationally intensive and time consuming Empirical Mode Decomposition (EMD) [4.34],[4.35] and Ensemble EMD [4.35]–[4.38] that require an exhaustive iterative 'sifting' process to generate intrinsic mode functions (IMF) [4.39],[4.40]. By adopting the tree–like decomposition technique, DWPA renders this gait analyzer suitable for the SPINE framework [4.21] and for other computer platforms with limited processing resources such as microcontrollers and FPGAs (field programmable gate arrays). The proposed gait analyzer is capable of tracking the user's gait behavior and providing prompt and regular feedback to the users and/or the clinicians, thus potentially leading towards early detection of anomalies in the functioning of musculoskeletal and nervous systems to facilitate healthy aging at home. This system, if coupled with smart textiles and modern communication and information technologies, may also enable long–term monitoring from a remote healthcare facility while ensuring maximum user comfort and unhindered day–to–day living.

4.2 Data acquisition system and protocols

4.2.1 Participants and protocols

A total of 74 healthy subjects with their ages ranging from 18 to 65 years participated in this study. Prior to acquiring walking signals, some key information such as motivation for the study, data acquisition procedure, and data security and privacy protocols were explained in detail to each subject and a written consent was obtained. Each participant was requested to answer a questionnaire prepared by a physician. The questionnaire was developed to collect some key physical features of the subjects including weight, sex, age, leg length and height. All participants were healthy and did not have any major health issues or prior surgery. Prior approval was obtained from the Hamilton Health Sciences Research Ethics Board for the study. Table 4.1 presents the summary of the subjects' characteristics.

Table 4.1 Participants' characteristics

	Male	**Female**	**18-40 years**	**41-65 years**
No. of sub.	45	29	50	24
Age [years]	36.5 (20-65)	37 (22-60)	29.22	52.6
Height [m]	1.76 (1.58-1.92)	1.66 (1.56-1.79)	1.73 (1.56-1.92)	1.71 (1.58-1.88)
Weight [kg]	81.8 (51 -149)	65.26 (49.3-118.5)	73.5 (49.3-126)	79 (54-149)

4.2.2 Data acquisition system

Walking signals were measured using an inertial measurement unit (IMU) from InvenSense Inc (MPU–9150). A photograph of the IMU is shown in Figure 4.1 (a). The IMU has dimensions of 43 mm × 37 mm and includes a tri–axial accelerometer and a tri–axial gyroscope. The accelerometer and the gyroscope has a full–scale range of ±16g and ±2000 degrees per second (dps), respectively, and acquires signal at a rate of 50 samples per second. The IMU is equipped with a Bluetooth transceiver module that can communicate with a computer over the wireless platform. The computer runs a Python program to receive the measured data and store them as text files. A program was developed in MATLAB to read the data from the text files for further processing and analyses.

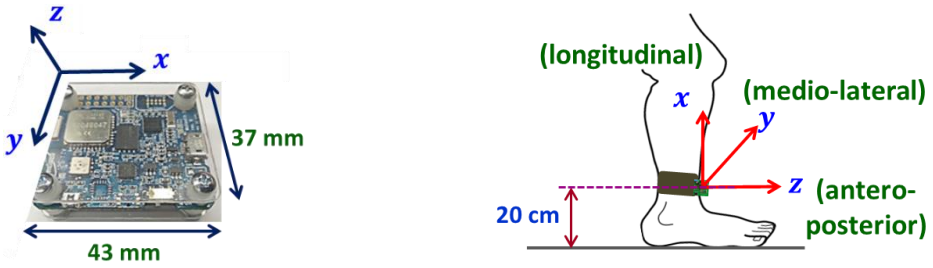

(a) (b)

Figure 4.1 Inertial measurement unit (a) commercial sensor (Invensense MPU–9150) (b) position of the sensor.

4.2.3 Data acquisition Protocol

The IMU was mounted on a Velcro belt in order to attach the device at the frontal section of the left and right shanks of the subject. The frontal section was preferred over the posterior section to minimize any possible artifacts that might be induced in the measured signal due to the movement of the muscles and the soft–tissues. The orientation of the attached device was such that the x–axis, y–axis and z–axis point towards the upright direction (longitudinal), the outward direction (medio–lateral) and the forward direction (antero–posterior), respectively. To maintain the uniformity of measurements among all subjects, the IMU was always attached at 20 cm above from the ground level (Figure 4.1 (b)). Each participant was asked to walk 40 m in a well–illuminated, obstacle free walkway at their preferred pace. The long and wide walkway (~70 m × ~4 m) allowed for the acquisition of stable walking signals.

4.3 Signal analysis and assessment

The general algorithm for signal analysis and gait assessment consists of three main sections. First, a set of statistical and temporal features was extracted from the height–normalized gait signals (linear acceleration and angular velocity). Second, the signals were decomposed using discrete wavelet packet analysis (DWPA) and the energy of each decomposed signal was calculated. Third, the significant features were extracted based on their statistical significance (t–test) and correlation coefficients. Following a dimensional reduction of the features, the features were finally classified using support vector machine (SVM). The method is described in detail in the following sections.

4.3.1 Preprocessing

The gait characteristics can be affected by the height and weight of the subjects. In order to minimize the effects of these physical factors, it is important to normalize the walking signals. It was observed in a previous study [4.40] that normalization of gait signals by the height of the subjects is more effective for discriminative analysis compared to the weight–normalized gait signals. The gait signals from the accelerometer were normalized according to Eq. 4.1 [4.40].

$$\breve{\boldsymbol{A}} = \frac{\boldsymbol{A}}{\sqrt{g.height}} \tag{4.1}$$

where g is the acceleration due to gravity (~9.81 ms^{-2}) and $\boldsymbol{A}$ represents walking signals from each axis of the accelerometer. The gait signals from the gyroscope were normalized according to Eq. 4.2,

$$\breve{\boldsymbol{G}} = \frac{\boldsymbol{G}}{\sqrt{height}} \tag{4.2}$$

where $\boldsymbol{G}$ represents walking signals from each axis of the gyroscope.

Since, the most significant features of the human gait signals remain in the low–frequency region, the high frequency components were removed by passing the normalized signal through a fourth order low–pass Butterworth filter (cut–off frequency = 12 Hz).

4.3.2 Signal decomposition

Gait signals, being non–linear and non–stationary in nature, can be effectively analyzed by decomposing them into their spectral components. For example, researchers in [4.40]–[4.44] used empirical mode decomposition (EMD) and complete ensemble EMD (CEEMD) methods, respectively for decomposing gait signals. As discussed earlier, these methods are computationally intensive and time consuming. In contrast, discrete wavelet transform (DWT) follows a fast and hierarchical tree–like decomposition algorithm, which makes it suitable for real–time applications.

The DWT decomposes a signal into approximation coefficients and detail coefficients by passing the discrete time–domain signal through several low–pas filters (LPF) and high–pass filters (HPF), respectively. While the approximation coefficients i.e. the lower–

frequency components at each level can be further decomposed in a similar fashion, the detail coefficients or the higher–frequency components remain unaltered. However, in the wavelet packet decomposition (WPD), both the detail and approximation coefficients are further decomposed at each level in a binary–tree like structure (Figure 4.2), thus allowing the signal to decompose evenly throughout its whole spectrum.

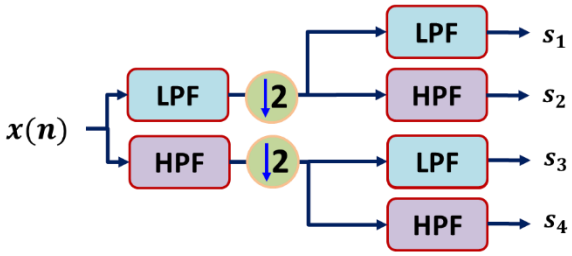

Figure 4.2 Wavelet packet decomposition tree up to 2nd level.

All components of the gyroscope signal around the medio–lateral axis decomposed at level 2 are shown in Figure 4.3. In our work, we used Symlets 4 (sym4) mother wavelet to decompose the filtered signals at level 8 using WPD.

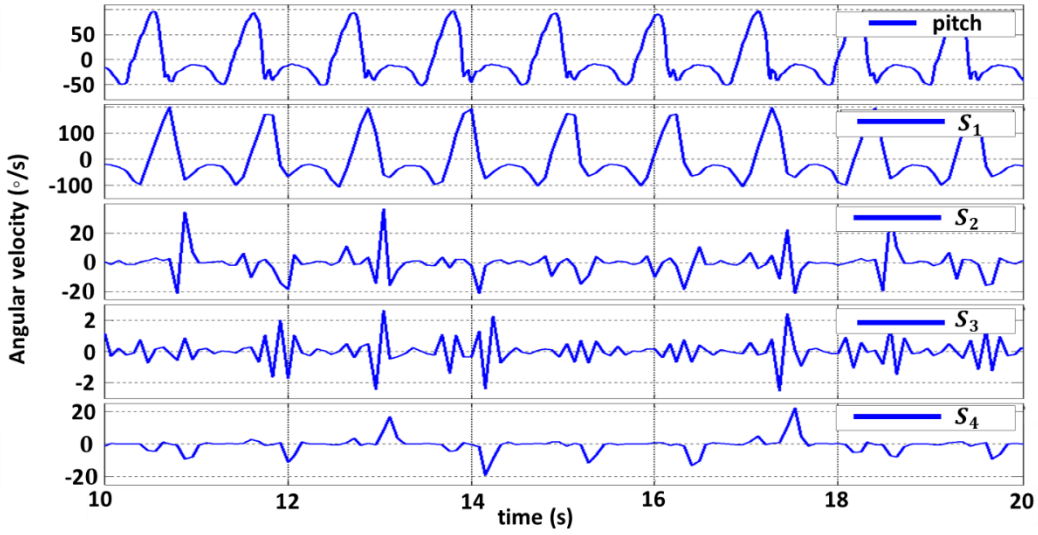

Figure 4.3 Four components of the medio–lateral signal decomposed at 2nd level with wavelet packet decomposition using sym4 as the mother wavelet.

4.3.3 Feature extraction

A large set of features were extracted from the preprocessed signals. The features included the energy of each decomposed signal, timing, and statistical parameters of the gait signals.

The gait signal energies are associated with the mechanical work done during locomotion [4.38],[4.40]. Also, the gait timing parameters vary with age and gender [4.44],[4.45] thus making them good candidates as suitable features. The energy E information of each decomposed signal during a straight walk was calculated using Eq. 4.3,

$$E = \frac{1}{M}\sum_{n=1}^{N}[S(n)]^2, \tag{4.3}$$

where S represents the components of decomposed signal, N is the total number of samples, and M is the total number of gait cycles in the signal. A gait cycle is the time between two consecutive heel–strike events of the same leg during locomotion.

Extracted features also include bipedal gait asymmetry (GA) and coefficient of variation (CV) that determine the degree of coordination between the legs. The swing time and stance time from both legs were also measured. The swing time was calculated from the gyroscope signal around the medio–lateral axis (g_y) by measuring the time difference between the last contact of the first support of the foot and the first contact of the following support. The stance time was obtained from the time difference between the first and the last contact of two consecutive supports of the same foot. As shown in Figure 4.3, the directionality of g_y changes rapidly at the contacts that results two valleys in each walking cycle. These contact valleys were detected automatically by calculating the time–derivative (dg_y/dt) of the low–pass filtered signal and identifying the points where the sign of (dg_y/dt) changes (zero crossing). The prior low pass filtering of g_y allows for removal of false zero–crossings due to high frequency noise and enables accurate identification of contact valleys.

The stride time, which is the duration of the gait cycle, was then obtained by adding both the swing time and the stance time in a gait cycle. The foot, which spent shorter and longer time during the swing phase was determined in order to calculate GA and CV [4.42], using Eq. 4.4 and Eq. 4.5, respectively.

$$GA = 100 \times \left|\ln\left(\frac{Sw_s}{Sw_l}\right)\right|, \tag{4.4}$$

where Sw_s is the mean shorter swing time and Sw_l is the mean longer swing time and

$$CV = 100 \times \left(\frac{\sigma}{\mu}\right), \quad (4.5)$$

where σ and μ are standard deviation and mean of swing time or stance time.

Table 4.2 presents all features that were extracted from the gait signals.

Table 4.2 Extracted gait features.

Temporal	Asymmetry	Energy	Statistical
• stride time (μ and σ)	• stance-to-swing time ratio	• acceleration (a)	• mean a, $\check{\theta}$
• swing time (μ and σ)	• gait asymmetry	• angular velocity ($\check{\theta}$)	• Correlation (right and left leg signals)
• stance time (μ and σ)	• coefficient of variation	• DWPA decomposed signals	• Covariance (right and left leg signals)

4.3.4 Dimensional reduction

Following the feature extraction process, an 8–length and a 32–length feature vector were derived for gender– and age–based gait classifications, respectively, based on the statistical significance (t–test) and correlation coefficients of the features. In order to reduce the redundancy and high dimensionality of the two feature vectors, a dimensional reduction was performed using Principal Component Analysis (PCA) [4.45]. PCA is a mathematical process that reduces the dimensionality of the data by projecting them onto a lower dimensional space after analyzing the covariance matrix of the data. The new lower dimensions represent most of the variance of the original data, thus ensuring minimal loss of information. Therefore, both the original 8–length and 32–length feature vectors can be projected on the 2–dimensional spaces using the first two principal components without losing much information.

4.3.5 Classification of the baseline gait data

We exploited and trained the linear support vector machine (SVM) with the reduced 2–length vectors, forming two distinct classes of baseline data corresponding to two specific gender and age groups. SVM is known to be very effective for classifying a two–class dataset with few samples [4.46],[4.47]. It is a supervised learning approach that determines a discriminative hyperplane in a multi–dimensional space by maximizing the geometric

margin between different classes. Feature vectors determining the hyperplane are called support vectors. Other feature vectors do not alter the position of the hyperplane.

4.3.6 Cross validation

The performance of the proposed algorithms was evaluated using a 15–fold cross validation. Each time, five random subjects out of 74 were excluded, without overlap. Fifteen such non–overlapping subsets of test subjects were thus developed. The SVM was then trained in each case with the remaining 69 subjects. Finally, the excluded 5 subjects from each subset were classified using the developed model. An overall accuracy of the analyzer was then calculated by combining the results from each of the 15–fold validation. The block diagram of the proposed gait analyzer is shown in Figure 4.4.

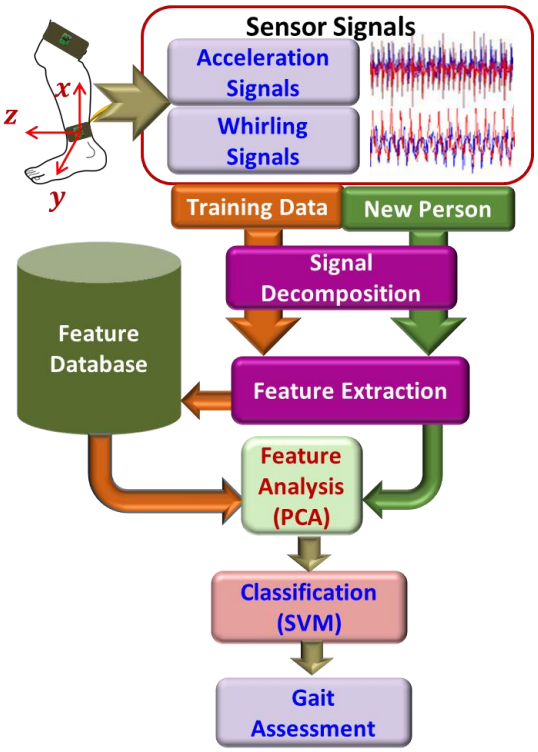

Figure 4.4 Block diagram of the gait analyzer.

4.4 Results and discussion

4.4.1 Stride characteristics

Although all subjects were asked to walk at their preferred pace, some gait characteristics

were found to be significantly different between the two groups. On average, the female subjects walked with a shorter stride time and a higher cadence (115.6 steps/min) compared to the male subjects (107.5 steps/min), which was statistically significant at $p < 0.001$. The higher cadence is generally attributed to the increased joint torque and power [4.48] during walking, thus indicating a tendency among the females towards spending more energy while walking. Higher cadence requires faster angular movements (flexion, extension) of the joints within its range, thus causing increased generation or absorption of joint power [4.48],[4.49]. It is observed that the differences in the magnitude of the temporal gait characteristics between two groups are not large (~ 6%), yet highly consistent – a fact that can be verified by their small standard deviation values and smaller p–value ($p < 0.001$).

It was observed that GA and CV do not differ much between the younger (< 40 years) males and females. The nervous systems as well as the musculoskeletal systems in younger persons are well–compensated. Any form of degeneration in any system possibly unmasks this asymmetry as age advances. According to previous studies [4.42],[4.50], gait asymmetry and variability are highly associated with cognitive function. It therefore possibly results in the same degree of balance, stability and coordination between right and left leg among the younger group of persons. A comparison of cadence, GA and CV between males and females is presented in Figure 4.5.

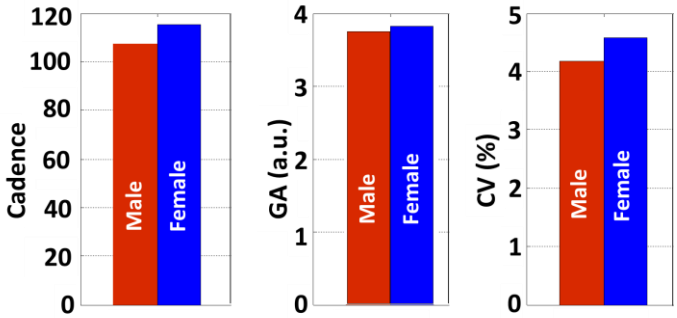

(a) (b) (c)

Figure 4.5 Comparison between male and female gait (a) cadence (b) GA (c) CV.

The energies of the significant components ($p < 0.009$) of the decomposed signals were calculated for all three axes. It was observed that the average energy of the antero–posterior

(*z*–axis) and medio–lateral (*y*–axis) acceleration were significantly higher for female subjects compared to their male counterparts. Females tend to have larger hip flexion and smaller knee extension before initial contact. They also have a tendency towards higher knee flexion moment and higher power absorption by the joints during the pre–swing phase of the gait cycle [4.48]. Since females exhibit a higher cadence compared to males, their joints and surrounding muscles need to perform higher amounts of mechanical work compared to males when walking a fixed distance in the same time.

The female subjects also exhibited higher rotational energy around the longitudinal, medio–lateral and antero–posterior axes than the male subjects. The distinct difference in medio–lateral (*y*–axis) acceleration energy, and rotational energy around the longitudinal and antero–posterior axes of females can be attributed to their greater pelvic tilt and larger swing while walking [4.8],[4.51].The female pelvis, commonly referred as gynecoid pelvis, has a distinctly different structure than male pelvis with a wider sacrum and pubic arch. This anatomical difference coupled with a relatively lax ligament of the female pelvis and hip joints results in a larger hip swing among the females. The comparison between male and female gait energies is presented in Figure 4.6.

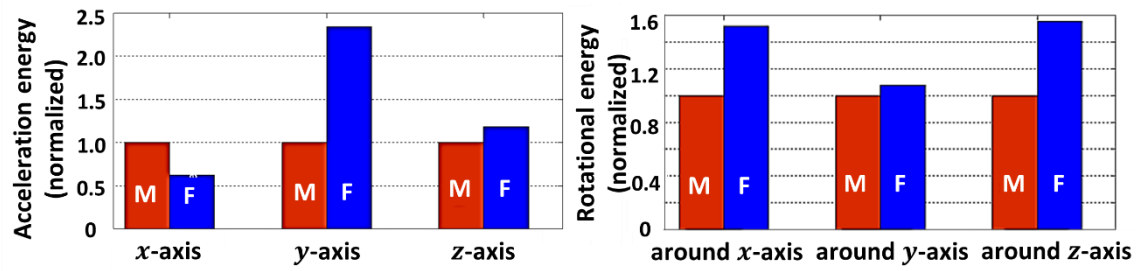

(a) (b)

Figure 4.6 Comparison between male and female gait energies (a) acceleration energy (b) rotational energy.

It was also observed that subjects from the older age group (> 40 years) walked with a shorter stride time ($p < 0.001$), which can be attributed to their shorter stride lengths compared to the younger adults. The bone and muscle mass as well as joint fluids among the older adults decline gradually with age. Therefore, they tend to compensate their

declining balance and stability by reducing their stride length. In the older age group, their stride frequency i.e. cadence, was observed to be ~3% higher. The GA and CV were found to be significantly higher in the older age group compared to the younger group. Stability, balance and cognitive function tend to decline with age, thus increasing the asymmetry and variability in gait among the older adults. The comparison of cadence, GA and CV between the two age groups is presented in Figure 4.7.

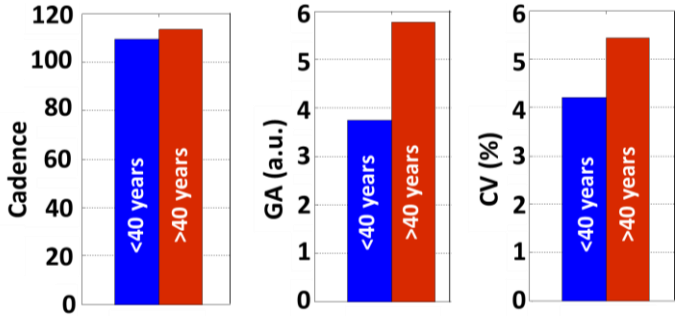

(a) (b) (c)

Figure 4.7 Comparison between two age groups (a) cadence (b) GA (c) CV.

As discussed earlier, higher cadence is usually associated with increased power and torque about the joint [4.48], [4.49]. However, the overall energies of the significant ($p < 0.009$) components of the signals were much lower (40%–60%) for the older age group, except for the energy of the frontal acceleration (z–axis) and angular velocity around the medio–lateral axis. The comparison of gait energies between younger and older adults is presented in Figure 4.8. The energy of these signals of the older age group were found to be significantly higher than the energy for the younger age group. This can be attributed to their shorter stride time and increased joint torques at hip extensors [4.52] during forward movement. Older people tend to spend less time in each stride, thus forcing the hip joints to perform more work in a gait cycle. However, the higher rotational energy around the longitudinal and antero–posterior in younger adults could be attributed to their tendency to maintain high ground clearance while maintaining an upright stance with enhanced control on the trajectory of their center of the mass.

Higher medio–lateral (y–axis) and longitudinal (x–axis) acceleration among the younger adults indicate stronger grip that ensures better control and balance during the gait cycles. The younger adults generally possess a healthy musculoskeletal system and an unimpaired

somatosensory system. Therefore, the basal energy expenditure among the younger adults is well controlled owing to their better postural balance and alignment, as well as superior coordination between the central nervous and the musculoskeletal systems [4.53]. However, the older age group demonstrates a significant decline in stride time and gait symmetry, thus confirming an overall weaker gait compared to the younger age group.

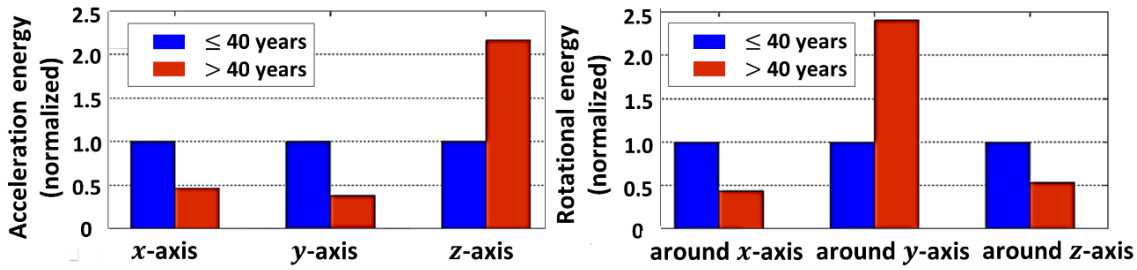

(a) (b)

Figure 4.8 Comparison between two age groups (a) acceleration energy (b) rotational energy.

In [4.52], it was hypothesized that as age increases, the joint torque and power gets redistributed gradually, resulting in an increase in joint torques at hip extensors and a decrease in knee extensors and ankle plantar flexors while walking. These changes in the walking physiology can be attributed to the slow but gradual decline of muscle mass and joint fluids [4.40], [4.54]. Muscles play the key role in moving the limbs by providing the necessary force and strength. Therefore, the gradual loss of muscle mass with age results in a deteriorating walking performance, resulting in a shorter step size, which causes a reduction in stride time and gait symmetry.

4.4.2 Gender–specific clustering of gait behavior

After extracting and standardizing the walking features, the first two principal components were projected on a 2–D space. The support vector machine was trained with the two principal components along with their corresponding classes. We observed that the hyperplane determined by the SVM can successfully arrange the first two principal components of the subjects' gait features into two separate classes with a high degree of accuracy which correspond to their gender identities, as shown in Figure 4.9.

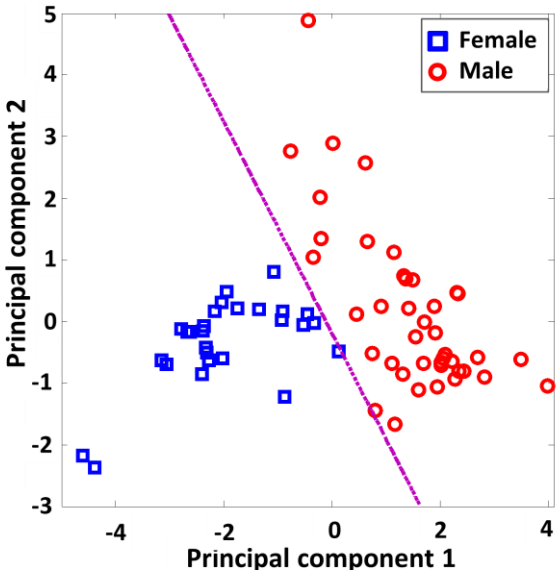

Figure 4.9 Classification results showing two distinct groups (excluding outliers).

Although, most of the subjects' gait patterns were found to truly correspond to their gender groups, a few subjects showed different gait patterns, resulting them being falsely classified. The classification accuracy was evaluated by a 15–fold cross validation. Figure 4.10 shows one instance of classifying 5 subjects based on a SVM trained with the remaining 69 subjects, where one subject was found to be misclassified.

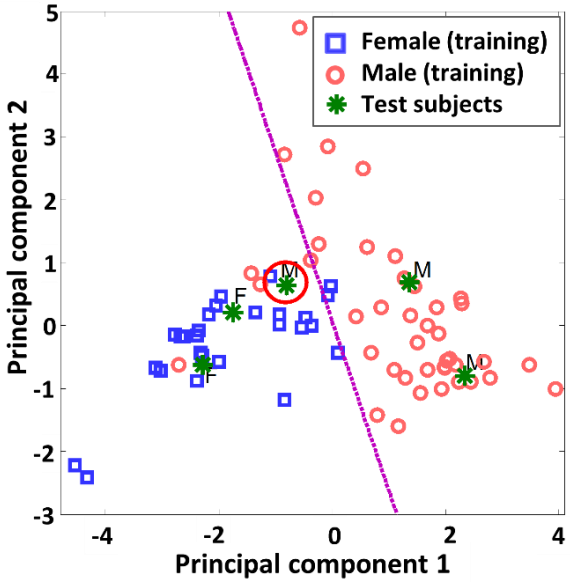

Figure 4.10 One instance of cross–validation showing one subject is falsely classified.

This observation may suggest a potential anomaly (inherent or developing) in the gait characteristics of the subject that prevents the gait behavior of that particular subject from being truly classified according to his/her gender identity. For example, the misclassified male was found to exhibit greater acceleration energy along the medio–lateral (y–axis), higher rotational energy around the longitudinal and antero–posterior axes, as well as shorter stride time, similar to that observed in healthy female subjects.

We obtain an overall classification accuracy of ~92% from the 15–fold cross validation, reflecting a reasonably accurate system capable of monitoring and evaluating the gait patterns in reference to the corresponding baseline clusters with a high degree of precision. The confusion matrix for the classifier is presented in Table 4.3. The high TPR (~92% on average) and accuracy (~92%) as well as corresponding low FPR (~8% on average) of the classification outcomes ensures the analyzer's capability in distinguishing potentially anomalous gait from healthy gaits with high confidence.

Table 4.3 Confusion matrix for gender–specific gait classifier.

	True positive rate (TPR)	False positive rate (FPR)	Accuracy
Male	91%	9%	92%
Female	93%	7%	

4.4.3 Age–specific clustering of gait behavior

In order to evaluate the age–specific differences in the baseline gait patterns, the gait features of the healthy subjects from two age groups were classified using the SVM algorithm, following the dimensional reduction using the PCA. Two distinct groups based on their "walking–age" [4.40],[4.42] were observed after the classification. One group comprises younger adults with their walking–age ranging from 18–40 years and the other group includes adults with walking–age from 41–65 years. The formation of two age groups is presented in Figure 4.11. Among all 74 subjects, 50 adults belonged to the chronological age group of 18–40. However, 47 of them have their walking–age matched to their chronological age. The remaining three subjects had their walking–age similar to those in the older "41–65 years" group.

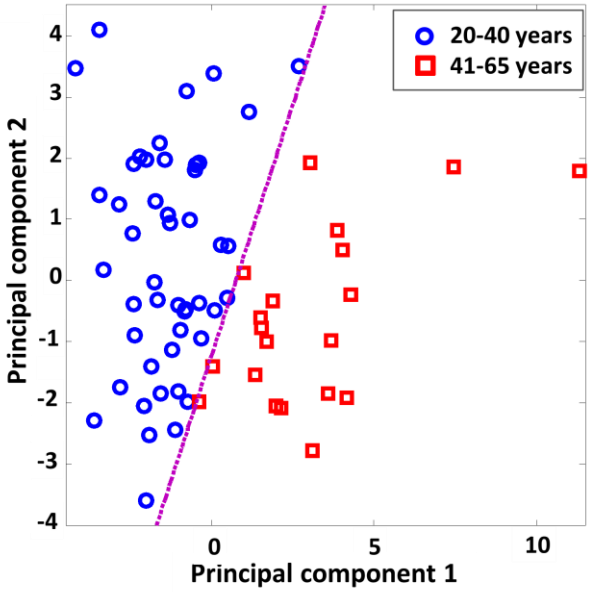

Figure 4.11 Classification results showing two distinct age groups (excluding outliers).

This aberration in the gait behavior may be attributed to an altered walking pattern caused by a potential health problem such as weak joints or degraded muscular strength. For example, the misclassified younger adults, on average show higher GA and CV and smaller stride time compared to the truly classified young adults, whereas the misclassified older adults exhibit higher stride time and better gait symmetry compared to the truly classified older adults. The accuracy of the gait classifier was evaluated by a 15–fold cross validation.

Table 4.4 Confusion matrix for age–specific gait classifier.

Age (years)	True positive rate (TPR)	False positive rate (FPR)	Accuracy
20-40 years	92%	8%	88%
41-65 years	79%	21%	

Figure 4.12 shows one instance of cross–validation where one subject of 52 years of age was classified having a walking–age "<40 years", potentially reflecting a better and healthier gait compared to the subjects of his/her chronological age group. An overall classification accuracy of ~88% was achieved from the 15–fold cross validation. The confusion matrix for the classifier is presented in Table 4.4.

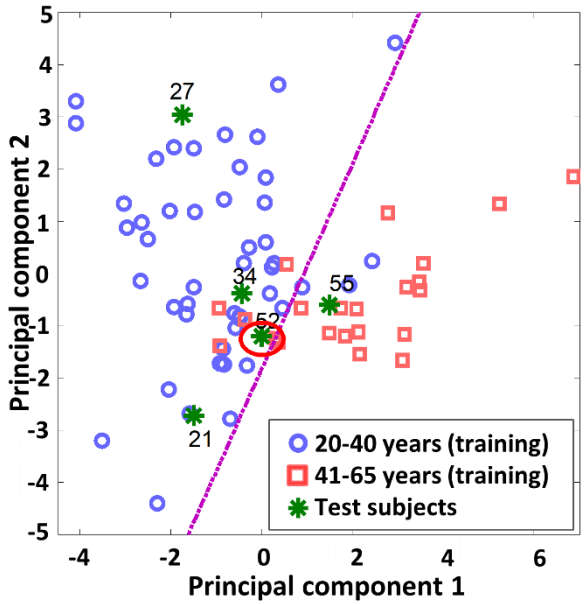

Figure 4.12 One instance of cross–validation showing one subject falls in a different age group than his/her actual age.

4.5 Conclusions

The continual increase of aging population, coupled with soaring costs associated with present–day healthcare services is likely to adversely affect the socio–economic structure of many countries. A simple, easy–to–use and cost–effective yet reliable health monitoring system would therefore be of immense benefit in keeping track of individuals' health status, thus facilitating healthy aging at home. Walking or gait, being reflective of the physiological functioning of the body, is a good indicator of overall health status. In this work, we report on a simple, low–cost and computationally efficient gait–analyzer based on MEMS inertial sensors to track the course of the gait health of an individual in a continuous fashion; thus potentially enabling early detection of health issues such as osteoporosis, osteoarthritis, dementia, Alzheimer's, and Parkinson's. The proposed system identifies an anomalous gait by evaluating its features with respect to the baseline clusters corresponding to an individual's peer group. The adoption of a computationally efficient signal analysis technique like DWPA renders the analyzer suitable for systems with limited processing capabilities.

However, a limitation of this work evolves from being unable to recruit patients with known pathological gaits. The gait pattern changes gradually through different disease processes and at different severities, thus it is likely to deviate from the healthy gaits corresponding to an individual's peer group. Although distinct clusters or patterns of healthy gait are reported in this work following a 15–fold cross validation, further in–depth study on different patient groups with a larger dataset from a wider age and BMI range, different walking surfaces as well as different walking speed would be useful to reinforce our inferences. Nevertheless, this research is critical and in fact mandatory in Canada according to our University's Research Ethics Board (REB) that requires us to demonstrate the feasibility of the gait analyzer on healthy individuals before it can be used on patients, which requires an additional approval from Health Canada.

Chapter 5

Wearable ECG system with automatic anomaly detection

Electrocardiography (ECG) has been proven to be among the most useful diagnostic tests in clinical medicine, which is now routinely used in the evaluation of patients with implanted defibrillators and pacemakers, as well as to detect myocardial injury, ischemia, and the presence of prior infarction. In addition to its usefulness in ischemic coronary disease, the electrocardiogram is also useful in diagnosing the disorders in the cardiac rhythm and evaluating syncope. Other common uses of the ECG include evaluation of metabolic disorders, direct and side effects of pharmacotherapy, and primary and secondary cardiomyopathy.

In the early days, realizing a highly sensitive ECG system was a significant challenge. The electrical heart signals attenuate while travelling through the body tissues and become weak at the skin's surface. However, Willem Einthoven [5.1] managed to improve the sensitivity of the ECG sensing systems by using a string galvanometer, which was considered to be a giant leap forward for electrocardiography. Einthoven's improvements were very significant, since the characteristic peaks of the ECGs, now familiar as P, Q, R, S, and T

---

* Adapted from S. Majumder, L. Chen, O. Marinov, C. H. Chen, T. Mondal, and M. Jamal Deen, "Noncontact Wearable Wireless ECG Systems for Long-Term Monitoring," *IEEE Rev. Biomed. Eng.*, vol. 11, pp. 306–321, 2018. (Appendix A)

waves, were apparently defined (Figure 5.1), while the scientists previously had demonstrated only ventricular depolarization and repolarization as it was shown in Waller's work [5.2].

Different types of ECG systems [5.3]–[5.6] have been introduced so far to improve the signal quality in the clinical settings. The conventional ECG method uses a hydrogel between the skin and the electrodes to increase the conductivity of the signal path. However, the wet electrode method uses conductive gels that contain toxic materials, which can cause irritation to the skin of the patients. Some patients may even be allergic to the nickel particles or the acrylic adhesive present in the popular disposable conductive hydrogel based ECG electrodes [5.7]–[5.11]. Therefore, the wet electrode method is not suitable for ambulatory and long–term monitoring of the ECG.

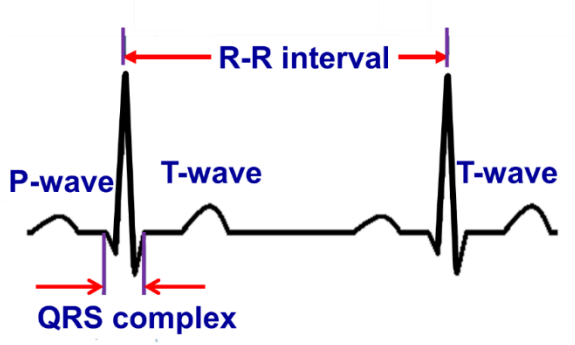

Figure 5.1 Basic features in the waveform of an ECG signal.

In this work, a dry capacitive–coupled flexible electrode is designed and used to develop a portable wireless ECG monitoring system for both inpatient and outpatient monitoring of the ECG. The capacitive dry electrode method [5.3], [5.4] requires neither a conductive interfacial medium, nor any direct contact to the skin, thus making it suitable for long–term monitoring. Despite having a layer of interfacial material between the skin and electrodes, the proposed electrode still allows the detection of the ECG signals from the skin's surface through capacitive coupling, thus making the system suitable for long–term monitoring of ECG in an ambulatory environment.

The interface material for capacitive electrodes can be a thin layer of textile material such as cotton, which is tightly attached to the skin to ensure an optimal signal quality. Cotton is a common fabric for clothes, which, along with other textile materials such as, wool, silk, or nylon, has higher dielectric constants, thus, resulting in better capacitive coupling [5.12]. These capacitive electrodes can potentially be integrated with the smart textiles [5.13]–[5.15] to realize a wearable and comfortable long–term ECG monitoring system. Both the capacitive dry electrodes and smart textiles are increasingly being studied and developed for flexible and wearable ECG monitoring systems.

5.1 Related works on ambulatory ECG systems

The primary purpose of the ambulatory ECG systems is to facilitate monitoring the heart's activity outside the clinical setting. It also allows for continuous monitoring of cardiovascular health thus enabling detection and diagnosis of any heart related issues at their early onset. Unlike the 10–electrode clinical ECG systems, ambulatory ECG systems are small, portable and generally exploit two to three electrodes to measure and record the electrical signals. Some systems incorporate wireless communication technologies such as Bluetooth, Bluetooth low energy (BLE), and ZigBee for real–time data transmission. A general architecture of ambulatory ECG monitoring system is shown in Figure 5.2.

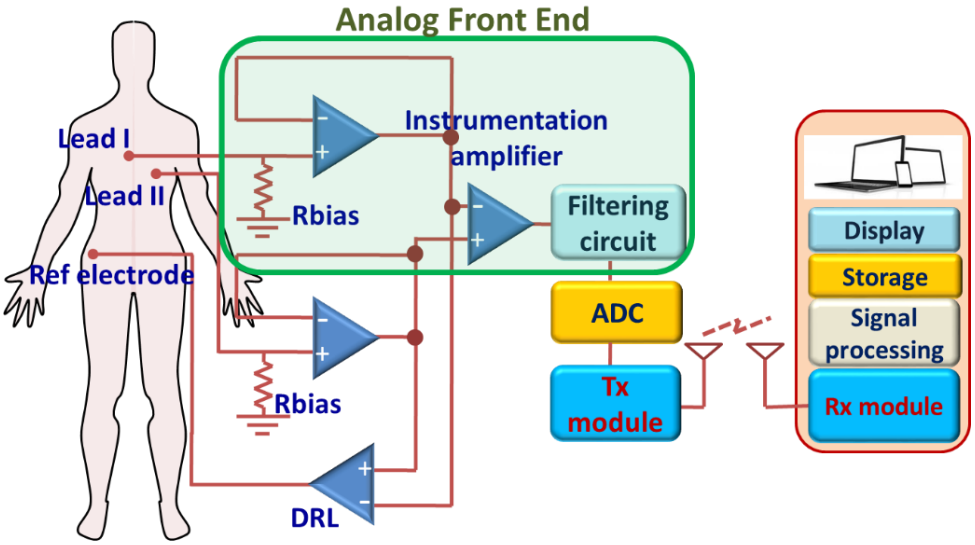

Figure 5.2 General architecture of the ambulatory ECG monitoring system.

Ambulatory ECG systems with inherent wireless transmission capability can thereby play a key role in a smart home–based long–term and remote health monitoring system. In this section, we present a detailed review on ambulatory ECG systems reported in recent years. We also present a discussion on the current state of the portable ECG system market by highlighting some commercially available devices.

5.1.1 ECG systems in the literature

One of the key problems in the ambulatory ECG systems evolves from the contamination of the electrical signals by the electrode motion artifacts. The impedance of the interface between the electrode and the skin is disturbed with the movement of the body that corrupts the ECG signal and decreases the SNR. Therefore, many researchers put their efforts in improving the motion tolerance and the noise performance of the ambulatory ECG systems by exploiting flexible electrodes, improved analog front ends (AFE) and on–chip signal processing techniques.

A. Flexible electrodes

In the conventional 12–lead clinical ECG systems, the heart's electrical activities are sensed using conventional Ag–AgCl gel electrodes. Although, the conductive gel offers superior signal quality and motion tolerance, it is, however, toxic and may cause skin irritation if used for a prolonged period of time, making it inappropriate for long–term ambulatory monitoring. Researchers in [5.17] integrated a miniature water reservoir in the Ag and Ti coated polyethylene terephthalate yarn–based textile electrode to moisturize the electrodes with the water vapor. Although the ECG signals thus obtained were of good quality, the presence of the water reservoir, however, may cause reliability issues, for example, in the case of a leakage. The water level in the reservoir needs to be monitored regularly in the case of long–term monitoring. A superabsorbent polymer was exploited in [5.18] to regulate the humidity around a conductive polymer–based flexible fabric electrode thus enabling faster discharge of any accumulated charges and resulting shorter stabilization

time for the signal. These electrodes showed high signal quality at rest and short stabilization time. However, the motion tolerance of these electrodes was not evaluated.

'Dry' electrodes, on the other hand, do not rely on any conductive gel or additional moisturizer and therefore, are suitable for long–term ambulatory monitoring systems. However, dry electrodes usually suffer from high electrode–tissue impedance (ETI) owing to the poor contact between the skin and the electrode and thereby, are prone to noise and motion artifacts. The electrode contact can be improved by using flexible substrates, which makes it highly conformable to the skin. Some researchers used polymer materials such as, polydimethylsiloxane (PDMS) [5.19], [5.20] and ethylene propylene diene monomer (EPDM) [5.21], urethane [5.22], [5.23] as the substrate to improve the contact between the electrode and the skin. The wearable dry electrodes can be realized by embedding conductive nanomaterials such as Ag–nanowire [5.19], [5.24], carbon nanoparticle [5.21], Ag–coated glass composite [5.25] and carbon nanotube (CNT) [5.20] in the flexible polymers or by employing a coating of conductive material such as Ni, Cu, and Au on the polymer substrate [5.22], [5.23]. With an adequate concentration of nanomaterials in the PDMS, these electrodes may achieve similar order of ETI to Ag–AgCl wet electrodes at lower frequencies. These flexible electrodes are tolerant to motion artifacts to some extent. In [5.24], an additional capacitive strain sensor was co–fabricated with the electrode on a self–adhesive, stretchable platinum silicone rubber–based substrate to estimate and minimize the motion artifacts through an adaptive filtering approach. These dry wearable electrodes are suitable for long–term monitoring systems. The signal quality, however, may degrade due to possible oxidation of the metal nanoparticles over time. For the CNT based electrodes, achieving homogenous dispersion of the CNT in PDMS may cause additional fabrication challenges due to the presence of strong van der Waals interactions in CNT. A novel concentric flexible multi–ring electrode was presented in [5.26], which consists of four hook–shaped silver electrodes and an inner disc fabricated on a flexible polyester substrate. The potential differences between the rings and the central disc contribute to achieving higher spatial resolution compared to the traditional disc electrodes.

Some researchers exploited microstructures to reduce the ETI by enhancing the adhesion, flexibility, and conformability of the electrodes. A 3D printed surface electrode was presented in [5.27]. An array of conical needles was printed on a truncated conical support by jetting thin layers of polymeric material and curing each layer by ultraviolet light. The developed model was then coated with Ti and Au to lower the ETI and prevent oxidation and corrosion. In [5.28], researchers exploited micro–electro–mechanical system (MEMS) process to fabricate a highly thin and flexible capacitive electrode. The electrode consists of two insulating layers, an active shield plate and a Ni sensing plate, forming a parallel–plate capacitor with the body, which enables sensing ECG over the cloth. In both works, the researchers reported to achieve ECG measurements comparable to the signal measured using wet electrodes. However, the impact of the MA on the measured signal was not reported. A filamentary serpentine mesh layout was exploited in [5.29] to realize a flexible and reusable epidermal capacitive sensor. Three such gold electrodes were embedded into silicone and connected to the anisotropic conductive film–based bonding pads. The stretchable membrane–like structure, with the aid of van–der Waals interaction, offers high conformability and ensures intimate contact to the skin. In addition, its low modulus and elastic properties allow the sensor to readily adapt to the skin deformation, thus making it less sensitive to MA compared to the traditional capacitive flat electrodes.

Researchers in [5.30] fabricated Si microneedles array (MNA) and bonded it over a PDMS substrate to realize a flexible structure of the electrode. The conductive PEDOT/PSS coated sharp MNA can penetrate the skin layer and thus can make intimate contact to the skin. An interesting microstructure, inspired from the gecko's toe pad was exploited in [5.31] to design a conductive dry adhesives (CDA) electrode. The CDA was fabricated by growing mushroom shaped micro–pillar structures of conductive elastomer on a Si platform, where the conductive elastomer was composed of 1D–2D hybrid carbon nano–fillers and PDMS. The structure showed a good adhesion force ($\sim$1.3 N/cm^2) on and conformity to the human skin. In addition, the surface of the pad showed super–hydrophobic property and thereby, having self–cleaning capability. Both structures showed close attachment and high

conformability to the skin even in the presence of movement, making them useful for long–term ambulatory monitoring systems with reduce motion artifacts.

There has also been a growing interest among the researchers in using textile materials for developing wearable, unobtrusive and comfortable health monitoring systems. Textile based sensors exploit conventional fabric manufacturing techniques such as weaving, knitting, embroidery, and stitching as well as advanced methods such as inkjet–printing, coating, lithography, chemical vapor deposition (CVD). Researchers in [5.32] fabricated a textile–based flexible and conformable electrode by screen printing Ag/AgCl based conductive ink on the propylene–based elastomeric nonwoven fabric. The dry electrode showed higher ETI than the commercial wet electrode as well as some motion artifacts. The impedance and motion artifacts, however, reduced significantly with the increase of the electrode area as well as with the application of hydrogel on the electrode. A similar electrode, based on nanofiber web textiles, was also reported in [5.33]. Another textile–based electrode was proposed in [5.34], where a flexible but un–stretchable textile was coated with the conductive PEDOT/PSS. A soft foam layer was introduced in the electrode to improve the contact pressure and keep the electrode wet, thus lowering the contact impedance. The dry electrodes showed similar order of ETI to the conventional Ag/AgCl gel electrodes but poor performance in terms of baseline stability. The impedance and signal quality, however, improves when the electrodes are wet. Although the electrodes are low–cost and follow a simple fabrication process, they require regular moistening to maintain a low ETI and high SNR, especially in the presence of movement. One may find several early implementations of textile electrodes in [5.35]–[5.38].

B. ECG systems

Ambulatory ECG systems are small in size and by using only a few electrodes compared to the clinical ECG systems can still provide limited yet useful information about the cardiovascular health. A wearable ECG system can facilitate continuous and long–term monitoring of cardiovascular health without affecting the daily activities and comfort of the user.

Researchers mostly used polymer [5.22],[5.26],[5.39],[5.40] and textile [5.41]–[5.46] based flexible and direct–contact electrodes to realize the sensing part of the wearable ECG systems. The non–contact electrodes are capacitive in nature and capable of sensing bio–potential over the cloth without having any direct contact to the skin. Such non–contact electrodes are embedded in chairs [5.43],[5.45] and bed covers [5.45] to measure the ECG at rest or during sleep. Direct–contact electrodes are usually embedded in textiles by using snap buttons [5.39],[5.40],[5.46]–[5.48], Velcro [5.49] or by means of conventional sewing, weaving or packaging techniques [5.42],[5.43],[5.44],[5.45].

The sensed bio–potential is fed to the analog front end (AFE), which filters and amplifies the ECG signal. The noise in a battery–operated ambulatory ECG system is primarily caused by the movement of the body. The flexible electrodes, due to their high conformability to the skin, can greatly reduce the motion artifacts (MA). The noise can be further reduced by designing the AFE with high input impedance and high common mode rejection ratio (CMRR). The input impedance of the AFE can be improved by using resistors [5.3],[5.44],[5.50],[5.51] or two anti–parallel diodes for biasing [5.49],[5.52]. However, anti–parallel diodes are preferred due to their low thermal noise and faster recovery time. Researchers also exploited advanced amplifier topologies, for example, differential difference amplifier (DDA) [5.40] to achieve high input impedance, high CMRR, low–power and low–noise performance. The filtered ECG signal is then digitized, which can be stored in a SD card and/or transmitted to a nearby computing platform such as computer, smartphone, and tablet, preferably over a wireless media.

Another key concern for the ambulatory ECG systems is achieving high energy efficiency and low power consumption. Lower power consumption increases the battery life, which is critical for long–term monitoring systems. Some researchers exploited energy harvesting techniques [5.53],[5.54] to meet the power requirements of the ambulatory systems. Power consumption can also be minimized by using low–power electronic components [5.39] and wireless communication technologies such as Bluetooth [5.22],[5.26],[5.43],[5.49], Bluetooth LE [5.41],[5.42],[5.46], ZigBee [5.39],[5.48] and ANT [5.3]. Researchers in [5.48] developed a dynamic power adjustment method to optimize the power consumption

of the transmitter by analyzing the distance between the transmitter and the receiver. The system periodically computes the relative received signal strength (RSSI) and automatically adjust the transmitter power until the RSSI falls within –60 dBm and –70 dBm. In [5.55], the human body was exploited as the low–power communication medium for transmitting ECG signal. They used impulse radio (IR)–type human body communication (HBC) technology to transmit ECG data. HBC generally operates in the megahertz (MHz) regime. The HBC transmitter generates a quasi–static electric field around and close to the body through capacitive coupling. As a result, HBC offers minimum interference with other wireless systems as well as high data security. The researchers reported to achieve low bit error rate (BER) at a data rate as high as 1.25 Mbps. The ECG data can be readily transferred to a computer by touching the receiver connected to the computer.

After receiving the ECG data, the computing platform can perform further processing, store and display the result in real time. The system can exploit signal processing techniques such as adaptive filtering [5.56],[5.57], wavelet decomposition [5.58]–[5.61] and empirical mode decomposition [5.60],[5.62],[5.63] techniques to further reduce the noise and improve the SNR. The platform can also make use of artificial intelligence (AI) technologies such as machine learning, deep learning and neural network to learn and evaluate the health status of the user. An Android–based mobile application was developed in [5.42] that can display the ECG traces and calculate the heart rate (HR) in real time with high accuracy. In [5.49], the researchers additionally included an alert generation mechanism in their application. The system is capable of detecting arrhythmia with high accuracy, and high sensitivity and can inform the user by a text message. The H–shirt system presented in [5.41] includes a mobile phone application, which can detect six types of anomalous ECG. The application can evaluate the user's health status by analyzing the ECG signal and warn the user about a potential health problem by sending voice messages to the phone. In [5.39], the researchers proposed and implemented a single integration platform to serve multiple ECG monitoring systems in a smart home, thus enabling management and long–term monitoring of multiple users at a reduced cost.

In order to realize seamless monitoring of the cardiovascular health from a remote facility, some researchers exploited cloud–based computing platform [5.43],[5.64]–[5.66]. Cloud–based monitoring systems allow the clinicians, designated family members and the users to share and access health information through a common web–based platform. In [5.43], researchers developed a mobile application for their ECG monitoring system, which can analyze, summarize and monitor the health status of the user. It can also communicate and share resources with the healthcare professional through a common web–based cloud computing server over the internet. Similar cloud–based ECG monitoring systems were also reported in [5.64]. Instead of analyzing the ECG in the local computing machine (e.g. smartphone, laptop, tablet), the system presented in [5.65] periodically transmits the measured ECG to the web server via a smartphone. The web server runs an algorithm that evaluates and enhances the quality of the ECG, displays and analyzes the signal in real time. It also functions as a common communication platform between the user and the healthcare professionals. Researchers in [5.66] also developed a cloud–based wearable ECG monitoring system, particularly for women. They installed two gold–nanowire based electrodes, electronic and transmission modules at the bottom layer of a brassiere. Unlike most ambulatory systems presented above, they employed GPRS communication technology for direct and long–range communication with the remote server, thus eliminating the need of any intermediate gateway, however, at the cost of increased power consumption. Table I presents a comparison among several ambulatory ECG monitoring systems presented in the literature recently.

5.1.2 Commercial portable ECG systems

The 12–lead clinical ECG systems are expensive, bulky and require trained personnel to operate, making them infeasible for in–home monitoring of the electrical activities of heart. Recent developments in flexible dry electrodes, low–power electronics, and short–range communication technologies coupled with high market penetration of computing devices such as smart phones, tablets, and laptops have propelled the medical product industries towards developing small, light–weight, and portable wireless ECG measurement systems in an effort to enable continuous in–home monitoring of basic cardiac activities and

arrhythmias. Several portable and small–size ECG monitoring systems are currently available in the market [5.67]–[5.78]. Some ECG monitoring systems, such as HeartCheck™ PEN [5.71] can be bought over–the–counter. Most of the systems, however, are sold with a doctor's prescription.

These portable systems are compact, affordable and can measure basic I–lead ECG by using two to three electrodes [5.67]–[5.74],[5.77]. However, some systems are capable of providing 3–lead ECG measurement [5.75],[5.76],[5.78]. Most systems are capable of measuring and recording the ECG signal for only a short period of time, usually 30 seconds. Some advanced systems facilitate continuous monitoring of the ECG signal up to 48 hours [5.68],[5.72],[5.74],[5.76]–[5.78]. The measured ECG data is stored either in a flash memory embedded in the system [5.69]–[5.72],[5.75]–[5.78] or in an external SD card [5.74], [5.76], which is later transmitted to a computing and storage platform over a wired communication protocol, for example, Universal Serial Bus (USB) [5.69]–[5.72],[5.74]–[5.76],[5.78]. Some systems also incorporate low–power wireless communication technologies, such as Bluetooth, Bluetooth Low Energy (BLE) to facilitate wireless transmission of ECG signal in real time [5.67],[5.68],[5.73],[5.74],[5.77].

5.2 Proposed ECG system

5.2.1 Overview

The purpose of using the proposed dry ECG electrode is to obtain the ECG traces in presence of a textile material between the skin and the electrodes. The electrodes do not require any conductive gel or direct contact to the skin, thus preventing any skin irritations or possible allergies. Figure 5.3 presents the block diagram of the proposed wireless ECG monitoring system, which includes the designed capacitive electrodes, data acquisition and transmission system, and a computer software. Two capacitive electrodes, one for the left arm (LA) and another for the right arm (RA), are placed on the forearms and connected to the portable ECG device by flexible wires. The portable data acquisition device is small in size, consumes low power, and transmits the ECG data to a personal computer over the low power Bluetooth communication medium [5.13].

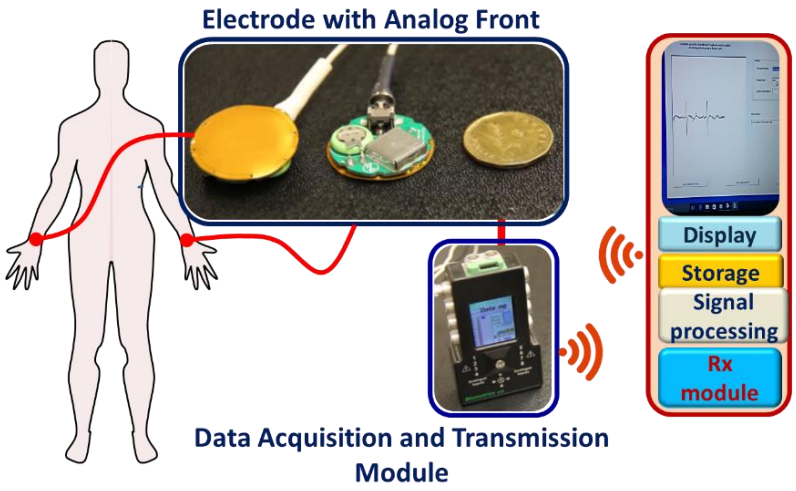

Figure 5.3 Block diagram of the proposed ECG sensing system.

A computer software was developed, which, upon receiving the ECG data, performs filtering of the raw data, stores and displays the filtered ECG signal. This entire system is designed to allow the user to carry the ECG device throughout the day, thereby enabling long– term monitoring of cardiac activities.

5.2.2 Capacitive electrodes

The capacitive electrodes sense the bio–potential through the capacitance between the electrode and skin surfaces [5.3],[5.4], as shown in Figure 5.4. Capacitive electrodes allow measuring the ECG over the cloth. In practice, the patient wears the electrodes over a thin layer of textile material such as cotton. The layer of the cotton material is expected to be thin and remain in tight contact to the skin for optimal pickup of the ECG signals.

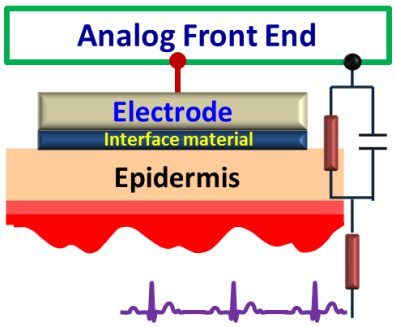

Figure 5.4 Electrode–body interface with capacitive coupling of ECG bio–potential.

Figure 5.5 presents the schematic of the designed capacitive electrode. The sensing area of the electrode is 6 cm², providing about 20pF capacitive coupling to the skin. A 3 V coin battery serves as the power source for the operational amplifiers (Op–Amps). The power switches on when the electrode is connected with the cable of the portable ECG device. Thus, the battery charge starts draining only when the wire is plugged into the electrode. The coin battery has a capacity of 40 mAh, allowing for the electrode to last for up to 2 weeks using the micro–power AD8617 CMOS dual Op–Amp.

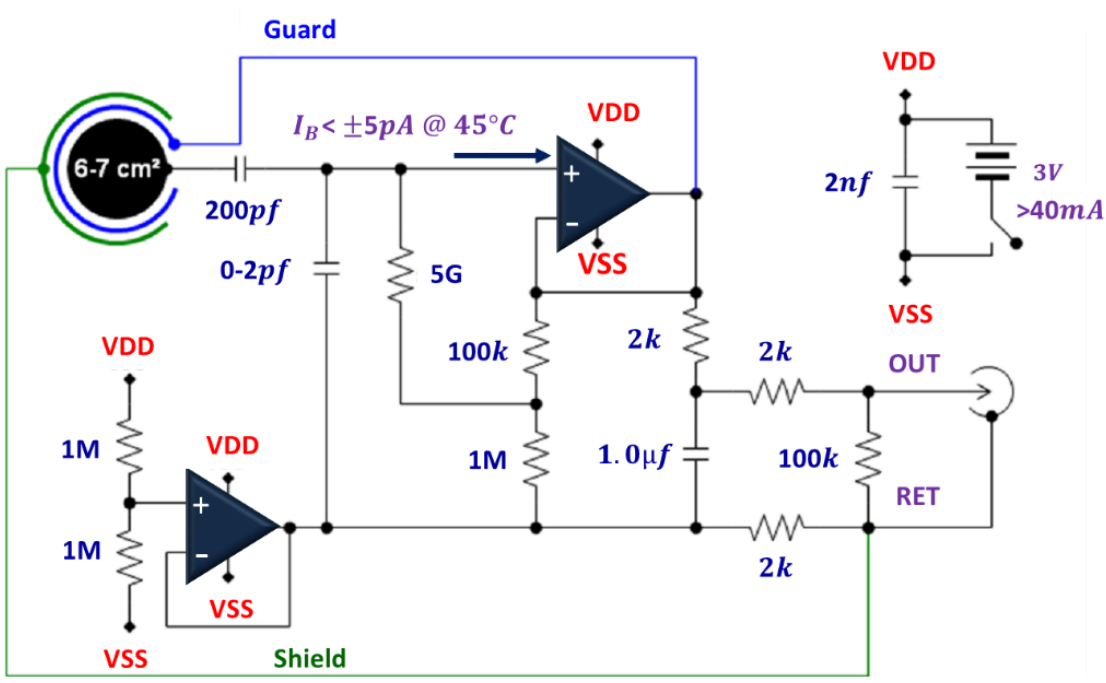

Figure 5.5 Schematic diagram of the capacitive electrode.

The operational amplifier (op–amp) AD8617 is selected for its low input bias current (< 5 pA) and low current consumption (< 0.1 mA). This op–amp also has a low offset voltage, a low input voltage, and current noise. The electrometric amplifier AD8617 is very suitable for portable medical devices. One of the op–amps is used for splitting the battery voltage symmetrically around the virtual ground (RET). The other op–amp is used for impedance buffering in the signal path, providing high impedance (50 GΩ) at the input and low impedance (few kΩ) at the output. The high input impedance of the electrodes makes them more tolerant to noise and artifacts. Shielding and guarding are carefully considered in the

layout in order to prevent external interferences being coupled to the sensitive input of the electrode.

Resistors and a capacitor are added at the output of the sensor in order to comply with safety requirements for the ECG systems, initial signal conditioning and lead–off detection. The safety requirements ask for very small or no current to keep the heart beating. Overall, the advantages of the proposed electrodes come from their small size and low power consumption, which enables both portability and long–term monitoring.

5.2.3 Portable ECG device

The Biometrics DataLog [5.79] is used as the data acquisition and transmission module for the portable ECG system. The size of the device is $104 \times 6 \times 22$ mm^3, weight is 129 g. The device is powered by two AA batteries and can run continuously for about 24 hours. The device is capable of transferring data in real time from up to 24 programmable channels. However, only one channel is used to realize the developed ECG system. The device also supports automatic data backup on a Micro SD card.

A photograph of the ECG measurement setup is shown in Figure 5.6. The electrodes are about 3 cm in diameter (Figure 5.3) and connected to the Biometrics DataLog device with flexible wires, which provides enhanced convenience to the user and also prevent the displacement of the electrodes in the case of body movement.

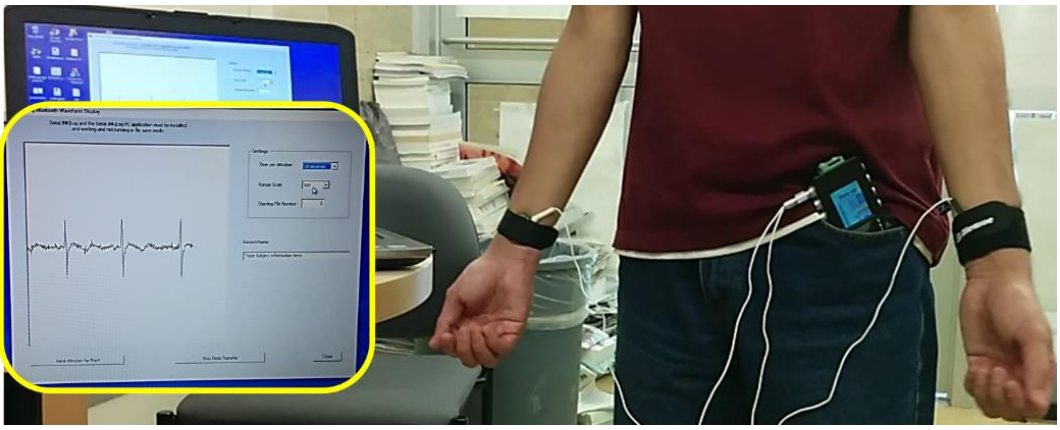

Figure 5.6 Photograph of the ECG measurement set–up.

5.2.4 Computer monitoring system

The Biometrics DataLog device acquires the ECG signals using the proposed capacitive–coupled electrodes. The portable ECG device transmits the measured ECG data over the Bluetooth platform in real time to a wireless receiver connected to the USB port of the computer. The ECG data received from the portable ECG device is processed by an infinite impulse response (IIR) notch (60 Hz) and a band–pass (1 Hz – 30 Hz) filter implemented in the software application to minimize the noise in the ECG traces. After performing the filtering, the ECG readings are displayed in real time. The software can also store the ECG readings in comma separated value (CSV) format. Each CSV file contains 10–seconds of ECG data. Consecutive acquisitions are automatically stored in files with filenames containing sequentially incremented numbers. Thus, the stored files contain the whole record of the ECG acquisition, until the storing function is stopped by the user. Therefore, the duration of the record is practically unlimited, or until the free disk space of the computer is consumed.

5.3 Performance evaluation

The proposed ECG monitoring system was used to measure the electrocardiogram from three different healthy subjects. The LA and RA electrodes were placed on the forearms of the left and right hand, respectively. The experiment was conducted in a standard room environment. A formal consent was taken from the McMaster Research Ethics Board (REB) to conduct the experiments. A simple questionnaire was prepared for the subjects to collect information about any known cardiac or significant health problems. The impact of different interface materials and body movements on the signal quality are also evaluated with experiments.

5.3.1 Experimental results

The ECG monitoring system was first tested by measuring the ECG signal at rest. The first set of measurements was taken by attaching the electrodes directly to the dry skin without applying any conductive gel or liquid (Figure 5.7 (a)). ECG was also measured by placing a thin cotton cloth between the electrodes and the skin (Figure 5.7 (b)). Reasonably good

ECG signals with distinguishable QRS complexes, P and T waves were observed in both cases. However, as shown in Figure 5.7 (a), the bare skin causes better coupling of signals to the electrodes compared to the textile–covered dry skin, thus resulting in signal with higher amplitude. However, since the ECGs were measured at rest, both signals were observed to be affected by a similar level of noise.

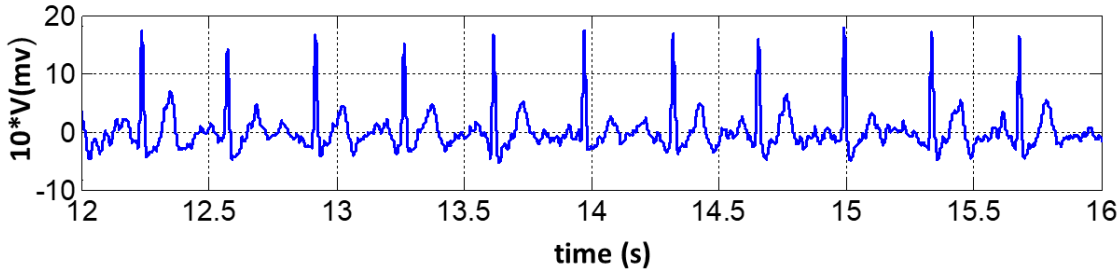

(a)

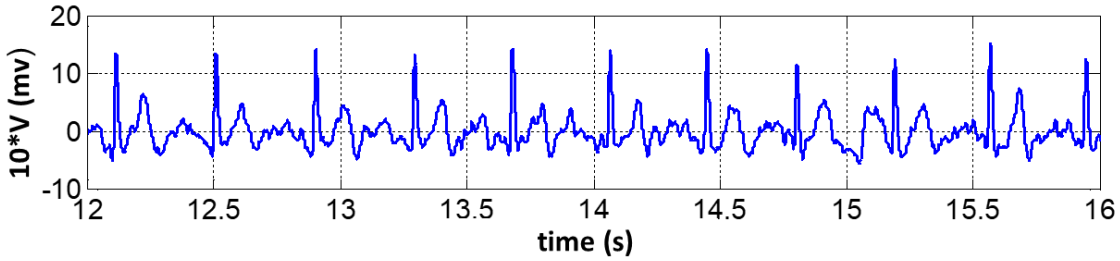

(b)

Figure 5.7 ECG acquisitions in the time domain without body movement, with electrodes on (a) bare dry skin and (b) cotton fabric covered dry skin.

A second set of experiments was performed to evaluate the impact of body movements on the ECG signals. Signals were measured with body movements, which include slow and fast abduction/adduction of hands, body rotation and normal walking. First, the ECG signals were measured by keeping the electrodes in direct contact with the dry skin. In the later experiments, the ECG signals were acquired by placing a thin cotton cloth between the electrodes and the dry skin. Figure 5.8 and Figure 5.9 show the ECG signals obtained by the direct–contact and contactless methods, respectively with different patterns of body movements.

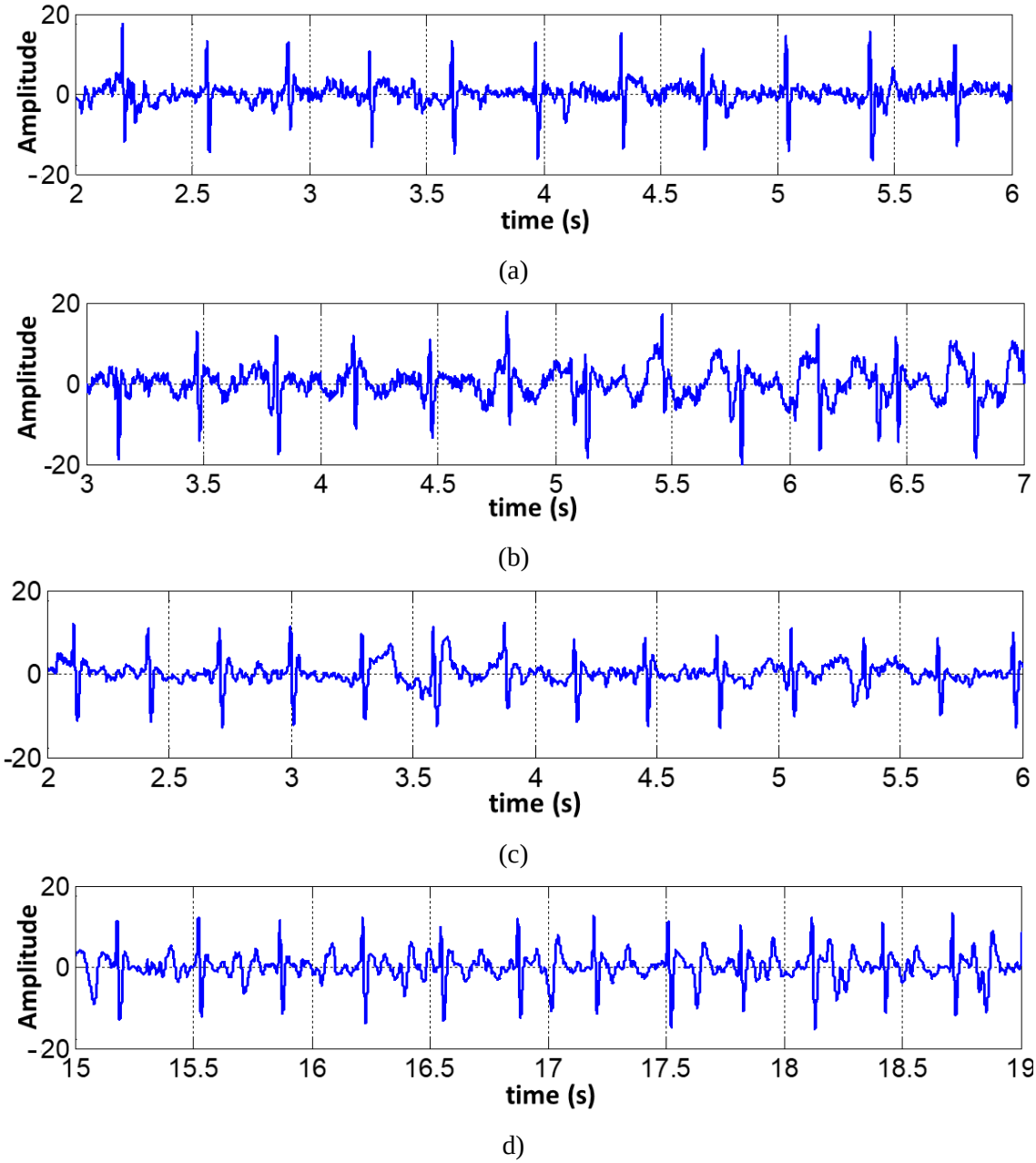

Figure 5.8 ECG measured from the bare dry skin with body movements: (a) slow abduction–adduction of both hands, (b) fast abduction–adduction of both hands, (c) body rotation, and (d) normal walking.

It was observed that the movement of the body contaminates the ECG signals in all cases, which is attributed to the displacement of the electrodes with movements. It can also be seen that the ECG signals obtained with a thin cotton cloth at the electrode–skin interface (Figure 5.9) are more affected by the motion–induced noise compared to the signals measured by direct–contact method (Figure 5.8). The textile material at the interface

experiences faster and larger displacement with the movements of the body, thus increasing the noise in the measured ECG signals. The QRS complex is, however, maintained in all cases although the P and T waves are heavily distorted by the movements.

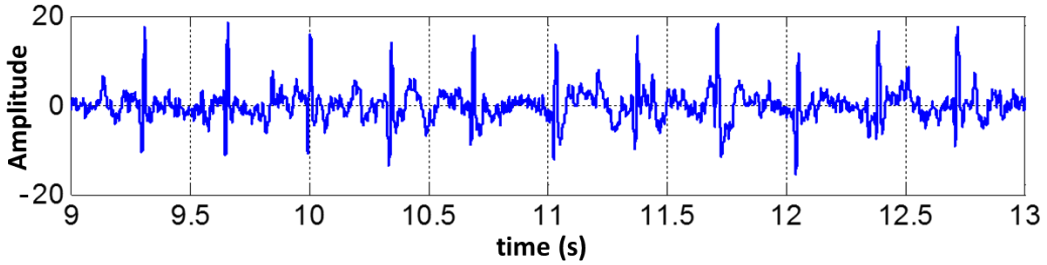

(a)

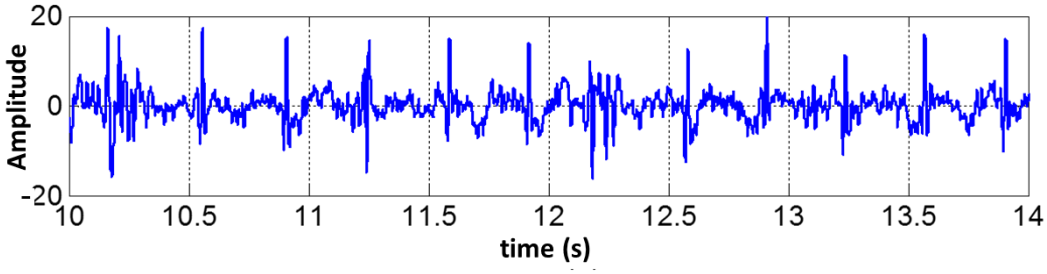

(b)

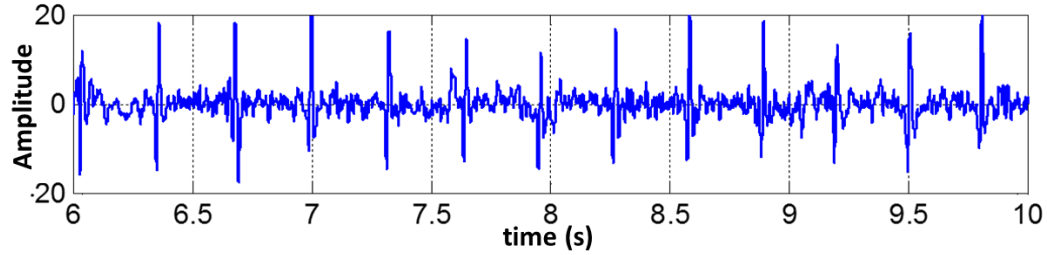

(c)

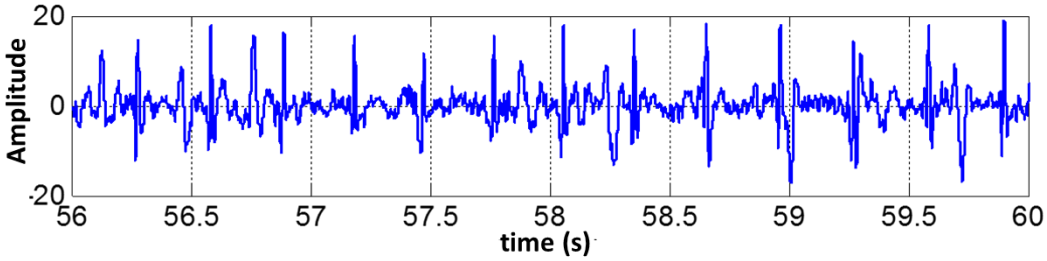

(d)

Figure 5.9 ECG measured from the textile covered dry skin with body movements: (a) slow abduction–adduction of both hands, (b) fast abduction–adduction of both hands, (c) body rotation, and (d) normal walking.

More experiments were performed at rest with the proposed electrode by placing different dry and moisturized (by water) textile materials at the interface. In Table 5.1, a summary

of the results in presence of different types of cotton interface materials and moisture is provided. A *good* result denotes waveforms with distinguishable QRS complex, P and T wave with a typical period of 5 seconds. The amplitude of the waveform varies depending on proximity of the electrodes to the heart. A stronger signal with higher amplitude of the waveform can be detected by placing the electrodes closer to the heart. On the contrary, a *poor* result refers to either no signal (flat) or waveform with significant fluctuations due to noise.

Table 5.1 Effects of interface materials and moisture on the ECG signal quality.

Interface materials and moisturizing		**Signal quality**
Electrode directly on skin surface	Dry	Good
	Moisturized	Good
Thin cotton cloth	Dry	Good
	Moisturized	Good
Cotton face towel	Dry	Poor
	Moisturized	Good
Cotton hand wipe	Dry	Good
	Moisturized	Good

5.3.2 Comparison with existing results

As discussed earlier, many ECG systems have been developed so far by the researchers by integrating different technologies such as, capacitive ECG electrodes, analog front ends, communication systems, and data processing techniques. Table 5.2 presents a comparison of key features between 10 different state–of–the–art ECG systems, including the proposed system. Compared to the technologies reported in these publications, the proposed ECG system presents a good balance among signal quality, size and power consumption. Although our proposed electrode is slightly larger than the electrodes presented in [5.5],[5.13],[5.80], it provides better flexibility in terms of integration with clothes. Additionally, the quality of the ECG signals obtained by the proposed system is similar to those reported in [5.4]–[5.14],[5.16],[5.22],[5.81]–[5.83]. The system also has lower power consumption and smaller size, which ensure better portability.

Table 5.2 Comparison between the proposed methods and recent alternatives for ECG sensing systems.

Ref.	Technology	Implement–ation	Advantages	Limitations	Com
[5.81]	Capacitive sensing	Integrated on chest belt	Portable and integrated to the Android phones	Power consumption issues	Zigbee
[5.80]	Flexible PDMS dry electrode	Integrated on wrist band	Small, low power consumption	Limited by the ECG recording systems	N/A
[5.13]	Capacitive sensing	Integrated on belt	Flexible electrodes integrated into garment, convenient integration on the body	Poor filtering (relatively small upper–corner frequency), Poor signal quality, Large Ref electrode – 250 cm^2	Bluetooth
[5.4]	Capacitive sensing	Integrated on chest vest	Picks up good signals through one or two layers of cotton	Large size of electrodes and devices gives poor portability	N/A
[5.5]	Capacitive sensing	Integrated on thin cloth	Small, low power electrodes	Limited by the phone and monitoring network	Bluetooth
[5.82]	Multiwall CNT/cotton–electrode	Integrated on cloth	Low cost, good conductivity on cotton materials	Limited by the circuits in electrodes and other part of the ECG system	N/A
[5.15]	Wet textile, Ag/AgCl electrodes	Integrated on belt	Good conductivity	Large in size, not portable	N/A
[5.83]	Dry electrode sensing	Integrated on cloth	Good noise filtering	Power consumption issues	Bluetooth/ ZigBee
[5.23]	Capacitive sensing using conductive foam	Embedded in chest belt	Flexible electrodes integrated with chest belt	3 electrodes, high resistor 5GΩ, Used for 24 hours, depends on clothing material, thickness, contact pressure and humidity	Bluetooth
[5.32]	Dry electrode sensing	Nanowoven fabrics with Ag/AgCl conductive inks	Screen printed dry electrode woven into fabric – comfortable, easy to use and suitable for wearable systems	Only sensing electrode demonstrated.	N/A
[5.6]	Dry–electrode, Active shielding	Integrated on cloth	Small electrodes (down to 8 mm diameter), conductive rubber electrodes	Relatively high power consumption, Low signal quality, Large sensor size	Bluesense AD module
This work	Capacitive sensing using flexible PCB	Integrable on a stretchable cloth	Very low power consumption compared to other systems, relatively small–size, ultra–thin flexible electrodes combined with standard 2–layer PCBs, easy to use	Semi–rigid electrodes using thin, flexible PCB	Bluetooth

In comparison with [5.5],[5.6],[5.13]–[5.15],[5.22],[5.83], our proposed method has better signal integrity primarily due to the flexible nature of the sensing material and better design of the capacitive electrode. Different wireless technologies have been adopted in different publications [5.5],[5.13],[5.16],[5.80]–[5.82]. For example, in [5.5],[5.13],[5.80],[5.81], it was suggested to develop mobile ECG monitoring applications in Android platforms for cell phones. However, cell phone consumes a significant amount of power during RF communications, which is an issue towards long term ECG monitoring. For long–term monitoring, an application specific transmitting device is preferred so that the battery can last for a minimum of one day of continuous operation of the portable unit.

The developed ECG monitoring system is tested, as routinely done, in an outpatient environment. Using our system, we aim to identify Tachy and Brady arrhythmias including atrial fibrillation, ventricular and supraventricular tachycardia (narrow complex and wide complex), sick sinus syndrome, episodic syncope which are particularly intermittent and may not be evident in short–term ECGs. The low power consumption allows the porotype system to monitor the ECG for prolonged periods. Apart from the long–term monitoring of ECG, one can also measure single lead short–term ambulatory ECGs using the proposed system.

5.4 Automatic anomaly detection

A single–lead ECG system, coupled with automatic detection of Atrial Fibrillation (AFib) is of paramount importance for early diagnosis that may otherwise lead to fatal consequences such as stroke and heart failure. In fact, approximately one–fourth of all strokes after the age of forty are caused by Afib [5.85]. The risk of developing AFib increases with age and other factors such as, high blood pressure, diabetes, and underlying heart disease, affecting approximately 200,000 Canadians[5.85]. In the case of AFib, the electrical impulses that contracts the atria to push the blood to the ventricles are fast and irregular, causing the heart to pump blood inefficiently at an irregular and faster pace. This results in irregular R–R intervals with missing P waves in the ECG signals. Figure 5.10 shows an example of single–lead ECG trace for normal and Afib signal.

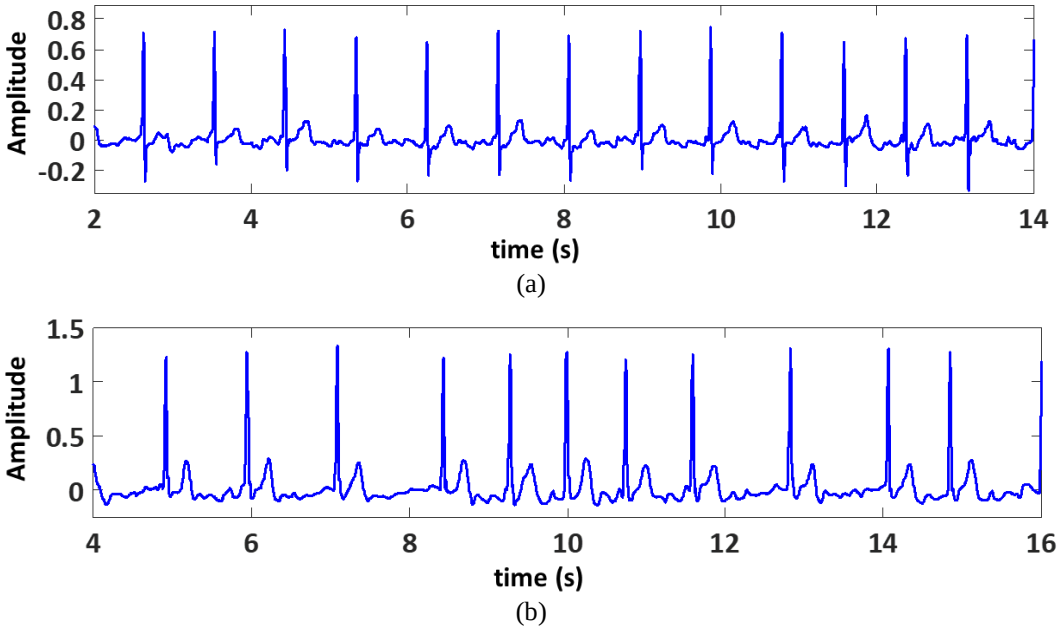

Figure 5.10 Single–lead ECG signal (a) normal rhythm and (b) atrial fibrilation [5.86].

Most AFib detection methods reported are based on binary classification between normal rhythms and AFib using high quality 12–lead clinical ECG signals. Although 12–lead ECG system can provide detailed information about heart health, it is not feasible for in–home ambulatory monitoring. In addition, the broad spectrum of cardiac anomalies such as, tachycardia, bradycardia, and arrhythmias exhibit similar pattern in HR and HRV, making high–specificity AFib detection even more challenging. Therefore, an automatic AFib detection method is developed as a potential extension of the system software that uses single–lead short ECG traces to detect normal, AFib, and other abnormal ECGs.

5.4.1 Data collection protocols

A total of 8528 single–lead ECG recordings are obtained from a publicly available dataset [5.86],[5.87]. The ECGs were measured with AliveCor's single–channel portable ECG device. The users held one electrode of the ECG device in each hand, thereby creating a lead I (LA–RA) equivalent of standard clinical ECG[5.88]. The ECGs were sampled at a rate of 300 samples per second and filtered by the AliveCor device. The ECG recordings are short with their duration varying from as short as 9s to 61s. The publicly available dataset comprises a heavily unbalanced set of four types of signals with 5076 normal ECG

traces, 785 AFib ECGs, 2415 other abnormal ECGs, and 279 noisy signals. The labelling of ECGs had been initially provided by the AliveCor that was further rechecked and relabelled by a group of experts [5.88]. However, for some ECG recordings even the experts could not reach to a consensus, further signifying the challenge associated with automatic anomaly detection [5.88].

5.4.2 Signal processing

Single–lead ECG signals measured by portable, non–clinical devices are generally vulnerable to noise and motion artifacts. The bodily movement and the rigid nature of the dry electrodes often disturb the contact interface between the skin and the electrode, thus corrupting the ECG signals and deteriorating the signal quality. Therefore, it is critical to improve the SNR of the ECG signals to ensure better classification performance.

The noise in the ECG signals may include low–frequency baseline wander due to breathing, and muscle movement as well as high–frequency impulse noise that evolves from occasional loss of contact between the skin and the electrode. A fast and hierarchical tree–like decomposition algorithm, discrete wavelet transform (DWT), is used to decompose the ECG signals into different frequency spectrums. As discussed before, the DWT decomposes a signal into approximation coefficients and detail coefficients by passing the discrete time–domain signal through several low–pas filters (LPF) and high–pass filters (HPF), respectively. While the approximation coefficients i.e. the lower–frequency components at each level can be further decomposed in a similar fashion, the detail coefficients or the higher–frequency components remain unaltered. A Daubechies 6 (db6) wavelet based discrete wavelet transform (DWT) method is used to decompose the ECG signals at level 9. The low–frequency approximation coefficients as well as the high–frequency detail coefficients are set to zero before reconstructing the ECG signal.

5.4.3 Feature extraction

Finding key discriminatory features are of paramount importance for a reliable and high performance classification tool. In this work, a large set of 371 features is extracted from the ECG signals. The features include statistical and entropy measures related to the timing

and morphological parameters. The timing parameters include the intervals between different characteristic peaks of the ECGs and HRV parameters such as pNN10, pNN20, pNN50, SDNN, SDSD and normalized RMSSD. The morphological features include the amplitude, rising and falling slopes and width of characteristic peaks. The normalized signal energy at different frequency spectrums are also calculated and fed to the classification algorithm. The energy E_c information of each component of the decomposed ECG signal is calculated using Eq. 5.1,

$$E_c = \frac{1}{B}\sum_{n=1}^{N} S_e(n)^2 \tag{5.1}$$

where S_e represents the components of decomposed ECG signal, N is the total number of samples, and B is the total number of ECG cycles in the signal.

In order to find the similarity measures among different segments of the ECG signal, the filtered ECG signals are segmented into three equal length windows (M_w) with overlap to form a $M_w \times 3$ matrix. A set of features associated with the singular values are then obtained from singular value decomposition (SVD) of the matrix.

Another measure of variation in the ECG parameters is obtained by calculating the coefficient of variation of the timing and morphological parameters. The coefficient of variation is given by,

$$CV = 100 \times \frac{\sigma_p}{\mu_p} \tag{5.2}$$

where σ_p and μ_p are standard deviation and mean of parameter p.

5.4.4 Predictive model

The ECGs were classified using a two stage process. In the first stage, a rule–based decision support technique was used to identify some of the noisy signals and AFib signals based–on some of the features' probability distribution and prior clinical knowledge. For example, based–on the distribution of HR as well as clinical knowledge, ECGs with HR above 98 bpm are identified as AFib. This simple rule–based identification in the first stage reduces computational burden in the second stage. However, ECGs showing normal and slower HR can still be AFib.

Therefore, a Bootstrap Aggregated tree (Bagged tree) is used in the second stage to classify normal, AFib, other rhythms and noisy signals. Decision tree is a very well–known and popular technique of decision making that uses a tree–like structure of decisions and their possible consequences. A decision tree can be a simple one with several branches, however, can get very complex in the case when many features and their values are interlinked or uncertain. A simple tree is prone to having a large model bias whereas a complex tree–based model may suffer from high variance. Bagged tree is one of the ensemble methods, which instead of using a single decision tree combines the outcomes from several decision trees to realize a better predictive model.

In an ensemble method, a strong learner is developed by combining a group of weak learners. In Bagged tree method, several subsets of the training data are picked randomly with replacement. Each subset of training data is then used to train a decision tree, thereby reducing the model variance associated with complex decision trees. The predictions from all such trees are then combined to obtain the final prediction, resulting in a more robust model than a single decision tree.

5.4.5 Model performance

The performance of the model was validated using 5–fold cross validation. Each time, 1706 ECGs out of 6822 were excluded randomly without overlap. Five such non–overlapping subsets of 1706 ECGs were thus obtained. The model was then trained in each case with the remaining 6822 ECGs. Finally, the excluded 1706 ECGs from each subset were classified using the model. The performance of the model was evaluated by calculating the F_1–scores for normal (F_{1n}), AFib (F_{1a}) and other rhythms (F_{1o}), separately as well as by the mean F_1–score of these three classes as recommended by [5.87]. The F_1–score of one class is given by,

$$F_{1x} = \frac{2TP}{2TP + (FP + FN)}; \qquad x = n, a, o \tag{5.3}$$

where, TP, FP, and FN represent the number of ECGs classified as true positive, false positive and false negative, respectively. The overall F_1–score is defined by [5.87] as,

$$\breve{F}_1 = \frac{F_{1n} + F_{1a} + F_{1o}}{3} \tag{5.4}$$

The performance of the classifier for all 5–fold validation is presented in Table 5.3.

Table 5.3 Performance of the anomalous ECG detector.

Folds	F_{1n}	F_{1o}	F_{1a}	$\breve{F}_1$
1	0.90	0.73	0.75	0.80
2	0.89	0.72	0.76	0.79
3	0.89	0.70	0.73	0.78
4	0.89	0.71	0.78	0.79
5	0.90	0.72	0.78	0.80
Overall	**0.90**	**0.73**	**0.78**	**0.80**

It can be seen that the classifier performs well across all five folds with a mean $\breve{F}_1$ of 0.80. The small standard deviation of 0.6% among $\breve{F}_1$ from different test scenarios ensures the model's robustness and stability. The model particularly achieves a very high F_1–score in classifying normal ECGs with a mean F_{1n} of 0.90 ($\pm$0.5%) and a moderately high F1–score in detecting AFib with a mean F_{1a} of 0.78 ($\pm$2.1%), reflecting a reasonably accurate classifier that can potentially be incorporated in the proposed ECG system to facilitate in–home detection atrial fibrillation at its onset.

It should be noted that even the experts could not reach to a consensus while labelling some of the ECGs, potentially causing some signals to be wrongly labelled. This may have affected the model accuracy to some extent, further signifying the challenges associated with automatic anomaly detection with ambulatory ECG systems.

5.5 Conclusions

An Electrocardiography (ECG) monitoring system has been developed to achieve improved signal detection, portability and reduced power consumption by addressing the trade–offs among size, power requirements, and signal quality. Recent developments in the ambulatory ECG monitoring systems have been leaning towards the idea of contactless bio–potential sensing. Since the contactless ECG monitoring system does not require any direct contact to the skin, it offers better user comfort during prolonged monitoring. The proposed system is capable of measuring the ECG signal on a biocompatible textile–based interface material such as cotton. The smaller size of the electrodes also allows for better

portability and convenience to the user. The proposed system does not require a ground electrode. As a result, the single lead ECG can be measured by using only two electrodes. The proposed ECG electrodes consume small amount power and can run continuously for 2 weeks from a 3V coin cell battery that makes the electrode suitable for long–term monitoring. The electrodes are connected to a portable ECG device that is capable of transmitting signals continuously for 24 hours over the Bluetooth platform to a personal computer in real time. Therefore, at present, the overall continuous run time of the system is limited by the battery life of the commercial data acquisition and transmission module. As observed from the results of the experiments, the proposed ECG monitoring system can properly acquire the ECG signals over the cloth with the QRS complexes, P and T waves being clearly distinguishable, when measured at rest. The proposed system, therefore, can potentially be used to detect abnormal ECGs by enabling long–term monitoring of cardiac activities.

Despite the advances that are being made in ECG monitoring systems, there is still room for further improvements. In order to reduce the displacement of the electrodes with motion, the electrodes need to be firmly integrated over the cloth. Furthermore, the electrostatic coupling of the electrodes to the skin potential can be improved by employing a dedicated film or membrane materials with increased dielectric permittivity. Conductive polymers or smart textiles can also be used to realize conductive sensing part of the electrodes, which may offer enhanced flexibility and user comfort.

Electrocardiography monitoring systems continue to be a very active area of research and technology development. So, a critical review and comparison of recent ambulatory ECG monitoring systems and ECG systems–on–chip solutions is presented and discussed. The major features and performance characteristics of recently published state–of–the–art ECG systems are compared and described. For long–term monitoring, electrodes integrated on skin and different types of interface clothing materials are desired. Therefore, a comparison of the advantages and limitations between the method proposed in this work and recent alternatives for ECG sensing systems is presented and discussed.

Chapter 6

Association between gait and heart

Walking is the most common daily physical activity that people perform on a regular basis. As mentioned in Chapter 4, healthy walking requires proper functioning and coordination between the nervous and musculoskeletal systems. Any damage to these systems can affect this process of coordination that can be manifested through an altered gait pattern. For example, patients suffering from neurodegenerative disorders such as Parkinson's disease, tend to walk with short and shuffling steps. Therefore, walking or gait is understandably rich in clinical information and can be used as a simple but effective biomarker in identifying chronologically aged people from geriatric i.e. biologically aged patients as well as to assess overall health and longevity of the older adults.

IMUs are the most suitable candidates for precise and accurate measurements of movements in a wearable platform, thus making them our device of interest for gait measurement. Furthermore, owing to the severity and global prevalence of cardiovascular diseases, we are particularly interested in studying the association between key cardiac features and gait features obtained from on–body IMUs. In this chapter, we investigate the quantitative association between human gait and cardiac activities measured with inertial sensors and single–lead portable ECG monitor, respectively. We present experimental results that show a good association between gait and heart activity. These associations can potentially enable realizing a low–cost monitoring tool to detect early signs of CVD–associated changes in gait features before the actual CVD symptoms are manifested.

6.1 Background

The central nervous system is both anatomically and physiologically linked to the cardiovascular system and the musculoskeletal system of the body, resulting in numerous interactions among them. The brain has three main parts: the *cerebrum*, *cerebellum* and *brainstem* (Figure 6.1). The *brainstem* part of the brain controls many automatic functions of the body including cardiac and lung function through the sympathetic and parasympathetic branches of the autonomic nervous system. It is thereby responsible for regulating the autonomic functions of the body, such as heart rate, respiratory rate, body temperature and blood pressure. The *brainstem* also serves as a relay hub, which connects the *cerebrum* and *cerebellum* of the brain to the *spinal cord*.

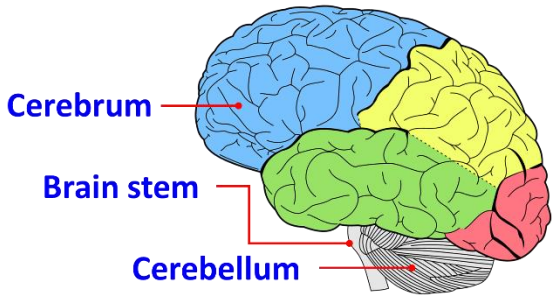

Figure 6.1 The brain has three main parts: the cerebrum, cerebellum and brain stem.

On the other hand, the *cerebellum* along with the spinal cord plays a vital role in motor coordination and regulating gait while maintaining postural stability and dynamic balance through a combination of voluntary and involuntary processes. The natural gait pattern results from the involuntary processes of the central nervous system (CNS). However, the gait and postural adjustments activate voluntarily or involuntarily upon receiving feedback about the environment from different sensory organs. In response to the sensory signals received from the spinal cord, the *cerebellum* sends signals to the *cerebral cortex* and the *brainstem*. These regions then relay the signals to the spinal cord that activates the motor neurons to adjust the gait pattern and postural stability and balance according to the environment.

Due to numerous intertwined interactions among the CNS, the cardiovascular system and the musculoskeletal system, it is understandable that some damage to or malfunctioning of one of these systems can disrupt this precise act of coordinated interactions, resulting in an altered gait pattern. For example, neurodegenerative disorders such as Parkinson's disease frequently cause slowly progressive autonomic failure that not only alters the gait pattern but also often causes cardiac autonomic dysfunction. However, the most prevalent cardiac abnormalities caused by CNS–associated disorders are arrhythmias.

One of the easy–to–measure, nevertheless, critical gait parameters is the gait speed, which reflects the overall status of health. The body adjusts its natural gait speed according to the ability of all the systems associated with the gait to adapt to the walking environment while minimizing the energy expenditure simultaneously. As persons become frail with age their gait speed decrease gradually in an attempt to maintain dynamic postural stability [6.1]. It was reported that gait speed reduces significantly after 50 years of age in both male and female [6.2]. In addition, decreased physical strength and flexibility [6.3] due to loss of muscle mass results into a reduced but highly variable step length, minimum toe clearance (MTC) [6.2],[6.1],[6.5] and range of motion (ROM) of the joints [6.3],[6.6]. A reduced and highly variable MTC and ROM of the knee and hip joints put an individual at a greater risk of accidentally contacting the walking surface during the swing phase of the gait, thus resulting in a trip or fall [6.1],[6.5].

Gait speed is also known to be associated with the risk of developing heart disease. People with slow walking pace were reported to be more vulnerable to cardiac and all–cause death compared to the brisk walkers that is likely associated with their physical fitness. Among the slow walkers, those with a low BMI are at the highest risk that is possibly attributed to the malnourishment or excessive levels of muscle tissue loss with age. However, it is uncertain whether physical fitness leads to a faster gait speed or faster gait speed results in better fitness. Nevertheless, it is well recognized that better physical fitness leads to better cardiac health.

Therefore, gait speed is understandably regarded as a reliable measure of frailty [6.7] and an indicator of an individual's likelihood of maintaining an independent and active life. In addition, gait speed, along with age and gender, has been shown to be a good predictor of life expectancy [6.1],[6.9]. Regular monitoring and trend analysis of a person's gait speed can therefore be very useful in identifying potential health problems at the very outset.

Alongside the gait speed, step length is also affected by health conditions. For example, patients with chronic heart failure (CHF) take short and frequent steps, which in severe cases may lead to a shuffling gait [6.1]. A weak heart potentially leads to higher gait variability, lower gait speed and angular velocity, shorter steps, and increased gait asymmetry. Possible reasons for this type of gait in CHF patients may be attributed to the abnormalities associated with their vascular system and strength of skeletal muscle alongside the histological and biochemical anomalies [6.9]. This short–shuffling gait in CHF patients also likely affects their oxygen consumption and thereby the ability to perform physical exercise. The muscle tissues possibly cannot support the contraction necessary to maintain a longer stride and consistent rhythmic steps as gait speed and cadence are highly associated with the strength of calf–muscle [6.9].

Another factor that links the cardiac health and gait is the energy expenditure during walking. Energy expenditure, which is measured by the rate of Oxygen consumption is reported to be linearly proportional to the gait speed over the range of 50–100 m/min [6.10], [6.11] and is also highly correlated with body weight [6.10]. However, oxygen consumption increases at a faster rate at higher gait speed [6.11]. In addition, motor impairments often reduces the efficiency of functional ability, resulting in increased oxygen expenditure [6.12]. Effective and efficient functioning of the heart is critical to maintain a sufficient supply of O_2 in the body to keep up with the body's demand of O_2 during the period of a submaximal workload such as walking, jogging, and climbing staircase.

A popular measure of gait efficiency that combines heart rate and gait velocity is the Physiological Cost Index (PCI), which was proposed by MacGregor [6.13] in 1979. PCI has since been extensively used in clinical and research settings [6.12]. MacGregor

assumed heart rate and oxygen consumption are linearly associated at submaximal workloads and proposed an indirect measure of oxygen expenditure during walking as,

$$PCI = \frac{\Delta HR(\text{bpm})}{v\ (\text{m/min})} \tag{6.1}$$

where, ΔHR is the difference between the steady–state walking heart rate (HR_w) during walk and resting heart rate (HR_r) and v is the gait velocity. Figure 6.2 shows how the HR changes with physical activities.

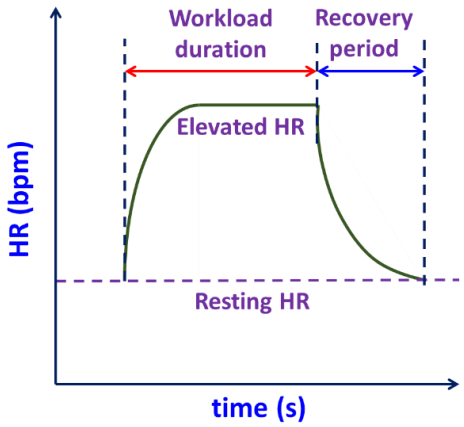

Figure 6.2 Change in HR due to submaximal workloads.

A smaller change in HR with walking results in a smaller PCI i.e. a lower energy cost of walking, thus indicating an efficient gait. On the contrary, a bigger change in HR with walking gives rise to a higher PCI that is indicative of an inefficient gait.

6.2 Data acquisition and protocols

6.2.1 Participants and protocols

In this study, we recruited 38 healthy persons with their age ranging from 18 to 65 years and obtained 50 set of ECG and walking measurements that includes an additional 12 set of measurements taken from the 12 participants at a different point of time. The participants were first briefed on the motivation of the study and the data privacy and security protocols prior to the experiment that was followed by a short session to familiarize the participants with the measurement systems and protocols. Each participant answered a questionnaire designed by a physician to collect information about some key physical features of the

participants such as their weight, sex, age, leg length, and height. For the experiments, we only recruited healthy subjects with no major health issues and/or prior surgeries and obtained a signed consent from each of them. Prior approval for the study was received from the Hamilton Health Sciences Research Ethics Board.

6.2.2 Data acquisition systems

Single lead ECG was measured using an FDA–approved portable, handheld ECG device (HeartCheck™). This device acquired 30s long ECG signals at a rate of 250 samples per second and stored the data on it. The ECG data were transferred to a computer via a USB cable and are stored there as text files. The motion signals corresponding to human walking were acquired using the inertial measurement units (IMUs) from InvenSense Inc (MPU–9150). The IMU measured 43 mm, 37 mm, and 12 mm in length, width and height, respectively and included a tri–axial accelerometer and a tri–axial gyroscope. The accelerometer and the gyroscope offered a full–scale range of ±16g and ±2000 degrees per second (dps), respectively. The IMU was configured to acquire signals at a rate of 50 samples per second. The measured motion data were transmitted to a computer in real-time using the IMUs onboard Bluetooth transceiver module. The computer runs a Python program to communicate with the IMUs over the Bluetooth medium and to store the data as text files. Finally, a program was developed in MATLAB to read both the ECG and walking data from the text files for further processing and analyses.

6.2.3 Data acquisition protocol

The IMU was mounted on a Velcro belt and attached at the frontal section of the shank of both legs (Figure 6.3a). The placement of the IMUs at the frontal section reduced the motion artifacts due to the movement of the muscles and the soft–tissues. The orientation of the attached device was such that the *x*–axis, *y*–axis and *z*–axis point towards the upright direction (longitudinal), the outward direction (medio–lateral) and the forward direction (antero–posterior), respectively. To maintain the uniformity of measurements among the subjects, the IMU was always attached at 20 cm above from the ground level.

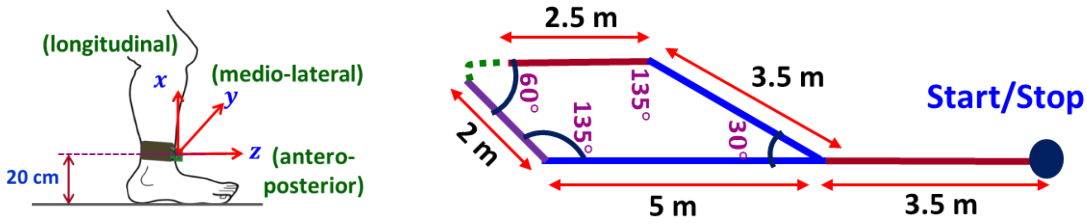

(a) (b)

Figure 6.3 Experimental setup a) IMU attachment in the shank b) 20 m walking loop.

The ECG was measured twice from each participant – at rest and immediately after walking. After measuring the resting ECG, the participant was taken to the starting point and asked to walk along a marked walkway at his/her preferred pace. The walkway was a well–illuminated 20m long loop and had 5 turns (45°, 120°, 45°, 30°, and 180°) along the path (Figure 6.3b). The participants were asked to complete 10 rounds along the path to complete walking a distance of 200m. This 200 m walk allowed the HR of the participants to reach a steady state during the walking. The participant started and stopped walking at the verbal commands of "start" and "stop" given by the investigator. The subject's ECG was measured again immediately after completing the specified walk.

6.3 Results and discussion

6.3.1 Association between Resting HR and Gait

Our study included a dataset of 50 measurements of ECG and gait signal from 38 participants. The participants were divided into two groups. Group 1 (G1) included 34 (68%) sets of measurements with a resting heart rate below 85 bpm and group 2 (G2) had 16 (86.9%) sets of measurements with a resting heart rate equals and above 85 bpm. The comparisons of the gait parameters between the two groups were made with one–way analysis of variance (ANOVA) method. ANOVA shows if there is a significant separation in the distributions of a parameter between two groups that is assessed by the *p*–value (*p*). A *p*–value < 0.05 is considered as significant for all statistical tests.

Among the physical characteristics, BMI was found to have a statistically significant association ($p < 0.0001$) with the two groups. It was observed that participants with higher BMI (mean BMI 28.1 vs 23.5) were more likely to having a higher resting HR. Overweight

and obesity occurs due to increase of white adipose tissue (WAT), which increases the body's metabolic rate, resulting into increased number or size of blood vessels [6.14]. As a result, the total blood volume and the cardiac output increases in overweight and obese people, thereby affecting the structure and function of vascular system and cardiac vessels [6.15]. Therefore, the cardiac output, which is determined by the cardiac stroke volume and heart rate, is likely to increase in overweight and obese people than in people with normal weight [6.15].

A total of 486 gait features were extracted from the accelerometer and gyroscope signals measured from both legs. After performing the ANOVA test, a set of 76 statistically significant gait variables ($p < 0.05$) were selected to use in three different types of classification algorithms – linear support vector machine (SVM), linear discriminant analysis (LDA) and logistic regression (LG). Gait variables with $p > 0.05$ were considered as statistically not significant and were discarded during the parameter selection and training process. A set of only five gait features were finally obtained that maximized the model accuracies in classifying the two groups of resting HRs with a five–fold cross validation. The classification performance was further evaluated by Positive Predictive Value (PPV), Negative Predictive Value (NPV), Sensitivity and Specificity. The confusion matrices of the five–fold cross validation from all three models are presented in Table 6.1. The high and consistent classification performance achieved from all three simple models with the five gait features validate their relevance in the association with the resting HR.

Table 6.1 Performance of the models after 5–fold cross validation.

Model	Accuracy	PPV	NPV	Sensitivity	Specificity
SVM	90%	89%	92%	97%	75%
LDA	88%	87%	92%	97%	69%
LR	84%	86%	79%	91%	69%

In order to find out the key contributors to the gait's association with the resting heart rate, we performed principal component analysis (PCA) on the set of these five features and created a biplot of the first three principal component coefficients. The first three principal component (PC1) explains 77.8% of total variance in the data. Table 6.2 presents the

description of the five gait features that are likely to be associated with the resting heart rate and their contributions (coefficients) in the first three principal components.

Table 6.2 Description of the five key gait features.

Feature	Description	PC1	PC2	PC3	2–norm
f1	Asymmetry between legs in terms of the proportion of gait cycles having more than 20% cycle–to–cycle variation in a_{p2pMS} *wrt* the mean a_{p2pMS}	–0.196	0.6588	0.464	0.8294
f2	Skewness of the peak acceleration during the mid–swing phases of the dominant leg	0.5861	0.1881	0.4045	0.7365
f3	Proportion of gait cycles having 10–20% cycle–to–cycle variation in a_{mxMS} *wrt* the mean a_{mxMS} of the dominant leg	0.5912	0.2708	–0.0038	0.6503
f4	Standard deviation of minimum angular velocities at foot–lift	–0.5096	0.1558	0.4067	0.6704
f5	Proportion of gait cycles having more than 20% cycle–to–cycle variation in ω_{fs} *wrt* the mean ω_{fs} of the dominant leg	0.094	–0.658	0.675	0.9473

a_{p2pMS}: Peak–to–peak acceleration during the mid–swing phase of the gait.
a_{mxMS}: Maximum acceleration during the mid–swing phase of the gait.
ω_{fs}: The rate at angular velocity changes following the mid–swing phase.

All five gait parameters are seen to be associated with resting HR are related with variability and asymmetry during the mid–swing phase of the gait, potentially suggesting an association of variability and asymmetry at the mid–swing phase of gait with cardiac output. The biplot of the first three principal component coefficients is presented in Figure 6.4.

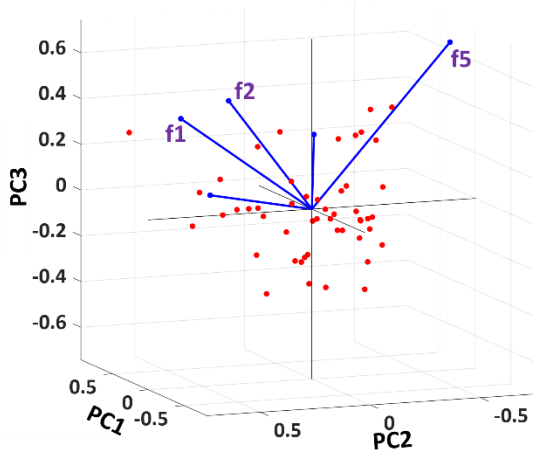

Figure 6.4 Biplot of the first three principal component coefficients.

It can be seen from the biplot as well as from the 2–norm (Table 6.2) that **f5**, **f1** and **f2** are the three highest contributions in the first three principal components that are associated with resting HR. Features **f1** explains the asymmetric pattern in the variability of a_{p2pMS} between two legs. On the other hand, feature **f2** explains the distortion in the distribution of peak acceleration during the mid–swing phases of the dominant leg, which along with feature **f5** explain the control on gait after mid–swing. A high variability in ω_{fs} following the mid–swing can be indicative of an individual's adaptability to the walking environment [6.15],[6.16]. Figure 6.5 shows the trend of the feature **f1**, **f3** and **f5** with respect to the resting HR. In a nutshell, a more symmetric and skewed acceleration during the mid–swing phase as well as high adaptability or controllability of the gait following the mid–swing are some potential good indicators of better resting cardiac output.

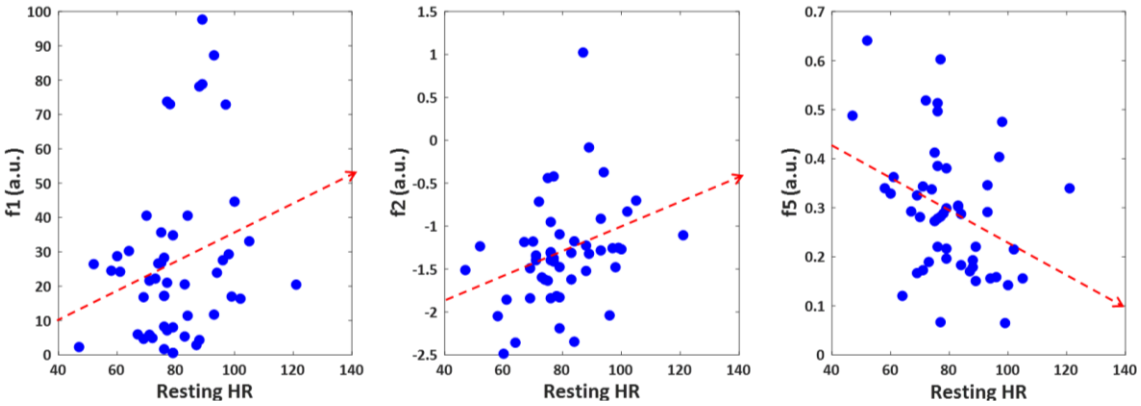

Figure 6.5 Association of key gait features with resting HR.

6.3.2 Association between HRV and Gait

Heart rate variability (HRV) is generally defined by beat–to–beat variations in the R–R intervals of the ECG signals. Although HRV manifests the variation in the heart's rhythmicity, it is regulated by the nervous system. The parasympathetic part of the nervous system that is often referred to as the rest and digest system decreases the heart rate, whereas the sympathetic nervous system or the *fight–or–flight* system, responds to situations like stress, anxiety, and exercise and increases the heart rate. In the case of a balanced and well–regulated Autonomic Nervous System (ANS), these two contrasting parts simultaneously send signals to the heart (Figure 6.6), resulting in a natural fluctuation

in R–R intervals. Therefore, HRV understandably represents the functioning of the ANS as well as overall health, endurance, and capacity to tolerate stress.

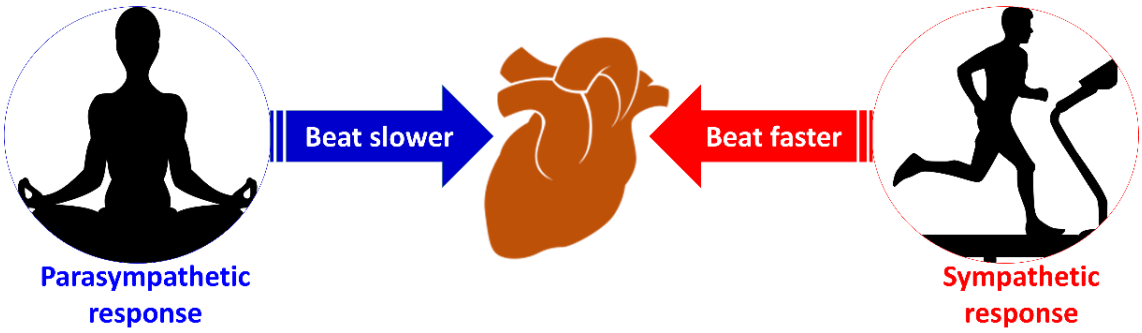

Figure 6.6 Heart rate variability evolves from the interaction between the sympathetic and parasympathetic parts of ANS.

A high resting–HRV is generally favorable that is indicative of a balanced ANS [6.18],[6.19]. A balanced ANS enables the body to effectively respond to both the parasympathetic and sympathetic inputs, making it highly adaptable to the environment and to perform efficiently. However, a low resting–HRV is indicative of disruption in the natural interaction between these two systems, leaving the body in a sympathetically dominant fight state even when the body is not involved in any activity. This results in inefficient use of bodily resources and leaves fewer resources available for actual *fight–or–flight* scenarios such as physical activities, stress, and anxiety [6.18],[6.19].

HRV can be described both in time–domain, frequency–domain [6.18],[6.19]. Time–domain HRV indices quantify the beat–to–beat variability in the ECG measurements, whereas frequency–domain indices explain the absolute or relative power into four frequency bands – ultra–low–frequency (≤ 0.003 Hz), very–low–frequency (0.0033–0.04 Hz), low–frequency (0.04–0.15 Hz), and high–frequency (0.15–0.4 Hz) bands. Table 6.3 presents the some of the HRV indices in time domain.

Table 6.3 HRV indices in time domain.

Parameter	Unit	Description
SDNN	ms	Standard deviation of NN intervals
pNN20	%	% of consecutive NN intervals that differ by more than 20 ms
pNN50	%	% of consecutive NN intervals that differ by more than 50 ms
RMSSD	ms	Root mean square of successive differences between NN intervals

A. HRV with aging

It can be seen that the HRV indices showed a negative correlation with aging. However, no HRV index showed any statistically significant correlation with BMI, gait speed, and stride length. Resting–HRV determined by pNN20 and pNN50 decreased following a quadratic regression pattern with aging (See Figure 6.7), with the Spearman correlation coefficient of -0.45 ($p < 0.002$) and -0.40 ($p < 0.02$), respectively that is consistent with the observations reported in [6.19].

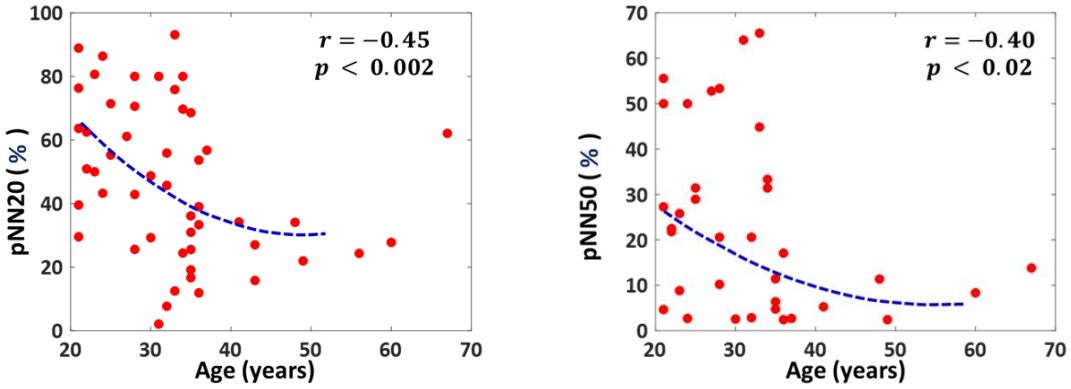

(a) (b)

Figure 6.7 Relations between age and resting–HRV of healthy participants determined by a) pNN20 and b) pNN50.

Although both SDNN and RMSSD at rest also showed a negative correlation with aging, they were not found statistically significant in this work. However, all four indices obtained from the ECGs immediately after the walking experiment showed statistically significant negative correlation with age. Table 6.4 presents the correlations of the four HRV indices with age both at rest and after walk.

Table 6.4 HRV indices with age both at rest and after walk.

	At rest		After walk	
	r	***p***	***r***	***p***
RMSSD	-0.23	0.11	-0.42	< 0.003
SDNN	-0.23	0.11	-0.42	< 0.003
pNN20	-0.45	< 0.002	-0.41	< 0.004
pNN50	-0.40	< 0.02	-0.42	< 0.007

The pNN50 is believed to reflect the parasympathetic activity of the body [6.20]. Therefore, the rapid decline of pNN50 as well as pNN20 with aging could be reflective of an early decline of parasympathetic activity compared to the sympathetic activity [6.20].

B. HRV with gait

The resting–HRV indices showed some association with the key gait parameters such gait speed, and stride length (Table 6.5). It was observed that participants who walked at a speed of or slower than 1.1 meter/s had on average a lower resting RMSSD (31 ms vs 59 ms) and SDNN (32 ms vs 60 ms) than the others that is statistically significant at $p < 0.05$. In addition, people with shorter stride length (≤ 1.1 m) had significantly lower ($p < 0.05$) pNN20, RMSSD and SDNN compared to the participants who had longer strides. The positive association of resting–HRVs and gait speed as well as stride length is likely indicative of the participants' physical fitness.

Table 6.5 Association of resting–HRVs with gait speed and stride length.

	Speed ≤ 1.1m/s		**Speed > 1.1 m/s**			**stride length ≤ 1.1**		**stride length >1.1**		
	$n = 17$		$n = 33$			$n = 22$		$n = 28$		
	μ	σ	μ	σ	p	μ	σ	μ	σ	p
pNN50	13.0	17.9	18.1	20.7	0.39	12.4	16.4	19.5	21.8	0.21
pNN20	41.7	23.7	49.5	24.3	0.29	39.1	24.0	52.9	22.9	< 0.05
RMSSD	31	19	59	52	< 0.05	34	22	62	55	< 0.05
SDNN	32	19	60	53	< 0.05	34	22	63	56	< 0.05

μ: mean, $\boldsymbol{\sigma}$: standard deviation

In addition, participants who spent more time in the stance phase i.e. showed a higher stance–to–swing time ratio, on average (1.36 vs 1.1) tend to have a lower resting RMSSD and SDNN at a significance of $p < 0.05$. Furthermore, participants with shorter swing time (47 ms vs 52 ms) had a lower pNN20 (30.5 vs 51.5), which was statistically significant at $p < 0.01$. Interestingly, participants showing a higher stance–to–swing time ratio and shorter swing time as well as lower resting HRV indices had a higher mean age (34 years vs 31 years and 36 years vs 32 years, respectively). As discussed in Chapter 5, the gradual decline in bone and muscle mass as well as joint fluids with age causes people to walk with

a shorter stride length as age progresses. To compensate for the declining balance and stability they tend to spend less time in the swing phase and more time in the stance phase. Besides, owing to their shorter stride length, older group of people have to exert higher torque [4.53] to the hip joints to perform more work in a gait cycle. As age progress, the basal energy expenditure efficiency declines owing to the gradual deterioration of gait symmetry, postural balance and alignment, as well as coordination between the central nervous and the musculoskeletal systems [4.54] that is likely to be associated with their reduced HRV.

The gait asymmetry (GA) and variation (CV) in stance time were observed to be associated with some HRV indices. A lower RMSSD (43 vs 78) and SDNN (44 vs 79) were found to be associated with increased gait asymmetry (0.216 vs 0.025), both at a statistical significance of $p < 0.05$. In addition, a smaller variation in stance time (40 vs 72) that explains for the reduced adaptability and balance control [6.21] was observed to be significantly (p <0.02) associated with lower pNN20 (34 vs 52).

6.4 Conclusions

In this chapter, we studied the association between human gait and cardiac activities quantitatively based–on measurements obtained with inertial sensors and single–lead portable ECG monitor, respectively. It was observed that gait asymmetry between two legs and variation in the gait are generally associated with key cardiac parameters such as HR and HRV as well as physical parameters such as age and BMI. These quantitative associations between gait and heart can potentially be useful in realizing an IMU–based predictive or screening tool to detect or screen for subtle changes in CVD–associated gait features much ahead of the actual CVD symptoms are manifested.

Although the reported observations mostly follow well–established and widely–accepted theories and results in the literature, there remain some limitations of this study. First, resting HRs are obtained from visibly healthy people and thus considered 'normal'. However, a recent study on 92,457 adults [6.24] showed that the normal resting HRs among people can vary as high as 70 bpm. Therefore, an HR, which is normal for an individual

can be abnormal for the other. The fluctuation of resting HR over a long period of time can be more useful for a more accurate assessment of cardiac health that further signifies the importance of a portable and wearable single–lead ECG monitor. Second, although the observed trends are similar to those reported in the literature, our observations may still have some inaccuracies due to a limited number of data. For example, resting–RMSSD and SDNN, although showed a negative correlation as reported in the literature, we, however, did not see a statistically significant association. Nevertheless, this work highlights the potential of using low–cost and small–size sensors and systems in quantifying the association between gait and heart in home–settings that otherwise have been done in the literature in clinical settings with medical devices.

Chapter 7
Conclusions, perspectives and future work

7.1 Conclusions

Global life expectancy has increased dramatically over the last several decades, thanks to remarkable progress in science and technology and public health. Consequently, the demand for affordable healthcare solutions is also rising all over the world. However, present–day healthcare solutions and services are still unaffordable for many owing to the ever–rising cost of pharmaceuticals, diagnostic procedures, and inpatient care services. In addition, a large elderly demographic requires personal support for their daily living and healthcare needs. Therefore, affordable and reliable healthcare and continuous monitoring services are urgently needed to enable early diagnoses of developing diseases for people with limited access to healthcare services or those living with very limited financial resources. Current monitoring practice requires frequent visits to or long term stays at expensive healthcare facilities that is financially consuming for both individuals and nations. Wearable healthcare systems coupled with modern computing and communication technologies can play a pivotal role in enabling a cost–effective viable solution for long–term health monitoring.

To ensure ubiquitous acceptance of wearable health monitoring systems, they need to be inexpensive, user–friendly, medically safe and ergonomic. In addition, the systems should have low power requirements to enable a longer operation time for long–term use.

Therefore, the key concern in designing wearable health monitoring systems is integrating sensors, electronic components, and on–board computing and communication systems while ensuring data accuracy and privacy, efficient computing for real–time monitoring, low–power consumption, and wearing comfort for the users.

In this research, we addressed some of the above–mentioned concerns and developed highly accurate and computationally efficient algorithms and low–cost, unobtrusive devices coupled with a prediction tool to enable continuous monitoring and assessment of mobility and cardiac health in a wearable platform. Next, we present short summaries of each chapter in this thesis.

In Chapter 1, a framework of a complete smart health–monitoring system and its requirements for developing low–cost, and computationally efficient systems are discussed. A brief discussion on interoperability issues and standardized platforms is presented next. Then, we highlight some recent research activities and the regulatory concerns associated with portable and wearable health monitoring systems. Finally, the contributions of this research and the thesis organization are presented.

In Chapter 2, a three–stage complementary filter–based approach for real–time orientation estimation is presented. The gyroscope–based estimation makes the proposed filter least affected by external acceleration and magnetic disturbances whereas the complementary filter–based approach makes it is inherently computationally efficient and well suited for real–time applications. The performance of the proposed algorithm is validated and some key gait parameters are derived using the proposed filter that shows high conformity to the ground–truth values.

In Chapter 3, a two–stage complimentary filter–based approach is presented that for real–time monitoring of lower–limb joint angles. The inclination of the IMUs estimated in the first stage are fused in the second stage to estimate the joint angles in real time. The gyroscope–based inclination estimation without requiring any magnetic field measurement makes the estimation least affected by any external acceleration and insensitive to magnetic disturbances. The performance of the proposed algorithm is validated for different walking

speeds and in presence of external acceleration that shows high conformity to the ground–truth.

In Chapter 4, a simple, low–cost, and computationally efficient gait–analyzer is presented that uses miniature IMUs to facilitate continuous monitoring of human gait health, potentially leading towards early detection of gait affecting neurodegenerative and musculoskeletal diseases. A comparative discussion on the gait characteristics between two gender and two age groups is presented. The gait analyzer distinguishes an abnormal gait by evaluating an individual's gait features with respect to the baseline information corresponding to his/her peer group.

In Chapter 5, the development of a flexible and dry capacitive electrode, a wireless ECG monitoring system, and an automatic anomalous ECG detection method is presented. The flexible capacitive electrodes allow ECG measurements over the fabric and offer better conformity to the surface of the body, thus reducing motion artifacts. Each electrode is virtually grounded that allows for obtaining single–lead ECG using only two electrodes. ECG measurements obtained over different types of textile materials and in presence of bodily movements show comparable results to other reported ECG monitoring systems. An automatic method of Atrial Fibrillation (AFib) detection from short single–lead ECGs is also presented as a future extension of the software developed for the ECG monitoring system.

In Chapter 6, the association between human gait and cardiac activities is presented. The gait characteristics are measured using wearable IMUs and the cardiac activity is measured by a single–lead handheld ECG monitor. Experimental results show that gait asymmetry between two legs and variation in the gait has an association with cardiac parameters such as HR and HRV as well as physical parameters such as age and BMI. Quantification of these associations can potentially lead towards realizing a low–cost monitoring tool for early detection of signs associated with CVD–related changes in gait features before the actual CVD symptoms are observed.

7.2 General perspectives

Owing to the emergence of low–power, miniature sensors, high–speed communication and computing technologies, there have been growing interests among researchers and manufacturers to develop wearable systems for healthcare and wellness purposes. However, there remain some key challenges that need to be addressed prior to achieving a global acceptance of these devices.

First, the hardware and computation resources for the on–body central node of a multi–sensor BSN system can be a limiting factor for seamless connectivity and data handling. The central processing node of the BSN network exchanges data with the on–body sensors as well as the home gateway, and sometimes performs limited processing. Therefore, a robust and efficient algorithm is required for the central BSN node to optimize its performance. In addition to that, an efficient data compression algorithm needs to be implemented in the central node in order to deal with a large volume of data and transmit them to the nearest gateway.

Second, a key concern for the seamless operation of the smart home system is associated with its energy requirement. Low power consumption and high energy efficiency are critical for the smart home, especially for the wearable and mobile systems used for long–term monitoring purposes. Advanced battery technologies as well as low–power electronic components can be used to increase the operating–time of the system. Researchers also may put their efforts into developing and integrating efficient energy harvesting technologies to fulfill the energy requirements of wearable and mobile systems in the smart home.

Third, most of the standalone products which are currently available in the market are proprietary and generally developed for one or a few specific tasks or functionalities. Although these systems use standard communication protocols, they are mostly not compatible to, or interoperable with similar systems from other manufacturers, thus leaving the consumers with few alternatives. A common platform for all systems will raise the competition among the manufactures that will result in many alternatives for the

consumers, thus increasing the market penetration of smart homes. Therefore, a global industry standard based on a well–defined layered architecture is critical for the widespread acceptance of the smart home technology. Researchers and industry groups may work together to develop and adopt a common and unified industry standard for the smart home system.

Fourth, textile based sensors or smart textiles, have great potential in wearable monitoring systems. For example, textile–based electrodes and temperature sensors can be used for physiological measurements, whereas textile–based strain sensors can be exploited for monitoring HR, respiration rate, pulse as well as human activities. However, ensuring high signal accuracy, sensitivity, SNR and stability in a textile–based platform are the key design challenges. Further, more work is needed for the proper selection of sensing materials and embedding technique as well as stable sensor–skin interface to ensure superior sensor performance. In addition, durability and signal integrity of the sensors with time and washing cycles should also be improved while fabricating smart textiles for long–term health monitoring.

Fifth, big communication and media companies, who already have high market penetration and robust infrastructures for high speed and secured data communication, may collaborate with third–party healthcare service providers such as hospitals, clinics, and ambulance services to bring healthcare facilities to the doorsteps of consumers. Addition of comprehensive health monitoring systems and healthcare services to their existing smart home solutions can potentially be a giant leap towards a ubiquitous and fully–functional smart home. In fact, some major technology companies such as Samsung, Alarm, and ADT (founded as American District Telegraph) have acquired several small smart home companies in recent years to facilitate health monitoring along with their existing home–security applications in the smart home platform. Also, the industry is still actively working to realize a fully functional smart home–based remote healthcare solution.

Sixth, although major regulatory bodies have their own guidelines for a system to be considered as a ‘medical device’, the boundaries between the fitness and wellness

devices/apps and the medical devices remain ambiguous, particularly in a situation when the self–monitoring thorough a fitness and wellness device and associated smartphone application is integrated within the patient care and treatment scheme. These blurred boundaries need to be resolved to safeguard the users from possible harmful consequences.

Seventh, unlike the US Food and Drug Administration (FDA), the intermediate– and high–risk devices in the EU require an authorized private and for–profit third–party organization called the 'Notified Body' (NB) to assess and certify the device's compliance with the corresponding directive. Although this process offers more flexibility to the manufacturers and reduces unnecessary delay in the approval process, it is, however, subject to the risk of compromised safety owing to varying standards, pricing and work ethics of different NBs.

Eighth, approving a medical device based on a predicate may cause safety concerns and was therefore criticized by some experts. It was argued that some predicates were in the market even before any regulatory policies were implemented. Some predicate devices were never tested on humans and some were even recalled voluntarily from the market due to their poor performance, thus questioning the credibility of the predicate itself. In addition, this process of device approval encourages the manufacturers to evade the expensive and time–consuming but critical clinical trials before bringing the product in the market.

7.3 Future work

This research work resulted in several advances towards the development of accurate, efficient and low–cost sensing systems for long–term monitoring of cardiac and gait health in a wearable platform. However, there remains some important research questions, which need to be addressed in the future.

First, the complementary filter approach used in designing the orientation filter and the knee joint monitor require appropriate tuning parameters for higher accuracy. An automatic calibration procedure needs to be developed to automate the tuning parameters selection process.

Second, a portable and low–cost health monitoring system can be developed and integrated into a complete wearable platform. Most current systems measure or monitor only specific bio–signals or parameters. However, it is necessary to monitor a set of key physiological signs such as HR or pulse, BP, respiratory rate and body temperature; often referred together as vital signs, as well as oxygen saturation level in the blood to perform a better assessment of an individual's health condition. Such a monitoring device is particularly important in a pandemic situation like the current coronavirus disease (COVID–19) during the self–quarantine period. However, it is neither practical nor ergonomically sound to use several on–body systems for continuous and ambulatory monitoring of each parameter.

A network of sensors for ECG, PPG, IMU, and temperature embedded in a wearable platform along with an on–body data acquisition and transceiver module can, therefore, be a viable solution for multi–parameter monitoring. An ECG sensor measures ECG signal, HR, and HRV while temperature sensor measures body temperature. Arterial oxygen saturation (SpO2) is calculated from the PPG signal. Besides, BP can be estimated from the pulse transit time (PTT), which is the time interval between the ECG and PPG signal peaks (See Figure 7.1a) using Moens–Korteweg or Bramwell–Hill relationships. Furthermore, ECG and PPG signals can also be used to determine the respiration rate (RR) by employing signal decomposition techniques such as empirical mode decomposition (EMD), principal component analysis (PCA) or wavelet transform. Figure 7.1b presents the concept of a multi–sensor monitoring system.

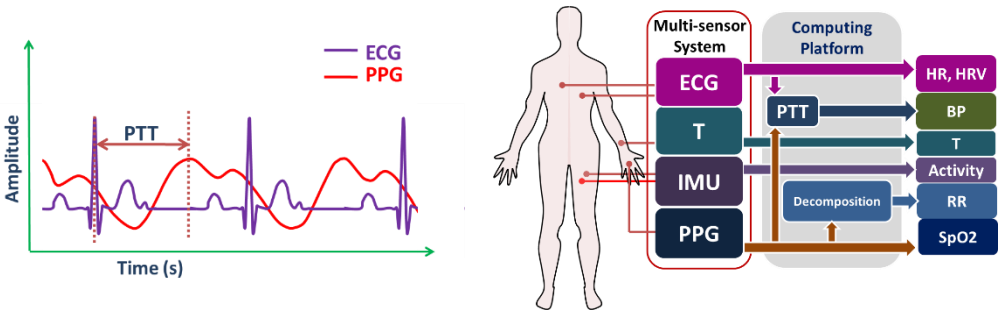

(a) (b)

Figure 7.1 (a) Pulse transit time (PTT) (b) Four sensor health monitoring system.

Third, a detailed analysis on quantitative correlation between the MIMU–based human gait signals and human cognitive and cardiovascular function would be worth looking into, to

realize low–cost, in–home prediction tool for neurodegenerative disorders and diseases associated with musculoskeletal and cardiovascular systems.

Fourth, the IMU data and information from the lower limb joints and gait patterns as well as the single–lead ECG signal can be fused together to formulate a ‘figure–of–merit’ like metric, for example, ‘Health index’ to quantitatively represent the general health status of an individual.

Fifth, a limitation of this work evolves from being unable to recruit patients with known pathological gaits. The gait pattern changes gradually through different disease processes and at different severities, thus it is likely to deviate from the healthy gaits corresponding to an individual’s peer group. Further in–depth study on different patient groups with a larger dataset from a wider age and BMI range, different walking surfaces as well as different walking speeds would be useful to reinforce our inferences.

Sixth, the electrostatic coupling of the electrodes to the skin potential can be improved by employing a dedicated film or membrane materials with increased dielectric permittivity. Conductive polymers or smart textiles can also be used to realize the conductive sensing part of the electrodes, which may offer enhanced flexibility and user comfort.

Seventh, a biofeedback system can be developed by combining the proposed gait and heart monitoring systems. The system may provide instant feedback about walking quality in terms of balance and foot clearance above ground. It may also raise an alarm when arrhythmia are detected and assess gait and lower–limb joints for potential health risks such as a slip or fall, and make recommendations to adjust gait pattern to reduce the risk. It may suggest appropriate and customized actions using sensor data and inputs from the user. For example, if the system knows the user’s blood glucose level (BGL) and BMI it would suggest the number of steps and walking speed required for the user to normalize the BGL based–on their historical data.

References

[1.1] L. Atzori, A. Iera, and G. Morabito, "The internet of things: A survey," *Comput. networks*, vol. 54, no. 15, pp. 2787–2805, 2010.

[1.2] "ITU Internet Reports 2005: The Internet of Things," *ITU*. [Online]. Available: https://www.itu.int/pub/S–POL–IR.IT–2005/e. [Accessed: 11–May–2017].

[1.3] Bassi and G. Horn, "Internet of Things in 2020: A Roadmap for the Future," *Eur. Comm. Inf. Soc. Media*, 2008.

[1.4] V. S. Thomas, S. Darvesh, C. MacKnight, and K. Rockwood, "Estimating the prevalence of dementia in elderly people: A comparison of the Canadian Study of Health and Aging and National Population Health Survey approaches," *Int. Psychogeriatrics*, vol. 13, no. 1, pp. 169–175, 2001.

[1.5] Kalache and A. Gatti, "Active Ageing: A Policy Framework," *Adv. Gerontol. Uspekhi Gerontol. Akad. Nauk. Gerontol. Obs.*, vol. 11, pp. 7–18, 2002.

[1.6] "Are you ready? What you need to know about ageing," *World Health Organization*, 27–Mar–2012. [Online]. Available: http://www.who.int/world–health–day/2012/toolkit/background/en/. [Accessed: 03–Jan–2019].

[1.7] T. Kulik, S. Ryan, S. Harper, and G. George, "Aging populations and management," *Acad. Manag. J.*, vol. 57, no. 4, pp. 929–935, 2014.

[1.8] "Disability and Health," *World Health Organization*. [Online]. Available: https://www.who.int/en/news–room/fact–sheets/detail/disability–and–health. [Accessed: 03–Jan–2019].

[1.9] "About Chronic Diseases," *Centers for Disease Control and Prevention*, 19–Nov–2018. [Online]. Available: https://www.cdc.gov/chronicdisease/about/index.htm. [Accessed: 03–Jan–2019].

[1.10] "Deaths and Mortality," *Centers for Disease Control and Prevention*, 17–Mar–2017. [Online]. Available: https://www.cdc.gov/nchs/fastats/deaths.htm. [Accessed: 11–May–2017].

[1.11] "2017 Budget in Brief: Strengthening health care," *Ontario*. [Online]. Available: https://www.ontario.ca/page/2017–budget–brief–strengthening–health–care. [Accessed: 23–May–2017].

[1.12] "National Health Expenditure Trends, 1975 to 2018," *CIHI*, 20–Dec–2018. [Online]. Available: https://www.cihi.ca/en/health–spending/2018/national–health–expenditure–trends. [Accessed: 12–Mar–2019].

[1.13] Venkat, R. Global Outlook of the Healthcare Industry; Frost & Sullivan: San Antonio, TX, USA, 2015.

[1.14] "Population ageing projections," *Helping older people live full and secure lives*. [Online]. Available: http://www.helpage.org/global–agewatch/populationageing–data/population–ageing–projections/. [Accessed: 03–Jan–2019].

[1.15] "Canada ranks fifth in well–being of elderly: study," *The Globe and Mail*, 11–May–2018. [Online]. Available: https://www.theglobeandmail.com/life/health–and–fitness/health/canada–ranks–fifth–in–well–being–of–elders–study/article14621721/. [Accessed: 03–Jan–2019].

[1.16] "National Health Expenditure Trends, 1975 to 2014", *Canadian Institute for Health Information*, [Online]. Available: https://www.cihi.ca/en/nhex_2014_report_en.pdf. [Accessed: 03–Jan–2019]

[1.17] "Working–age shift," *The Economist*, 26–Jan–2013. [Online]. Available: https://www.economist.com/finance–and–economics/2013/01/26/working–age–shift. [Accessed: 03–Jan–2019]

[1.18] G. Anderson and J. R. Knickman, "Changing the chronic care system to meet people's needs," *Health Aff.*, vol. 20, no. 6, pp. 146–160, 2001.

[1.19] "Advantages & Disadvantages of Nursing Homes," *AmeriGlide Stair lifts and Vertical Platform lifts*. [Online]. Available: http://www.ameriglide.com/advantages–disadvantages–nursing–homes.htm. [Accessed: 03–Jan–2019].

[1.20] S. Majumder, T. Mondal, and M. Deen, "Wearable Sensors for Remote Health Monitoring," *Sensors*, vol. 17, no. 1, p. 130, 2017.

[1.21] M. J. Deen, "Information and communications technologies for elderly ubiquitous healthcare in a smart home," *Pers. Ubiquitous Comput.*, vol. 19, no. 3–4, pp. 573–599, 2015.

[1.22] N. Agoulmine, M. Jamal Deen, J. S. Lee, and M. Meyyappan, "U–Health Smart Home: Innovative solutions for the management of the elderly and chronic diseases," *IEEE Nanotechnol. Mag.*, vol. 5, no. 3, pp. 6–11, 2011.

[1.23] "National Center for Chronic Disease Prevention and Health Promotion | CDC," *Centers for Disease Control and Prevention*, 19–Dec–2018. [Online]. Available: https://www.cdc.gov/chronicdisease/. [Accessed: 03–Jan–2019].

[1.24] K. Takei, W. Honda, S. Harada, T. Arie, and S. Akita, “Toward flexible and wearable human–interactive health–monitoring devices,” *Adv. Healthc. Mater.* vol. 4, no. 4, pp. 487–500, 2015.
[1.25] Pantelopoulos and N. G. Bourbakis, “A survey on wearable sensor–based systems for health monitoring and prognosis,” *IEEE Trans. Syst. Man Cybern. Part C Appl. Rev.*, vol. 40, no. 1, pp. 1–12, 2010.
[1.26] S. Madakam, R. Ramaswamy, and S. Tripathi, “Internet of Things (IoT): A Literature Review,” *J. Comput. Commun.*, vol. 03, no. 05, pp. 164–173, May 2015.
[1.27] R. Aggarwal and M. L. Das, “RFID security in the context of ‘internet of things,’” in *Proceedings of the First International Conference on Security of Internet of Things – SecurIT ’12*, 2012, pp. 51–56.
[1.28] “National Intelligence Council,” *National Intelligence Council*. [Online]. Available: https://fas.org/irp/nic/. [Accessed: 11–May–2017].
[1.29] Miorandi, S. Sicari, F. De Pellegrini, and I. Chlamtac, “Internet of things: Vision, applications and research challenges,” *Ad Hoc Networks*, vol. 10, no. 7, pp. 1497–1516, Sep. 2012.
[1.30] M. Weiser, “The Computer for the 21st Century,” *Sci. Am.*, vol. 265, no. 3, pp. 94–104, Sep. 1991.
[1.31] N. Noury, G. Virone, P. Barralon, J. Ye, V. Rialle, and J. Demongeot, “New trends in health smart homes,” in *Enterprise Networking and Computing in Healthcare Industry, 2003. Healthcom 2003. Proceedings. 5th International Workshop on*, 2003, pp. 118–127.
[1.32] Zhou, W. Huang, and X. Zhao, “Study on architecture of smart home management system and key devices,” in *Computer Science and Network Technology (ICCSNT), 2013 3rd International Conference on*, 2013, pp. 1255–1258.
[1.33] Li and J. Yu, “Research and Application on the Smart Home Based on Component Technologies and Internet of Things,” *Procedia Eng.*, vol. 15, pp. 2087–2092, 2011.
[1.34] S. Majumder *et al.*, “Smart Homes for Elderly Healthcare—Recent Advances and Research Challenges,” *Sensors*, vol. 17, no. 11, p. 2496, 2017.
[1.35] M. R. Alam, M. B. I. Reaz, and M. A. M. Ali, “A Review of Smart Homes—Past, Present, and Future,” *IEEE Trans. Syst. Man, Cybern. Part C (Applications Rev.*, vol. 42, no. 6, pp. 1190–1203, Nov. 2012.
[1.36] G. Amato, D. Bacciu, M. Broxvall, S. Chessa, S. Coleman, M. D. Rocco, M. Dragone, C. Gallicchio, C. Gennaro, H. Lozano, T. M. Mcginnity, A. Micheli, A. K. Ray, A. Renteria, A. Saffiotti, D. Swords, C. Vairo, and P. Vance, “Robotic Ubiquitous Cognitive Ecology for Smart Homes,” *Journal of Intelligent & Robotic Systems*, vol. 80, no. S1, pp. 57–81, Jan. 2015.
[1.37] Huijnen, A. Badii, H. V. D. Heuvel, P. Caleb–Solly, and D. Thiemert, ““Maybe It Becomes a Buddy, But Do Not Call It a Robot” – Seamless Cooperation between Companion Robotics and Smart Homes,” *Lecture Notes in Computer Science Ambient Intelligence*, pp. 324–329, 2011.
[1.38] “HomeOS: Enabling smarter homes for everyone,” *Microsoft Research*. [Online]. Available: https://www.microsoft.com/en–us/research/project/homeos–enabling–smarter–homes–for–everyone/. [Accessed: 11–May–2017].
[1.39] S. Mumtaz, A. Alsohaily, Z. Pang, A. Rayes, K. F. Tsang, and J. Rodriguez, “Massive Internet of Things for Industrial Applications: Addressing Wireless IIoT Connectivity Challenges and Ecosystem Fragmentation,” *IEEE Industrial Electronics Magazine*, vol. 11, no. 1, pp. 28–33, 2017.
[1.40] S. JaeSeung, A. Kunz, N. Al Marzouqi, C. Legare, and J. Costa, “Standards News,” *IEEE Communications Magazine* , vol. 54, no. 7, pp. 14–16, Jul. 2016.
[1.41] Meddeb, “Internet of things standards: who stands out from the crowd?,” *IEEE Communications Magazine*, vol. 54, no. 7, pp. 40–47, 2016.
[1.42] NGMN. (2106, June). 5G prospects—Key capabilities to unlock digital opportunities, v. 1.1. [Online]. Available: https://www.ngmn.org/uploads/media/160701_NGMN_BPG_Capabilities_Whitepaper_v1_1.pdf
[1.43] “ABB–free@home®,” *ABB–free@home – Home and Building Automation*. [Online]. Available: http://new.abb.com/low–voltage/products/building–automation/product–range/abb–freeathome. [Accessed: 25–Aug–2017].
[1.44] “WHAT IS THREAD?,” *Connected Home*. [Online]. Available: https://threadgroup.org/What–is–Thread/Connected–Home. [Accessed: 25–Aug–2017].
[1.45] “A new age of industrial production: The internet of things, services and people.,” *ABB*. [Online]. Available: http://new.abb.com/docs/default–source/technology/a–new–age–of–industrial–production—–iotsp.pdf. [Accessed: 25–Aug–2017].
[1.46] K. Hughes, “CoAP 4 Plugtests,” *ETSI*. [Online]. Available: http://www.etsi.org/news–events/events/741–plugtests–2014–coap4. [Accessed: 25–Aug–2017].
[1.47] C. A. Sfez, “6LoWPAN Plugtests,” *ETSI*. [Online]. Available: http://www.etsi.org/news–events/events/663–2013–6lowpan–plugtest. [Accessed: 25–Aug–2017].
[1.48] “Neighbor Discovery Optimization for IPv6 over Low–Power Wireless Personal Area Networks (6LoWPANs),” *IETF Tools*. [Online]. Available: https://tools.ietf.org/html/rfc6775. [Accessed: 25–Aug–2017].

[1.49] J. Mineraud, O. Mazhelis, X. Su, and S. Tarkoma, “A gap analysis of Internet–of–Things platforms,” *Computer Communications*, vol. 89–90, pp. 5–16, 2016.
[1.50] L. Atzori, A. Iera, and G. Morabito, “From "smart objects" to "social objects": The next evolutionary step of the internet of things,” *IEEE Communications Magazine*, vol. 52, no. 1, pp. 97–105, 2014.
[1.51] Tao, Y. Wen, and R. Hong, “Multicolumn Bidirectional Long Short–Term Memory for Mobile Devices–Based Human Activity Recognition,” *IEEE Internet Things J.*, vol. 3, no. 6, pp. 1124–1134, 2016.
[1.52] S. Morris, G. Fawcett, L. Brisebois, and J. Hughes, “A demographic, employment and income profile of Canadians with disabilities aged 15 years and over, 2017,” *Statistics Canada: Canada's national statistical agency*, 28–Nov–2018. [Online]. Available: https://www150.statcan.gc.ca/n1/pub/89–654–x/89–654–x2018002–eng.htm. [Accessed: 05–Feb–2019].
[1.53] S. F. Coutinho, K. V. Bloch, and C. M. Coeli, “One–year mortality among elderly people after hospitalization due to fall–related fractures: comparison with a control group of matched elderly,” *Cad. Saude Publica*, vol. 28, no. 4, pp. 801–805, 2012.
[1.54] P. Rolfe, “In Vivo Near–Infrared Spectroscopy,” *Annu. Rev. Biomed. Eng.*, vol. 2, no. 1, pp. 715–754, 2000.
[1.55] S. A. Siddiqui, Y. Zhang, Z. Feng, and A. Kos, “A Pulse Rate Estimation Algorithm Using PPG and Smartphone Camera,” *J. Med. Syst.*, vol. 40, no. 5, p. 126, 2016.
[1.56] Bánhalmi, J. Borbás, M. Fidrich, V. Bilicki, Z. Gingl, and L. Rudas, “Analysis of a Pulse Rate Variability Measurement Using a Smartphone Camera,” *J. Healthc. Eng.*, vol. 2018, p. 15 pages, 2018.
[1.57] Y. Nam, Y. Kong, B. Reyes, N. Reljin, and K. H. Chon, “Monitoring of heart and breathing rates using dual cameras on a smartphone,” *PLoS One*, vol. 11, no. 3, p. e0151013, 2016.
[1.58] N. Koenig *et al.*, “Validation of a New Heart Rate Measurement Algorithm for Fingertip Recording of Video Signals with Smartphones,” *Telemed. e–Health*, vol. 22, no. 8, pp. 631–636, 2016.
[1.59] K. Matsumura, P. Rolfe, J. Lee, and T. Yamakoshi, “iPhone 4s photoplethysmography: Which light color yields the most accurate heart rate and normalized pulse volume using the iPhysioMeter application in the presence of motion artifact?” *PLoS One*, vol. 9, no. 3, 2014.
[1.60] M. P. Lavanya, “Real Time Motion Detection Using Background Subtraction Method and Frame Difference,” *Int. J. Sci. Res.*, vol. 3, no. 6, pp. 1857–1861, 2014.
[1.61] N. Singla, “Motion Detection Based on Frame Difference Method,” *Int. J. Inf. Comput. Technol.*, vol. 4, no. 15, pp. 1559–1565, 2014.
[1.62] R. Krishnan, B. Natarajan, and S. Warren, “Two–stage approach for detection and reduction of motion artifacts in photoplethysmographic data,” *IEEE Trans. Biomed. Eng.*, vol. 57, no. 8, pp. 1867–1876, 2010.
[1.63] Lamonaca, Y. Kurylyak, D. Grimaldi, and V. Spagnuolo, “Reliable pulse rate evaluation by smartphone,” in *MeMeA 2012 – 2012 IEEE Symposium on Medical Measurements and Applications, Proceedings*, 2012, pp. 234–237.
[1.64] S. Kwon, H. Kim, and K. S. Park, “Validation of heart rate extraction using video imaging on a built–in camera system of a smartphone,” in *Proceedings of the Annual International Conference of the IEEE Engineering in Medicine and Biology Society, EMBS*, 2012, pp. 2174–2177.
[1.65] M.–Z. Poh, D. J. McDuff, and R. W. Picard, “Non–contact, automated cardiac pulse measurements using video imaging and blind source separation,” *Opt. Express*, vol. 18, no. 10, p. 10762, 2010.
[1.66] W. Verkruysse, L. O. Svaasand, and J. S. Nelson, “Remote plethysmographic imaging using ambient light.,” *Opt. Express*, vol. 16, no. 26, pp. 21434–21445, 2008.
[1.67] Y. Sun, C. Papin, V. Azorin–Peris, R. Kalawsky, S. Greenwald, and S. Hu, “Use of ambient light in remote photoplethysmographic systems: comparison between a high–performance camera and a low–cost webcam,” *J. Biomed. Opt.*, vol. 17, no. 3, p. 037005, 2012.
[1.68] S. Sanyal and K. K. Nundy, “Algorithms for Monitoring Heart Rate and Respiratory Rate from the Video of a User’s Face,” *IEEE J. Transl. Eng. Heal. Med.*, vol. 6, pp. 1–11, 2018.
[1.69] Guede–Fernandez, V. Ferrer–Mileo, J. Ramos–Castro, M. Fernandez–Chimeno, and M. A. Garcia–Gonzalez, “Real time heart rate variability assessment from Android smartphone camera photoplethysmography: Postural and device influences,” in *Proceedings of the Annual International Conference of the IEEE Engineering in Medicine and Biology Society, EMBS*, 2015, vol. 2015–Novem, pp. 7332–7335.
[1.70] R. B. Lagido, J. Lobo, S. Leite, C. Sousa, L. Ferreira, and J. Silva–Cardoso, “Using the smartphone camera to monitor heart rate and rhythm in heart failure patients,” in *2014 IEEE–EMBS International Conference on Biomedical and Health Informatics, BHI 2014*, 2014, pp. 556–559.
[1.71] J. B. Bolkhovsky, C. G. Scully, and K. H. Chon, “Statistical analysis of heart rate and heart rate variability monitoring through the use of smart phone cameras,” in *Proceedings of the Annual International Conference of the IEEE Engineering in Medicine and Biology Society, EMBS*, 2012, pp. 1610–1613.
[1.72] M. J. Gregoski *et al.*, “Development and validation of a smartphone heart rate acquisition application for health promotion and wellness telehealth applications,” *Int. J. Telemed. Appl.*, vol. 2012, p. 7 pages, 2012.

[1.73] S. Majumder and M. J. Deen, "Smartphone sensors for health monitoring and diagnosis," *Sensors (Switzerland)*, vol. 19, no. 9. 2019.
[1.74] M. Derawi and P. Bours, "Gait and activity recognition using commercial phones," *Comput. Secur.*, vol. 39, no. PART B, pp. 137–144, 2013.
[1.75] A. Ronao and S. B. Cho, "Human activity recognition using smartphone sensors with two–stage continuous hidden Markov models," in *2014 10th International Conf. on Natural Computation, ICNC 2014*, 2014, pp. 681–686.
[1.76] M. Seera, C. K. Loo, and C. P. Lim, "A hybrid FMM–CART model for human activity recognition," in *Conference Proceedings – IEEE Int. Conf. on Systems, Man and Cybernetics*, 2014, vol. 2014–January, no. January, pp. 182–187.
[1.77] M. Eastwood and C. Jayne, "Evaluation of hyperbox neural network learning for classification," *Neurocomputing*, vol. 133, pp. 249–257, 2014.
[1.78] Catal, S. Tufekci, E. Pirmit, and G. Kocabag, "On the use of ensemble of classifiers for accelerometer–based activity recognition," *Appl. Soft Comput. J.*, vol. 37, pp. 1018–1022, 2015.
[1.79] De, P. Bharti, S. K. Das, and S. Chellappan, "Multimodal wearable sensing for fine–grained activity recognition in healthcare," *IEEE Internet Comput.*, vol. 19, no. 5, pp. 26–35, 2015.
[1.80] Wang, G. Chen, J. Yang, S. Zhao, and C. Y. Chang, "A Comparative Study on Human Activity Recognition Using Inertial Sensors in a Smartphone," *IEEE Sens. J.*, vol. 16, no. 11, pp. 4566–4578, 2016.
[1.81] Z. Chen, Q. Zhu, Y. C. Soh, and L. Zhang, "Robust Human Activity Recognition Using Smartphone Sensors via CT–PCA and Online SVM," *IEEE Trans. Ind. Informatics*, vol. 13, no. 6, pp. 3070–3080, 2017.
[1.82] Anguita, A. Ghio, L. Oneto, X. Parra, and J. L. Reyes–Ortiz, "Human activity recognition on smartphones using a multiclass hardware–friendly support vector machine," in *Lecture Notes in Computer Science (including subseries Lecture Notes in Artificial Intelligence and Lecture Notes in Bioinformatics)*, 2012, vol. 7657 LNCS, pp. 216–223.
[1.83] Y. Kwon, K. Kang, and C. Bae, "Unsupervised learning for human activity recognition using smartphone sensors," *Expert Syst. Appl.*, vol. 41, no. 14, pp. 6067–6074, 2014.
[1.84] A. Ronao and S. B. Cho, "Human activity recognition with smartphone sensors using deep learning neural networks," *Expert Syst. Appl.*, vol. 59, pp. 235–244, 2016.
[1.85] A. Ronao and S. B. Cho, "Deep convolutional neural networks for human activity recognition with smartphone sensors," in Lecture Notes in Computer Science (including subseries Lecture Notes in Artificial Intelligence and Lecture Notes in Bioinformatics), 2015, vol. 9492, pp. 46–53.
[1.86] Tao, Y. Wen, and R. Hong, "Multicolumn Bidirectional Long Short–Term Memory for Mobile Devices–Based Human Activity Recognition," *IEEE Internet Things J.*, vol. 3, no. 6, pp. 1124–1134, 2016.
[1.87] J. Ordóñez and D. Roggen, "Deep convolutional and LSTM recurrent neural networks for multimodal wearable activity recognition," *Sensors (Switzerland)*, vol. 16, no. 1, p. 115, 2016.
[1.88] Y. He, Y. Li, and S. Di Bao, "Fall detection by built–in tri–accelerometer of smartphone," in Proceedings – IEEE–EMBS International Conference on Biomedical and Health Informatics: Global Grand Challenge of Health Informatics, BHI 2012, 2012, pp. 184–187.
[1.89] Thammasat and J. Chaicharn, "A simply fall–detection algorithm using accelerometers on a smartphone," in *5th 2012 Biomedical Engineering International Conference, BMEiCON 2012*, 2012, pp. 1–4.
[1.90] Lee, S. Lee, Y. S. Choi, Y. Seo, and E. Shim, "A new posture monitoring system for preventing physical illness of smartphone users," in *2013 IEEE 10th Consumer Communications and Networking Conference, CCNC 2013*, 2013, pp. 713–716.
[1.91] Fleury, Q. Mourcou, C. Franco, B. Diot, J. Demongeot, and N. Vuillerme, "Evaluation of a Smartphone–based audio–biofeedback system for improving balance in older adults – A pilot study," in *Proceedings of the Annual International Conference of the IEEE Engineering in Medicine and Biology Society, EMBS*, 2013, pp. 1198–1201.
[1.92] Z. Chen, C. Jiang, and L. Xie, "A Novel Ensemble ELM for Human Activity Recognition Using Smartphone Sensors," *IEEE Transactions on Industrial Informatics*, pp. 1–1, 2018.
[1.93] Vaughn, P. Biocco, Y. Liu, and M. Anwar, "Activity Detection and Analysis Using Smartphone Sensors," *2018 IEEE International Conference on Information Reuse and Integration (IRI)*, 2018
[1.94] M. M. Hassan, M. Z. Uddin, A. Mohamed, and A. Almogren, "A robust human activity recognition system using smartphone sensors and deep learning," *Futur. Gener. Comput. Syst.*, 2018.
[1.95] S. Li, C. Li, W. Li, Y. Hou, and C. Cook, "Smartphone–sensors Based Activity Recognition Using IndRNN," Proceedings of the 2018 ACM International Joint Conference and 2018 International Symposium on Pervasive and Ubiquitous Computing and Wearable Computers – UbiComp 18, 2018
[1.96] Li and M. Trocan, "Deep learning of smartphone sensor data for personal health assistance," *Microelectronics Journal*, 2018.

[1.97] Bort–Roig *et al.*, "Monitoring sedentary patterns in office employees: validity of an m–health tool (Walk@Work–App) for occupational health," *Gac. Sanit.*, vol. 32, no. 6, pp. 563–566, 2018.
[1.98] N. Wan and G. Lin, "Classifying Human Activity Patterns from Smartphone Collected GPS data: A Fuzzy Classification and Aggregation Approach," *Trans. GIS*, vol. 20, no. 6, pp. 869–886, 2016.
[1.99] M. Shoaib, H. Scholten, and P. J. M. Havinga, "Towards physical activity recognition using smartphone sensors," in Proceedings – IEEE 10th International Conference on Ubiquitous Intelligence and Computing, UIC 2013 and IEEE 10th International Conference on Autonomic and Trusted Computing, ATC 2013, 2013, pp. 80–87.
[1.100] W. Wu, S. Dasgupta, E. E. Ramirez, C. Peterson, and G. J. Norman, "Classification accuracies of physical activities using smartphone motion sensors," *J. Med. Internet Res.*, vol. 14, no. 5, 2012.
[1.101] Y. Lee, H. Yeh, K.–H. Kim, and O. Choi, "A Real–time Fall Detection System Based on the Acceleration Sensor of Smartphone," *International Journal of Control and Automation*, vol. 10, no. 1, pp. 315–326, 2017.
[1.102] Hakim, M. S. Huq, S. Shanta, and B. S. K. K. Ibrahim, "Smartphone Based Data Mining for Fall Detection: Analysis and Design," in *Procedia Computer Science*, 2017, vol. 105, pp. 46–51.
[1.103] M. Ashfak Habib, M. S. Mohktar, S. Bahyah Kamaruzzaman, K. Seang Lim, T. Maw Pin, and F. Ibrahim, "Smartphone–based solutions for fall detection and prevention: Challenges and open issues," *Sensors (Switzerland)*, vol. 14, no. 4. pp. 7181–7208, 2014.
[1.104] V. R. L. Shen, H. Y. Lai, and A. F. Lai, "The implementation of a smartphone–based fall detection system using a high–level fuzzy Petri net," *Appl. Soft Comput. J.*, vol. 26, pp. 390–400, 2015.
[1.105] Y. W. Hsu, K. H. Chen, J. J. Yang, and F. S. Jaw, "Smartphone–based fall detection algorithm using feature extraction," in Proceedings – 2016 9th International Congress on Image and Signal Processing, BioMedical Engineering and Informatics, CISP–BMEI 2016, 2017, pp. 1535–1540.
[1.106] R. Luque, E. Casilari, M. J. Morón, and G. Redondo, "Comparison and characterization of android–based fall detection systems," *Sensors (Switzerland)*, vol. 14, no. 10, pp. 18543–18574, 2014.
[1.107] M. P. Støve, T. S. Palsson, and R. P. Hirata, "Smartphone–based accelerometry is a valid tool for measuring dynamic changes in knee extension range of motion," *Knee*, vol. 25, no. 1, pp. 66–72, 2018.
[1.108] Y. Jenny, A. Bureggah, and Y. Diesinger, "Measurement of the knee flexion angle with smartphone applications: Which technology is better?" *Knee Surgery, Sport. Traumatol. Arthrosc.*, vol. 24, no. 9, pp. 2874–2877, 2016.
[1.109] Nemati, M. J. Deen, and T. Mondal, "A wireless wearable ECG sensor for long–term applications," in *IEEE Communications Magazine*, 2012, vol. 50, no. 1, pp. 36–43.
[1.110] S. Majumder, L. Chen, O. Marinov, C. H. Chen, T. Mondal, and M. Jamal Deen, "Noncontact Wearable Wireless ECG Systems for Long–Term Monitoring," *IEEE Rev. Biomed. Eng.*, vol. 11, pp. 306–321, 2018.
[1.111] M. Hadjem, O. Salem, and F. Nait–Abdesselam, "An ECG monitoring system for prediction of cardiac anomalies using WBAN," *2014 IEEE 16th International Conference on e–Health Networking, Applications and Services (Healthcom)*, 2014.
[1.112] Andreoni, P. Perego, and C. Standoli, "Wearable monitoring of elderly in an ecologic setting: the SMARTA project," *Proceedings of 2nd International Electronic Conference on Sensors and Applications*, May 2015.
[1.113] C. Tseng, B.–S. Lin, L.–D. Liao, Y.–T. Wang, and Y.–L. Wang, "Development of a Wearable Mobile Electrocardiogram Monitoring System by Using Novel Dry Foam Electrodes," *IEEE Systems Journal*, vol. 8, no. 3, pp. 900–906, 2014.
[1.114] J. Lee, J. Heo, W. Lee, Y. Lim, Y. Kim, and K. Park, "Flexible Capacitive Electrodes for Minimizing Motion Artifacts in Ambulatory Electrocardiograms," *Sensors*, vol. 14, no. 8, pp. 14732–14743, Dec. 2014.
[1.115] T. Komensky, M. Jurcisin, K. Ruman, O. Kovac, D. Laqua, and P. Husar, "Ultra–wearable capacitive coupled and common electrode–free ECG monitoring system," *2012 Annual International Conference of the IEEE Engineering in Medicine and Biology Society*, pp. 1594–1597, 2012.
[1.116] J.–H. Park, D.–G. Jang, J. Park, and S.–K. Youm, "Wearable Sensing of In–Ear Pressure for Heart Rate Monitoring with a Piezoelectric Sensor," *Sensors*, vol. 15, no. 9, pp. 23402–23417, 2015.
[1.117] Y. Shu, C. Li, Z. Wang, W. Mi, Y. Li, and T.–L. Ren, "A Pressure sensing system for heart rate monitoring with polymer–based pressure sensors and an anti–interference post processing circuit," *Sensors*, vol. 15, no. 2, pp. 3224–3235, Feb. 2015.
[1.118] Derawi and P. Bours, "Gait and activity recognition using commercial phones," *Computers & Security*, vol. 39, pp. 137–144, 2013.
[1.119] De, P. Bharti, S. K. Das, and S. Chellappan, "Multimodal Wearable Sensing for Fine–Grained Activity Recognition in Healthcare," *IEEE Internet Computing IEEE Internet Comput.*, vol. 19, no. 5, pp. 26–35, 2015.
[1.120] M. Bertolotti, A. M. Cristiani, P. Colagiorgio, F. Romano, E. Bassani, N. Caramia, and S. Ramat, "A Wearable and Modular Inertial Unit for Measuring Limb Movements and Balance Control Abilities," *IEEE Sensors J. IEEE Sensors Journal*, vol. 16, no. 3, pp. 790–797, 2016.

[1.121] Panahandeh, N. Mohammadiha, A. Leijon, and P. Handel, "Continuous Hidden Markov Model for Pedestrian Activity Classification and Gait Analysis," *IEEE Trans. Instrum. Meas. IEEE Transactions on Instrumentation and Measurement*, vol. 62, no. 5, pp. 1073–1083, 2013.
[1.122] C. Bejarano, E. Ambrosini, A. Pedrocchi, G. Ferrigno, M. Monticone, and S. Ferrante, "A Novel Adaptive, Real–Time Algorithm to Detect Gait Events From Wearable Sensors," *IEEE Transactions on Neural Systems and Rehabilitation Engineering*, vol. 23, no. 3, pp. 413–422, 2015.
[1.123] T. T. Ngo, Y. Makihara, H. Nagahara, Y. Mukaigawa, and Y. Yagi, "Similar gait action recognition using an inertial sensor," *Pattern Recognition*, vol. 48, no. 4, pp. 1289–1301, 2015.
[1.124] Alshurafa, W. Xu, J. J. Liu, M.–C. Huang, B. Mortazavi, C. K. Roberts, and M. Sarrafzadeh, "Designing a Robust Activity Recognition Framework for Health and Exergaming Using Wearable Sensors," *IEEE Journal of Biomedical and Health Informatics IEEE J. Biomed. Health Inform.*, vol. 18, no. 5, pp. 1636–1646, 2014.
[1.125] Ghasemzadeh, N. Amini, R. Saeedi, and M. Sarrafzadeh, "Power–Aware Computing in Wearable Sensor Networks: An Optimal Feature Selection," *IEEE Transactions on Mobile Computing IEEE Trans. on Mobile Comput.*, vol. 14, no. 4, pp. 800–812, Jan. 2015.
[1.126] Chen, E. Zheng, Q. Wang, and L. Wang, "A new strategy for parameter optimization to improve phase–dependent locomotion mode recognition," *Neurocomputing*, vol. 149, pp. 585–593, 2015.
[1.127] M. Cristiani, G. M. Bertolotti, E. Marenzi, and S. Ramat, "An Instrumented Insole for Long Term Monitoring Movement, Comfort, and Ergonomics," *IEEE Sensors Journal*, vol. 14, no. 5, pp. 1564–1572, 2014.
[1.128] W. Tang and E. S. Sazonov, "Highly Accurate Recognition of Human Postures and Activities Through Classification With Rejection," *IEEE Journal of Biomedical and Health Informatics IEEE J. Biomed. Health Inform.*, vol. 18, no. 1, pp. 309–315, 2014.
[1.129] Friedman, J. B. Rowe, D. J. Reinkensmeyer, and M. Bachman, "The Manumeter: A Wearable Device for Monitoring Daily Use of the Wrist and Fingers," *IEEE Journal of Biomedical and Health Informatics*, vol. 18, no. 6, pp. 1804–1812, 2014.
[1.130] M. El–Gohary and J. Mcnames, "Human Joint Angle Estimation with Inertial Sensors and Validation with A Robot Arm," *IEEE Transactions on Biomedical Engineering IEEE Trans. Biomed. Eng.*, vol. 62, no. 7, pp. 1759–1767, 2015.
[1.131] Y. L. Hsu *et al.*, "Gait and balance analysis for patients with Alzheimer's disease using an inertial–sensor–based wearable instrument," *IEEE J. Biomed. Heal. Informatics*, vol. 18, no. 6, pp. 1822–1830, 2014.
[1.132] Pierleoni, A. Belli, L. Palma, M. Pellegrini, L. Pernini, and S. Valenti, "A High Reliability Wearable Device for Elderly Fall Detection," *IEEE Sens. J.*, vol. 15, no. 8, pp. 4544–4553, 2015.
[1.133] Rai, P. S. Kumar, S. Oh, H. Kwon, G. N. Mathur, V. K. Varadan, and M. P. Agarwal, "Smart healthcare textile sensor system for unhindered–pervasive health monitoring," *Nanosensors, Biosensors, and Info–Tech Sensors and Systems 2012*, vol. 8344, 2012.
[1.134] P. Rai, S. Oh, P. Shyamkumar, M. Ramasamy, R. E. Harbaugh, and V. K. Varadan, "Nano– Bio– Textile Sensors with Mobile Wireless Platform for Wearable Health Monitoring of Neurological and Cardiovascular Disorders," *Journal of the Electrochemical Society*, vol. 161, no. 2, pp. B3116–B3150, 2014.
[1.135] Merritt, H. Nagle, and E. Grant, "Fabric–Based Active Electrode Design and Fabrication for Health Monitoring Clothing," *IEEE Transactions on Information Technology in Biomedicine IEEE Trans. Inform. Technol. Biomed.*, vol. 13, no. 2, pp. 274–280, 2009.
[1.136] Fonseca, J. P. S. Cunha, R. E. Martins, V. M. Ferreira, J. P. M. D. Sa, M. A. Barbosa, and A. M. D. Silva, "A Novel Dry Active Electrode for EEG Recording," *IEEE Transactions on Biomedical Engineering IEEE Trans. Biomed. Eng.*, vol. 54, no. 1, pp. 162–165, 2007.
[1.137] T. Keller and A. Kuhn, "Electrodes for transcutaneous (surface) electrical stimulation," *Journal of Automatic Control J Autom Control*, vol. 18, no. 2, pp. 35–45, 2008.
[1.138] L. Li, W. M. Au, Y. Li, K. M. Wan, S. H. Wan, and K. S. Wong, "Design of Intelligent Garment with Transcutaneous Electrical Nerve Stimulation Function Based on the Intarsia Knitting Technique," *Textile Research Journal*, vol. 80, no. 3, pp. 279–286, Jul. 2009.
[1.139] N. M. Malešević, L. Z. Maneski, V. Ilić, N. Jorgovanović, G. Bijelić, T. Keller, and D. B. Popović, "A multi–pad electrode based functional electrical stimulation system for restoration of grasp," *Journal of NeuroEngineering and Rehabilitation*, vol. 9, no. 1, p. 66, 2012.
[1.140] Paul, R. Torah, S. Beeby, and J. Tudor, "Novel active electrodes for ECG monitoring on woven textiles fabricated by screen and stencil printing," *Sensors and Actuators A: Physical*, vol. 221, pp. 60–66, 2015
[1.141] Z. Lim, Z. Chia, M. Kevin, A. Wong, and G. Ho, "A facile approach towards ZnO nanorods conductive textile for room temperature multifunctional sensors," *Sensors and Actuators B: Chemical*, vol. 151, no. 1, pp. 121–126, 2010.
[1.142] T. Inoh, S. Yoon, T. E. Kim, H. Wi, K. J. Kim, E. J. Woo, and R. J. Sadleir, "Nanofiber Web Textile Dry Electrodes for Long–Term Biopotential Recording," *IEEE Transactions on Biomedical Circuits and Systems*, vol. 7, no. 2, pp. 204–211, 2013.

[1.143] T. N. Shaikh, S. Chaudhari, B. H. Patel, and M. Patel. "Study of conductivity behavior of nano copper loaded nonwoven polypropylene based textile electrode for ECG." *International Journal of Emerging Science and Engineering*, vol. 3, no. 4, pp. 11–14, 2015.
[1.144] L. Rattfält, F. Björefors, D. Nilsson, X. Wang, P. Norberg, and P. Ask, "Properties of screen printed electrocardiography smartware electrodes investigated in an electro–chemical cell," *BioMedical Engineering OnLine*, vol. 12, no. 1, p. 64, 2013.
[1.145] Cho, K. Jeong, M. J. Paik, Y. Kwun, and M. Sung, "Performance Evaluation of Textile–Based Electrodes and Motion Sensors for Smart Clothing," *IEEE Sensors Journal*, vol. 11, no. 12, pp. 3183–3193, 2011.
[1.146] M. A. Mestrovic, R. J. N. Helmer, L. Kyratzis, and D. Kumar, "Preliminary study of dry knitted fabric electrodes for physiological monitoring," *2007 3rd International Conference on Intelligent Sensors, Sensor Networks and Information*, pp. 601–606, 2007.
[1.147] Cho, H. Lim, S. Cho, and J.–W. Lee, "Development of textile electrode for electrocardiogram measurement based on conductive electrode configuration," *Fibers Polym Fibers and Polymers*, vol. 16, no. 10, pp. 2148–2157, 2015.
[1.148] M. Weder, D. Hegemann, M. Amberg, M. Hess, L. Boesel, R. Abächerli, V. Meyer, and R. Rossi, "Embroidered Electrode with Silver/Titanium Coating for Long–Term ECG Monitoring," *Sensors*, vol. 15, no. 1, pp. 1750–1759, 2015.
[1.149] Q. Jiang, E. Newton, C. W. M. Yuen, and C. W. Kan, "Chemical silver plating on polyester/cotton blended fabric," *Journal of Applied Polymer Science*, vol. 100, no. 6, pp. 4383–4387, 2006.
[1.150] P. Xue and X. M. Tao, "Morphological and electromechanical studies of fibers coated with electrically conductive polymer," *Journal of Applied Polymer Science.*, vol. 98, no. 4, pp. 1844–1854, 2005.
[1.151] A. Brevnov, "Electrodeposition of Porous Silver Films on Blanket and Patterned Aluminum–Copper Films," *Journal of The Electrochemical Society*, vol. 153, no. 4, pp. C249–C253, 2006.
[1.152] N. N. Z. M. Rajdi, A. A. Bakira, S. M. Saleh, and D. H. Wicaksono, "Textile–based Micro Electro Mechanical System (MEMS) Accelerometer for Pelvic Tilt Mesurement," *Procedia Engineering*, vol. 41, pp. 532–537, 2012.
[1.153] M. Amjadi, A. Pichitpajongkit, S. Lee, S. Ryu, and I. Park, "Highly Stretchable and Sensitive Strain Sensor Based on Silver Nanowire–Elastomer Nanocomposite," *ACS Nano*, vol. 8, no. 5, pp. 5154–5163, 2014.
[1.154] Lee, S. Kim, J. Lee, D. Yang, B. C. Park, S. Ryu, and I. Park, "A stretchable strain sensor based on a metal nanoparticle thin film for human motion detection," *Nanoscale*, vol. 6, no. 20, pp. 11932–11939, 2014.
[1.155] T.–W. Shyr, J.–W. Shie, C.–H. Jiang, and J.–J. Li, "A Textile–Based Wearable Sensing Device Designed for Monitoring the Flexion Angle of Elbow and Knee Movements," *Sensors*, vol. 14, no. 3, pp. 4050–4059, 2014.
[1.156] Zhang, "Flexible textile–based strain sensor induced by contacts," *Measurement Science and Technology Meas. Sci. Technol.*, vol. 26, no. 10, p. 105102, 2015.
[1.157] O. Atalay, W. Kennon, and M. Husain, "Textile–Based Weft Knitted Strain Sensors: Effect of Fabric Parameters on Sensor Properties," *Sensors*, vol. 13, no. 8, pp. 11114–11127, 2013.
[1.158] Seyedin, J. M. Razal, P. C. Innis, A. Jeiranikhameneh, S. Beirne, and G. G. Wallace, "Knitted Strain Sensor Textiles of Highly Conductive All–Polymeric Fibers," *ACS Appl. Mater. Interfaces ACS Applied Materials & Interfaces*, vol. 7, no. 38, pp. 21150–21158, 2015.
[1.159] F. D. Silva, R. Pedro, J. Paulo, and J. Higino, "Photonic Sensors Based on Flexible Materials with FBGs for Use on Biomedical Applications," *Current Trends in Short– and Long–period Fiber Gratings*, pp. 105–132, 2013.
[1.160] M. Krehel, R. Rossi, G.–L. Bona, and L. Scherer, "Characterization of Flexible Copolymer Optical Fibers for Force Sensing Applications," *Sensors*, vol. 13, no. 9, pp. 11956–11968, Sep. 2013.
[1.161] M. N. Kamel Boulos, A. C. Brewer, C. Karimkhani, D. B. Buller, and R. P. Dellavalle, "Mobile medical and health apps: state of the art, concerns, regulatory control and certification," *Online J. Public Health Inform.*, vol. 5, no. 3, 2014.
[1.162] G. A. Van Norman, "Drugs and Devices: Comparison of European and U.S. Approval Processes," *JACC Basic to Transl. Sci.*, vol. 1, no. 5, pp. 399–412, 2016.
[1.163] W. G. Buijink, B. J. Visser, and L. Marshall, "Medical apps for smartphones: Lack of evidence undermines quality and safety," *Evidence–Based Medicine*, vol. 18, no. 3. pp. 90–92, 2013.
[1.164] Cummings, E. M. Borycki, and E. Roehrer, "Issues and considerations for healthcare consumers using mobile applications," *Stud. Health Technol. Inform.*, vol. 183, pp. 227–231, 2013.
[1.165] O'Neill and R. R. W. Brady, "Colorectal smartphone apps: Opportunities and risks," *Color. Dis.*, 2012.
[1.166] P. Demidowich, K. Lu, R. Tamler, and Z. Bloomgarden, "An evaluation of diabetes self–management applications for Android smartphones," *J. Telemed. Telecare*, vol. 18, no. 4, pp. 235–238, 2012.
[1.167] N. A. Ferrero, D. S. Morrell, and C. N. Burkhart, "Skin scan: A demonstration of the need for FDA regulation of medical apps on iPhone," *Journal of the American Academy of Dermatology*, vol. 68, no. 3. pp. 515–516, 2013.

[1.168] A. Wolf *et al.*, "Diagnostic inaccuracy of smartphone applications for melanoma detection," *JAMA Dermatology*, vol. 149, no. 4, pp. 422–426, 2013.
[1.169] Visvanathan, A. Hamilton, and R. R. W. Brady, "Smartphone apps in microbiology–is better regulation required?," *Clin. Microbiol. Infect.*, vol. 18, no. 7, 2012.
[1.170] Y. Robson, S. Blackford, and D. Roberts, "Caution in melanoma risk analysis with smartphone application technology," *British Journal of Dermatology*, vol. 167, no. 3. pp. 703–704, 2012.
[1.171] Huckvale, M. Car, C. Morrison, and J. Car, "Apps for asthma self–management: A systematic assessment of content and tools," *BMC Med.*, vol. 10, no. 1, p. 144, 2012.
[1.172] McKinstry, "Currently available smartphone apps for asthma have worrying deficiencies," *Evid. Based. Med.*, vol. 18, no. 5, p. e45, 2013.
[1.173] S. O'neill, and R. R. Brady, "Clinical involvement and transparency in medical apps; not all apps are equal." *Colorectal Disease*, vol. 15, no. 1, p. 122, 2013.
[1.174] Sucala *et al.*, "Anxiety: There is an app for that. A systematic review of anxiety apps," *Depression and Anxiety*, vol. 34, no. 6. pp. 518–525, 2017.
[1.175] Strickland, "The FDA Takes On Mobile Health Apps," *IEEE Spectrum: Technology, Engineering, and Science News*, 12–Sep–2012. [Online]. Available: https://spectrum.ieee.org/biomedical/devices/the–fda–takes–on–mobile–health–apps. [Accessed: 06–Jan–2019].
[1.176] Food and Drug Administration/ U.S., "Mobile medical applications: Guidance for industry and food and drug administration staff," *Food Drug Adm. U.S. Dep. Heal. Hum.*, pp. 1–44, 2015. [Online]. Available: https://www.fda.gov/downloads/medicaldevices/.../ucm263366.pdf. [Accessed: 06–Jan–2019].
[1.177] "Premarket Notification 510(k)," *U S Food and Drug Administration Home Page*. [Online]. Available: https://www.fda.gov/MedicalDevices/DeviceRegulationandGuidance/HowtoMarketYourDevice/PremarketSubmissions/PremarketNotification510k/default.htm. [Accessed: 06–Jan–2019].
[1.178] Institute of Medicine (US). Committee on the Public Health Effectiveness of the FDA 510 (k) Clearance Process., *Medical devices and the public's health: the FDA 510(k) clearance process at 35 years*. Washington, D.C.: National Academies Press, 2011.
[1.179] A. Waxman, "H.R.3095 – 101st Congress (1989–1990): Safe Medical Devices Act of 1990," *Congress.gov*, 28–Nov–1990. [Online]. Available: https://www.congress.gov/bill/101st–congress/house–bill/3095. [Accessed: 06–Jan–2019].
[1.180] Cain, "One company's experience: blazing the trail with the first FDA–approved medical imaging app.," *Biomed. Instrum. Technol.*, vol. 46, no. suppl, pp. 87–90, 2012.
[1.181] Dolan, "FDA clears first diagnostic radiology app, Mobile MIM," *MobiHealthNews*, 04–Feb–2011. [Online]. Available: https://www.mobihealthnews.com/10173/fda–clears–first–diagnostic–radiology–app–mobile–mim. [Accessed: 06–Jan–2019].
[1.182] "KardiaMobile," *AliveCor, Inc.* [Online]. Available: https://store.alivecor.com/products/kardiamobile. [Accessed: 06–Jan–2019].
[1.183] "iExaminer," *iEXAMINER*. [Online]. Available: http://www.welchallyn.ca/en/microsites/iexaminer.html. [Accessed: 06–Jan–2019].
[1.184] "Product," *Welldoc Inc*. [Online]. Available: https://www.welldoc.com/product/. [Accessed: 06–Jan–2019].
[1.185] "Healthcare solutions | PureWeb | ResolutionMD," *PureWeb*. [Online]. Available: https://www.pureweb.com/
healthcare. [Accessed: 06–Jan–2019].
[1.186] The European Parliament and the Council of the European Union, "Medical Device Directive 93/42/EEC," Off. J. Eur. Union, 1993. [Online]. Available: https://eur–lex.europa.eu/LexUriServ/LexUriServ.do?uri=CONSLEG:1993L0042:20071011:en:PDF [Accessed: 06–Jan–2019].
[1.187] The European Parliament and the Council of the European Union, "Medical Device Directive 2007/47/EC," Off. J. Eur. Union, 2007. [Online]. Available: https://eur–lex.europa.eu/LexUriServ/LexUriServ.do?uri=OJ:L:2007:247:0021:0055:en:PDF [Accessed: 06–Jan–2019].
[1.188] "CE marking," *Together Against Trafficking in Human Beings*, 30–Aug–2017. [Online]. Available: http://ec.europa.eu/growth/single–market/ce–marking/. [Accessed: 06–Jan–2019].
[1.189] "Adjuvant Calculator– Oncology Apps – ONCOassist healthcare professional," *ONCOassist*. [Online]. Available: https://oncoassist.com/. [Accessed: 06–Jan–2019].
[1.190] European Parliament and Council of the European Union, "Regulation (EU) 2017/746 of the European Parliament and of the Council of 5 April 2017 on medical devices," *Off. J. Eur. Union*, vol. 60, no. April 2014, pp. 1–175, 2017. [Online]. Available: https://eur–lex.europa.eu/legal–content/EN/TXT/PDF/?uri=CELEX:32017R0745 [Accessed: 06–Jan–2019].

[1.191] Edwards, "EU medical device regulation changes: What do they mean?" *Verdict Medical Devices*, 16–Oct–2018. [Online]. Available: https://www.medicaldevice–network.com/features/eu–medical–device–regulation–changes/. [Accessed: 06–Jan–2019].
[1.192] "Making a success of Brexit," *GOV.UK*. [Online]. Available: https://www.gov.uk/government/news/medicines–and–healthcare–products–regulatory–agency–statement–on–the–outcome–of–the–eu–referendum. [Accessed: 06–Jan–2019].
[1.193] "How medicines, medical devices and clinical trials would be regulated if there's no Brexit deal," *GOV.UK*. [Online]. Available: https://www.gov.uk/government/publications/how–medicines–medical–devices–and–clinical–trials–would–be–regulated–if–theres–no–brexit–deal/how–medicines–medical–devices–and–clinical–trials–would–be–regulated–if–theres–no–brexit–deal. [Accessed: 06–Jan–2019].
[1.194] Medicines & Healthcare products Regulatory Agency, "Medical device stand– alone software including apps," *GOV.UK*, 2014. [Online]. Available: https://assets.publishing.service.gov.uk/government/uploads/system/uploads/attachment_data/file/548313/Software_flow_chart_Master.pdf.
[1.195] Lightley, "When is a mobile app classed as a medical device | MHRA compliant apps," *Genetic Digital*, 09–Dec–2013. [Online]. Available: https://www.geneticdigital.co.uk/2013/03/when–should–an–app–be–classed–as–a–device/. [Accessed: 06–Jan–2019].
[1.196] Heather, "Explainer: when is an app not an app (but a medical device)?," *Digital Health*, 07–Mar–2017. [Online]. Available: https://www.digitalhealth.net/2016/09/explainer–when–is–an–app–not–an–app–but–a–medical–device/. [Accessed: 06–Jan–2019].
[1.197] "Medical Device Technology Forum on the use of software as a medical device – 12 May 2010," *Ofcom | Statutory Duties and Regulatory Principles*, 11–Jan–2012. [Online]. Available: https://webarchive.nationalarchives.gov.uk/20150113200213/http://www.mhra.gov.uk/Howweregulate/NewTechnologiesForums/DevicesNewTechnologyForum/Forums/CON084987. [Accessed: 06–Jan–2019].
[1.198] "Approval of Medical Devices," *Planning D–Day (April 2003) – Library of Congress Information Bulletin*, 01–Sep–2014. [Online]. Available: http://www.loc.gov/law/help/medical–devices/. [Accessed: 06–Jan–2019].
[1.199] B. Kramer, S. Xu, and A. S. Kesselheim, "Regulation of Medical Devices in the United States and European Union," *N. Engl. J. Med.*, vol. 366, no. 9, pp. 848–855, 2012.
[1.200] Sorenson and M. Drummond, "Improving medical device regulation: The United States and Europe in perspective," *Milbank Q.*, vol. 92, no. 1, pp. 114–150, 2014.
[1.201] Cohen, "How a fake hip showed up failings in European device regulation," *BMJ*, vol. 345, p. e7090, 2012.
[1.202] Cohen and M. Billingsley, "Europeans are left to their own devices.," *BMJ*, vol. 342, p. d2748, 2011.
[1.203] D. Curfman and R. F. Redberg, "Medical Devices — Balancing Regulation and Innovation," *N. Engl. J. Med.*, vol. 365, no. 11, pp. 975–977, 2011.
[1.204] "EUROPE – Overview of medical device industry and healthcare statistics," *Emergo*, 23–Oct–2018. [Online]. Available: https://www.emergobyul.com/resources/market–europe. [Accessed: 27–Apr–2019].
[1.205] Legislative Services Branch, "Consolidated federal laws of Canada, Medical Devices Regulations," *Medical Devices Regulations.* [Online]. Available: https://laws–lois.justice.gc.ca/eng/regulations/sor–98–282/fulltext.html. [Accessed: 27–Apr–2019].
[1.206] "Health Canada Medical Device License (MDL) and MDEL Registration," *Emergo*, 12–Nov–2018. [Online]. Available: https://www.emergobyul.com/services/canada/canada–device–license. [Accessed: 27–Apr–2019].
[1.207] Australian Government Department of Health, "Consultation: Designation of Australian conformity assessment bodies for medical devices – Implementation," *Therapeutic Goods Administration (TGA)*, 14–Jun–2017. [Online]. Available: https://www.tga.gov.au/consultation/consultation–designation–australian–conformity–assessment–bodies–medical–devices–implementation. [Accessed: 27–Apr–2019].
[1.208] Australian Government Department of Health, "Use of market authorisation evidence from comparable overseas regulators / assessment bodies for medical devices (including IVDs)," *Therapeutic Goods Administration (TGA)*, 28–Nov–2018. [Online]. Available: https://www.tga.gov.au/publication/use–market–authorisation–evidence–comparable–overseas–regulators–assessment–bodies–medical–devices–including–ivds. [Accessed: 27–Apr–2019].
[1.209] Australian Government Department of Health, "Medical Device Single Audit Program (MDSAP)," *Therapeutic Goods Administration (TGA)*, 06–Dec–2016. [Online]. Available: https://www.tga.gov.au/medical–device–single–audit–program–mdsap. [Accessed: 27–Apr–2019].
[1.210] H. Canada, "Notice: Medical Device Single Audit Program (MDSAP) Transition Plan – Frequently Asked Questions (FAQ)," *Canada.ca*, 22–Apr–2016. [Online]. Available: https://www.canada.ca/en/health–canada/services/drugs–health–products/medical–devices/activities/international/notice–transition–plan–medical–device–audit–program.html. [Accessed: 27–Apr–2019].

[2.1] S. Majumder, T. Mondal, and M. J. Deen, "Wearable Sensors for Remote Health Monitoring," *Sensors*, vol. 17, no. 1, p. 130, doi:10.3390/s17010130, January 2017.

[2.2] A. I. Faisal, S. Majumder, T. Mondal, D. Cowan, S. Naseh, and M. J. Deen, "Monitoring methods of human body joints: State–of–the–art and research challenges," *Sensors (Switzerland)*, vol. 19, no. 11, 2019.

[2.3] M. J. Deen, "Information and communications technologies for elderly ubiquitous healthcare in a smart home," *Personal and Ubiquitous Computing*, vol. 19, no. 3–4, pp. 573–599, 2015.

[2.4] S. Majumder and M. J. Deen, "Smartphone sensors for health monitoring and diagnosis," *Sensors (Switzerland)*, vol. 19, no. 9. 2019.

[2.5] P. Gope and T. Hwang, "BSN–Care: A Secure IoT–Based Modern Healthcare System Using Body Sensor Network," *IEEE Sens. J.*, vol. 16, no. 5, pp. 1368–1376, 2016.

[2.6] S. Majumder, T. Mondal, and M. J. Deen, "A Simple, Low–Cost and Efficient Gait Analyzer for Wearable Healthcare Applications," *IEEE Sens. J.*, vol. 19, no. 6, pp. 2320–2329, 2019.

[2.7] Y. Liu *et al.*, "A Novel Cloud–Based Framework for the Elderly Healthcare Services Using Digital Twin," *IEEE Access*, vol. 7, pp. 49088–49101, 2019.

[2.8] S. Majumder *et al.*, "Smart homes for elderly healthcare—Recent advances and research challenges," *Sensors (Switzerland)*, vol. 17, no. 11, p. 2496, 2017.

[2.9] "Your Walking Speed May Be Linked to Risk of Heart Disease," *Health Essentials from Cleveland Clinic*, 19–Nov–2019. [Online]. Available: https://health.clevelandclinic.org/your–walking–speed–may–be–linked–to–risk–of–heart–disease/. [Accessed: 11–Mar–2020].

[2.10] R. Best and R. Begg, "A method for calculating the probability of tripping while walking," *J. Biomech.*, vol. 41, no. 5, pp. 1147–1151, 2008.

[2.11] C. Rosano, J. Brach, S. Studenski, W. T. Longstreth, and A. B. Newman, "Gait variability is associated with subclinical brain vascular abnormalities in high–functioning older adults," *Neuroepidemiology*, vol. 29, no. 3–4, pp. 193–200, 2008.

[2.12] J. L. Marins, X. Yun, E. R. Bachmann, R. B. McGhee, and M. J. Zyda, "An extended Kalman filter for quaternion–based orientation estimation using MARG sensors," in *Proc. IEEE/RSJ Int. Conf. Intell. Robots Syst.*, vol. 4, Oct. 2001, pp. 2003–2011.

[2.13] X. Yun and E. R. Bachmann, "Design, implementation, and experimental results of a quaternion–based Kalman filter for human body motion tracking," *IEEE Trans. Robot.*, vol. 22, no. 6, pp. 1216–1227, Dec. 2006.

[2.14] Y. S. Suh, "Orientation estimation using a quaternion–based indirect Kalman filter with adaptive estimation of external acceleration," *IEEE Trans. Instrum. Meas.*, vol. 59, no. 12, pp. 3296–3305, 2010.

[2.15] A. M. Sabatini, "Quaternion–based extended Kalman filter for determining orientation by inertial and magnetic sensing," *IEEE Trans. Biomed. Eng.*, vol. 53, no. 7, pp. 1346–1356, Jul. 2006.

[2.16] A. M. Sabatini, "Kalman–filter–based orientation determination using inertial/magnetic sensors: Observability analysis and performance evaluation," *Sensors*, vol. 11, no. 10, pp. 9182–9206, 2011.

[2.17] M. D. Shuster and S. D. Oh, "Three–axis attitude determination from vector observations," *J. Guid. Control, Dyn.*, vol. 4(1), pp. 70–77, 1981.

[2.18] J. L. Crassidis, F. L. Markley, "Unscented filtering for spacecraft attitude estimation," *J. Guid. Control. Dyn.*, vol. 26(4), pp. 536–542, 2003.

[2.19] G. F. Welch, "HISTORY: The use of the Kalman filter for human motion tracking in virtual reality," *Presence: Teleoperators and Virtual Environments*, vol. 18, no. 1. pp. 72–91, 2009.

[2.20] W. T. Higgins, "A comparison of complementary and Kalman filtering," *IEEE Trans. Aerosp. Electron. Syst.*, vol. AES–11, no. 3, pp. 321–325, May 1975.

[2.21] A. M. Khan, M. H. Siddiqi, and S.–W. Lee, "Exploratory data analysis of acceleration signals to select light–weight and accurate features for real–time activity recognition on smartphones," *Sensors*, vol. 13, no. 10, pp. 13099–13122, 2013.

[2.22] R. Mahony, T. Hamel, and J.–M. Pflimlin, "Complementary filter design on the special orthogonal group SO(3)," in *Proc. IEEE Conf. Decision Control Eur. Control Conf.*, Dec. 2005, pp. 1477–1484.

[2.23] S. O. H. Madgwick, A. J. L. Harrison, and R. Vaidyanathan, "Estimation of IMU and MARG orientation using a gradient descent algorithm," in *Proc. IEEE Int. Conf. Rehabil. Robot.*, Jun./Jul. 2011, pp. 1–7.

[2.24] R. G. Valenti, I. Dryanovski, and J. Xiao, "Keeping a good attitude: A quaternion–based orientation filter for IMUs and MARGs," *Sensors (Switzerland)*, vol. 15, no. 8, pp. 19302–19330, 2015.

[2.25] A. Makni, H. Fourati, and A. Y. Kibangou, "Energy–Aware Adaptive Attitude Estimation under External Acceleration for Pedestrian Navigation," *IEEE/ASME Trans. Mechatronics*, vol. 21, no. 3, pp. 1366–1375, 2016.

[2.26] X. Li and Q. Li, "External acceleration elimination for complementary attitude filter," in *2017 IEEE International Conference on Information and Automation, ICIA 2017*, 2017, pp. 208–212.

[2.27] B. Fan, Q. Li, and T. Liu, "Improving the accuracy of wearable sensor orientation using a two–step complementary filter with state machine–based adaptive strategy," *Meas. Sci. Technol.*, 2018.

[2.28] G. H. Lee, M. Achtelik, F. Fraundorfer, M. Pollefeys, and R. Siegwart, "A benchmarking tool for MAV visual pose estimation," in *11th International Conference on Control, Automation, Robotics and Vision, ICARCV 2010*, 2010, pp. 1541–1546.

[2.29] R. G. Valenti, I. Dryanovski, and J. Xiao, "Keeping a good attitude: A quaternion–based orientation filter for IMUs and MARGs," *Sensors (Switzerland)*, vol. 15, no. 8, pp. 19302–19330, 2015.

[2.30] A. H. Snijders, B. P. van de Warrenburg, N. Giladi, and B. R. Bloem, "Neurological gait disorders in elderly people: clinical approach and classification," *Lancet Neurol.*, vol. 6, no. 1, pp. 63–74, 2007.

[2.31] J. Dumurgier, A. Elbaz, P. Ducimetière, B. Tavernier, A. Alpérovitch, and C. Tzourio, "Slow walking speed and cardiovascular death in well functioning older adults: Prospective cohort study," *BMJ*, vol. 339, no. 7731, p. 1187, 2009.

[2.32] D. T. H. Lai, S. B. Taylor, and R. K. Begg, "Prediction of foot clearance parameters as a precursor to forecasting the risk of tripping and falling," *Hum. Mov. Sci.*, vol. 31, no. 2, pp. 271–283, 2012.

[2.33] R. Zhang, H. Yang, F. Höflinger, and L. M. Reindl, "Adaptive Zero Velocity Update Based on Velocity Classification for Pedestrian Tracking," *IEEE Sens. J.*, vol. 17, no. 7, pp. 2137–2145, 2017.

[2.34] H. Benzerrouk, A. Nebylov, and P. Closas, "MEMS IMU/ZUPT Based Cubature Kalman Filter Applied to Pedestrian Navigation System," in *Proceedings of International Electronic Conference on Sensors and Applications*, 2014, pp. 1–7.

[3.1] S. Majumder, T. Mondal, and M. J. Deen, "Wearable Sensors for Remote Health Monitoring," *Sensors*, vol. 17, no. 1, p. 130, doi:10.3390/s17010130, January 2017.

[3.2] M. Basso, M. Galanti, G. Innocenti, and D. Miceli, "Pedestrian Dead Reckoning Based on Frequency Self–Synchronization and Body Kinematics," *IEEE Sens. J.*, vol. 17, no. 2, pp. 534–545, 2017.

[3.3] M. J. Deen, "Information and communications technologies for elderly ubiquitous healthcare in a smart home," *Personal and Ubiquitous Computing*, vol. 19, no. 3–4, pp. 573–599, 2015.

[3.4] S. Majumder and M. J. Deen, "Smartphone sensors for health monitoring and diagnosis," *Sensors (Switzerland)*, vol. 19, no. 9. 2019.

[3.5] P. Gope and T. Hwang, "BSN–Care: A Secure IoT–Based Modern Healthcare System Using Body Sensor Network," *IEEE Sens. J.*, vol. 16, no. 5, pp. 1368–1376, 2016.

[3.6] S. Majumder, T. Mondal, and M. J. Deen, "A Simple, Low–Cost and Efficient Gait Analyzer for Wearable Healthcare Applications," *IEEE Sens. J.*, vol. 19, no. 6, pp. 2320–2329, 2019.

[3.7] Y. Liu *et al.*, "A Novel Cloud–Based Framework for the Elderly Healthcare Services Using Digital Twin," *IEEE Access*, vol. 7, pp. 49088–49101, 2019.

[3.8] S. Majumder *et al.*, "Smart homes for elderly healthcare—Recent advances and research challenges," *Sensors (Switzerland)*, vol. 17, no. 11, p. 2496, 2017.

[3.9] A. I. Faisal, S. Majumder, T. Mondal, D. Cowan, S. Naseh, and M. J. Deen, "Monitoring methods of human body joints: State–of–the–art and research challenges," *Sensors (Switzerland)*, vol. 19, no. 11, 2019.

[3.10] M. Ha and D. Han, "The relationship between knee joint angle and knee flexor and extensor muscle strength," *J. Phys. Ther. Sci.*, vol. 29, no. 4, pp. 662–664, 2017.

[3.11] K. Moromizato, R. Kimura, H. Fukase, K. Yamaguchi, and H. Ishida, "Whole–body patterns of the range of joint motion in young adults: Masculine type and feminine type," *J. Physiol. Anthropol.*, vol. 35, no. 1, 2016.

[3.12] A. Turkiewicz, A. A. Kiadaliri, and M. Englund, "Cause–specific mortality in osteoarthritis of peripheral joints," *Osteoarthr. Cartil.*, vol. 27, no. 6, pp. 848–854, 2019.

[3.13] L. Bilro, J. Lemos Pinto, J. Oliveira, and R. Nogueira, "Gait monitoring with a wearable plastic optical sensor," in *Proceedings of IEEE Sensors*, 2008, pp. 787–790.

[3.14] D. Z. Stupar, J. S. Bajic, L. M. Manojlovic, M. P. Slankamenac, A. V. Joza, and M. B. Zivanov, "Wearable low–cost system for human joint movements monitoring based on fiber–optic curvature sensor," *IEEE Sens. J.*, vol. 12, no. 12, pp. 3424–3431, 2012.

[3.15] J. H. M. Bergmann, S. Anastasova–Ivanova, I. Spulber, V. Gulati, P. Georgiou, and A. McGregor, "An attachable clothing sensor system for measuring knee joint angles," *IEEE Sens. J.*, vol. 13, no. 10, pp. 4090–4097, 2013.

[3.16] P. T. Gibbs and H. H. Asada, "Wearable conductive fiber sensors for multi–axis human joint angle measurements," *J. Neuroeng. Rehabil.*, vol. 2, 2005.

[3.17] P. Mandal, K. Tank, T. Mondal, C. H. Chen, and M. J. Deen, "Predictive Walking–Age Health Analyzer," *IEEE J. Biomed. Heal. Informatics*, vol. 22, no. 2, pp. 363–374, 2018. Priyanka's paper

[3.18] B. Jin *et al.*, "Walking–age analyzer for healthcare applications," *IEEE J. Biomed. Heal. Informatics*, vol. 18, no. 3, pp. 1034–1042, 2014.
[3.19] M. D. Djurić–Jovičić, N. S. Jovičić, and D. B. Popović, "Kinematics of gait: New method for angle estimation based on accelerometers," *Sensors*, vol. 11, no. 11, pp. 10571–10585, 2011.
[3.20] E. Allseits, K. J. Kim, C. Bennett, R. Gailey, I. Gaunaurd, and V. Agrawal, "A novel method for estimating knee angle using two leg–mounted gyroscopes for continuous monitoring with mobile health devices," *Sensors (Switzerland)*, vol. 18, no. 9, 2018.
[3.21] W. T. Higgins, "A comparison of complementary and Kalman filtering," *IEEE Trans. Aerosp. Electron. Syst.*, vol. AES–11, no. 3, pp. 321–325, May 1975.
[3.22] S. Majumder and M. J. Deen, "A Robust Orientation Filter for Wearable Sensing Applications," in *IEEE Sensors Journal*, doi: 10.1109/JSEN.2020.3009388.
[3.23] M. El–Gohary, S. Pearson, and J. McNames, "Joint angle tracking with inertial sensors," in *Proceedings of the 30th Annual International Conference of the IEEE Engineering in Medicine and Biology Society, EMBS'08 – "Personalized Healthcare through Technology,"* 2008, pp. 1068–1071.
[3.24] G. Cooper *et al.*, "Inertial sensor–based knee flexion/extension angle estimation," *J. Biomech.*, vol. 42, no. 16, pp. 2678–2685, 2009.
[3.25] P. Daponte, L. De Vito, M. Riccio, and C. Sementa, "Design and validation of a motion–tracking system for ROM measurements in home rehabilitation," *Meas. J. Int. Meas. Confed.*, vol. 55, pp. 82–96, 2014.
[3.26] J. L. Crassidis, F. L. Markley, "Unscented filtering for spacecraft attitude estimation," *J. Guid. Control. Dyn.*, vol. 26(4), pp. 536–542, 2003.
[3.27] G. F. Welch, "HISTORY: The use of the Kalman filter for human motion tracking in virtual reality," *Presence: Teleoperators and Virtual Environments*, vol. 18, no. 1. pp. 72–91, 2009
[3.28] A. M. Khan, M. H. Siddiqi, and S.–W. Lee, "Exploratory data analysis of acceleration signals to select light–weight and accurate features for real–time activity recognition on smartphones," *Sensors*, vol. 13, no. 10, pp. 13099–13122, 2013.
[3.29] T. Seel, T. Schauer, and J. Raisch, "Joint axis and position estimation from inertial measurement data by exploiting kinematic constraints," in *Proceedings of the IEEE International Conference on Control Applications*, 2012, pp. 45–49.
[3.30] T. Seel, J. Raisch, and T. Schauer, "IMU–based joint angle measurement for gait analysis," *Sensors (Switzerland)*, vol. 14, no. 4, pp. 6891–6909, 2014.
[3.31] F. Alonge, E. Cucco, F. D'Ippolito, and A. Pulizzotto, "The use of accelerometers and gyroscopes to estimate hip and knee angles on gait analysis," *Sensors (Switzerland)*, vol. 14, no. 5, pp. 8430–8446, 2014.
[3.32] F. Alonge, E. Cucco, and F. D'Ippolito, "Use of accelerometers and gyros for hip and knee angle estimation," in *2013 IEEE International Conference on Mechatronics and Automation, IEEE ICMA 2013*, 2013, pp. 939–944.
[3.33] L. Meng, B. Li, C. Childs, and A. Buis "IMU–based angle measurement – algorithm validation by Vicon motion capture," *University of Strathclyde, Glasgow, Scotland. DOI; 10.15129/91cc1c74–4aa1–4d66–8476–ff6ab0e7a196*, 31–Jul–2018.
[3.34] L. Meng, B. Li, C. Childs, A. Buis, F. He, and D. Ming, "Effect of walking variations on complementary filter based inertial data fusion for ankle angle measurement," in *2019 IEEE International Conference on Computational Intelligence and Virtual Environments for Measurement Systems and Applications, CIVEMSA 2019 – Proceedings*, 2019.
[3.35] L. J. Millar, L. Meng, and P. J. Rowe, "Routine clinical motion analysis: comparison of a bespoke real–time protocol to current clinical methods," *Comput. Methods Biomech. Biomed. Engin.*, vol. 22, no. 2, pp. 149–158, 2019.
[3.36] H. Zheng, N. D. Black, and N. D. Harris, "Position–sensing technologies for movement analysis in stroke rehabilitation," *Medical and Biological Engineering and Computing*, vol. 43, no. 4. pp. 413–420, 2005.
[4.1] S. Majumder, T. Mondal, and M. J. Deen, "Wearable Sensors for Remote Health Monitoring," *Sensors*, vol. 17, no. 1, 45 pages, doi:10.3390/s17010130, January 2017.
[4.2] M. Patton, "U.S. Health Care Costs Rise Faster Than Inflation," Available: http://www.forbes.com/sites/mikepatton/2015/06/29/u–s–health–care–costs–rise–faster–than–inflation/#2a6017656fa1 [Accessed: 16–Mar–2018].
[4.3] N. Agoulmine, M.J. Deen, J.S. Lee, M. Meyyappan, "U–health smart home," *IEEE Nanotech Magazine*, vol. 5, no. 3, pp. 6–11, Sep. 2011;
[4.4] S. Majumder, E. Aghayi, M. Noferesti, H. Memarzadeh–Tehran, T. Mondal, Z. Pang, M.J. Deen "Smart Homes for Elderly Healthcare—Recent Advances and Research Challenges," *Sensors*, vol. 17, no. 11, pp. 2496–2511, 2017.

[4.5] S. J. Jung, R. Myllyla, and W. Y. Chung, "Wireless machine–to–machine healthcare solution using android mobile devices in global networks," *IEEE Sens. J.*, vol. 13, no. 5, pp. 1419–1424, 2013.

[4.6] S. Majumder, L. Chen, O. Marinov, C.–H. Chen, T. Mondal, and M. J. Deen, "Non–Contact Wearable Wireless ECG Systems for Long Term Monitoring," *IEEE Rev. Biomed. Eng.*, vol. 11, pp. 306–321, 2018.

[4.7] M. J. Deen, "Information and communications technologies for elderly ubiquitous healthcare in a smart home," *Personal and Ubiquitous Computing*, vol. 19, no. 3–4, pp. 573–599, 2015.

[4.8] S. Mulroy, J. Gronley, W. Weiss, C. Newsam, and J. Perry, "Use of cluster analysis for gait pattern classification of patients in the early and late recovery phases following stroke," *Gait & Posture*, vol. 18, no. 1, pp. 114–125, 2003.

[4.9] L. K. Smith, J. L. Lelas, and D. C. Kerrigan, "Gender differences in pelvic motions and center of mass displacement during walking: Stereotypes quantified," *Journal of Women's Health & Gender–Based Medicine*, vol. 11, no. 5, pp. 453–458, Jun. 2002.

[4.10] K. Keller and M. Engelhardt, "Strength and muscle mass loss with aging process. Age and strength loss," *Muscles, Ligaments and Tendons Journal*, vol. 3, no. 4, pp. 346–350, Oct. 2013.

[4.11] P. Lorenzi, R. Rao, G. Romano, A. Kita, and F. Irrera, "Mobile Devices for the Real–Time Detection of Specific Human Motion Disorders," *IEEE Sens. J.*, vol. 16, no. 23, pp. 8220–8227, 2016.

[4.12] A. Lung, N. E. Shakhsheer, Y. Gonzalez, P. Shrivastava, A. Roy, A. Craig, M. Faisal, J. Boley, S. Oh, and Y. Zhang, "21.3 A 6.45 μW self–powered IoT SoC with integrated energy–harvesting power management and ULP asymmetric radios," *2015 IEEE International Solid–State Circuits Conference–(ISSCC)*, pp. 1–3, Feb. 2015.

[4.13] P. Gope and T. Hwang, "BSN–Care: A Secure IoT–Based Modern Healthcare System Using Body Sensor Network," *IEEE Sens. J.*, vol. 16, no. 5, pp. 1368–1376, 2016.

[4.14] A. H. Abdul Razak, A. Zayegh, R. K. Begg, and Y. Wahab, "Foot plantar pressure measurement system: A review," *Sensors*, vol. 12, no. 7. pp. 9884–9912, 2012.

[4.15] J. A. Ramirez–Bautista, J. A. Huerta–Ruelas, S. L. Chaparro–Cárdenas, and A. Hernández–Zavala, "A Review in Detection and Monitoring Gait Disorders Using In–Shoe Plantar Measurement Systems," *IEEE Reviews in Biomedical Engineering*, vol. 10. pp. 299–309, 2017.

[4.16] Y. Makihara, H. Mannami, and Y. Yagi, "Gait Analysis of Gender and Age Using a Large–Scale Multi–view Gait Database," *Computer Vision – ACCV 2010 Lecture Notes in Computer Science*, pp. 440–451, 2011.

[4.17] M. Okumura, H. Iwama, Y. Makihara, and Y. Yagi, "Performance evaluation of vision–based gait recognition using a very large–scale gait database," *2010 Fourth IEEE International Conference on Biometrics: Theory, Applications and Systems (BTAS)*, 2010.

[4.18] Z. Wang, M. Jiang, Y. Hu, and H. Li, "An incremental learning method based on probabilistic neural networks and adjustable fuzzy clustering for human activity recognition by using wearable sensors," *IEEE Trans. Inf. Technol. Biomed.*, vol. 16, no. 4, pp. 691–699, 2012.

[4.19] S. Qiu, Z. Wang, H. Zhao, and H. Hu, "Using Distributed Wearable Sensors to Measure and Evaluate Human Lower Limb Motions," *IEEE Trans. Instrum. Meas.*, vol. 65, no. 4, pp. 939–950, 2016.

[4.20] Q. Yuan, I. M. Chen, and A. Caus, "Human velocity tracking and localization using 3 IMU sensors," in *IEEE Conference on Robotics, Automation and Mechatronics, RAM – Proceedings*, 2013, pp. 25–30.

[4.21] G. Fortino, R. Giannantonio, R. Gravina, P. Kuryloski, and R. Jafari, "Enabling effective programming and flexible management of efficient body sensor network applications," *IEEE Trans. Human–Machine Syst.*, vol. 43, no. 1, pp. 115–133, 2013.

[4.22] R. Gravina, P. Alinia, H. Ghasemzadeh, and G. Fortino, "Multi–sensor fusion in body sensor networks: State–of–the–art and research challenges," *Inf. Fusion*, vol. 35, pp. 1339–1351, 2017.

[4.23] N. Raveendranathan *et al.*, "From modeling to implementation of virtual sensors in body sensor networks," *IEEE Sens. J.*, vol. 12, no. 3, pp. 583–593, 2012.

[4.24] H. Ghasemzadeh, P. Panuccio, S. Trovato, G. Fortino, and R. Jafari, "Power–aware activity monitoring using distributed wearable sensors," *IEEE Trans. Human–Machine Syst.*, vol. 44, no. 4, pp. 537–544, 2014.

[4.25] H. Ghasemzadeh, N. Amini, R. Saeedi, and M. Sarrafzadeh, "Power–aware computing in wearable sensor networks: An optimal feature selection," *IEEE Trans. Mob. Comput.*, vol. 14, no. 4, pp. 800–812, 2015.

[4.26] S. Mulroy, J. Gronley, W. Weiss, C. Newsam, and J. Perry, "Use of cluster analysis for gait pattern classification of patients in the early and late recovery phases following stroke," *Gait Posture*, vol. 18, no. 1, pp. 114–125, 2003.

[4.27] A. H. Snijders, B. P. van de Warrenburg, N. Giladi, and B. R. Bloem, "Neurological gait disorders in elderly people: clinical approach and classification," *Lancet Neurol.*, vol. 6, no. 1, pp. 63–74, 2007.

[4.28] A. Jalal, M. Z. Uddin, and T.–S. Kim, "Depth video–based human activity recognition system using translation and scaling invariant features for life logging at smart home," *IEEE Transactions on Consumer Electronics*, vol. 58, no. 3, pp. 863–871, Aug. 2012.

[4.29] N. D. Nguyen, D. T. Bui, P. H. Truong, and G. M. Jeong, "Classification of Five Ambulatory Activities Regarding Stair and Incline Walking Using Smart Shoes," *IEEE Sens. J.*, vol. 18, no. 13, pp. 5422–5428, 2018.

[4.30] S. Qiu *et al.*, "Body Sensor Network based Robust Gait Analysis: Toward Clinical and at Home Use," *IEEE Sensors J.*, 2018.

[4.31] A. Baghdadi, L. A. Cavuoto, and J. L. Crassidis, "Hip and trunk kinematics estimation in gait through kalman filter using IMU data at the ankle," *IEEE Sens. J.*, vol. 18, no. 10, pp. 4253–4260, 2018.

[4.32] C. Mizuike, S. Ohgi, and S. Morita, "Analysis of stroke patient walking dynamics using a tri–axial accelerometer," *Gait & Posture*, vol. 30, no. 1, pp. 60–64, 2009.

[4.33] F. Verdini, T. Leo, S. Fioretti, M.G. Benedetti, F. Catani, and S. Giannini, "Analysis of ground reaction forces by means of wavelet transform," *Clinical Biomechanics*, vol. 15, pp. 607–610, 2000.

[4.34] S. Mallat, A wavelet tour of signal processing: the sparse way. 3rd edition, Academic Press Inc., Burlington, MA, 2008.

[4.35] N. E. Huang, Z. Shen, S. R. Long, M. C. Wu, H. H. Shih, Q. Zheng, N. Yen, C. C. Tung, and H. H. Liu, "The empirical mode decomposition and the Hilbert spectrum for nonlinear and non–stationary time series analysis," presented at *Royal Society*, London, pp. 903–995, 1998.

[4.36] N. Wang, E. Ambikairajah, B. G. Celler, and N. H. Lovell, "Accelerometry based classification of gait patterns using empirical mode decomposition," *2008 IEEE International Conference on Acoustics, Speech and Signal Processing*, pp. 617–620, 2008.

[4.37] R. K. Ibrahim, E. Ambikairajah, B. G. Celler, and N. H. Lovell, "Gait pattern classification using compact features extracted from intrinsic mode functions," in *Proc. 30th Ann. Int. IEEE Eng. Med. Biol. Soc.*, pp. 3852–3855, Aug. 2008.

[4.38] Z.H. Wu, and N.E. Huang, "Ensemble empirical mode decomposition: a noise assisted data analysis method," *Advances in Adaptive Data Analysis* vol. 1, pp. 1–41, 2009.

[4.39] X. Cui, Chung–Kang Peng, M. D. Costa, A. Weiss, A. L. Goldberger and J. M. Hausdorff, "Development of a new approach to quantify stepping stability using Ensemble Empirical Mode Decomposition," *Gait Posture*, vol. 39(1), pp.495–500, 2014.

[4.40] N. Mammone, F. La Foresta, and F. C. Morabito, "Automatic artifact rejection from multichannel scalp EEG by wavelet ICA," *IEEE Sens. J.*, vol. 12, no. 3, pp. 533–542, 2012.

[4.41] S. Majumder, L. Chen, O. Marinov, C–H. Chen, T. Mondal and M.J. Deen, "Noncontact Wearable Wireless ECG Systems for Long–Term Monitoring," *IEEE Reviews in Biomedical Eng.*, vol. 11, pp. 306– 321, May 2018.

[4.42] P. Mandal, K. Tank, T. Mondal, C. H. Chen, and M. J. Deen, "Predictive Walking–Age Health Analyzer," *IEEE J. Biomed. Health. Informatics*, vol. 22, no. 2, pp. 363–374, 2018.

[4.43] G. Yogev, P. Meir, P. Chava, G. Nir, and J. M. Hausdorff, "Gait asymmetry in patients with Parkinson's disease and elderly fallers: when does the bilateral coordination of gait require attention?.," *Experimental Brain Research*, vol. 177, no. 3, pp. 336–346, Mar. 2007.

[4.44] J. Bo, T. Hoai Thu, E. Baek, S. H. Sakong, J. Xiao, T. Mondal, and M. J. Deen, "Walking–Age Analyzer for Healthcare Applications," *IEEE J Biomedical and Health Informatics*, vol. 18, no. 3, pp. 1034–1042, 2014.

[4.45] J. J. He, *Principal Component Analysis*, Springer, New York, 1986.

[4.46] R. K. Begg, M. Palaniswami, and B. Owen, "Support vector machines for automated gait classification," *IEEE Transactions on Biomedical Engineering*, vol. 52, no. 5, pp. 828–838, May 2005.

[4.47] L. Lee and W. E. L. Grimson, "Gait analysis for recognition and classification," *Fifth IEEE International Conference on Automatic Face and Gesture Recognition, 2002 May 20*, pp. 155–162.

[4.48] D. A. Winter, "Energy generation and absorption at the ankle and knee during fast, natural, and slow Cadences," *Clinical Orthopaedics and Related Research*, no. 175, pp. 147–154, 1983.

[4.49] D. A. Winter, "Biomechanical motor patterns in normal walking," *Journal of Motor Behavior*, vol. 15, no. 4, pp. 302–330, Dec. 1983.

[4.50] S. O'Shea, M. E. Morris, R. Iansek, "Dual Task Interference during Gait in People with Parkinson Disease: Effects of Motor versus Cognitive Secondary Tasks," *Physical Therapy*, vol. 82, no. 9, p. 888, Sep. 2002.

[4.51] K. M. T. Goutier, S. L. Jansen, C. G. C. Horlings, U. M. Kung, and J. H. J. Allum, "The influence of walking speed and gender on trunk sway for the healthy young and older adults," *Age and Ageing*, vol. 39, no. 5, pp. 647–650, Jun. 2010.

[4.52] P. DeVita and T. Hortobagyi, "Age causes a redistribution of joint torques and powers during gait," *Journal of Applied Physiology*, vol. 88, no. 5, pp. 1804–1811, May 2000.

[4.53] H. Shimokata and F.Kuzuya, "Aging, Basal Metabolic Rate, and Nutrition," *Japanese Journal of Geriatrics*, vol. 30, pp. 572–576, 1993.

[4.54] M. F. Schulz Aellen. (2008). Healthy Ageing. Continuing Psychology Education, Austin, Texas. [Online]. Available: http://texcpe.com/html/pdf/HealthyAging.pdf

[5.1] W. Einthoven, "Un nouveau galvonometre," *Nat. Arch Neerl Sci Exactes*, vol. 6, pp. 623–33, 1901.

[5.2] W. Einthoven, "Le telecardiogramme," *Arch Int Physiol.*, vol. 4, pp. 132–63, 1906.

[5.3] E. Nemati, M. J. Deen, and T. Mondal, "A wireless wearable ECG sensor for long–term applications," *IEEE Communications Magazine*, vol. 50, pp. 36–43, 2012.

[5.4] A. Arcelus, M. Sardar, and A. Mihailidis, "Design of a capacitive ECG sensor for unobtrusive heart rate measurements," *2013 IEEE International Instrumentation and Measurement Technology Conference* (*I2MTC*), 2013, pp. 407–410.

[5.5] B. S. Lin, W. Chou, H. Y. Wang, Y. J. Huang, and J. S. Pan, "Development of novel non–contact electrodes for mobile electrocardiogram monitoring system," *IEEE Translational Engineering in Health and Medicine*, vol. 1, pp. 1–8, 2013.

[5.6] G. Gargiulo, P. Bifulco, M. Cesarelli, M. Ruffo, M. Romano, R. A. Calvo, C. Jin, and A. van Schaik, "An ultra–high input impedance ECG amplifier for long–term monitoring of athletes," *Med. Dev. Evid. Res.*, vol. 3, pp. 1–9, 2010.

[5.7] L. Stingeni, E. Cerulli, A. Spalletti, A. Mazzoli, L. Rigano, L. Bianchi, and K. Hansel, "The role of acrylic acid impurity as a sensitizing component in electrocardiogram electrodes," *Contact Dermatitis*, vol. 73(1), pp. 44–8, 2015.

[5.8] E. Ozkaya and P. Kavlak Bozkurt, "Allergic contact dermatitis caused by self–adhesive electrocardiography electrodes: a rare case with concomitant roles of nickel and acrylates," *Contact Dermatitis*, vol. 70(2), pp. 121–123, 2014.

[5.9] N. Sakamoto, N. Sato, M. Goto, M. Kobayashi, N. Takehara, T. Takeuchi, A. K. Talib, E. Sugiyama, A. Minoshima, Y. Tanabe, K. Akasaka, J. Kawabe, Y. Kawamura, A. Doi, and N. Hasebe, "Three cases of corticosteroid therapy triggering ventricular fibrillation in J–wave syndromes," *Heart Vessels*, vol. 29(6), pp. 867–872, 2014.

[5.10] A. C. Deswysen, E. Zimerson, A. Goossens, M. Bruze, M. Baeck, "Allergic contact dermatitis caused by self–adhesive electrocardiography electrodes in an infant," *Contact Dermatitis*, vol. 69(6), pp. 379–381, 2013.

[5.11] B. Nunez–Acevedo, M. T. Gonzalez–Fernandez, M. M. Juangorena, and C. Vidal, "Multifunctional acrylates as possible sensitizers in electrocardiogram electrode allergy," *Ann Allergy Asthma Immunol*, vol. 111(1), pp. 77–78, 2013.

[5.12] M. S. Naidu and V. Kamaraju, *High Voltage Engineering*, 4th ed.; Publisher: New Delhi, India, pp. 107–108, 2009.

[5.13] S. Fuhrhop, S. Lamparth, and S. Heuer, "A textile integrated long–term ECG monitor with capacitively coupled electrodes," *IEEE Biomedical Circuits & Systems Conference*, 2009, pp. 21–24.

[5.14] C. L. Lam, N. N. Z. M. Rajdi, and D. H. B. Wicaksono, "MWCNT/ Cotton–based flexible electrode for electrocardiography," *Sensors IEEE*, pp. 1–4, 2013.

[5.15] G. Andreoni, A. Fanelli, I. Witkowska, P. Perego, M. Fusca, M. Mazzola, and M. G. Signorini, "Sensor validation for wearable monitoring system in ambulatory monitoring: Application to textile electrodes," *2013 7th International Conference on Pervasive Computing Technologies for Healthcare and Workshops* (*PervasiveHealth*), 2013, pp. 169–175.

[5.16] M. J. Deen, "Information and communications technologies for elderly ubiquitous healthcare in a smart home," *Personal and Ubiquitous Computing*, vol. 19(3–4), pp. 573–599, 2015.

[5.17] M. Weder, D. Hegemann, M. Amberg, M. Hess, L. Boesel, R. Abächerli, V. Meyer, and R. Rossi, "Embroidered Electrode with Silver/Titanium Coating for Long–Term ECG Monitoring," *Sensors*, vol. 15, no. 1, pp. 1750–1759, 2015.

[5.18] E.–M. Fong and W.–Y. Chung, "A Hygroscopic Sensor Electrode for Fast Stabilized Non–Contact ECG Signal Acquisition," *Sensors*, vol. 15, no. 8, pp. 19237–19250, May 2015

[5.19] A. C. Myers, H. Huang, and Y. Zhu, "Wearable silver nanowire dry electrodes for electrophysiological sensing," *RSC Adv.*, vol. 5, no. 15, pp. 11627–11632, 2015.

[5.20] H.–C. Jung, J.–H. Moon, D.–H. Baek, J.–H. Lee, Y.–Y. Choi, J.–S. Hong, and S.–H. Lee, "CNT/PDMS Composite Flexible Dry Electrodes for Long–Term ECG Monitoring," *IEEE Transactions on Biomedical Engineering*, vol. 59, no. 5, pp. 1472–1479, 2012.

[5.21] Y.–H. Chen, M. O. D. Beeck, L. Vanderheyden, E. Carrette, V. Mihajlovic, B. Grundlehner, S. Gadeyne, P. Boon, and C. V. Hoof, "Soft, Comfortable Polymer Dry Electrodes for high Quality ECG and EEG Recording," *Proceedings of International Electronic Conference on Sensors and Applications*, Feb. 2014.
[5.22] K. C. Tseng, B.–S. Lin, L.–D. Liao, Y.–T. Wang, and Y.–L. Wang, "Development of a Wearable Mobile Electrocardiogram Monitoring System by Using Novel Dry Foam Electrodes," *IEEE Systems Journal*, vol. 8, no. 3, pp. 900–906, 2014.
[5.23] J. Lee, J. Heo, W. Lee, Y. Lim, Y. Kim, and K. Park, "Flexible Capacitive Electrodes for Minimizing Motion Artifacts in Ambulatory Electrocardiograms," *Sensors*, vol. 14, no. 8, pp. 14732–14743, Dec. 2014.
[5.24] F. Lin, S. Yao, M. Mcknight, Y. Zhu, and A. Bozkurt, "Silver nanowire based wearable sensors for multimodal sensing," *IEEE Topical Conference on Biomedical Wireless Technologies, Networks, and Sensing Systems (BioWireleSS)*, 2016, pp. 55–58.
[5.25] P. Sarati Das and J.–Y. Park, "A flexible touch sensor based on conductive elastomer for biopotential monitoring applications," *Biomedical Signal Processing and Control*, vol. 33, pp. 72–82, Nov. 2017.
[5.26] Y. Ye–Lin, J. Bueno–Barrachina, G. Prats–Boluda, R. R. D. Sanabria, and J. Garcia–Casado, "Wireless sensor node for non–invasive high precision electrocardiographic signal acquisition based on a multi–ring electrode," *Measurement*, vol. 97, pp. 195–202, 2017.
[5.27] P. Salvo, R. Raedt, E. Carrette, D. Schaubroeck, J. Vanfleteren, and L. Cardon. "A 3D printed dry electrode for ECG/EEG recording." *Sensors and Actuators A: Physical*, vol. 174, pp. 96–102, 2012.
[5.28] L.–F. Wang, J.–Q. Liu, H.–L. Peng, B. Yang, H.–Y. Zhu, and C.–S. Yang. "MEMS–based flexible capacitive electrode for ECG measurement." *Electronics Letters*, vol. 49, no. 12, pp. 739–740, 2013.
[5.29] J.–W. Jeong, M. K. Kim, H. Cheng, W.–H. Yeo, X. Huang, Y. Liu, Y. Zhang, Y. Huang, and J. A. Rogers, "Epidermal Electronics: Capacitive Epidermal Electronics for Electrically Safe, Long–Term Electrophysiological Measurements (Adv. Healthcare Mater. 5/2014)," *Advanced Healthcare Materials*, vol. 3, no. 5, pp. 621–621, 2014.
[5.30] H. Zhang, W. Pei, Y. Chen, X. Guo, X. Wu, X. Yang, and H. Chen, "A motion interference–insensitive flexible dry electrode," *IEEE Trans. on Biomedical Engineering*, vol. 63, no. 6, pp. 1136–1144, 2016.
[5.31] T. Kim, J. Park, J. Sohn, D. Cho,and S. Jeon. "Bioinspired, highly stretchable, and conductive dry adhesives based on 1D–2D hybrid carbon nanocomposites for all–in–one ECG electrodes," *ACS Nano*, vol. 10, no. 4, pp. 4770–4778, 2016.
[5.32] M. A. Yokus and J. S. Jur, "Fabric–Based Wearable Dry Electrodes for Body Surface Biopotential Recording," *IEEE Transactions on Biomedical Engineering*, vol. 63, no. 2, pp. 423–430, 2016.
[5.33] T. Inoh, S. Yoon, T. E. Kim, H. Wi, K. J. Kim, E. J. Woo, and R. J. Sadleir, "Nanofiber Web Textile Dry Electrodes for Long–Term Biopotential Recording," *IEEE Transactions on Biomedical Circuits and Systems*, vol. 7, no. 2, pp. 204–211, 2013.
[5.34] D. Pani, A. Dessi, J. F. Saenz–Cogollo, G. Barabino, B. Fraboni, and A. Bonfiglio, "Fully Textile, PEDOT:PSS Based Electrodes for Wearable ECG Monitoring Systems," *IEEE Transactions on Biomedical Engineering*, vol. 63, no. 3, pp. 540–549, 2016.
[5.35] S. Majumder, T. Mondal, and M. J. Deen, "Wearable Sensors for Remote Health Monitoring," *Sensors*, vol. 17, no. 1, 45 pages, doi:10.3390/s17010130, January 2017.
[5.36] A. Gruetzmann, S. Hansen, and J. Müller, "Novel dry electrodes for ECG monitoring," *Physiological Measurement*, vol. 28, no. 11, pp. 1375–1390, Dec. 2007.
[5.37] Y. M. Chi, T.–P. Jung, and G. Cauwenberghs, "Dry–Contact and Noncontact Biopotential Electrodes: Methodological Review," *IEEE Reviews in Biomedical Engineering*, vol. 3, pp. 106–119, 2010.
[5.38] P. J. Xu, H. Zhang, and X. M. Tao, "Textile–structured electrodes for electrocardiogram," *Textile Progress*, vol. 40, no. 4, pp. 183–213, 2008.
[5.39] E. Spanò, S. D. Pascoli, and G. Iannaccone, "Low–Power Wearable ECG Monitoring System for Multiple–Patient Remote Monitoring," *IEEE Sensors Journal*, vol. 16, no. 13, pp. 5452–5462, Jul. 2016.
[5.40] C.–Y. Chen, C.–L. Chang, C.–W. Chang, S.–C. Lai, T.–F. Chien, H.–Y. Huang, J.–C. Chiou, and C.–H. Luo, "A Low–Power Bio–Potential Acquisition System with Flexible PDMS Dry Electrodes for Portable Ubiquitous Healthcare Applications," *Sensors*, vol. 13, no. 3, pp. 3077–3091, Apr. 2013.
[5.41] F. Sun, C. Yi, W. Li, and Y. Li, "A wearable H–shirt for exercise ECG monitoring and individual lactate threshold computing," *Computers in Industry*, vol. 92–93, pp. 1–11, 2017.
[5.42] V. P. Rachim and W.–Y. Chung, "Wearable Noncontact Armband for Mobile ECG Monitoring System," *IEEE Transactions on Biomedical Circuits and Systems*, vol. 10, no. 6, pp. 1112–1118, 2016.
[5.43] E.–M. Fong and W.–Y. Chung, "Mobile Cloud–Computing–Based Healthcare Service by Noncontact ECG Monitoring," *Sensors*, vol. 13, no. 12, pp. 16451–16473, Feb. 2013.
[5.44] Y. Qin a, M.M.R. Howlader, M.J. Deen, Y.M. Haddara, and P.R. Selvaganapathy, "Polymer integration for packaging of implantable sensors", *Sensors and Actuators B: Chemical*, vol. 202, pp. 758–778, 31xOctober 2014.

[5.45] B. Chamadiya, K. Mankodiya, M. Wagner, and U. G. Hofmann, "Textile–based, contactless ECG monitoring for non–ICU clinical settings," *Journal of Ambient Intelligence and Humanized Computing*, vol. 4, no. 6, pp. 791–800, 2012.
[5.46] G. Andreoni, P. Perego, and C. Standoli, "Wearable monitoring of elderly in an ecologic setting: the SMARTA project," *Proceedings of 2nd Int. Electronic Conference on Sensors and Applications*, May 2015.
[5.47] E. S. Winokur, M. K. Delano, and C. G. Sodini, "A Wearable Cardiac Monitor for Long–Term Data Acquisition and Analysis," *IEEE Transactions on Biomedical Engineering*, vol. 60, no. 1, pp. 189–192, 2013.
[5.48] Y. Wang, S. Doleschel, R. Wunderlich, and S. Heinen, "A Wearable Wireless ECG Monitoring System With Dynamic Transmission Power Control for Long–Term Homecare," *Journal of Medical Systems*, vol. 39, no. 3, 2015.
[5.49] B.–S. Lin, W. Chou, H.–Y. Wang, Y.–J. Huang, and J.–S. Pan, "Development of Novel Non–Contact Electrodes for Mobile Electrocardiogram Monitoring System," *IEEE Journal of Translational Engineering in Health and Medicine*, vol. 1, pp. 1–8, 2013.
[5.50] Z.X. Yan, M.J. Deen and D.S. Malhi, "Gate–Controlled Lateral LPNP BJT: Characteristics, Modeling and Circuit Applications", *IEEE Trans. on Electron Devices*, vol. 44, no. 1, pp. 118–128, January 1997.
[5.51] E. Spinelli, F. Guerrero, P. García, and M. Haberman, "A simple and reproducible capacitive electrode." *Medical Engineering & Physics*, vol. 38, no. 3, pp. 286–289, 2016.
[5.52] T. Komensky, M. Jurcisin, K. Ruman, O. Kovac, D. Laqua, and P. Husar, "Ultra–wearable capacitive coupled and common electrode–free ECG monitoring system," *2012 Annual International Conference of the IEEE Engineering in Medicine and Biology Society*, 2012, pp. 1594–1597.
[5.53] Y. Zhang, F. Zhang, Y. Shakhsheer, J. D. Silver, A. Klinefelter, M. Nagaraju, J. Boley, J. Pandey, A. Shrivastava, E. J. Carlson, A. Wood, B. H. Calhoun, and B. P. Otis, "A Batteryless 19 □W MICS/ISM–Band Energy Harvesting Body Sensor Node SoC for ExG Applications," *IEEE Journal of Solid–State Circuits*, vol. 48, no. 1, pp. 199–213, 2013.
[5.54] C. Tsou, C.–H. Hsieh, M.–C. Liang, P.–W. Huang, and S.–Y. Lee, "ECG acquisition system with heart rate detection and energy harvesting for drivers," *2015 International Symposium on Bioelectronics and Bioinformatics (ISBB)*, 2015, pp. 180–183.
[5.55] J. Wang, T. Fujiwara, T. Kato, and D. Anzai, "Wearable ECG Based on Impulse–Radio–Type Human Body Communication," *IEEE Transactions on Biomedical Engineering*, vol. 63, no. 9, pp. 1887–1894, 2016.
[5.56] S. Poungponsri and X.–H. Yu, "An adaptive filtering approach for electrocardiogram (ECG) signal noise reduction using neural networks," *Neurocomputing*, vol. 117, pp. 206–213, 2013.
[5.57] N. Thakor and Y.–S. Zhu, "Applications of adaptive filtering to ECG analysis: noise cancellation and arrhythmia detection," *IEEE Trans. on Biomedical Engineering*, vol. 38, no. 8, pp. 785–794, 1991.
[5.58] P. Agante and J. M. D. Sa, "ECG noise filtering using wavelets with soft–thresholding methods," *Computers in Cardiology 1999.* (*Cat. No.99CH37004*), vol. 26 pp. 535–538, 1999.
[5.59] V. Bhateja, S. Urooj, R. Mehrotra, R. Verma, A. Lay–Ekuakille, and V. D. Verma, "A Composite Wavelets and Morphology Approach for ECG Noise Filtering," *Lecture Notes in Computer Science Pattern Recognition and Machine Intelligence*, pp. 361–366, 2013.
[5.60] M. A. Kabir and C. Shahnaz, "Denoising of ECG signals based on noise reduction algorithms in EMD and wavelet domains," *Biomedical Signal Processing and Control*, vol. 7, no. 5, pp. 481–489, 2012.
[5.61] H.–Y. Lin, S.–Y. Liang, Y.–L. Ho, Y.–H. Lin, and H.–P. Ma, "Discrete–wavelet–transform–based noise removal and feature extraction for ECG signals," *Irbm*, vol. 35, no. 6, pp. 351–361, 2014.
[5.62] H. Li, X. Wang, L. Chen, and E. Li, "Denoising and R–Peak Detection of Electrocardiogram Signal Based on EMD and Improved Approximate Envelope," *Circuits, Systems, and Signal Processing*, vol. 33, no. 4, pp. 1261–1276, 2013.
[5.63] J. Jenitta and A. Rajeswari, "Denoising of ECG signal based on improved adaptive filter with EMD and EEMD," *IEEE Conference On Information And Communication Technologies* (*ICT* 2013), 2013, pp. 957–962.
[5.64] B. Jeon, J. Lee and J. Choi, "Design and Implementation of a Wearable ECG System," *Int. Journal of Smart Home*, vol. 7, no. 2, pp. 61–70, 2013.
[5.65] H. Xia, I. Asif, and X. Zhao, "Cloud–ECG for real time ECG monitoring and analysis," *Computer Methods and Programs in Biomedicine*, vol. 110, no. 3, pp. 253–259, 2013.
[5.66] H. Kwon, S. Oh, P. S. Kumar, and V. K. Varadan, "E–Bra system for women ECG measurement with GPRS communication, Nanosensor, and motion artifact remove algorithm," *Proc. SPIE – Nanosystems in Engineering and Medicine*, vol. 8548, 9 pages, 24 October 2012.
[5.67] "Peace of mind," *AliveCor*. [Online]. Available: https://www.alivecor.com/?gclid=EAIaIQobChMI8u2iz_fw1gIVEIJpCh2HOwkTEAAYASABEgLdv_D_BwE. [Accessed: 14–Oct–2017].
[5.68] "Smart Wearable ECG EKG Monitor – QardioCore," *Qardio*. [Online]. Available: https://www.getqardio.com/qardiocore–wearable–ecg–ekg–monitor–iphone/. [Accessed: 14–Oct–2017].

[5.69] "AfibAlert – Heart Rhythm Monitor with Instant Atrial Fibrillation Detection," *Lohman Technology*. [Online]. Available: http://www.lohmantech.com/. [Accessed: 14–Oct–2017].
[5.70] *Gima, articoli medicali, apparecchi per medicina, elettromedicali, endoscopi, misuratori medicali, arredo ambulatorio, elettrobisturi, articoli per il pronto soccorso, articoli per la sterilizzazione*. [Online]. Available: http://www.gimaitaly.com/prodotti.asp?sku=33261&dept_selected=580&dept_id=5800. [Accessed: 14–Oct–2017].
[5.71] *The HeartCheck™ PEN handheld ECG Device*. [Online]. Available: http://www.cardiocommsolutions.com/QTStudy/. [Accessed: 14–Oct–2017].
[5.72] "PHYSICIANS," *The HeartCheck™*. [Online]. Available: http://www.theheartcheck.com/physician.html. [Accessed: 14–Oct–2017].
[5.73] "Home – ECG Check | iPhone & Android heart monitor," *Home – ECG Check | iPhone & Android heart monitor*. [Online]. Available: http://cardiacdesigns.com/. [Accessed: 14–Oct–2017].
[5.74] "Color Portable ECG Recorder Dicare m1CC." [Online]. Available: http://www.dimetekus.com/Color–Portable–ECG–Recorder–Dicare–m1CC_p234.html. [Accessed: 14–Oct–2017].
[5.75] *Handheld—超思*. [Online]. Available: http://www.choicemmed.com/info.aspx?m=photo&id=447#. [Accessed: 14–Oct–2017].
[5.76] *Handheld—超思*. [Online]. Available: http://www.choicemmed.com/info.aspx?m=photo&id=537#. [Accessed: 14–Oct–2017].
[5.77] "Easy ECG Monitor — PC–80A (Bluetooth 4.0)," *Easy ECG Monitor — PC–80A (Bluetooth 4.0)–Portable ECG Monitors–Heal Force Bio–meditech Holdings Limited*. [Online]. Available: http://www.healforce.com/en/index.php?ac=article&at=read&did=176. [Accessed: 14–Oct–2017].
[5.78] "H3 ," *H3 :: Mortara Website*. [Online]. Available: https://www.mortara.com/products/healthcare/holter–monitoring/h3/. [Accessed: 14–Oct–2017].
[5.79] Biometrics Ltd. Biometrics DataLog. Available online: http://www.biometricsltd.com/datalog.htm (accessed on 26 January 2014)
[5.80] C. Y. Chen, C. L. Chang, C. W. Chang, S. C. Lai, T. F. Chien, H. Y. Huang, J. C. Chiou, and C. H. Luo, "A low–power bio–potential acquisition system with flexible PDMS dry electrodes for portable ubiquitous healthcare applications," *Sensors*, vol. 13, pp. 3077–3091, 2013.
[5.81] P. C. Hii and W. Y. Chung, "A comprehensive ubiquitous healthcare solution on an Android™ mobile device," *Sensors*, vol. 11, pp. 6799–6815, 2011.
[5.82] B. Jin, T. H. Thu, E. H. Baek, S. H. Sakong, J. Xiao, T. Mondal, and M. J. Deen, "Walking–age analyzer for healthcare applications," *IEEE Journal of Biomedical and Health Informatics*, vol. 18(3), pp. 1034– 1042, 2014.
[5.83] M. Magno, L. Benini, C. Spagnol, and E. Popovici, "Wearable low power dry surface wireless sensor node for healthcare monitoring application," *2013 IEEE 9th International Conference on Wireless and Mobile Computing, Networking and Communications (WiMob)*, pp. 189–195, 2013(*WiMob*), Lyon, France, pp. 189–195, 7–9 October 2013.
[5.84] F. Miao, Y. Cheng, Y. He, Q. He, and Y. Li, "A Wearable Context–Aware ECG Monitoring System Integrated with Built–in Kinematic Sensors of the Smartphone," *Sensors*, vol. 15, no. 5, pp. 11465–11484, 2015.
[5.85] Atrial fibrillation. https://www.heartandstroke.ca/heart/conditions/atrial–fibrillation (accessed Aug 29, 2020).
[5.86] Goldberger, A. L.; Amaral, L. A.; Glass, L.; Hausdorff, J. M.; Ivanov, P. C.; Mark, R. G.; Mietus, J. E.; Moody, G. B.; Peng, C. K.; Stanley, H. E. PhysioBank, PhysioToolkit, and PhysioNet: Components of a New Research Resource for Complex Physiologic Signals. *Circulation* 2000, *101* (23). https://doi.org/10.1161/01.cir.101.23.e215.
[5.87] AF Classification from a Short Single Lead ECG Recording – The PhysioNet Computing in Cardiology Challenge 2017. https://physionet.org/content/challenge–2017/1.0.0/ (accessed Aug 29, 2020).
[5.88] Clifford, G. D.; Liu, C.; Moody, B.; Lehman, L.–W. H.; Silva, I.; Li, Q.; Johnson, A. E.; Mark, R. G. AF Classification from a Short Single Lead ECG Recording: the Physionet Computing in Cardiology Challenge 2017. *2017 Computing in Cardiology Conference (CinC)* 2017.

[6.1] C. A. Miller, A. H. Feiveson, and J. J. Bloomberg, "Effects of speed and visual–target distance on toe trajectory during the swing phase of treadmill walking," *J. Appl. Biomech.*, vol. 25, no. 1, pp. 32–42, 2009.
[6.2] T. Oberg, A. Karsznia, and K. Oberg, "Basic gait parameters: Reference data for normal subjects, 10–79 years of age," *J. Rehabil. Res. Dev.*, vol. 30, no. 2, pp. 210–223, 1993.
[6.3] H. G. Kang and J. B. Dingwell, "Separating the effects of age and walking speed on gait variability," *Gait Posture*, vol. 27, no. 4, pp. 572–577, 2008.
[6.4] P. M. Mills, R. S. Barrett, and S. Morrison, "Toe clearance variability during walking in young and elderly men," *Gait Posture*, vol. 28, no. 1, pp. 101–107, 2008.
[6.5] B. W. Schulz, "Minimum toe clearance adaptations to floor surface irregularity and gait speed," *J. Biomech.*, vol. 44, no. 7, pp. 1277–1284, 2011.
[6.6] T. Oberg, A. Karsznia, and K. Oberg, "Joint angle parameters in gait: Reference data for normal subjects, 10–79 years of age," *J. Rehabil. Res. Dev.*, vol. 31, no. 3, pp. 199–213, 1994.
[6.7] G. Pulignano *et al.*, "Incremental Value of Gait Speed in Predicting Prognosis of Older Adults With Heart Failure: Insights From the IMAGE–HF Study," *JACC Hear. Fail.*, vol. 4, no. 4, pp. 289–298, 2016.
[6.8] S. W. Davies, C. A. Greig, S. L. Jordan, D. W. Grieve, and D. P. Lipkin, "Short–stepping gait in severe heart failure," *Heart*, vol. 68, no. 11, pp. 469–472, 1992.
[6.9] L. D. Alexander, S. E. Black, K. K. Patterson, F. Gao, C. J. Danells, and W. E. Mcllroy, "Association between gait asymmetry and brain lesion location in stroke patients," *Stroke*, vol. 40, no. 2, pp. 537–544, 2009.
[6.10] R. Passmore and J. V. Durnin, "Human energy expenditure," *Physiol. Rev.*, vol. 35, no. 4, pp. 801–840, 1955..
[6.11] R. L. Waters, B. R. Lunsford, J. Perry, and R. Byrd, "Energy-speed relationship of walking: Standard tables," *J. Orthop. Res.*, vol. 6, no. 2, pp. 215–222, 1988.
[6.12] V. L. Hood, M. H. Granat, D. J. Maxwell, and J. P. Hasler, "A new method of using heart rate to represent energy expenditure: The total heart beat index," *Arch. Phys. Med. Rehabil.*, vol. 83, no. 9, pp. 1266–1273, 2002.
[6.13] MacGregor J, "The objective measurement of physical performance with long term ambulatory physiological surveillance equipment (LAPSE). Proceedings of the Third International Symposium on Ambulatory Monitoring," *Proc. 3rd Int. Symp. Ambul. Monit. 1979*, pp. 29–39, 1979.
[6.14] Z. Tahergorabi and M. Khazaei, "The relationship between inflammatory markers, angiogenesis, and obesity," *ARYA Atheroscler.*, vol. 9, no. 4, pp. 247–253, 2013.
[6.15] C. J. Lavie, R. V. Milani, and H. O. Ventura, "Obesity and Cardiovascular Disease. Risk Factor, Paradox, and Impact of Weight Loss," *Journal of the American College of Cardiology*, vol. 53, no. 21. pp. 1925–1932, 2009.
[6.16] J. S. Brach, J. E. Berlin, J. M. VanSwearingen, A. B. Newman, and S. A. Studenski, "Too much or too little step width variability is associated with a fall history in older persons who walk at or near normal gait speed," *J. Neuroeng. Rehabil.*, vol. 2, 2005.
[6.17] S. Lord, T. Howe, J. Greenland, L. Simpson, and L. Rochester, "Gait variability in older adults: A structured review of testing protocol and clinimetric properties," *Gait and Posture*, vol. 34, no. 4. pp. 443–450, 2011.
[6.18] F. Shaffer and J. P. Ginsberg, "An Overview of Heart Rate Variability Metrics and Norms," *Front. Public Heal.*, vol. 5, 2017.
[6.19] K. J. Hunt and J. Saengsuwan, "Changes in heart rate variability with respect to exercise intensity and time during treadmill running," *Biomed. Eng. Online*, vol. 17, no. 1, 2018.
[6.20] K. Umetani, D. H. Singer, R. McCraty, and M. Atkinson, "Twenty–four hour time domain heart rate variability and heart rate: Relations to age and gender over nine decades," *J. Am. Coll. Cardiol.*, vol. 31, no. 3, pp. 593–601, 1998.
[6.21] H. Shimokata and F.Kuzuya, "Aging, Basal Metabolic Rate, and Nutrition," *Japanese Journal of Geriatrics*, vol. 30, pp. 572–576, 1993.
[6.22] M. F. Schulz Aellen. (2008). Healthy Ageing. Continuing Psychology Education, Austin, Texas. [Online]. Available: http://texcpe.com/html/pdf/HealthyAging.pdf
[6.23] J. M. Hausdorff, "Gait variability: Methods, modeling and meaning," *Journal of NeuroEngineering and Rehabilitation*, vol. 2. 2005.
[6.24] G. Quer, P. Gouda, M. Galarnyk, E. J. Topol, and S. R. Steinhubl, "Inter– And intraindividual variability in daily resting heart rate and its associations with age, sex, sleep, BMI, and time of year: Retrospective, longitudinal cohort study of 92,457 adults," *PLoS One*, vol. 15, no. 2, pp. 1–12, 2020.

Appendix

Copyright permissions

BACK CLOSE WINDOW
Comments? We would like to hear from you. E–mail us at customercare@copyright.com

Home Help Email Support Sign in Create Account

RightsLink
Noncontact Wearable Wireless ECG Systems for Long–Term Monitoring
Author: Sumit Majumder
Publication: Biomedical Engineering, IEEE Reviews in
Publisher: IEEE
Date: 2018

Thesis / Dissertation Reuse
The IEEE does not require individuals working on a thesis to obtain a formal reuse license, however, you may print out this statement to be used as a permission grant:
Requirements to be followed when using of any portion (e.g., figure, graph, table, or textual material) of an IEEE copyrighted paper in a thesis:
1) In the case of textual material (e.g., using short quotes or referring to the work within these papers) users must give full credit to the original source (author, paper, publication) followed by the IEEE copyright line © 2011 IEEE.
2) In the case of illustrations or tabular material, we require that the copyright line © [Year of original publication] IEEE appear prominently with each reprinted figure and/or table.
3) If a substantial portion of the original paper is to be used, and if you are not the senior author, also obtain the senior author's approval.
Requirements to be followed when using an entire IEEE copyrighted paper in a thesis:
1) The following IEEE copyright/ credit notice should be placed prominently in the references: © [year of original publication] IEEE. Reprinted, with permission, from [author names, paper title, IEEE publication title, and month/year of publication]
2) Only the accepted version of an IEEE copyrighted paper can be used when posting the paper or your thesis online.
3) In placing the thesis on the author's university website, please display the following message in a prominent place on the website: In reference to IEEE copyrighted material which is used with permission in this thesis, the IEEE does not endorse any of [university/educational entity's name goes here]'s products or services. Internal or personal use of this material is permitted. If interested in reprinting/republishing IEEE copyrighted material for advertising or promotional purposes or for creating new collective works for resale or redistribution, please go to http://www.ieee.org/publications_standards/publications/rights/rights_link.html to learn how to obtain a License from RightsLink.
If applicable, University Microfilms and/or ProQuest Library, or the Archives of Canada may supply single copies of the dissertation.
BACK CLOSE WINDOW
Comments? We would like to hear from you. E–mail us at customercare@copyright.com

---

Sensors Editorial Office Sun, Sep 27, 2:45 AM (8 days ago)

to me, sensors

Dear Dr. Majumder,
Sensors is an open access journal. The authors retain the copyright of the papers.
The two papers are open access articles distributed under the Creative Commons Attribution License

Please feel free to let us know if we can be of any assistance.

Kind regards,

Ms. Fancy Chai
Managing Editor
Sensors Editorial Office
E–Mail: fancy.chai@mdpi.com
MDPI
St. Alban–Anlage 66, 4052 Basel, Switzerland
http://www.mdpi.com/

Sensors Impact Factor 2019: 3.275

On 2020/9/23 21:11, SUMIT MAJUMDER wrote:
> Dear Sensors editorial team,
> I published the following papers
> "Wearable sensors for remote health monitoring", S Majumder, T Mondal,
> MJ Deen, Sensors 17 (1), 130 in MDPI that is available at
> https://www.mdpi.com/1424–8220/17/1/130
>
> "Smart Homes for Elderly Healthcare—Recent Advances and Research
> Challenges" S Majumder, E Aghayi, M Noferesti, H Memarzadeh–Tehran, T
> Mondal, ...Sensors 17 (11), 2496 that is available at
> https://www.mdpi.com/1424–8220/17/11/2496
>
> "Smartphone Sensors for Health Monitoring and Diagnosis" S Majumder,
> MJ Deen, Sensors 19 (9), 2164 that is available at
> https://www.mdpi.com/1424–8220/19/9/2164
>
> I would like to request permission to reuse the contents of these papers
> in my Ph. D. dissertation. Thank you for your consideration and support.
>
> Kind regards,
> Sumit Majumder
> Ph.D. Candidate
> Department of Electrical & Computer Engineering